Reactive Jet Impingement Bioprinting for In Vitro Model Development

A thesis submitted to the Faculty of Science, Agriculture and Engineering for the Degree of

Doctor of Philosophy

By

Aidan Bowes

School of Engineering

Newcastle University

October 2021

I Abstract

3D bioprinting allows for the production of living tissue in vitro through the printing of cells and supporting materials into complex 3D structures. The applications for this are far reaching including the production of microtissues and organs for transplant [1], as well as for drug testing applications. Furthermore there is evidence to show that 3D cell culture models more accurately replicate in vivo conditions than traditional 2D models by more accurately replicating the in vivo microenvironment [2].

Newcastle University have developed a method of inkjet bioprinting known as the Reactive Jet Impingement (ReJI) method. This method allows for deposition of the desired high viscosity, high cellular density gel at a high deposition rate on a drop on demand basis.

The aim of this project was to develop this method to increase the throughput capability, and to evaluate the printhead for production of stratified hydrogel co-cultures incorporating multiple cell types, and in printing cells as part of a cancer invasion model

Over the course of this work the ability to print high cellular density bioinks (of the order of 10^7 cells/ml) with a high cell viability was demonstrated and cell viability remained high in both high and low cell density gels. Additionally, culture type did not affect viability as cell viability remained high in printed stratified co-cultures as well as cultures with only one cell type.

Cell density was demonstrated to have had a significant effect on maturation rate of 3D printed tissue models, with higher cell densities producing tissue models with greater extracellular matrix content. This was assessed quantitatively through imaging and qualitatively through ELISA analysis and mechanical testing.

The ReJI system was demonstrated to be capable of printing on delicate, uneven surfaces of unknown stiffnesses through printing on sectioned liver tissue slices for use in a cancer invasion model.

II Acknowledgements

I would firstly like to thank my main supervisor Prof. Kenny Dalgarno for providing me with opportunities that I otherwise wouldn't have thought would ever be available to me, challenging me to be a better engineer, providing me with a job that reminded me daily just how much I enjoy engineering, and for making me feel like someone always had my back. None of this would have been possible without Kenny's continued, unbiased and honest support.

To Brian and Stuart in the Stephenson Building workshop for their help with manufacturing the ReJI components but also for providing a level-headed voice of reason throughout, I am very grateful.

Thank you to Glyn Nelson, David Bulmer and the rest of the Bioimaging team for providing the expertise and guidance in selecting and applying stainings and imaging processes.

Thank you to Prof. Fiona Oakley and Amy Collins for their help in choosing appropriate analysis techniques and their help carrying these out, as well as for providing general help and support with a great deal of the biological aspects of this project. Also, for their help in providing samples and imaging for the cancer invasion model.

Thank you to my mother Angela for being so incredibly helpful and for always being there to put others first.

I would like to thank my wife Charlotte for her continued unbridled, emphatic, and seemingly bottomless support throughout all of my studies. For believing I could do it when I was convinced I couldn't, and for putting up with me when no one else would. But mainly just for being there to share this and everything else with me.

Finally, I would like to thank my father David. For introducing me to engineering, for challenging me to always think that if something seemed too difficult; "why shouldn't I be able to do that, and why shouldn't I be able to do it better", and for being the type of person who I would like to be.

For all of these people, and the roles they played I will always be grateful.

III Table of Contents

IV Table of abbreviations

2D	Two Dimensional
3D	Three dimensional
ECM	Extracellular Matrix
ReJI	Reactive Jet Impingement
CT	Computed Tomography
MRI	Magnetic Resonance Imaging
CAD	Computer Aided Design
CAF	Collagen Alginate Fibrinogen
DOD	Drop on Demand
LAB	Laser-Assisted Bioprinting
IAMF	In Air Micro-Fluidic
AFM	Atomic Force Microscopy
TFM	Traction Force Microscopy
PEG	Polyethylene Glycol
RWV	Rotating-Wall-Vessel
GAGS	Glycosaminoglycans
FRAP	Fluorescence Recovery After Photobleaching
OCT	Optimum Cutting Temperature
OA	Osteoarthritis
MMPs	Matrix Metalloproteinases
ACI	Autologous Chondrocyte Implantation
NICE	National Institute for Health and Care Excellence
CPC	Calcium Phosphate Cement
AlgMC	Alginate-methylcellulose
FBS	Fetal Bovine Serum
DPBS	Dulbecco's Phosphate Buffered Saline
PFA	Paraformaldehyde Solution
PG	Proteoglycan
hCol1	Human collagen type I
ELISA	Enzyme-linked Immunosorbent Assay
RD	Reagent Diluent
3T3	3-day transfer, inoculum 3×10^5 cells
eGFP	Enhanced Green Fluorescent Protein

V List of Figures

VI List of Tables

VII List of Equations

Chapter 1. Introduction, Aim and Objectives

1.1 Introduction

Additive manufacture or 3D printing is a rapidly developing field of research. Its development is instigating changes to manufacturing processes across a wide variety of sectors including engineering, medicine, art and design[3]. One area at the forefront of these developments is the printing of biocompatible and biological materials.

In this body of work the Reactive Jet Impingement (ReJI) system [4,5], developed by Newcastle University, is developed and novel capabilities demonstrated through applying the technique to two applications; the production of 3D printed stratified osteochondral co-cultures, and the deposition of cells within a cancer invasion model. Using a novel jet impingement process this system is able to produce high viscosity, high cell density, cell filled hydrogels on an accurate drop-on-demand basis. Using this system, high cell density gels are produced and assessed to determine cell viability post print as well as the effect of cell density on the maturation of the printed cultures. Moreover, the scalability and throughput of the process is demonstrated along with the versatility of the system for use in numerous applications.

Osteoarthritis is a painful degenerative disease that affects people globally. Arthritis treatments range from pain management to invasive joint replacement surgeries dependent on the severity of the disease and the need for new and alternative treatment options, especially in the time between the early and late stages of the disease where pain management is difficult but invasive surgical treatments are not yet warranted, is evident [6,7]. Producing a more accurate model of the osteochodral interface using a scalable high throughput method would make studying the cellular behaviour in this area in greater depth easier, and aid in undertaking repeatable, accurate lab trials for use in arthritis and tissue research. In addition to drug testing for osteoarthritis, cell filled gel scaffolds could also be printed in complex geometries for use as implants in the repair of damaged cartilage.

The second application demonstrated for the ReJI system is the production of cancer invasion models. Cancer is a condition where cells proliferate and grow in an uncontrolled way, these cells can become invasive and destroy healthy tissues. Many of the current most popular chemical drug treatments, such as chemotherapy, focus on the destruction of the rapidly proliferating cells and overall reducing cell growth. However due to the difficulties of representing suitable conditions in current in vitro tissue models, drugs that prevent the

spreading of cancerous cells throughout the body are more difficult to study and therefore not commonly offered as treatment options, instead this leads to a focus skewed towards more aggressive drug treatments that tend to be more effective on traditional 2D in vitro models. Using the ReJI system as a high throughput method of 3D printing cancer cell invasion models could allow for easier study of cell motility whilst also demonstrating the versatility of the system in printing different cell types and accurately depositing gels of smaller volumes (in some cases single droplet) on to delicate, uneven, and soft tissue substrates.

Currently, a number of in vitro models are used for drug development in pre-clinical trials, however many share the same common drawbacks, in the case of 2D models this is that they oversimplify conditions found in vivo and can lead to misrepresentative results [8,9], or in the case of aggregate based culture methods cell-ECM interaction is not represented fully[10]. Additionally, animal models are used for this purpose and are currently thought to be the most representative models of human in vivo conditions, however, animal testing raises a host of issues, including expense, low throughput, animal welfare concerns and there is no guarantee that drugs that succeed in animal trials will also succeed in human trials due to immunogenic properties of the drugs going undetected in animal trials [11]. There is significant expense involved in the process of drug development, Schlander et al estimate the total average capitalized pre-launch R&D costs for developing a new drug can vary significantly, ranging from $161 million to $4.54 billion (2019 US$). With the highest estimates being for anticancer drugs (between $944 million and $4.54 billion) [12]. The drug development process generally adheres to the following main stages:

- Basic Research
- Drug Discovery
- Pre-Clinical trials
- Clinical Trials
- Regulatory Agency review
- Post approval Research and monitoring

With each of these phases being comprised of multiple sub phases. Total drug development time can average between 10 – 15 years [13].

Whilst new lead compounds are continually being identified and explored it is preferable that unsuccessful compounds are identified as early in the testing process as possible in order to

save as much time and money in development as possible. To this end the development of reliable in vitro models of tissue that can be created in large quantities as early in the testing process as possible is very important as it would allow for earlier detection of adverse effects [14].

For a number of years researchers have used hydrogels to act as tissue culture scaffold for the production of more representative tissue with some relevant studies dating back to 1992 [15]. Using natural hydrogels such as collagen and fibrin, and by controlling mechanical properties of the crosslinked gel it is possible to mimic the conditions found in native tissue [16]. However, methods of producing hydrogel cultures manually can be time consuming. Gels have to be manually mixed and seeded with cells. Additionally, due to the high viscosity of hydrogels the number of high throughput options for producing cultures through 3D bioprinting have previously been limited. Suitable methods include microextrusion, which lacks accuracy and can damage cells through excessive sheer stresses, and laser assisted bioprinting, to which access is limited by the cost of the process. Due to the demand for high throughput as well as the need to minimise costs, few suitable high throughput methods for the production of cell filled hydrogels using drop-on-demand technology have been demonstrated. Furthermore, the printed cell density within the gels is also limited due to viscosity as excessive viscosities can induce shear stresses in the print nozzles which harm cells or are simply too viscous to print successfully.

This thesis develops and demonstrates an accessible and effective method of high throughput bioprinting of high cellular density hydrogel tissue models.

1.2 Project Aim

The aim of this project was to develop the ReI system from a concept system into a working, commercially viable bioprinter and demonstrate it's efficacy as a high throughput bioprinter through the production of a stratified osteochondral co-culture model s well as demonstrate the system's efficacy for other applications such as cancer cell motility research.

1.3 Project Objectives

- Carry out printer development through the design, production and testing of a number of different designs.
- Produce cell filled hydrogels of varying cell densities using the newly developed printer demonstrating the printer's ability to produce gels with a high cell density.
- Assess the effect of cell density on in vitro tissue maturation.

- Produce a printed stratified co-culture model and assess the effect of cells in co-culture on tissue maturation.
- Demonstrate the effect of high cell density printed structures in other applications, namely the production of tumour models.
- Print on to uneven, biological substrates.

Chapter 2. Literature review

2.1 Introduction

This literature review aims to assess relevant literature in the field of 3D bioprinting, it's application to drug development models and the potential future uses. The different stages of the bioprinting process will be outlined as well as different bioprinting processes, the current limitations of the technology and areas of future development.

Following this, impingement based technologies including the ReJI system are reviewed.

The current methods for producing in vitro tissue models for drug screening applications are summarised and reviewed in the context of how 3D bioprinting can be applied to these applications.

Finally, an overview of osteoarthritis, and cancer invasion models, their impact and current drug development methods are outlined as these were the main applications of the ReJI system throughout the course of this work.

2.2 3D Bioprinting

2.2.1 Overview

3D bioprinting allows for the production of living tissue through the printing of cells and supporting materials into complex 3D structures. Jürgen Groll et al 2016 define bioprinting to be *"a process that resultis in a defined product with a biological function"*[17]. Materials used for this application are often referred to as bioinks and generally comprise of cells suspended in either liquid media or a gel. The applications for this are far reaching including the production of microtissues and organs for transplant such as urethras [18], muscle [1], multi layered skin and bone.

Furthermore, 3D bioprinting shows promise as a reliable method for the production of 3D tissue models for research, toxicology and drug discovery. In order to gain the most accurate understanding possible of the biological processes involved in the human body it is necessary for in vitro assays to replicate in vivo conditions as closely as possible. However this is often not the case as practically the use of 2D models is still widespread [19] and there is evidence to show that 3D cell culture models more accurately replicate in vivo conditions by more accurately replicating the microenvironment where cells reside in tissues [2]. Therefore, the development of 3D bioprinting as a method for the production of 3D tissue models could not only provide more effective replication of in vivo conditions but do so in a way that provides

increased repeatability and reliability in terms of production process with a potential for an overall increased manufacturing process speed.

In the majority of 3D bioprinting processes there are six common steps, these are as follows:

1. Imaging and CAD – An image is created of the tissue to be constructed.
2. Design – A design for the tissue to be made is produced.
3. Material Selection – Suitable material is selected for the application.
4. Cell Selection – Suitable cell types are chosen for the application.
5. Bioprinting – The Bioprinting methodology is selected and the part if fabricated.
6. Application – The completed part is used in its application.

Figure 2-1 below shows the process as a flowchart with a selection of potential options for each step. The sections below consider each step in more detail.

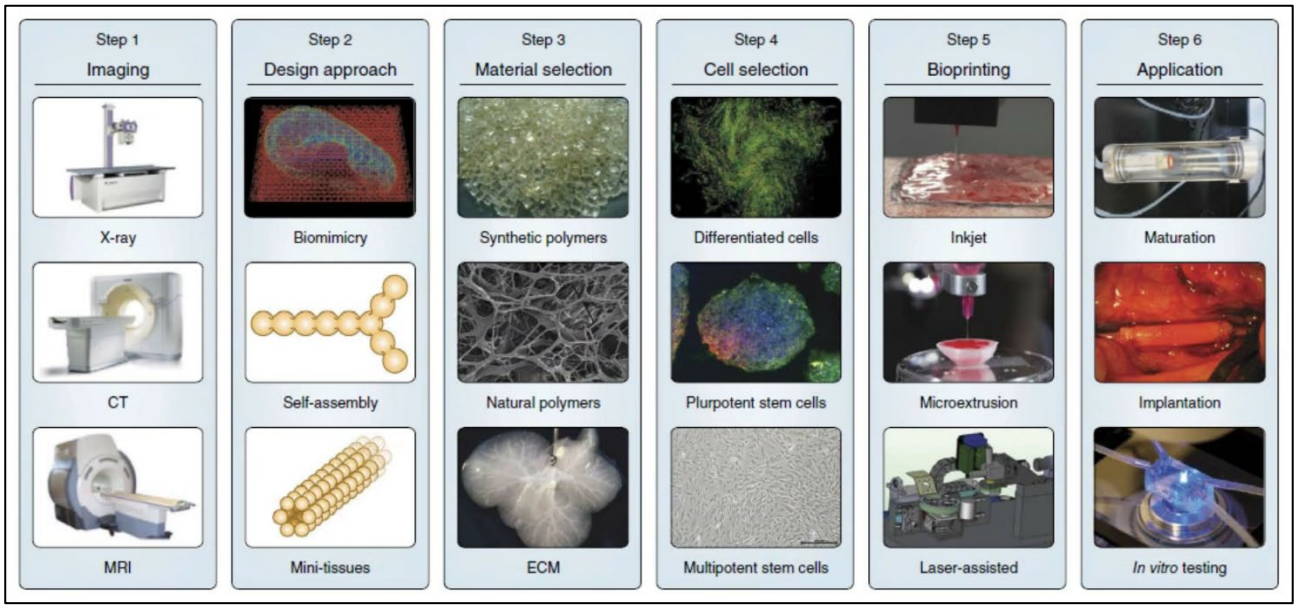

Figure 2-1: Typical tissue printing process showing different options for each step. Described in further detail in the below sections. From [3].

2.2.2 **Imaging and CAD**

In order to produce an accurate replication of any kind of biological tissue, it is first necessary to understand its composition and cellular structure. Computed tomography (CT) and magnetic resonance imaging (MRI) are both common and non-invasive medical scanning techniques used to compile 3D images of tissue structure and function down to the cellular level.

CT Scanning works through rotating an x-ray source around the object desired to be scanned. As the absorption of the x-rays will vary across different tissues, by measuring the beam intensity and angle it is possible to build a tomographic or sliced image of the 3D object converting the measured data to an array of pixels. Once these tomographic images have been produced a 3D image of the full volume of tissue can then be assembled through editing techniques such as surface rendering.

MRI scanning makes use of nuclear magnetic resonance, this produces a strong magnetic field that causes a number of nuclei in the scanned tissue to align with the magnetic field. This induces changes in energy states of the nuclei which produces radiofrequency signals, this can then be picked up by the receiver coils in the MRI machine. MRI offers the advantage of not introducing ionising radiation to the tissue while still offering high contrast resolution in soft tissues within close proximity to each other.

Post processing of the raw data that these two scanning techniques provide is the next step and this involves volumetric rendering of the 2D images produced to create one solid 3D image created using computer aided design (CAD). By creating a 3D image using CAD not only can a greater understanding of the scanned tissue be gained, but the digital construction of the scanned tissue may even be modified before printing. Modification may occur if the patient's scanned tissue was damaged or if the 3D model to be printed included geometry which would be unsuitable for large scale in vitro testing. Furthermore once a 3D model has been created it is then possible to undertake computational and structural analysis and simulation of the tissue. Once analysis has been carried out it may even be necessary to undertake modification to change structural properties or to make the structure more suitable for the chosen printing techniques as some methods of printing may have difficulty in printing certain shape profiles or patterns. One reason for this is that before any tissue can be printed, the 3D CAD image is then again sliced into a 2D image which allows the bioprinter to build the part effectively by depositing bioink layer by layer. It is important to note that the printing method and also the materials chosen will have a large input on the final desired 'tissue design' to be printed [20].

2.2.3 **The Design Phase**

There are currently three overarching approaches to the design phase in bioprinting, these are tissue engineering by self-assembly, biomimicry and the use of mini-tissue building blocks [3]. In order to provide suitable context for the background of this project these will be briefly summarised.

2.2.3.1 ***Biomimicry***

Biomimetics involves solving technological problems with solutions derived from nature. Its application can be found in many fields including robotics [21], cell culture and bioengineering methods [22], and materials science [23]. Biomimicry is used in 3D bioprinting to attempt to directly replicate the cellular or extracellular components of a tissue. For example in the production of functional bioprinted organs it is crucial to create complex tissues with full vascularisation. Biomimicry can be used in conjunction with bioprinting techniques to replicate aspects of biological tissues such as the patterns of the vascular tree on a microscale [24]. For this technique to be successful it is necessary to have a detailed understanding of the microstructure of the biological tissues that are being replicated including the arrangement of the cells, the composition of the extracellular matrix (ECM) and the biological forces involved. One such application of biomimicry in 3D bioprinting is the production of porous scaffolds designed to mimic the structure of ECMs at the nanoscale in order to provide the base for growth and regeneration of cellular tissue. In this application not only does the scaffold need to mimic the ECM in terms of structure, mechanical strength and biological activity, but also the materials used must be biologically compatible[25].

2.2.3.2 ***Self-assembly***

As the name would suggest, self-assembly is the autonomous organisation of cellular structures without any intervention from external sources. Living organisms, in particular developing embryo are extremely efficient as self-organising systems. Through cell-cell and cell-ECM reactions histogenesis and organogenesis are examples of processes through which organisms autonomously self-assemble to reach their final form [26]. This is also possible without scaffold through the use of self-assembling spheroids, these spheroids fuse together mimicking tissue development. This method relies on the cell to be the primary driver of histogenesis and requires precise control of the environment to aid development.

2.2.3.3 ***Micro-Tissues***

Micro-tissues can be described as the smallest functioning structural component of a tissue. These are effectively the building blocks that organs are comprised of. Examples of micro-tissues include kidney nephrons, lung alveoli and liver lobuli [27]. In the context of bioengineering mini-tissues can be fabricated in two ways. The first method is through planned rational biomimetic design process, self-assembling cell spheres can be arranged to form larger tissue constructs [28]. The second involves producing a high resolution design of

a tissue construct and then allowing self-assembly of micro-tissues into a larger tissue construct [26].

2.2.4 **Material Selection**

Conventional 3D printing methods were not designed for the application of bioprinting. Processes were instead developed with a view to printing materials such as polymers, metals and ceramics. As a result, these processes often involve steps that would be considered too invasive for printing biocompatible materials as they are likely to have an effect on the health of the cells. For example, prolonged exposure to a high temperature heat source or high extrusion pressures are likely to adversely affect the health of cells. Therefore, in material selection for bioprinting the problem is twofold, firstly it is necessary for the material to be compatible with, and resilient to the printing process, and secondly the final printed tissue must have the desired mechanical and operational requirements.

Currently the most common materials used in biofabrication are naturally derived polymers such as collagen, alginate and fibrinogen, or synthetic polymers such polyethylene glycol, polylactic acid (PLA), polyglycolic acid (PGA), polylactic-co-glycolic acid (PLGA). It is clear that the use of natural polymers is advantageous due to their bioactivity and similarity to the human ECM, conversely synthetic polymers can have biocompatibility issues as well as a toxic degradation which results in a loss of the desired mechanical properties. Even so, some synthetic polymers and hydrogels are attractive for use in bioprinting for the ability to control their physical properties to meet the requirements of individual applications. Due to the use of biocompatible materials in medical applications the desired requirements can be extensive and difficult to achieve. Some key requirements are as follows.

2.2.4.1 Mechanical Properties

Materials must have good short term mechanical properties and stability. In the case of something like a scaffold this is to ensure that they do not fail causing channels and porosities to be crushed. Biocompatibility is also necessary to ensure that the material is not rejected by the host and will degrade properly over time. Furthermore during in vivo development they should effectively facilitate cell growth, and be capable of structural change and degradation in order for this growth to proliferate. Additionally the aim of biocompatibility in materials is now not only for the material to be able to exist within the host without rejection, but instead for the material to positively affect the host tissue through providing useful mechanical properties, encouraging cell growth or through some other means [29].

2.2.4.2 *Printability*

Another significant factor involved with materials selection is printability. For example, inkjet printing, while providing the accuracy of 'drop on demand', requires the bioinks to be of a suitably low viscosity to pass through the jet orifice. As the jet orifice diameter also contributes to the droplet size, with small sizes required for single cell deposition, this has a large effect on the choice of material especially when attempting to print cell media and materials such as CAF (Collagen Alginate Fibrinogen) hydrogels [30]. Conversely due to the nature of the microextrusion process this can often use materials of a much higher viscosity.

2.2.4.3 *Working Temperature*

Another complication in considering material printability are temperature constraints, thermal inkjetting and laser assisted bioprinting both involve subjecting the material to a high temperature heat source and therefore it is advantageous in these instances for the bioink to offer some protection to the cells. One method for this may be to have a cell media with a low thermal conductivity [31].

2.2.4.4 *Degradation*

Degradation properties are also an important factor of consideration in bioprinting. Ultimately the aim for most tissue scaffold is to eventually degrade and be replaced with new healthy tissue grown from the embedded cells [32]. Due to this, the rate of degradation of the scaffold must synchronise with the rate of new tissue growth. If the scaffold degrades too quickly the loss of structure is likely to affect cell growth as there are no channels and porosities for the cells to adhere to, but also if the rate of degradation is much greater than the rate of new tissue growth then there is likely to be a significant loss of structural mechanical properties. Furthermore as has been mentioned previously, degrading materials must not release any toxins into the host or cause any unwanted side effects that may affect cell health such as swelling, inflammation or temperature changes.

2.2.5 **Cell selection**

The next stage in the bioprinting process is the selection of cells. It is clear that living tissue is made of multiple cells that all provide a particular biological purpose. It is important for any fabricated or transplanted tissue construct to match this as closely as possible in order for growth and renewal to be possible. However this makes the task of cell selection for printing difficult as not only is it necessary to include in the printed object the desired functional primary cells, but also the cells that perform a supporting role such as providing structural

stability or aiding in vascularisation. The current approach for replication of cell types in a printed structure is either printing multiple primary cell types in a stratified co-culture that best represents the tissue that the print is trying to replicate, or printing stem cells such as MSCs or hPSCs that can then differentiate into the desired cell types. Using the latter method has been found to improve certain functions of the primary cells that they are in co-culture with, for example increases chondrogenesis when in co-culture with chondrocytes [33]. However controlling the differention of the MSCs can be complex and dependent on multiple features of the co-culture environment.

What is more, it is important that the cell types chosen are able to maintain desired functionality and stability in vivo. Cell proliferation is a very important function of this. If cell growth is not sufficient then the tissue is likely to lose functionality whereas if cell growth is too great there is risk of hyperplasia.

Ultimately cells chosen for bioprinting applications must firstly be suitable for achieving the desired growth and proliferation rates but they must also be amenable to the printing process. Cells can be subject to numerous damaging factors, for example high temperatures, as has been previously mentioned. Mechanical stresses can also have an adverse effect on cells, processes such as microextrusion involve compressing the cell media in order to extrude it through an orifice, as well as this, cells are subject to wall shear stress in both inkjet and microextrusion. Additionally there are potential biological risks such as the presence of toxins or enzymes that the cells must be robust enough to overcome.

2.2.6 **Bioprinting Methodologies**

Bioprinting methodologies have been mentioned briefly in previous sections but will be covered in greater detail in this section. Essentially there are currently 3 prime methods of producing 3D tissue by bioprinting. These are inkjet bioprinting, which can be further divided into continuous jetting and drop on demand (DOD) printing [34,35], microextrusion [36,37], and laser-assisted bioprinting (LAB) [38]. Figure 2-2 below shows the 3 main methods described in this section in more detail.

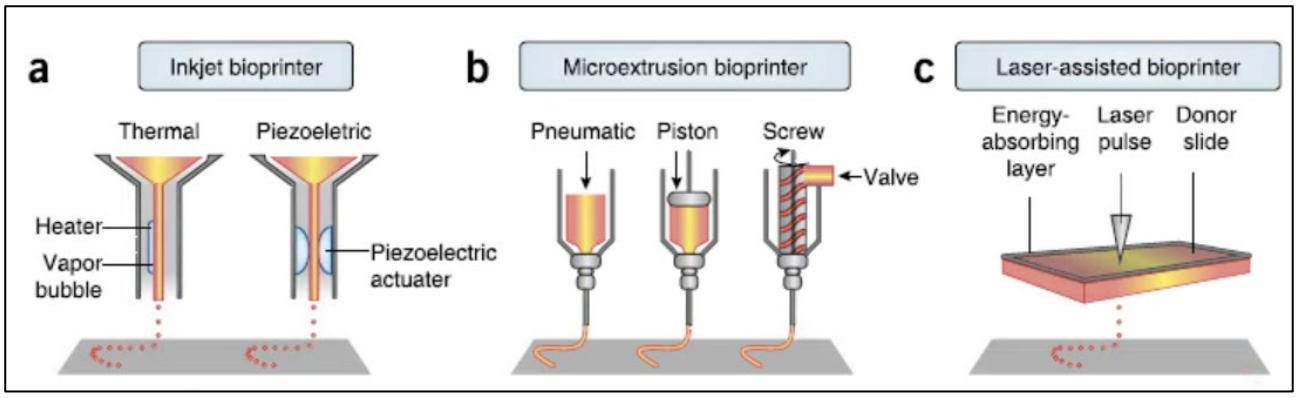

Figure 2-2: The three most popular methods of 3D bioprinting. (a) Inkjet Bioprinting. (b) Microextrusion bioprinting. (c) Laser-assisted bioprinting. From [3].

Additionally the below table taken from Murphy and Atala [3] summarises some of the main features of each methodology.

	Bioprinter type		
	Inkjet	**Microextrusion**	**Laser assisted**
Material viscosities	3.5–12 mPa/s	30 mPa/s to >6 × 10_7 mPa/s	1–300 mPa/s
Gelation methods	Chemical, photo-crosslinking	Chemical, photo-crosslinking, sheer thinning, temperature	Chemical, photo-crosslinking
Preparation time	Low	Low to medium	Medium to high
Print speed	Fast (1–10,000 droplets per second)	Slow (10–50 µm/s)	Medium-fast (200–1,600 mm/s)
Resolution or droplet size	<1 pl to >300 pl droplets, 50 µm wide	5 µm to millimeters wide	Microscale resolution
Cell viability	>85%	40–80%	>95%
Cell densities	Low, $<10^6$ cells/ml	High, cell spheroids	Medium, 10^8 cells/ml
Printer cost	Low	Medium	High

Table 2-1: Table showing comparison of features of each of the three most popular bioprinting methodologies taken from Murphy & Atala [3]

2.2.6.1 ***Inkjet bioprinting***

Inkjet bioprinting was initially developed by modifying conventional inkjet printers. By replacing the conventional inks with bioinks and the paper with an adjustable build platform or 'z-axis' it was possible to develop a system that is able to deliver precisely controlled

volumes of bioinks, repeatedly, to a defined area [39]. The design of inkjet bioprinters has now evolved such that they are now designed to achieve specific build rates, function correctly with a range of bioinks and achieve a high level of precision. There are three main methods of inkjet bioprinting, these are thermal, pressure and acoustic.

Thermal inkjet bioprinting functions by applying heat to the inkjet valve electrically, this induces the formation of heat bubbles in the valve chamber to induce pressure pulses in the bioink. This causes a droplet to be released from the nozzle orifice. This method offers multiple advantages in the form of high speed, high resolution, low cost and widespread availability. However due to the introduction of a heat source there is the risk of exposing cells to unnecessary levels of thermal stress, furthermore other issues such as nozzle clogging and non-uniform droplet size are present [34]. Common nozzle diameter for a thermal inkjet valve is approximately 50 µm which leads to a droplet diameter range of 30-80 µm [40–42]. Although the heat source can be in the range of 200-300 °C it has been shown that the short duration of this temperature does not necessarily have an effect on the functionality of printed cells [25] and that the total maximum temperature rise of the bioink in the printhead due to this method is only 10°C [41,42]. Thermal microvalves often have slower response times (greater than 100ms to complete a cycle). Slower valve actuation time results in longer thruster on-times and consequently larger impulse bits. With thermally actuated valves there is also the risk of the valve opening at random if ambient heating or cooling occurs, resulting in uncontrolled initiation of the actuation mechanism[43].

Piezoelectric inkjet printers introduce pressure into the print nozzle through either an ultrasound pulse or through the actuation of a piezoelectric crystal. Piezoelectric systems will often have a nozzle seated within a piezoelectric ring or some other form of piezo actuator, a voltage can be applied to this causing it to deform and apply pressure to the bioink. Alternatively ultrasound systems induce a wave in the bioink which causes a droplet to separate itself from the air liquid interface in the nozzle [44]. The advantages of this method are that parameters such as the duration, pulse and amplitude can be controlled. This not only means that cells are not exposed to stresses such as high temperature, but droplet size and directionality can be controlled with a greater degree of accuracy. This method is also less susceptible to nozzle clogging. Piezoelectrically actuated microvalves are usually available with nozzle diameters ranging from 18-120 µm [45,46] with droplet diameters varying commonly between 50-100 µm.

Although inkjet bioprinters offer many advantages there are still some drawbacks of this method. Firstly printable materials must be in liquid form with a relatively low viscosity to allow for droplets to form correctly [47]. This drawback has a large effect on the material choice when selecting bioinks compatible with this method. It has also lead to the development of methods that will independently print or extrude a gel precursor and a cross-linker, allowing these to mix and cross-link either one printed atop the other, or in a common, larger diameter mixing chamber before being extruded. Companies such as Aspect Biosystems have attempted to develop commercial answers to this issue but it still continues to be a significant limiting factor of microextrusion as a 3D bioprinting methodology.

The most common method of inkjet bioprinting is DOD printing, however there is also continuous inkjet bioprinting. Continuous inkjet bioprinting results in a continuous flow of droplets through a nozzle rather than individual drop on demand. This is achieved by applying a pressure to a bioink to force a continuous flow through a nozzle. Simultaneously a piezoelectric frequency is applied to the nozzle causing the continuous flow to break up into a continuous flow of droplets. This is similar to the concept of conventional inkjet printing.

2.2.6.2 ***Microextrusion***

Microextrusion bioprinters work in a similar manner to conventional fused deposition modelling 3D printers, in that the print material, in this instance the bioink, is extruded through a nozzle as one continuous filament and the 3D construct is built up in layers of filament. The material is extruded through the nozzle through one of three methods, these are; pneumatic actuation whereby a pneumatic pressure is applied to the material in the printhead, mechanical actuation by means of a piston physically applying pressure to the bioink, and mechanical extrusion by use of a screw to extrude the material through the nozzle.

Pneumatic actuation offers the advantage of having fewer mechanical components and thus is a simpler and easier to maintain system however it is thought that the delay in bioink reaction due to changes in the pneumatic pressure may result in less reliable spatial control than that offered by one of the purely mechanical methods. Conversely both purely mechanical methods are more complex systems than the pneumatic extrusion method, using a greater amount of small, complex mechanical components, this is especially true of the screw driven method. Due to the small component size extrusion force and consequently material viscosity is often limited.

The main advantage of microextrusion is the ability to deposit high cell densities due to the ability to extrude higher viscosity materials. It has been demonstrated that it is possible to deposit bioinks comprised of only cells to create 3D tissue [48]. However, although high cell densities are achievable, this often comes with an increase in bioink viscosity, meaning print resolution may have to be sacrificed due to the necessary increase in nozzle size, so as to not have an adverse effect on cell survival rates due to increased shear stresses. Furthermore print speed is much slower than that of inkjet or even LAB at approximately 10-50 µm/s [3].

2.2.6.3 ***Laser-Assisted Bioprinting***

Despite being less common that inkjet or microextrusion bioprinting LAB has proven a successful method for the deposition of bioinks including both cells and DNA [48,49] and is increasing in use for bioprinting applications. It is based on the concept of laser induced forward transfer that was initially developed for use with metals. A typical LAB setup includes a pulsed laser beam with a focusing system, an energy absorbing film followed by a glass ribbon coated in the print material and a receiving substrate. The received laser pulses cause a pressure bubble to form, resulting in the print material being ejected in droplets towards the receiving substrate.

The resolution of LAB can be affected by many factors including the laser energy delivered per unit area, surface tension of the build material and the viscosity of the bioink. Despite this, due to there being no nozzle involved in the LAB process, not only is nozzle clogging not an issue but the system can handle materials with high viscosities and cell densities with little effect on cell survival rate [50].

Despite these positives there are a number of negatives involved in the lab process, for example bioinks are difficult to prepare for this process and different bioinks need to be prepared separately and changed over during print. This can be time consuming and difficult. Additionally achieving single cell deposition is more complex than using the inkjet method. LAB systems are often more expensive than the other described methods of bioprinting and although this price is likely to decrease, they are still less accessible at present [50].

2.2.6.4 ***Light assisted Bioprinting***

Another method for the production of 3D tissue constructs is through photo-curing bioinks. This method is similar in process to how a typical stereolithography 3D printer works in that

the working material is cured in layers usually by a UV laser or light, but this is dependent on the curing properties of the photo-curing material used.

This method offers some advantages in the field of 3D bioprinting in that it is possible to produce high cellular density components due to there being no requirement for cells or high viscosity bioinks to be extruded or ejected through small orifices which usually lead to a high cell mortality rate. Instead, cells can be suspended in the working material which is held within a build tray, and gradually photo-cured in layers.

There are however, some issues with this method currently, the most detrimental of which at this point in time being the biocompatibility of the majority of materials used for this process not being suitable [51]. Furthermore, the working material would need to be continually agitated to prevent cells from agglomerating and forming sediment at the bottom of the build tray, this would be especially true of high cellular density bioinks.

2.2.7 **Alternative Fabrication Techniques**

A reliable and effective high throughput method for the production of high cellular density 3D tissue scaffold has the potential to have a great deal of impact across a range of sectors such as in biomedical science, drug testing, as well as the development of tissue implants. As a result of this, there has been a number of studies related to ReJI into developing a successful method for this.

The Kenzan method [52] is a method of producing a high cell density 3D tissue construct without the use of a bioink or a material developed as an adaptation from a more standard 3D printing methodology for bioprinting. Unlike the RejI system that prints cells encapsulated within a gel matrix, the Kenzan method is one of a number of methods that relies on the assembly of aggregates however the main novelty of the process is that it is entirely automated, meaning that it could be well suited for high throughput production. The Kenzan method utilises a method of closely arranging compacted cell spheroids into a physical tissue geometry. In its simplest form this is a three step process, the first step being the production of adequately sized cell spheroids from either single or mixed cell types. The cell spheroids are then arranged into a 3D shape by individually placing them onto an array of small stainless-steel needles. The 3D shape is governed by the desired 3D design data being used but shapes such as flat films, plugs and hollow tubes are achievable. The structure is then cultured in a

bioreactor to allow for self-organisation of the cell spheroids until a desired form and functional properties, such as strength are reached. Figure 2-3 illustrates this process.

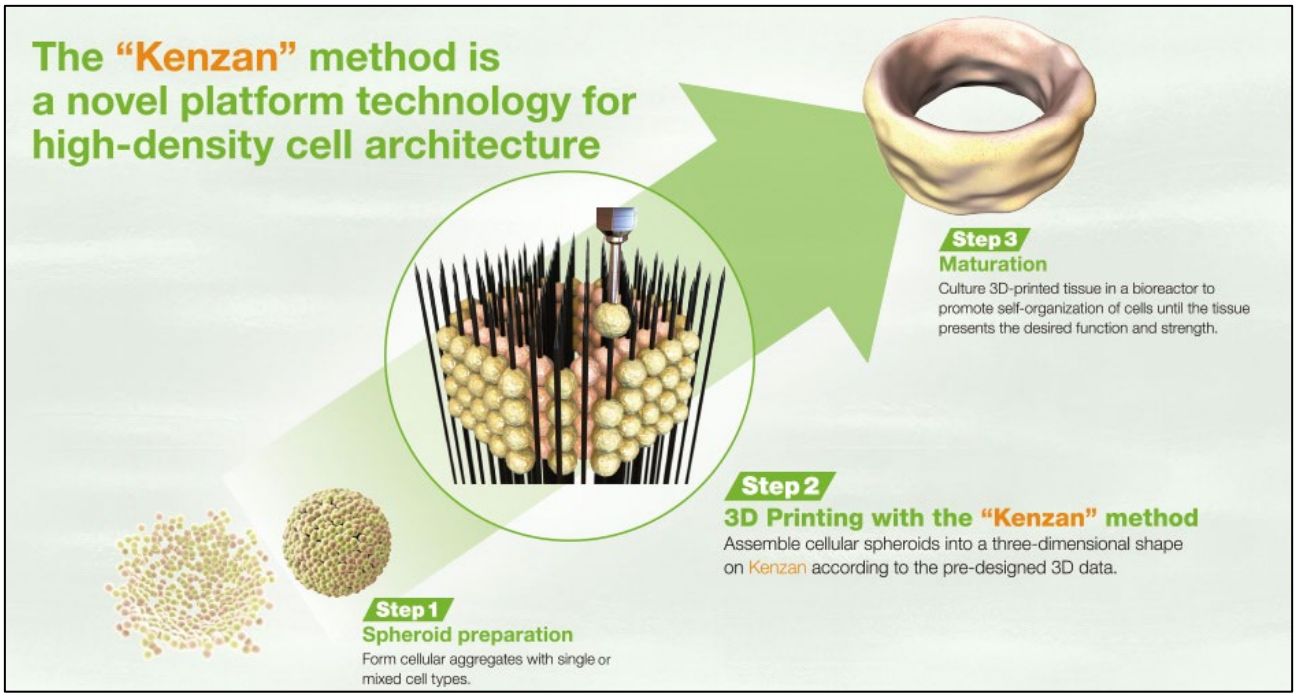

Figure 2-3: Illustration of the Kenzan method taken from [53]

This method appears to be an effective method for the effective production of high cellular density scaffold and tissue constructs. This is especially true as it does not have the drawbacks that some other methods of cell deposition that were developed from existing 3D printing methods, such as microextrusion, have in not being ideally suited to cell deposition. In microextrusion the drawback being cell mortality rates being high due to high shear stresses in the nozzle. As well as this, cells are not supported in a bioink but instead the structure is entirely made of cell spheroids, there may however, be both positive and negative effects from this. The absence of a surrounding bioink matrix clearly means that the cell density achieved from this method is very high, cells are in direct contact with each other and this encourages communication within the cells and allows for cells to more easily self-organise. However this tightly compacted structure of cells may lead to a deficiency in nutrients in cells in the centre of the construct as nutrients in the growth medium are unable to diffuse through the tightly compacted organoid structure. Due to this, the assembled spheroid construct must be submerged in a media immediately following the print.

Another feature of this method is that cell spheroid size is dependent on needle size which can be as small as 0.17 mm in diameter with a 0.4 mm spacing between needles [54]. To

ensure the construct can be arranged correctly and effectively allowing for optimal cell mobility between spheroids without causing cell compaction it is necessary to optimise spheroid size before printing, which can be time consuming and difficult, what is more, changes in cell types, incubation times or other tissue culture factors can result in suboptimal spheroid sizes. Further to this an added complexity in the formation of spheroids comes through the essential deposition of a robust extracellular matrix and the requirement for effective intercellular interactions [54]. In order to effectively deposit cell spheroids there needs to be an adequate level of cell adhesiveness. However, this has an inversely proportional relationship with the deposition of the extracellular matrix. To add an additional complexity to this cell survival rate at the core of the spheroid also decreases with the amount of time in the culture.

As well as this when the needles are removed from the structure it is left with a number of holes that are usually replaced and infilled as the cells have a tendency to repair and bridge gaps, however this may make this method unsuitable for the production of microvascularised structures as this same tendency to infill holes will cause the microvascularisation to be closed in on. Finally the process is not particularly fast, with each structure requiring approximately 4 days in culture before needles can even be removed to prevent damage to the structure [54].

2.2.8 **Application**

The final phase of the 3D bioprinting process is application. Common bioprinting applications include but are not limited to, creating implants for regenerative medicine and creating in vitro test samples for the testing of new drugs. When considering applications such as these inkjet bioprinting is one of the most cost effective printing methods whilst also being able to to accurately print high cell density constructs on a drop on demand basis.

2.2.9 **Limitations and Future Development**

3D bioprinting is approaching a point where bioprinters are no longer modified conventional printers but are instead bespoke designed machines. As with all machine design, refinement of machine performance will always be a factor in future development, this may involve increasing build speed, resolution, the ability to print higher cell densities or the ability to print a wide range of bioinks. Currently printability is still a large factor involved in bioink selection and aspirationally it would be better if bioinks could be chosen purely on their suitability for use in the construction of the 3D tissue, with a manufacturing method that is robust enough

to cope with this. Additionally, for almost any drug testing application the ability to produce samples at a high throughput is a must have.

A long-term aspiration of bioprinting would likely be to remove the need for transplantation by printing directly into open tissue in vivo. Having been proposed as early as 2007 [55] The ability to print synthetic tissue directly in to the site of a defect has numerous advantages. For example, printing tissue models in vitro has advanced a great deal however there is still a need for a more robust understanding of bioreactor technology specific to the growth of each specific cell type in order to ensure cells grow effectively, if printed directly in vivo cells are able to grow in the conditions of their native tissue [56,57]. Additionally, surgical procedures through which prior printed scaffold are implanted pose a great deal of risk to the printed constructs for a number of reasons, such as damage occurring to the scaffold due to its inherent fragility, damage to the fragile native tissue, risk of contamination during transportation and implementation, the cost and time required to culture the scaffold before implementation, and finally the shape or morphology of the printed scaffold not matching the defect morphology due to unreliable imaging techniques. Printing the scaffold directly in situ overcomes a great deal of these hurdles, however it does pose new difficulties, such as the need to print on to surfaces that are complex shapes with varying mechanical properties such as stiffness and surface roughness as opposed to the traditional smooth flat substrates of lab based printers [58,59] as well as the aseptic nature of any in situ process needing to be extensively screened before undertaken in a surgical environment [60]. Despite this, there have been rapid developments in the field in recent years in skin, bone and cartilage repair [61–65].

2.3 Impingement Bioprinting

There have been a small number of impingement-based studies used in the field of 3D bioprinting. Impingement-based technologies all work on the principle of having a system with two opposing deposition nozzles, these nozzles deposit either individual droplets or a continuous stream that impinge either in the air or on the print substrate. This means that bioinks with high viscosities such as gels that cannot normally be extruded through a single nozzle can be printed. This can be achieved by having a gel pre-cursor extruded from one nozzle and a crosslinking agent extruded from another nozzle meaning when the two inks impinge, a crosslinking reaction takes place. Additionally this can allow for printing inks with higher cell densities. There is a wide range of potential materials that can be used in

impingement based bioinks, the main requirement being that the ink components are biocompatible and able to crosslink instantly. One common combination of gel precursor and crosslinking agent are alginate and calcium carbonate respectively. Alginate and calcium carbonate solutions are popular as they crosslink easily and quickly at room temperature, they are relatively cheap and they form a biocompatible hydrogel. During impingement based printing the calcium carbonate solution often has a much lower viscosity than the alginate solution and as such this is usually the preferred solution to add cells to during the print process. Care must be taken if this approach is taken as if the calcium carbonate concentration is too high the solution can be cytotoxic. Additionally fibrin and throbin act as effective gel precursor and cross linking agents respectively. These have the advantage of not being cytotoxic prior to crosslinking however these are more expensive and following crosslinking fibrin based hydrogels are subject to gradual breakdown over time due to natural fibrinolysis in the gel.

2.3.1 **Valve Based Techniques**

Visser et al [66] have developed a method that they refer to as the IAMF (in air micro-fluidic) method which comprises of two nozzles, one actuated on a drop on demand bases with a second continually jetting, see Figure 2-4 below.

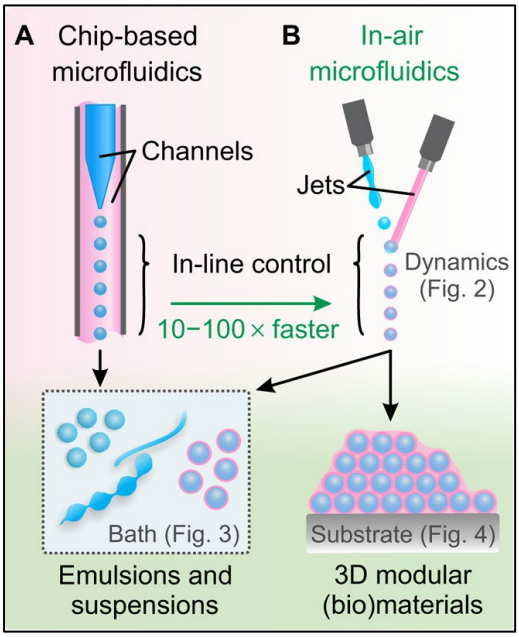

Figure 2-4: A – Chip based microfluidic gel printing method B – In Air Micro-fluidic method taken from [66]

This appears to be an effective method of producing on the fly 3D printed tissue structures however it may lack the control that the Newcastle University ReJI system has, as with the ReJI system it is possible to independently actuate and provide a drop on demand from each valve. Further to this, because of this feature of the ReJI system it is also possible to adjust the deposition settings for each nozzle to account for factors such as material viscosity.

The German company GeSiM have a device called the TwinTip Nano-Plotter. This is a deposition head comprised of two piezo-actuated microvalves than can provide drop on demand bioprinting, Figure 2-5 below shows this arrangement. This appears to be an effective system however this differs from the ReJI system in two distinct ways. Firstly in this system the two droplets do not truly impinge in the air but rather the two droplets mix on the substrate. This means that in order to ensure that both droplets mix perfectly on the substrate the deposition height would need to be carefully calibrated to the substrate printed on, which in itself would be time consuming during the print process. This would also add difficulty when needing to print into a deep container with a small area for access such as a well plate and it may not even be possible to print into something as deep and a well plate where there is not a great deal of room for the pipets to get close to the bottom of the well.

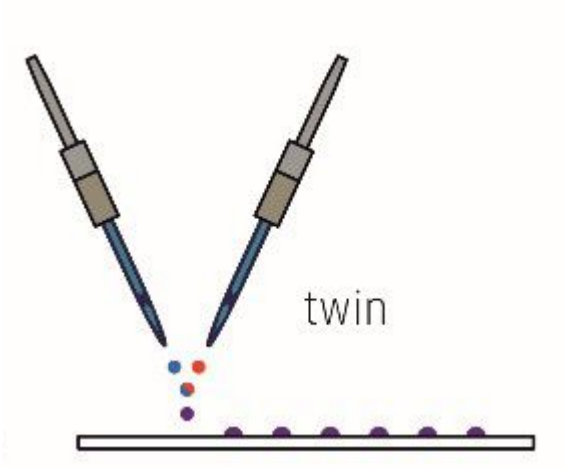

Figure 2-5: GeSiM TwinTip Piezo Pipette Nano-Plotter [67]

2.3.2 **Inkjet Based Techniques**

Albanna et al. demonstrated the ability of their impingement based method for in situ printing of autologous skin cells directly into extensive skin wounds to accelerate healing. The in-situ printing methodology demonstrated that they were able to directly print with some accuracy on to the wound site. Additionally they demonstrated the use of a collagen and fibrin based gel crosslinked by thrombin [68]. However the process did not seem to be able to achieve

significantly high cell densities (approx. $2x10^6$) and as a result the improvement observed did not appear to be significant. Additionally, in their printing process a layer of collagen-fibrin precursor containing cells was printed, followed by a layer of thrombin to crosslink this layer, then after 15 mins the process was repeated. This is unlike the ReJI system by which the gel precursor is printed at the same time as the crosslinking solution resulting in instant crosslinking, and as such 15 minute wait times between layers can be avoided.

Sakurada et al. have also developed a similar impingement based system [69]. This is a microvalve based system that demonstrates the printing of impressive detailed structures, with the paper demonstrating that using a fibrous substrate that can absorb additional moisture whilst printing improves the print quality of gels that use calcium chloride/alginate based inks. Additionally, they demonstrate that their system is able to print cells with a viability of 80% however, again, cell density is still low at $5x10^6$ cells/ml.

Additionally the need to print onto a substrate to remove excess uncrosslinked material demonstrates that calibration of the system in order to achieve efficient crosslinking may be difficult.

2.3.3 **Reactive Jet Impingement (ReJI)**

Newcastle University have developed a new, high-throughput method of inkjet bioprinting known as the Reactive Jet Impingement (ReJI) method of bioprinting. This is a high throughput method of depositing high cellular density gel on a drop on demand basis. The setup comprises of two piezo-actuated microvalves which are both independently connected to a reservoir containing print material. Both microvalves are then actuated simultaneously to eject two droplets. One droplet of a gel precursor, and one droplet of a cross-linker containing the desired cells. These droplets interact with each other in the air, simultaneously cross-linking to form a gel before landing on the target media. Individually depositing the gel precursor and cross-linker is how it is possible to deposit the desired high viscosity, high cellular density gel at a high rate.

In this body of work, the ReJI system is demonstrated to be capable of high throughput, high accuracy and high cell density (approx. $40x10^6$ cells/ml) bioprinting. This is supported through using the system for applications such as the production of an effective stratified osteochondral co-culture, and the printing of a high cell density tumour invasion model on to a tissue substrate. This not only demonstrates the effectiveness and versatility of the system,

but also how it could be applied to high throughput applications such as the development of representative 3D in vitro cell culture models for drug screening. Furthermore, through printing on a tissue substrate that is not smooth or flat, with unknown mechanical properties this demonstrates the systems potential for adaptation for use as an in situ printing solution.

Finally, due to the ReJI system's design it can easily be scaled in size, meaning it can be used for intricate drop on demand applications where only very small volumes of ink are required, or it can be scaled up to increase throughput or to simultaneously print different inks, or cell types for use in stratified, complex co-culture studies.

2.3.4 **ReJI Materials**

The ReJI system is able to print 3D hydrogel scaffolds containing cells by depositing an uncrosslinked gel precursor through one microvalve and a crosslinking agent through the other. As the crosslinking agent is often lower viscosity than the gel precursor this usually contains the cells that are printed. All of the cellular gels demonstrated in this thesis are comprised of collagen, alginate and fibrin (CAF), this is crosslinked with a thrombin and calcium chloride solution as described in Montalbano et al. [70]. The acellular gels used for calibration experiments are all alginate based and crosslinked with calcium chloride. The main component materials of bioinks used with the ReJI system currently are detailed below:

- Collagen – Chosen for its biocompatibility, significance as a major component of ECM and ease of crosslinking
- Alginate – Chosen for it's biocompatibility and instant crosslinking with calcium chloride
- Fibrin – Chosen for it's biocompatibility and quick crosslinking
- Thrombin – Crosslinker for the fibrin
- Calcium Chloride – crosslinker for the thrombin

More detail on the use of collagen, alginate and fibrin as hydrogel scaffolds for in vitro cell culture models can be found in 2.4.3. Figure 2-6 shows how hydrogel components are added to the ReJI system.

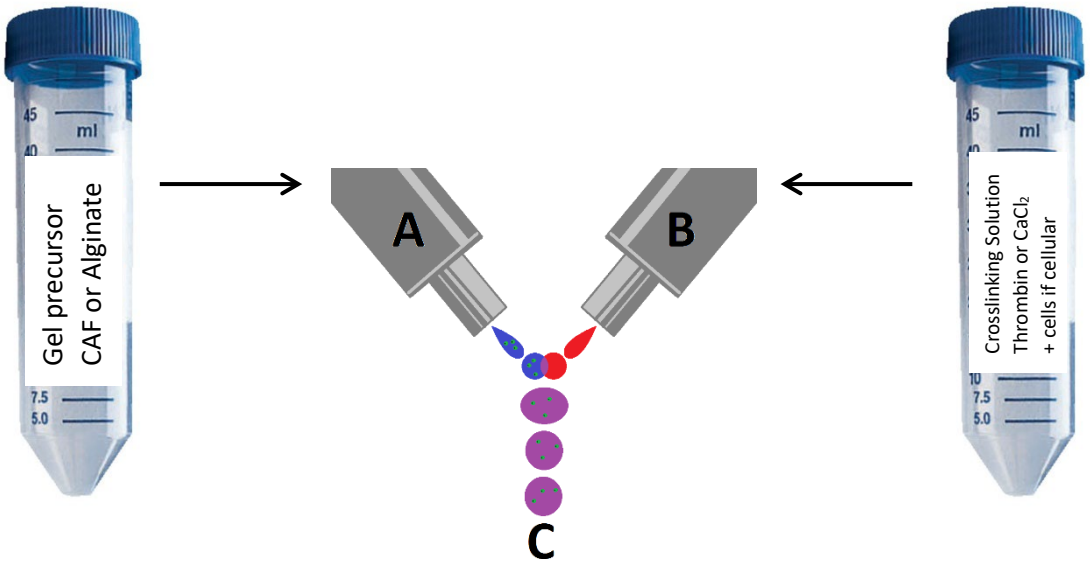

Figure 2-6: Diagram showing how gel components are added to ReJI microvalves when printing hydrogels.

2.4 Drug development and cell culture for drug testing

2.4.1 Current In Vitro Drug Development models

A number of methods have been developed in order to replicate the complex conditions for cell growth in human tissue in vitro. This ranges from basic 2D monolayer cell culture methods using a single cell type through to insert based 3D culture methods and the more complex aggregate based methods for the production of organoids and 3D tissue models (see Figure 2-7).

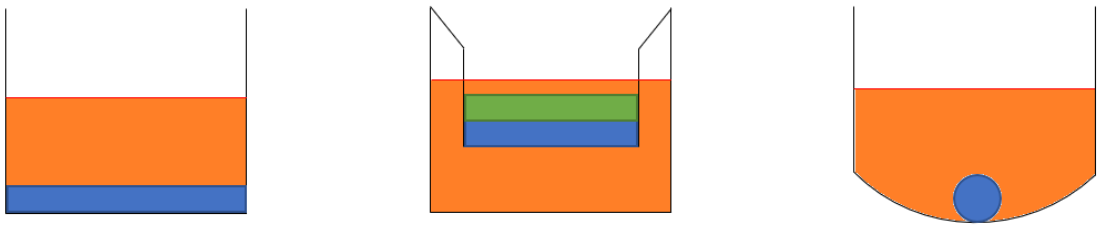

Figure 2-7: Methods for culturing cells for use in drug screening research, from left to right: Basic 2D molo-layer culture, layered co-culture in a trans-well insert, aggregate. Orange colour represents culture media, blue and green represent cells.

The simplest method of cell culture is 2D monoculture. This is widely used for the relatively low cost and complexity, as well as scalability for larger experiments. The method involves seeding a single cell type in a single monolayer on to a tissue culture substrate and assessing

the cell reaction to chemical or environmental stimuli. Whilst 2D cell culture can be a good indicator for cell response in more simplistic studies, due to the lack of 3D structure, the complex cellular structure that is observed in cell growth in vivo is not represented accurately. Additionally extracellular matrix (ECM) is not formed in the same way and at the same rate when compared to 3D culture [71,72]. 2D monolayer culture is widely regarded as over simplistic of modelling complex multi-cellular structures such as a joint, where there are a number of cell types present that continuously interact to maintain normal tissue function [8,9]. This can lead to deceptive research conclusions which are not an accurate representation of how a treatment will perform in vivo [73]. Therefore the development of in vitro 3D modelling techniques that are more representative of cell behaviour in vivo is imperative for more accurate study of factors that lead to the onset of diseases such as OA or cancer [74–76]. 3D cell culture techniques allows for closer replication of the 3D spacial organisation found in vivo [77].

Aggregate culture methods are one way of producing 3D cell culture environments that enable the construction of larger scale micro-tissues. In aggregate based culture techniques, cells are in direct cell to cell contact and are less dependent on tissue culture substrates for adherence and as such have a more representative nutrient diffusion gradient within the 3D culture [76,78,79]. Some common methods for the production of aggregates include in-well, hanging droplet culture and spinner flasks. However matrix based methods as well as microfluidic methods have also been developed [80–82]. Aggregate based cultures allow for a greater degree of spatial organisation and as a result, cellular interaction as well as ECM formation [83], and as such, are used as a more representative method of replication in vivo conditions than traditional 2D culture. Additionally, as mentioned previously aggregates can be arranged through various biofabrication methods [84,85] in order to produce larger 3D micro-tissues.

However, there are a number of drawbacks to the production of aggregates. For example, aggregate production Is a complex and time consuming process. It involves the use of a large amount of cell culture resources in order to produce a large number of cells in 2D prior to the aggregate construction. Some methods, such as hanging drop are very sensitive to disturbances from vibrations which can make simple things like culture and media change very difficult. Additionally due to the densely packed nature of the organoids produced, nutrients are not always able to fully diffuse through the culture, this can result in a ‘necrotic core’ [10] of dead cells within the organoid. Due to this inhibited nutrient diffusion assays that are

developed for cells in traditional 2D monolayer culture are often ineffective or unrepresentative when performed on 3D aggregate culture, and there is difficulty with many common imaging techniques in imaging the core of the aggregate, making cell behaviour difficult to analyse.

One more common method for replicating co-culture environments such as those found within an osteochondral interface is the use of well inserts. Well inserts increase the surface area of the culture allowing increased access to growth medium. This means that cells can be grown in inserts in layered co-culture. Co-culture models help to further replicate in vivo conditions by allowing for the observation of intercellular interaction in response to stimuli [86] which in turn helps to increase the accuracy of the culture model [87].

Indeed, it has been found in studies that certain cells, for example cultured MSCs produce a number of cytokines and growth factors [88], including chondrogenic inducers such as TGF-ß [89], BMP-2 [90] and IGF-1 [91], this, combined with the increased direct cell-cell contact in 3D co-culture can lead to improved chondrogenesis in chondrocyte-MSC co-cultures [33]. Additionally studies have shown that chondrocytes can induce chondrogenesis in MSCs and those MSCs may directly contribute to cartilage formation [92–94]. This can be observed in several different culture models, species and culture conditions [95]. Meretoja et al. for example, observed more robust chondrogenesis in their chondrocyte-MSC co-cultures than in any other observed culture type, leading to the conclusion that the most promising cell source for cartilage engineering was from their co-cultures rather than mono-cultures [86].

By increasing the surface area of the cells exposed to culture medium this method can avoid a number of the previously mentioned drawbacks of aggregate culture whereby nutrients cannot be reached by all of the cells in culture. These methods generally employ a porous membrane that is suspended within the wells of standard size multiwell plates. Polycarbonate and polyethylene terephthalate are materials commonly used in the membranes and features such as pore size and height within the well can be controlled. This allows for studies of cell growth and migration across the membrane as well as molecular transport studies. Additionally some studies incorporate interlinked wells within the multiwell plate [96] to allow for media to be circulated between multiple wells and across multiple samples. This can be aided by incubating the samples on a rocker plate. Insert based culture techniques have been adopted for the development of models to assess cell migration and drug absorption and are also able to be adapted for larger plates sizes for use in high throughput applications [97]. One

additional benefit of this method is, because the membrane is suspended within the well, interactions between cells in co-culture without the cells being in contact with each other can be monitored.

2.4.2 **Growth Media for Co-culture Models**

The formulation of bespoke cell culture media for co-cultures can be a complex process as there are many variables in the media selection process that can influence the growth of the constituent component cells [98].

Each individual cell type has its own individual function and has specific requirements from the culture medium used in order to help it fulfil that function. When multiple cell types are in culture together media selection becomes complex and demanding requirement [93].

There are multiple approaches to media selection for co-culture including mixed medium, supplemented medium and partitioned culture. In a mixed medium study, the specific medium used for the culture of each cell type is combined, sometimes with varied ratios. This is the simplest method of co-culture media formulation however care must be taken when blending media types so that supplements included in each medium do not interfere with the growth of the other cell type [99,100]. There are, however, studies where this has been implemented effectively and this is often when both media used are general cell growth media which are unlikely to have a negative effect on other cell types [101–103]. Additionally, the blending of two general cell growth media types may be the preferred method of media selection if the desire of the study is to assess the effect of one cell type on the growth of another. In this case, if soluble factors were added to one just one general media type to supplement the growth of each cell type, it would be difficult to discern the effect of the added soluble growth factors from those naturally secreted from each cell type and thus it would be difficult to assess the effect that the two cell types have on each other's growth in co-culture [104]. Nakaoka et al for example, used a mix of F12/DMEM and α-MEM - medium types very similar to those used in this study - in their ostecochondral co-culture study where they found that proliferation of the co-cultured chondrocytes was enhanced using soluble factors produced from the osteoblasts, and the level of differentiation of the osteoblasts influenced that of the chondrocytes [103].

Another common approach is to use a general base medium such as α-MEM, DMEM, or DMEM/F12 for the co-culture, sometimes this can be additionally be supplemented with

soluble factors providing each cell type with the required nutrients without harming either of them [105–107]. This means that each individual cell type will receive the nutrients they need without risking harm to either of them. However, it is complex and time consuming to find suitable supplements for each cell type, additionally, if soluble factors are added to aid cell growth it may be difficult to differentiate between the effect of soluble factors that are produced by the cells in co-culture and the soluble factors that have been added to the medium. Moreover, if additional soluble factors are not added to the general base medium there is the risk that not all cell types will have the required supplements for their growth [98,104].

Finally, a culture method that allows two mediums to be used independently can also be used. This often involves a process of physically partitioning a flowing medium through culture in a bioreactor . This can be a very complex method that requires a high level of precision to ensure that media types are correctly partitioned and that each cell types are able to receive enough of the media that they require whilst ensuring they are effectively partitioned from the other media types used. For example Xue at al developed a bespoke system in which the osteochondral co-culture scaffold is placed and the chondrogenic medium is perfused through the top of the scaffold and osteogenic through the bottom layer with no mixing of mediums [108].

2.4.3 **Hydrogels for 3D culture models**

Matrix and hydrogel-based techniques have also been employed for the production of 3D cell culture models. Gel based methods offer the benefit of providing a 3D culture environment with the cells encapsulated within the gels. This allows for 3D cell to cell interactions such as those observed in aggregate based methods. However unlike in aggregate based methods, gels are not so densely packed in close contact so as to restrict media and other nutrients from diffusing through the scaffold, meaning gel-based culture methods are less likely to develop a ‘necrotic core’. Whilst matrix-based methods may be less well suited for the observation of cell to cell interactions of cells in contact, they are well suited for the observation of cell to ECM interactions which is in turn likely more representative of the native tissue [16]. Additionally in many matrix based methods cells are able to move throughout the matrix and in some cases even locally degrade areas of the matrix to allow for cell growth and proliferation [109] however this is dependent on the matrix material.

Anseth et al. have investigated the process of the dynamic modification of local cell environment in hydrogels through the study of cells suspended in PEG gels and have found that cells begin with a spherical morphology and gradually degrade their local matrix. This allows for greater movement and the ability to change their morphology and proliferate [109–111]. Although this provides some information on cell behaviour within the gels they explain that understanding the mechanisms by which cells receive information from their local environment combined with how the matrix responds to changes caused by the cells becomes increasingly difficult. Researchers have carried out techniques such as real-time cell tracking to monitor the rate at which cells migrate through their local environment [112,113]. This is particularly important to monitor in 3D culture as opposed to 2D as the process is substantially different for cells moving on a surface vs those moving through a 3D matrix. One such method for this is in reported based systems where gene and protein expression are linked with the production of reporter proteins, such as green fluorescence protein. This allows for non-destructive monitoring of cell behaviour via fluorescence imaging [114,115].

It is worth note that the matrix composition has a significant effect on the health and growth of the cells. 3D cellular scaffolds cannot be considered to be simply another method of analysing cell function in the same way that 2D cell culture methods are. It has long been established that the cellular microenvironment plays a large part in the complex special and temporal signalling domain that directs cell phenotype. Petersen et al have in fact shown that phenotype can supersede genotype due to interactions in the ECM through their demonstration that human breast epithelial cells develop like tumour cells in 2D but exhibit normal growth behaviour when cultured in a 3D environment similar to their native tissue [15].

Furthermore, microscopic mechanical changes may be monitored micromechanically, such as with micro-rheology and atomic force microscopy (AFM) [116]. Baker et al . have used micro-rheology to demonstrate prostate cancer cells show increased intracellular creep compliance, which is a measure of cytoplasmic modulus, as the matrix modulus is increased, whereas no relationship was found in 2D, this may account for phenotypical differences observed in cancer cells when cultured in 2D versus 3D [117]. Forces on the matrix by the cells can be measured with traction force microscopy (TFM), using this method it has been demonstrated that fibroblasts migrating on polyacrylamide surfaces exert forces in 3D [118]. Cell to cell

mechanical communication was also observed with TFM, where the modulus of the matrix was found to have an influence on transmitted traction stresses between cells [119].

Banerjee et al found that in analysing the effect of gel modulus on the growth of neural stem cells, that the rate of proliferation decreased as the gel modulus increased [120]. In this study gel stiffness was varied over two orders of magnitude but notably, the least stiff hydrogels also expressed the greatest amount the neuronal marker β-tubulin III. It is also worth noting that the lowest stiffness hydrogels had a stiffness comparable to that of brain tissue inferring that it is not just that cells grow better in gels with a lower modulus but that cells grow best in gels with a modulus that closely matches the relevant tissue type. This infers that cartilage cells such as chondrocytes or osteoblasts may grow better in stiffer hydrogels or even gels that are held in compression as it is a closer replication of the in vivo conditions.

These works highlight the importance of not only replicating the native growth environment but also the influence that the ECM has on cell growth and the importance of Cell to ECM interaction. In 2D culture only a very small portion of the cell can interact with the ECM and other cells, with a large portion of the cell being exposed to growth medium. This leads to reactions with soluble factors in the growth medium that would not naturally occur in 3D culture. Whereas in 3D culture soluble factors that influence cell migration, cell-cell interaction and differentiation have been proven to exhibit special gradients in vivo [121].

2D growth environments also have an effect on cell morphology as well as cell migration. Morphology has been shown to influence proliferation, apoptosis [122], differentiation and gene expression [8] and in 3D cultures cells exhibit more complex morphologies that when they are constricted to a 2D growth environment. In 2D there is little resistance to migration either from other cells or from surrounding ECM. This is significant when observing changes that occur over longer time periods such as the metastasis of cancer cells or tissue organisation where interactions with the surrounding microenvironment influence cell behaviour. All of the above demonstrates that if factors such as cell physiology, migration, and tissue construction are to be studied in vitro, cells must be cultured in a 3D model that best replicates the important mechanical and biometric factors present in their native tissue in order to best facilitate this [74].

The fabrication of hydrogel-based 3D cultures usually fundamentally involves one of two methods, either viable cells are encapsulated within the gel or substrates are fabricated and

cells are later seeded on top. In all cases gels are formed by the gelation of a liquid gel precursor either through physical (noncovalent), or chemical (covalent) crosslinking. Peptide or protein-based gels are often formed through physical crosslinking, for example in collagen hydrogels, interactions between solubilized fibrils lead to fibre and network assembly over time. Chemical crosslinking polymers are also commonly used for the production of hydrogels and are advantageous when seeking rapid gelation of pre-cursor materials. However, considerations must be made in order to keep polymerization times short and to use non-toxic components in order to maintain a high cell viability as, for example in photopolymerization, free radicals generated through this process have been shown to damage cells [123].

Generally hydrogels can be divided in to two types, either natural or synthetic with each type having its own advantages and disadvantages. There are a number of factors to consider in choosing a hydrogel material for cell culture, some of the more relevant factors include, cell adhesion, stability in culture and physical properties such as mechanical stiffness. Some of the more common and commercially available materials will be discussed below.

Collagen is the most ubiquitous protein in the human body and is present in bone, cartilage, skin, tendons and muscle. The most common type of collagen is type I, which is a major structural component of many tissues [124]. The most popular types of collagen for use in hydrogel culture are types I, II and III, this is commonly derived from solution of acid, or pepsin soluble type I collagen is often derived from rat tail and is readily commercially available. Crosslinking commonly takes approximately 20 mins and is often initiated by raising the temperature of the collage. The gelation temperature does affect the collagen fibre length which in turn can influence cell growth and behaviour. Fibroblasts have been found to grow better in collagen gels with larger fibrils [125]. Collagen provides a natural viscoelastic 3D scaffold and the main advantage of collagen is its cytocompatibility. Collagen hydrogels have been used in a number of in vitro and in vivo cell culture studies with great success [125,126]. Some potential drawbacks for collagen as a 3D scaffold include stability over long culture periods, variation between batches, and also relatively low stiffness, although this is not always a drawback. Collagen is one of the main constituent components of the commonly used commercially available Matrigel® (Corning). Matrigel is a widely used commericallialy available gel matrix and is composed of 60% laminin, 30% collagen IV, and 8% entactin.

Entactin is a bridging molecule that interacts with laminin and collagen IV this aids in the structural organization of these extracellular matrix molecules [127].

Alginate is a natural polymer ink derived from brown algae that is biocompatible, low cost and low toxicity. It is particularly valued for its fast ionic crosslinking method using divalent cations such as calcium or magnesium, meaning that in some cases alginate bioinks can be crosslinked simply by adding these cations to the culture media. This makes cell encapsulation and gel digestion very simple. Unlike collagen and Fibrin an adhesive ligand such as RGD to allow cells to adhere.

Fibrin is a naturally occurring polymer found in blood clots that is formed through the coagulation process. Fibrin crosslinking is fast and can be activated by thrombin, both of which are readily available from commercial suppliers and fibrin sealants are widely used for medical applications. The ration of thrombin to fibrin can also be controlled in order to alter the hydrogel properties, for example a greater amount of thrombin results in a gel with smaller fibrils and pores [128]. The main drawback with fibrin based hydrogels is that they are unstable over longer culture periods, his is because, similarly to blood clots, the thrombin initiate the process of fibrinolysis which gradually breaks down the gel. For this reason fibrin can be combined with other, more stable natural hydrogels, such as alginate or collagen to provide a temporary scaffold as the encapsulated cells begin to produce ECM and form tissue [129,130].

Polyethylene Glycol (PEG) is a hydrophilic and relatively inert synthetic polymer. PEG can be modified with a number of functional groups and hydrogels formed using multiple polymerization techniques [131]. Through the photopolymerization of PEG precursors modified with either acrylate or methacrylate moieties in the presence of photoinitiators PEG hydrogels can be fabricated[132,133]. When exposed to UV light, photoinitiators are fragmented to yield free radicals. These radicals attack carbon–carbon double bonds present in the acrylate groups, initiating polymerization which forms a hydrogel network. This network can then be exposed to aqueous solvents, which causes swelling of the crosslinked network until the swelling forces of the hydrogel are balanced by the elastic forces of the polymer [ref]. A hydrogel with a more tightly crosslinked structure will result in a lower amount of contained water. Nguyen et al have demonstrated that by altering PEG molecular weight and concentration, a number of the hydrogel properties such as, swelling property, equilibrium confined compressive modulus, compressive dynamic stiffness, hydraulic permeability of PEG hydrogels in static/dynamic confined compression tests, and equilibrium tensile modulus can

be influenced [134]. PEG hydrogels have a large amount of design flexibility, including the modification of stiffness and how ligands are presented to cells, due to this and have been used in numerous cell culture applications, including stem cell differentiation and mechanobiology studies [135–137]. PEG has particularly been used effectively in photoencapsulation experiments [138].

It is important that for use in gel-based drug discovery models that a process with a sufficiently high throughput and level of repeatability be selected. This would be a perfect application for a high throughput method of reliably 3D printing gel-based culture models.

2.4.3.1 ***Dynamic In Vitro Evaluation Systems***

As mentioned previously one of the most common methods for cell culture is to seed cells into a tissue culture flask for 2D growth and to add growth medium on top of the cell monolayer. However, the 2D nature of this method discussed previously is not the only aspect that is unrepresentative of conditions found in vivo. There are other factors that influence cell growth in vivo that are not represented adequately by traditional static culture methods. For example, studies have shown that by circulating growth medium in a rotating-wall-vessel (RWV) type bioreactor there is a significant enhancement in GAGS (glycosaminoglycans) and hydroxyproline synthesis in both human and bovine chondrocytes [139]. RWVs that provide steady laminar flow of medium have also been proven to be more effective than more simplistic stirrer or mixer flask culture methods that often have a more turbulent flow resulting in higher shear stresses applied to the cells. Another common type of bioreactor is the stirrer or spinner flask. Stirrer flask bioreactors are used both for seeding cells onto 3D scaffolds and for the culture of these scaffold. Cells are seeded onto and through the scaffolds by convection. Stirring of the media increases external mass-transfer however this also generates turbulent eddies, which may have an adverse effect on tissue developement[140]. Figure 2-8 shows a schematic illustration of two of the most common bioreactor types; (a) stirrer flask and (b) RWV.

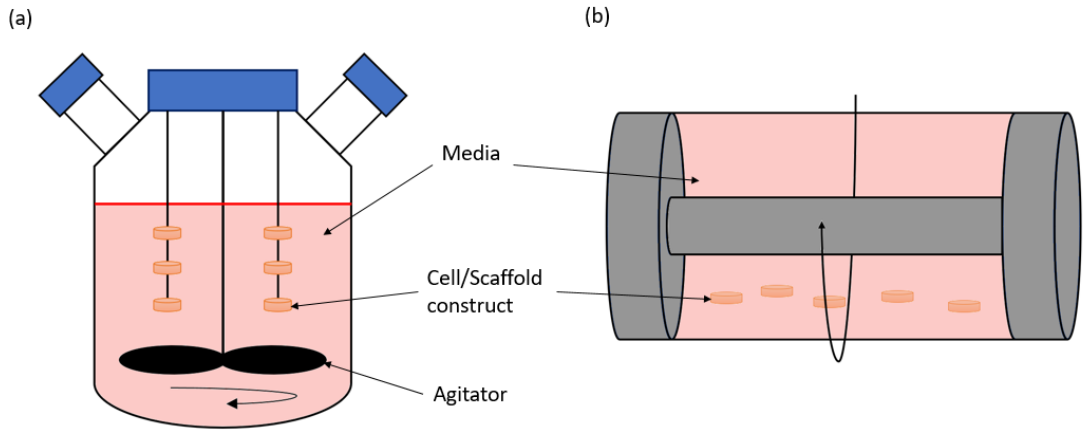

Figure 2-8: Two common types of bioreactor (a) spinner flask in which scaffold are suspended and the liquid medium is agitated by an agitator within the flask (b) Rotating wall vessel in which scaffold are placed and the entire vessel is rotated to ensure the medium is flows continually

There are some cell types that grow more effectively when subject to mechanical stimulus such as shear stresses, compression or tension. For example, in vivo, cartilage in joints is subject to a number of mechanical stimuli with compression and shear being the most prevalent. Cochis et al. have demonstrated with MSCs seeded in to a porous polyurethan matrix that after 21 days in culture when subject to a combination of compressive and shear loading there is a significant increase in chondrogenic gene expression, with histological analysis detecting sulphated GAGs and collagen II only in specimens subjected to loading [141].

Aside from loading there are other factors of 3D culture that can be difficult to replicate in vivo. For example the reproduction of vascularised tissue has in recent years given rise to a great deal of research in the area of 'organs on chips'. This involves the production of microfluidic chips through either newer manufacture methods such as stereo or photolithography or more traditional methods such as machining to create a series of small channels in a chip through which culture medium can be circulated and on which the tissue sample can be grown.

One notable 'organ on a chip' study was carried out by Huh, D .et al. whereby human alveolar epithelial cells were cultured in close contact with human pulmonary microvascular endothelial cells separated by a porous membrane to form a tissue interface that replicates

the in vivo alveolar-capillary interface. In this model that interface membrane could also be mechanically stretched cyclically to replicate breathing [142]. This model has allowed for the observation of previously unobserved phenomena such as the reaction of blood-borne immune cells in response to bacteria, inflammatory cytokines and environmental nanoparticulates.

Bioreactors and alternative culture methods are produced for numerous purposes, some of the most popular including, proliferation of cells on both large and small scales, generation of 3D tissue constructs in vitro and direct organ support devices. The ability to control environmental factors such as oxygen concentration, pH, temperature and stresses, as well as being simple to use aseptically (for example in exchanging media or cleaning) are all of high importance. Additionally bioreactors should be designed with automation in mind for both accurate, repeatable and robust small scall and high throughput studies [143]. These are all factors that will be common in all bioreactor design however specific requirements for different culture types, for example compressive and shear loading, will also need to be considered for individual applications.

2.4.3.2 ***Hydrogel characterisation***

Some of the most important properties to consider in hydrogel characterisation include, mechanical properties, mesh size, swelling and degradation. The properties of hydrogels are important as they are likely to affect the cells suspended in culture and can influence behaviours such as spreading, differentiation and migration [16].

Mechanical properties are often described in terms of stiffness and can be quantified through the calculation of the shear modulus or Young's modulus. There are a number of methods used for evaluating gel stiffness including indentation, atomic force microscopy as well as compression and tensile testing. Indentation is well suited to the analysis of viscoelastic gel cultures due to the minimal sample preparation requirements as well as it only impacting a small are and thus being non-destructive, meaning the same gel can be analysed over multiple timepoints in a study. However, this method only gives a measure of a small, localised area of the culture, so if the stiffness is suspected to vary throughout the structure this may not be the most suited method. Atomic force microscopy is useful for measuring mechanical properties on a cellular level. Compression and tensile testing methods act upon the entire hydrogel and so give an idea of average stiffness throughout the entire structure through the

measurement of applied load and corresponding deformation. The shear modulus of the material can be evaluated through rheometry.

Hydrogel mesh size or porosity can influence the diffusion of nutrients through the gel. Scanning electron microscopy is often used for the imaging of gel porosity. However, the process of preparing the gels for imaging often includes a dehydration step, which can affect the structure of the gel so this method may not be best suited for all cases. Additional methods for measuring pore size include fluorescence recovery after photobleaching (FRAP) [144] and DNA electrophoresis [145].

Swelling is a measure of the water uptake and is an indicator of hydrophilicity and crosslinking density with stiffer gels often exhibiting lower swelling. Swelling is useful for measuring variations between batches of hydrogels when consistency is important.

Hydrogel degradation can lead to changes in the gel mechanical properties which ultimately can affect cell behaviour over time. The desired rate of degradation may vary dependent on the nature of the study. For example, it may be desirable for the hydrogel scaffold to gradually degrade whist being replaced by ECM and natural tissue formed by the cells. Gel degradation is usually hydrolytic or enzymatic. Hydrolytic degradation occurs at the same rate throughout the entire gel and is due to hydrolytically unstable chemical bonds. The rate of hydrolysis can in some cases be controlled by altering factors such as crosslinking density. Natural hydrogels such as fibrin and collagen degrade through cell mediated proteases. Degradation can be monitored by analysing the culture supernatant for quantities of degradation by-products for example soluble collagen. Other methods such as simply monitoring the mass of the hydrogel over a given time can also be used.

2.4.3.3 ***Characterising cells in hydrogel cultures***

Analysis of properties such as cell viability or metabolic activity can be difficult in gel based 3D cultures. Due to the varying rates of diffusion of the assays throughout the culture when compared to the immediate exposure of all cells in 2D culture, it can be difficult to compare 3D cultures to established standards and protocols. Furthermore, when working with hydrogel cultures with a very high concentration of encapsulated cells it can be difficult to achieve an assay dilution that that will not be immediately saturated when the fluorescence is read. For these reasons and also for applications such as flow cytometry it may be necessary to digest or dissolve the gel scaffold to recover cells. One of the most popular methods of doing this in

natural hydrogels is to use enzyme based degradation methods such as collagenase, nattokinase [146] or dispase. However, when using these enzymes exposure time must be minimised in order to ensure the cells are not harmed by the process.

For applications where it is necessary to image cells in the surrounding matrix there are a number of imaging methods that can be employed. Many natural hydrogels are optically transparent, meaning confocal microscopy can be a suitable method for visualising cells in situ. Cells, proteins or other markers of cell growth can be stained with fluorofours which can the be imaged in three dimensions. However depending on the microscope power, and gel opacity, it is not always possible to image through the entire depth of the gel. Multiphoton imaging can also be used to image deeper, more opaque sections of tissue approximately up to 1 mm. Gels are processed for histology in the same manner as soft tissue, however, the paraffin embedding process may not be best suited for sample preparation as it can result in a significant amount of deformation and leave the remaining gel too brittle to section [147]. Optimum Cutting Temperature (OCT) is a suitable alternative for embedding samples for cryosectioning which circumvents the dehydration step and makes sectioning easier. Standard immunostaining and immunohistochemical staining protocols can be used on gels, and cells contained within, again to observe factors such as cell growth, morphology or the presence of of growth indicators, for example the presence of aggrecan in cartilage tissue. However it may be necessary to extend the exposure time when compared to a 2D assay to allow enough time for the staining to diffuse through the gel.

2.5 Osteoarthritis and models of osteoarthritis

2.5.1 Significance

Osteoarthritis (OA) is the most prevalent joint disease worldwide, it affects approximately 10% of men and 18% of women over the age of 60 [148]. The effects of OA can be debilitating due to both loss of joint function and the associated pain, as a result, in developed countries, the socioeconomic cost is significant at approximately 1-2.5% of gross domestic product [149]. Additionally, 80% of those with arthritis suffer from a limited range of movement and 25% cannot adequately perform their major daily activities of life. It is most commonly found in load bearing joints such as knees, hips, spine and hands. Additionally age related changes to the articular cartilage have shown to be contributing factors to pathophysiology [150]. Some risk factors include age, sex, body-mass index (specifically obesity), genetics, occupation and socioeconomic standing.

2.5.2 **Pathology**

Originally thought to be solely based around the mechanical degradation of cartilage, osteoarthritis is in fact a complex disease that effects the entirety of the joint [7]. For a long time, osteoarthritis has been characterised as the failure of joint repair due to the mechanical and biochemical changes in the joint. Due to the fact that cartilage is not vascularised, the supply of oxygen and nutrients to the chondrocytes – which are the cell type present in the cartilage and and are also responsible for the maintenance of the extracellular matrix (ECM) – is difficult and as such articular cartilage has a limited capacity for repair. In the early stages of osteoarthritis, clusters of chondrocytes form in the affected areas, in an attempt to repair the damage, this causes the concentration of growth factors in the ECM to rise [94,151]. This attempt often fails and leads to an imbalance in the degradation-repair cycle favouring degradation. This leads to greater production of proteases that degrade the local tissue such as matrix metalloproteinases (MMPs) and aggricanases, increases apoptosis and a lack of production of matrix components, ultimately this results in the matrix being unable to adequately withstand mechanical stresses [152,153]. This cycle of breakdown continues, often unnoticed by the patient, due to cartilage being aneural, until additional tissues become involved, often by this point the damage is significant, this is one explanation for the often late diagnosis of OA. Figure 2-8 shows the changes that take place within the joint due to OA.

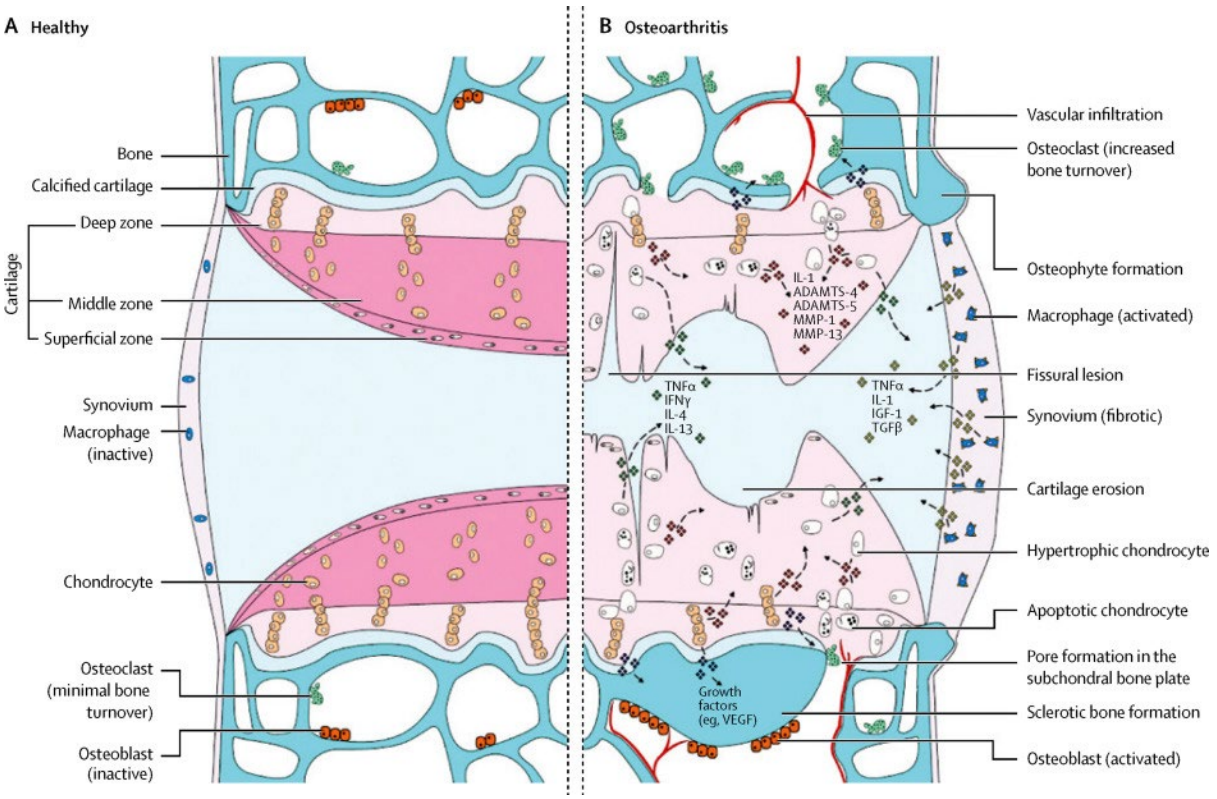

Figure 2-9: The effect of osteoarthritis on an articular joint (taken from Glyn-Jones et al.) [7]

Evidence also shows that the behaviour of bone and synovial tissue also play a role in disease progression, with cartilage, bone and synovium releasing mediators such as cytokines and prostaglandins, resulting in local tissue changes and synovitis which is one of the most common symptoms of OA [6]. Synovial inflammation corresponds to clinical symptoms such as joint swelling and inflammatory pain, and it is thought to be secondary to cartilage debris and catabolic mediators entering the synovial cavity [154]. Synovial inflammation occurs both in the early and late stages of OA however it is often not as severe as in rheumatoid arthritis, although it may add to the cycle of progressive joint degeneration.

One of the most characteristic features of OA are the changes it makes to the subchondral bone. The formation of osteophytes, sclerosis and the changes in the subchondral bone are all important factors for diagnosis with radiology. Due to the often late diagnosis of OA often these are not found until the late stages of the diseases however many of these changes to the bone may actually occur before cartilage damage [155,156]. This infers that the changes to the bone may influence or even initiate cartilage damage.

2.5.3 **Cartilage**

The main component of cartilage of ECM which comprises approximately 95-99% of its total tissue volume with the other 1-5% comprising of chondrocytes [157]. The most common component of ECM within the cartilage is collagen type II which comprises approximately 50% of the total amount of protein. Collagen type II produces a mesh within the cartilage which is reinforced by other collagen types as well as other proteins which results in increased tensile strength of the cartilage. Proteoglycans such as aggrecan are also included within this framework and these draw up water into the cartilage resulting in resistance to compression. The mechanical and biochemical structure of this cartilage is regulated by the chondrocytes [158]. The orientation, shape and density of the chondrocytes and ECM fibres vary significantly throughout cartilage tissue creating stratified layers throughout the tissue. Figure 2-9 shows the osteochondral interface in more detail, highlighting the stratification of the tissue.

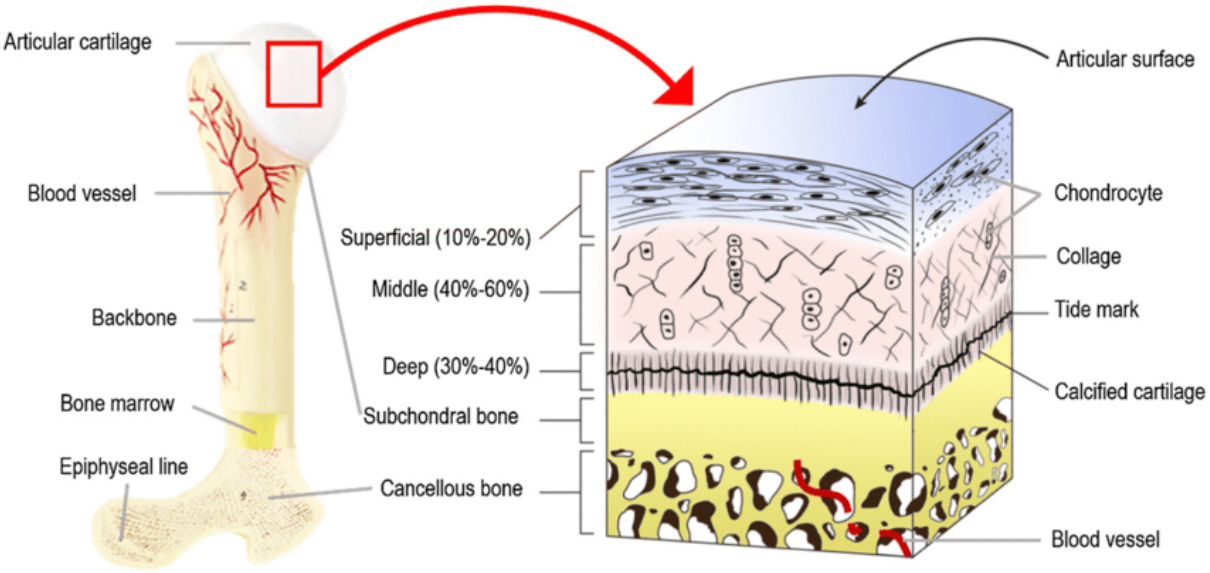

Figure 2-10: Diagram showing the stratification of cartilage tissue, with the changes in fibre and cell, size, orientation, shape and density represented taken from [159]

The ECM can be damaged by the biochemical processes within the joint leading to development of OA [158].

2.5.4 **Subchondral Bone**

The subchondral bone is found between the calcified cartilage layer and the trabecular bone. In osteoarthritis significant changes occur to both the subchondral and trabecular bone [160,161] with osteophytes and subchondral cysts being formed and the subchondral bone thickening and reducing porosity. Advances in imaging now allow bone-marrow lesions to be

identified on MRI that are related to several histological changes, including microfractures at different stages of healing. For some time there have been a number of studies that indicate that the formation of osteophytes and changes in the subchondral bone actually occur before cartilage degradation [162,163]. However these studies are limited by the sensitivity of the imaging technique. Sanchez et al. demonstrated that in response to mechanical stimulation osteoblasts produce inflammatory cytokines and degradative enzymes, similarly to chondrocytes [164]. These enzymes could act directly upon the cartilage or changes in the adjacent subchondral bone could have an adverse effect on the cartilage. Alternatively, the degradation of cartilage could lead to a greater load applied to the subchondral bone which results in it's remodelling. Unlike cartilage, subchondral bone is innervated meaning this is likely one of the main causes of pain in patients.

2.5.5 **Synovium**

One of the common elements of OA is an enflamed synovium and this can occur even early in the disease. As the disease advances there is an increase of synoviocyte proliferation, as well as an increase in size and vascularity of the synovium [164]. In a healthy joint the role of synoviocytes is to produce lubricants such as hyaluronic acid [165] and lubricin [166] help to keep the joint lubricated and ease movement. However in patients with OA synovial fluid viscosity is reduced and lubrication functionality is poor [165–167]. Similar to chondrocytes and osteoblasts, synoviocytes also release inflammatory cytokines and degradative enzymes.

2.5.6 **Treatment**

Treatments offered for OA depend on the severity of the disease. Figure 2-10 adapted from Dieppe and Lohmander [168] shows the treatment response as the disease progresses. Initial treatment for early stages of the disease often involve patient education, advising possible lifestyle changes such as reducing strenuous activity or losing weight if the patient is obese as these are both risk factors due to them contributing to overloading of the joints. This progresses to analgesics and topical non-steroidal anti-inflammatory or pian killer medication to manage pain.

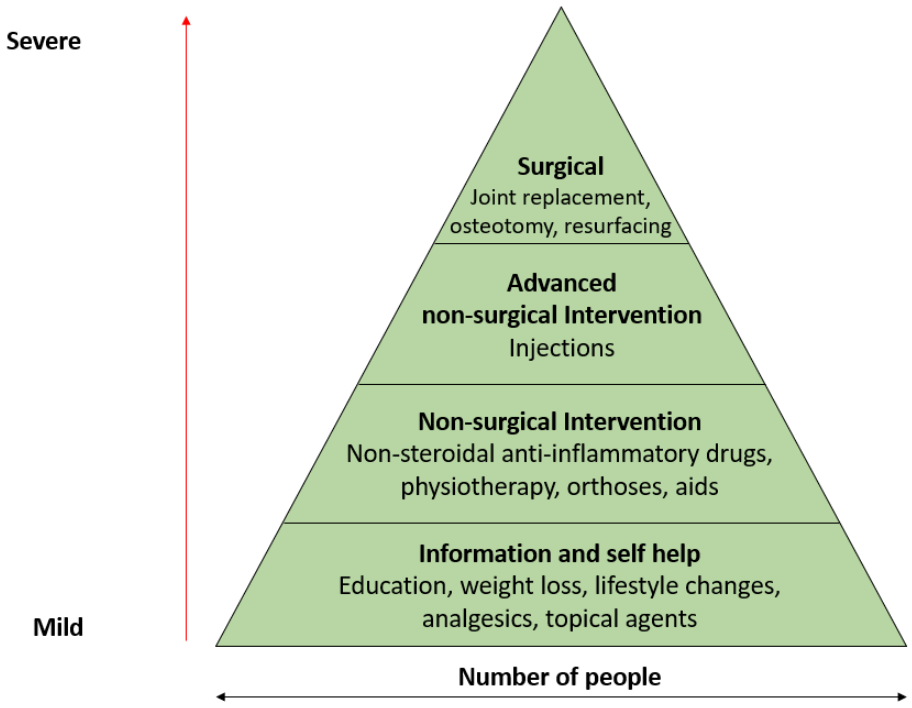

Figure 2-11: Treatment options available as the severity of OA increases, adapted from Dieppe and Lohmander [168]

The next stage of non-surgical interventions includes physical therapy and occupational therapy. Additionally patients may be offered localised injections of opioids, or cortico-steroids to assist in pain management and reduce inflammation in addition to the above treatments. Finally, if symptoms progress and pain cannot be managed patients may be offered aids such as orthoses or surgical intervention.

Traditional surgical methods include arthroplasty or osteotomy, practically this includes either fusing, realigning, resurfacing or even replacing the joint entirely. Clearly this level of surgery is a significant undertaking and always comes with some level of inherent risk. Additionally, although surgeries such as hip osteotomy are on average very successful and cost effective [169], due to the average lifespan of an artificial hip joint being approximately 15 years [170] and revision hip-surgeries being significantly more invasive, expensive and with greater potential morbidity [171], surgeons may want to delay surgical options in favour of pharmacological and non-pharmacological treatments for as long as possible, especially in younger patients where the probability of having to undertake a future revision due to a worn joint is higher.

More recently newer surgical methods been employed. One such method is osteochondral transplantation also called (osteochondral autograft or mosaicplasty), whereby a number of small cylindrical plugs are taken from healthier and less weightbearing areas of the cartilage, holes are then drilled in the damaged cartilage and these healthy cartilage plugs are inserted in order to stimulate new cartilage growth. Additionally microfracture surgery involves inducing a number of small fractures in the subchondral bone, in an effort to repair these there is an increase of cells that form a clot which in turn triggers the repair of cartilage [172].

Tissue engineering options have also been explored. Autologous matrix-induced chondrogenesis is a method that combines microfracture with implantation of a in order to restore large areas of damage that would not be suitable for repair by microfracture alone. This improves the filling of the cartilage defect and increases the stability of the clot formed at the location of the defect.

Additionally, autologous chondrocyte implantation (ACI) is a method that is also employed in combination with microfracture surgery. Using this technique healthy cells are removed from a healthier less load bearing area of the cartilage and grown ex-vivo for 4-6 weeks in order to generate a large enough number to repair the damaged area of cartilage. A second surgery is then caried out whereby microcracking is carried out and the grown chondrocyte cells are applied to the damaged tissue. A tissue scaffold can also be used to supply support to the area or a collagen membrane or periosteal flap can be applied. Clearly this procedure is limited in that it requires multiple surgeries, the first to harvest the cells and the second to re-apply them, and with any surgery there is an inherent risk and cost involved. Additionally, rigorous and involved laboratory practices must be employed to select, screen and grown healthy cells that will produce healthy hyaline cartilage, minimising the amount of fibrocartilage formation. Indeed, this is one of the know issues with microfracture treatment in that the method tends to produce fibrocartilage which is not ideal in joint repair [7]. Harris et al. believe that from initial findings ACI shows an improvement in outcomes over just microfracture surgery, however long-term data is lacking and so it is difficult to conclusively state that there is an improvement, additionally ACI has a higher expense for reasons such as the requirement of additional surgery and the necessary cell culture. That said both methods do show an improvement to short and medium term patient outcomes and ACI appears to induce the production of greater amounts of hyaline cartilage [173]. With additional long-term data,

presumably it would be possible to compare these methods with established methods such as osteotomy by means of a cost/benefit analysis.

In a comprehensive review of cartilage repair techniques and the use of ACI Neimeyer et al. found that ACI is best suiter for repair of damaged tissue in sizes between 3-4 cm^2 however a smaller area of 2.5cm^2 is considered for younger patients and those with active sporting lifestyles. One key conclusion is that the author suggests not to view microfracture and ACI as opposing treatments but rather as complementary treatments that a cartilage surgeon should be able to use adaptively and flexibly dependent on the patient requirement. Additionally the author does also find that the quality of repaired cartilage does appear to be better following ACI when compared to microfracture, but that there is not enough evidence to conclude that ACI performs more effectively than mosaicplasty [174].

2.5.7 **Novel future treatment methods**

In 2016 Di Bella et al. presented a study of the application of their new novel in situ bioprinting method for use in repairing cartilage defects in large animals. In this study they demonstrated their handheld biopen 3D printing device. This works by extruding stem cells, in this case MSCs recovered from the infra-patellar fat pad of a sheep, coaxially through a nozzle into a cartilage defect, whereby the inner layer of the extruded bioink is culture media containing cells and the outer layer is a gelatine methacrylamide and hyaluronic acid hydrogel, a gel know to perform well in cartilage repair [175,176], which acts as a scaffold. 6 sheep were studied and in each sheep 4 cartilage defects were created by means of making an 8 mm hole in the distal femoral condyles. The treatment groups were: in situ bioprinted scaffold using the biopen, preconstructed bench based scaffolds, microfracture, and no treatment. The defects treated with the biopen showed better macroscopic and microscopic characteristics than any other treatment group [177], showing a great deal of promise for this method and for the future application of in situ bioprinting as a treatment process as a whole. However, there is a clear lack of long term data presented in this study and so it is difficult to say how this process compares to established methods over a long time frame and if the additional cost associated with the bioprinting and cell culture is reflected in the benefits of the process. Additionally, it may have been fairer to compare this methodology to ACI rather than microfracture as a control, as microfracture does not have the additional advantage of being able to add cells that stimulate cartilage regrowth to the defect.

Targeted pharmacotherapy or gene therapy may be used as a future treatment for OA. As a number of factors of OA can be hereditary, this indicates there may be genetic risk factors. Both viral, and non viral vectors have been developed in order to transfer therapeutic genes into the target cells (autologous chondrocytes) by direct intra-articular injection. Proof of concept has been achieved in animal models for both in vivo and ex vivo gene delivery using a variety of vectors, genes, and cells [178,179]. These treatments have the potential to improve the quality of life, reduce the symptoms or potentially completely eliminate the disease in patients. Additionally, they provide an alternative to invasive surgeries with a lower associated risk. However there are still some hurdles to overcome before these can be accepted as treatments such as the safety of the procedures, cost effectiveness and the general lack of understanding of the pathophysiology of OA [180–182].

Another method of addressing OA is through drugs that affect the subchondral bone. Strontium ranelate is a drug previously used for osteoporosis that prevents bone resorption and increases bone formation making it a potentially viable bone treatment for OA [183].

In addition to ACI numerous other cell-based treatments are also being explored for the treatment of OA. One such method is the injection of MSCs to the damaged area that have previously been recovered from either adipose tissue or bone marrow concentrate. Numerous studies have assessed a range of cell sources, culture conditions and application methods however there currently there is a great deal of conflict between research outcomes as to weather this method provides any significant benefit. As a result these methods are currently not recommended in the UK [184,185].

Other methods seek to develop on the ACI procedure, one such method, Chondrosphere®, uses a sample of cartilage harvested from the patient that cells are removed from and cultured for 4-8 weeks. Rather than directly re-apply cells to the damaged tissue they are then placed into 96-well plates that are coated in a hydrogel in order to allow aggregates to form. Aggregates are then combined to make larger tissue constructs which are in turn applied to the damaged cartilage. This treatment is currently recommended as a treatment option by the National Institute for Health Care and Excellence with similar requirements as ACI and has an estimated cost effectiveness per quality-adjusted life year of £18,000. To give context to this figure The U.K. National Institute for Health and Care Excellence (NICE) have a threshold in the range of £20,000 to £30,000 per quality-adjusted life year for the reimbursement of new drugs in the NHS [186,187].

It is worth noting that despite the development of new and novel therapies, new treatments options are still limited by the general lack of understanding of OA, its complex pathophysiology and the multiple contributing factors [6,7]. Therefore, there is a need for further research in order to fully understand the disease progression. Additionally, there are limited options for patients between early and late stages of the disease. This leads to some patients not meeting the requirements for costly risk adverse surgical procedures being left to manage their own pain until the disease worsens enough to warrant surgical intervention. This is not helped by the difficulty of diagnosing early-stage OA. Future treatments options should address the disease before the need for surgical intervention.

The development of new drugs and treatment therapies requires a significant amount of testing, screening, optimisation and calibration in order to identify potential lead compounds, which then need to be studied further. Once identified, extensive in vitro tests are carried out to firstly assess biocompatibility and also to assess their effectiveness in the treatment of OA. Additionally there are a number of stages before a new treatment is accepted for clinical use including, preliminary testing, pre-clinical testing and clinical trials [188]. The increasing cost of the drug development process in combination with less lead compounds progressing to clinical trials means the productivity of research and development has reduced, meaning total costs have increased [188]. In order to increase productivity one of the main requirements is the need for more efficient and productive early phase testing. This requires greater automation and speed to improve efficiency in candidate screening as well as the development of more robust testing methodologies [189].

Due to this there is an increasing interest in the development of in vitro models of OA that are more representative of in vivo conditions to speed up the transition between lead compound discovery and preclinical trial.

2.5.8 **Osteochondral models**

It is clear that the best method of testing the efficacy of an OA treatment is through human clinical trial however given the significant steps that need to be taken to advance to the point of clinical trial there are a number of models currently utilised as an alternative. Each of these models has advantages and drawbacks which must be considered.

Often seen as the most representative of human in vivo conditions, in vivo mammalian models are used for studies that have progressed to the more advanced stages of development or in larger studies where the influence of the full body physiological functions need to be studied.

In the study of OA, mammalian models can be divided into broadly three types which are defined by the method through which OA is induced in the animal. Surgical models physically modify the joint to create a cartilage defect, for example Di Bella et al. replicated arthritis in sheep in their 2016 study by creating an 8 mm hole in the cartilage [177]. Chemical models involve locally injecting the animal to induce joint degradation [190,191]. Thought to be the most effective method for drugs testing, spontaneously induced models [192] rely on the development of OA over a longer time period [193]. This method can also include the use of genetic modifications to prematurely induce the degradation of cartilage. Animals that have fully developed musculoskeletal systems that are also of a larger size (similar mass to humans) provide a better model for drug testing. They also allow for better comparison between data such as gait, histological and wear analysis. One area of research that heavily relies on animal models are pain based studies as there is not enough knowledge of the markers of pain to assess this effectively in vitro [194,195].

Although in vivo animal studies are often more representative there are other factors to consider that limit their use, for example the cost, the relatively low throughput as well as the welfare of the animals studied [181].

As a result, there is a constant demand to reduce the use of animal models where possible and only to use animal models where there are no viable alternative models and the outcomes should contribute significantly to research in the area studied [196]. To meet the demand for research models but reduce the use of animal studies there is an increased demand for the development of more accurate, high throughput, in vitro models of OA.

There has been some research into the development of an in vitro osteochondral interface model. With many of these studies involving researchers manually seeding cells on to a porous scaffold [108,197]. He et al [198] were not only able to observe increased chondrogenesis and ECM production in their in vitro cultured implants over an 8 week period but they were also able to ascertain that cartilage constructs cultured in vitro over longer periods such as 4 and 8 weeks, when implanted into cartilage defects in porcine test subjects, demonstrated a greater amount of cartilage repair than scaffolds only cultured for 2 weeks in vitro, thus demonstrating the clear merit of extending in vitro culture time.

More recently there have been attempts to produce layered osteochondral scaffolds with cells encapsulated within the inks in order to forgo the additional step of cell seeding. Kilian et al have demonstrated the production of multi-layered osteochondral tissue models using an extrusion based printing method and calcium phosphate cement (CPC) and a bioink based on

alginate-methylcellulose (algMC) based bioinks. These were found to successfully produce ECM however the cell viability was on average low (60% or less). This can likely attributed to the higher viscosity of the cellular bioink causing high shear stresses to be exerted on the cells during extrusion [199]. Other studies have produced chondrocyte laden constructs for cartilage tissue engineering application using inks of lower viscosities such as Nanocellululose-alginate inks [200] with a viability of approximately 70% and Gelatin-Methacrylamide inks with a viability of 80% however the latter did not allow for the production of volumetric constructs without support [201]. Further to this, Castilho et al have demonstrated the influence of varying the stiffness in multi-layered scaffolds using 3D printed meshes as a basis for representing different zones of cartilage with more dense zones being represented by a denser print and less dense zones represented by prints with higher porosity. The least dense zones were represented by hydrogels with encapsulated chondrocytes. Whilst it was not possible to possible to directly replicate the moduli found in native cartilage the peak stress to equilibrium stress, as well as in the relaxation rates, were very similar [202]. The density of printed meshes is one of the most important factors as not only is replicating the stiffness of native tissue important, but also the porosity of the scaffold, which in turn has an effect on the density, also plays a large role in the ability of nutrients to diffuse through the structure.

Whilst the production of volumetric constructs is important, specifically for defect repair where it may be necessary to produce a construct that will fit exactly in to the defect site, ultimately it is necessary that the ECM produced by the cells also begins to provide sufficient support for the construct in order to best replicate in vivo conditions. In addition to this, when attempting to produce optimised constructs.

Finally, the process of culturing osteochondral models must be considered. In less complex single cell cultures selecting suitable culture media and growth factors is relatively simple however as soon as co-cultures are considered, selecting an optimised media blend to ensure suitable growth rates for both cell types becomes significantly more complex. Additionally simply placing co-culture constructs in to well plates and covering with media is unlikely to be the most effective method for cell culture and as such there have been a number of developments in the field of bioreactor design in order to effectively simulate in vitro conditions [140,143,203].

2.6 Cancer Invasion models

The second application explored in this work is the high throughput production of tumour invasion models. Like in OA research and most other pharmacological research, there is also a need for the development of a high throughput 3D in vitro model for drug screening for use in cancer research. As in OA research, traditional 2D cell culture methods for use in cancer research are highly reductive and may even negatively influence research by providing misleading outcomes. For example, when grown on artificial plastic surfaces, due to a loss of a physical 3D ECM and also due to high concentrations of additives such as serum in growth media, properties such as differentiation, polarization, cell-cell and cell-ECM communication are lost whereas properties such as wound healing and hyper-proliferation are emphasised [204]. As a result, the most effective treatments for cells grown in 2D culture tend to be chemotherapeutic drugs as these target mitosis and proliferation. 3D culture architecture as well as ECM have a strong effect on the effectiveness of a drug and as a result, properties not promoted in 2D growth such as cell-cell interaction, maturation, epithelial to mesenchymal transition, and cancer stem cells are difficult to detect [205]. Additionally, in cases where drug resistance or the lack of response to chemotherapeutic drugs is to be studied better models are also needed. It is believed that mitotic inhibitors do not actually have a significant effect on the slow proliferating, cells that act to regenerate and re-constitute tumour mass [206,207].

Cancer metastasis is a complex process comprised of multiple stages, however the first and most important stage of this process is migration of cancer cells from the primary tumour through the ECM, this is called tumour invasion [208–210]. Therefore, for a cancer treatment to be considered successful it should not only involve the slowing or stopping of cancer cell proliferation but should also prevent cancer cell invasion. Despite this process being key in the metastasis of cancer, current knowledge of this process leaves something to be desired [75,211]. This is in part due to a key aspect of studying this process being understanding the process through which cells migrate through the ECM and current cancer invasion models being unable to accurately replicate this behaviour. To this end, single and multi-cellular spheroid models have become more common as a 3D culture model more accurately representing the microenvironment of a solid tumour [76,212].

The most common use for these spheroid models is the testing of new drugs [213,214] however they also provide effective models of tumour development and initiation [215,216].

Spheroids can both be cultured in ECM or in the absence of ECM. Most commonly spheroids and organoids are cultured in aqueous cell culture media, which limits their suitability for studying cancer invasion due to the lack of a surrounding ECM. Therefore the next logical step is the use of biomaterials in order to synthesis a microtissue for culture that replicates the cell ECM. Cells or spheroids can then be encapsulated in this matrix and properties such as stiffness can be adjusted to replicate the native tissue as closely as possible in order to study cell invasion [217].

For the applications of tissue engineering or regenerative medicine, scaffold based methods are generally favoured, however scaffold-free methods are regularly used in a number of studies as they are cheap, relatively simple and can generate spheroids rapidly. Tumour spheroids are some of the simplest 3D cell culture models in use but remain very popular as they replicate many properties of solid tumours effectively. Crucially they demonstrate cell-cell and cell-ECM interaction that is not found in simple 2D culture. Additionally, due to the close adhesion between cells, tumour spheroids act as an effective model for poorly vascularised tumours and in diameters of larger than 500 µm even exhibit metabolic gradients. The structures tend to exhibit three distinct layers, an outer layer of proliferating cells, a middle layer of quiescent cells and a necrotic core[218]. As a result of this tumour spheroids exhibit a similar anti-cancer drug resistance and resistance to radiation, found in human cancers. Therefore, tumour spheroids are widely used in drug screening. Furthermore, tumour spheroids can be used in combination with other cell types in studies of cancer cell migration and [76].

Multiple methods exist to determine the invasive potential of cells in a spheroid. The current standard methods of assessing tumour cell invasion invitro include, transwell-based or Boyden chamber assays [219,220]. Using these methods single cell suspensions are seeded on top of a filter coated with proteins derived from the ECM. Responding to a chemo-attractant placed in the lower chamber of the well plate, cells then migrate from the upper to the lower chamber. The most frequently used ECM proteins include type I collagen, or a matrix such as Matrigel that simulates the natural construction of basement membranes.

Lehman et al. demonstrate a modified Boyden chamber-based invasion assay, in which a mixture of spheroid and liquid matrix is applied in a thin layer to the underside of an insert which covers the entire surface of a porous membrane. When the liquid matrix material gelates at room temperature the spheroids become embedded within it.

Added to the bottom of the well chamber that the insert is placed in is a serum free media and a media supplemented with growth factors which act as the chemoattractant is added to the top chamber. Cells begin to migrate from the spheroid within a few hours, they break down the matrix proteolytically and migrate to the upper chamber [221].

The invasiveness of cells moving through the cellular barrier can be further assessed by modifying the assay through placing endothelial cells on top of the porous membrane. Media is removed from the insert after 24 hours, the layer containing the spheroids and matrix is removed, and then stained with crystal violet to visualize the invasive cells that have migrated to the upper side of the membrane. Further to this, if the cells have been genetically modified to express fluorescent protein they can be imaged and counted using fluorescence microscopy. One of the main drawbacks of the Boyden chamber-based assay is that it does not allow real-time monitoring of cell invasion and there is a limited time period in which the assay needs to be terminated. An alternative technique to this is Real Time Cell Analyzer (RTCA) allowing for continuous monitoring of invasion throughout the assay. The RTCA assay uses bespoke designed culture plates know as CIM plates, these have gold-coated microelectrodes which are placed below a porous membrane coated with ECM. The membrane sits between the upper and lower chambers of a two chamber well. One top of the matrix a monolayer of mesothelial or endothelial cells seeded to further assess the invasiveness through the cellular barrier. Invasive cells migrate through this barrier and when they move through the membrane case an electrical impedance which can in turn be measured and quantified [222]. Additionally the Celigo cytometer allows for real-time monitoring of invasiveness, it is able to capture images and use them to calculate the area that is occupied by the first leading influx of invasive cells [223]. From these an ‘Invasive index’ of cells is given as the number of cells with invasive extensions divided by the total number of cells [224]. There are additional methodologies available to study migration of spheroids guided by electric field or oxygen gradients [225,226].

A complication that arises as a direct result of allowing cells within the spheroids to naturally rearrange themselves is that cells will not remain randomly distributed but will instead rearrange themselves into an ordered structure. Often this may be beneficial for example when a layered construct is needed, however a direct impact that this behaviour has on cell spheroid arrangements is that the stronger interacting cells will tend to arrange themselves into the core of the spheroid, with the weaker interacting cells forming graduated concentric

layers [46]. This may lead to the cell type that is always arranged at the core of the spheroid becoming nutrient deficient, hindering growth and proliferation.

There are a number of drawbacks to the production of aggregates. For example, aggregate production Is a complex and time consuming process. It involves the use of a large amount of cell culture resources in order to produce a large number of cells in 2D prior to the aggregate construction. Some methods, such as hanging drop are very sensitive to disturbances from vibrations which can make simple things like culture and media change very difficult. Additionally due to the densely packed nature of the organoids produced, nutrients are not always able to fully diffuse through the culture, this can result in a 'necrotic core' [10] of dead cells within the organoid. Due to this inhibited nutrient diffusion assays that are developed for cells in traditional 2D monolayer culture are often ineffective or unrepresentative when performed on 3D aggregate culture, and there is difficulty with many common imaging techniques in imaging the core of the aggregate, making cell behaviour difficult to analyse.

Chapter 3. ReJI Print Head and Machine Development

3.1 Introduction

The purpose of this chapter is to provide a technical description of the ReJI (Reactive Jet Impingement) bioprinter head and the design changes made to the ReJI system during the course of this project. This will include an overview of the version 1 proof of concept system, the main design requirements for the production of the version 2 system and their implementation, as well as an overview of the design changes implemented in the version 3 system which was adapted for a commercial bioprinter. This will include a summary of mechanical components, electronic components and control, current software requirements and the next steps for further design refinement.

3.2 Printhead version 1 Overview and Background

3.2.1 Machine operation

Figure 3-1 and Figure 3-2 below provide an overview of the operation of the ReJI system and the components involved respectively. The basic method of operation is that two bio-inks, one a crosslinking solution Figure 3-1(A) and one a gel precursor Figure 3-1(B) are processed through micro-valves to create droplet streams. One of the bioinks, usually the ink with the lowest viscosity can also contain a number of cells in suspension. The valves are arranged such that the droplet streams impinge in air. When this happens the gel precursor and crosslinking solutions react to produce a stream of gel droplets at C. If one of the inks contains cells in solution then the gel will be a cell filled gel.

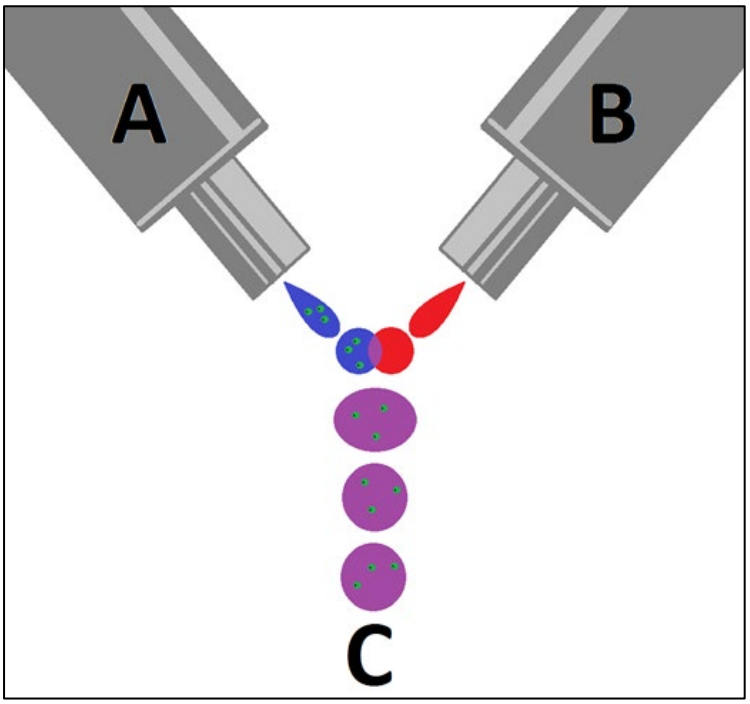

Figure 3-1: ReJI Basic principle of operation showing a crosslinking solution (A) and a gel precursor (B) impinging in the air to create a crosslinked hydrogel. The crosslinking solution (A) contains cells that are encapsulated in the gel

Figure 3-2 shows a general assembly, with reservoirs for the bio-inks, print head which holds the micro-valves as well as the microvalve controllers.

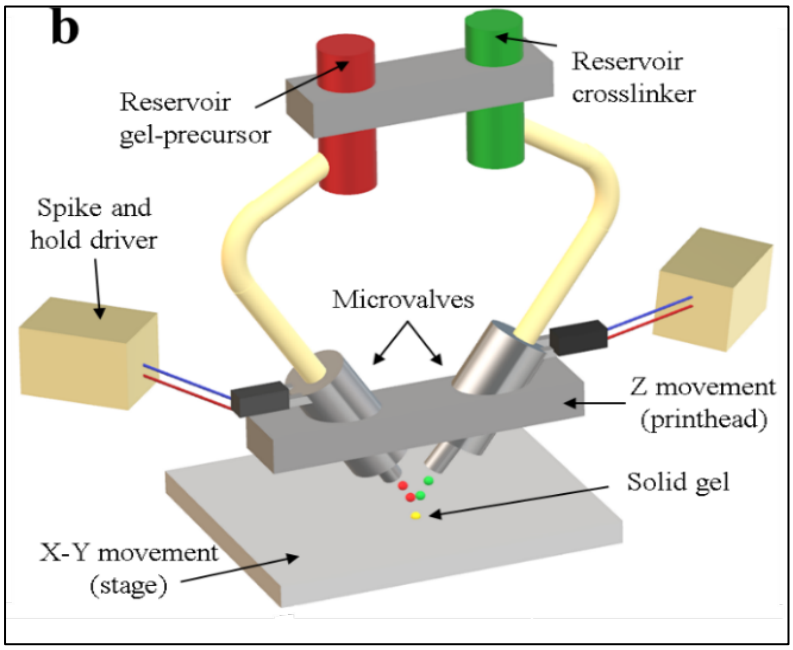

Figure 3-2: ReJI system set up and component overview

The ReJI system is comprised of a printhead that is mounted on to a JetLab® 4 XL (MicroFab, USA) printing work station combined with the JetDrive® printer drive electronics unit (Figure

3-3). Pneumatic back pressure is supplied through the use of an 25l benchtop air compressor (Orasio 241184) and is controlled by the MicroFab CT-PT4 Pneumatic controller using an analogue control dial with digital pressure readout in mmHg. This was used as the on board Jetlab pneumatic controller is unable to provide sufficient back pressure, being designed for inkjet printing rather than microvalve printing use. Figure 3-4 details the main pneumatic components.

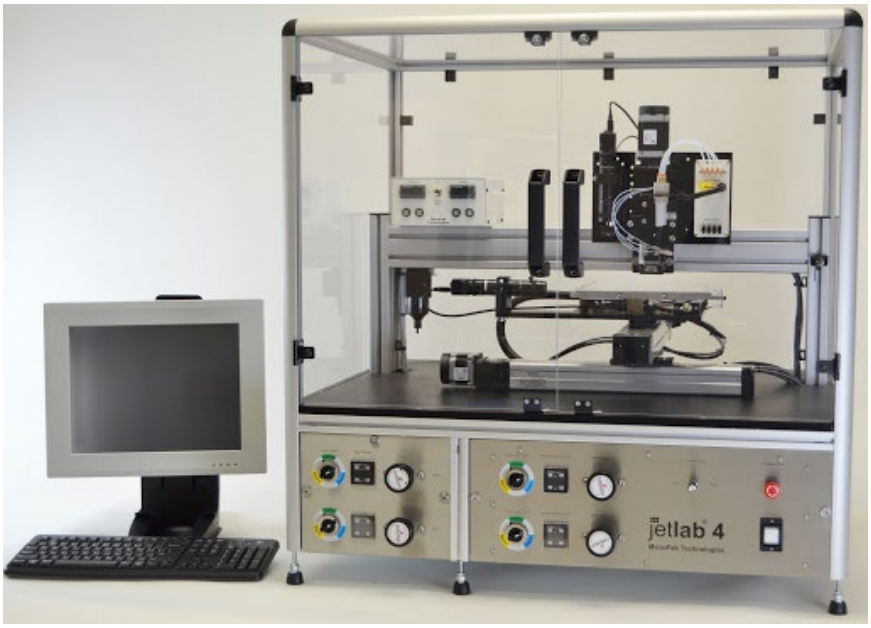

Figure 3-3: JetLab® 4 XL (MicroFab, USA) printing work station combined with the JetDrive® printer drive electronics unit

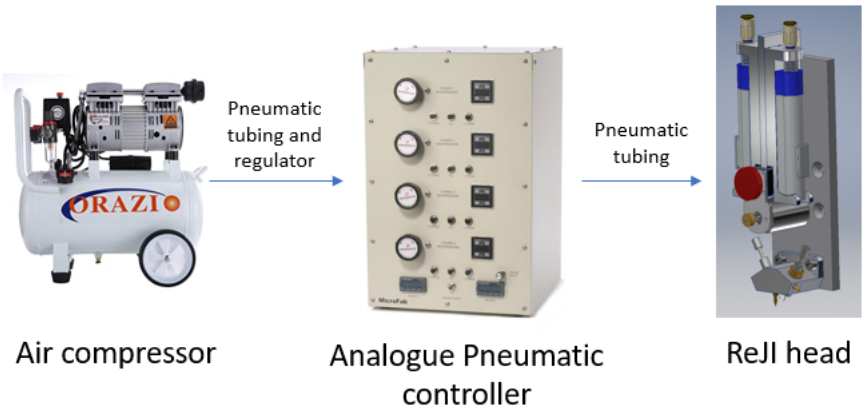

Figure 3-4: ReJI main pneumatic components for accurate control of system back pressure

3.3 Printhead version one

At the start of this project a proof of concept version 1 system had been manufactured and trialled with success [4].The initial studies showed the system was effective in producing high cellular density, cell filled gel scaffolds. However, the machine was a prototype produced for proof-of-concept studies and as such had a number of design issues to be addressed before any significant further printing would could be carried out. Figure 3-5 below shows the version 1 ReJI system.

For practical printing and research applications there are a number of features that needed to be addressed. These included:

1. The lack of fixing points for the ReJI system on the Jetlab machine, meaning that the reservoirs and the printhead needed to be clamped on using temporary clamps for printing. This meant that reliably repeating the setup process was very difficult and time consuming as the print head was not always at a set height and could not be guaranteed to be level, sometimes this would even lead to the need to rewrite scripts. As this was not the only printhead used on the Jetlab machine a printhead that could be simply and quickly mounted and dismounted from the system was necessary, this also meant that features to mount the print head on that could be attached to the machine needed to be developed, such as a mounting plate.
2. The lack of a method of adjusting the valves by a known quantity. An adjustable valve holding collet had been manufactured and trialled, however this was found to be ineffective and unreliable, and for most print sessions, researchers would remove the collet and instead use temporary fixes to secure the valves. Clearly this was not an accurate positioning method and droplet impingement with this method was very hard and time consuming to calibrate. Additionally, this made cleaning the valves or the printhead very difficult.
3. Other design issues to be addressed include:
    a. Cable management
    b. Positioning of the spike and hold controllers
    c. Bioink agitation - the prototype system required the user to manually agitate the bioinks to prevent cell sedimentation, due to this, valve blocking was more frequent.

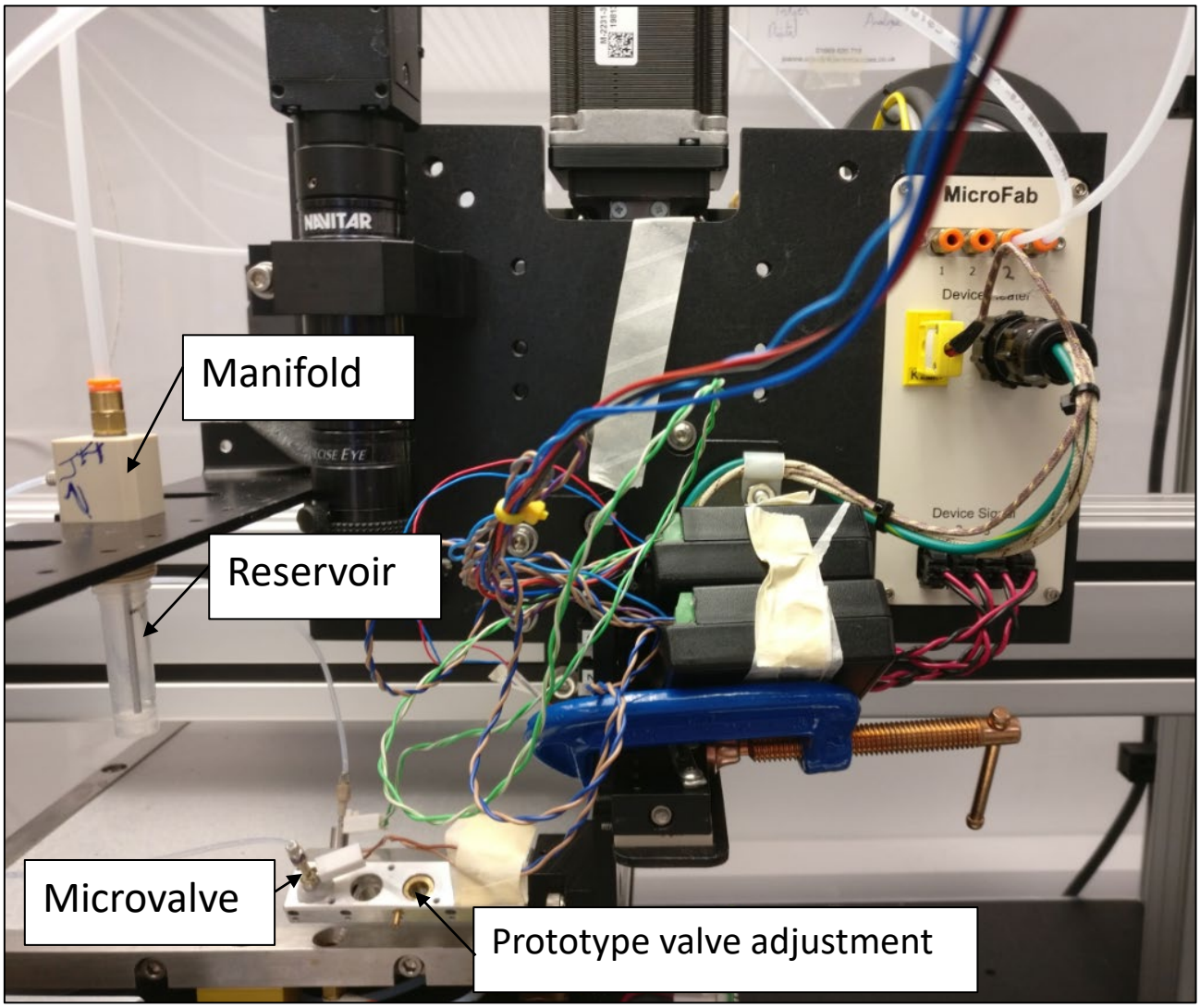

Figure 3-5: ReJI version 1, proof of concept print head used in initial studies

3.4 Hardware and Components

The main mechanical and electronic components and their operation are described in greater detail below.

3.4.1 **'V Block' Printhead**

The microvalves sit in an aluminium V block on opposing sides at a 120 degree angle. The simplest system has one set of valves, but V blocks can currently be configured for up to 4 different sets of valves. This allows for the independent printing of 4 different types of inks.

As shown below in Figure 3-6, in the V block there is one side on which valves are fixed in place by a set screw, allowing the valve to be fixed securely but also easily adjusted in height and replaced. On the opposing side of the block the valves are fixed into an eccentric collet (Figure 3-7) rather than directly into the block. The eccentric collet has a thread which meshes with

an adjuster screw. As the valve is set into the collet off-centre, turning the adjuster screw allows adjustment in order to make sure that the valves are aligned.

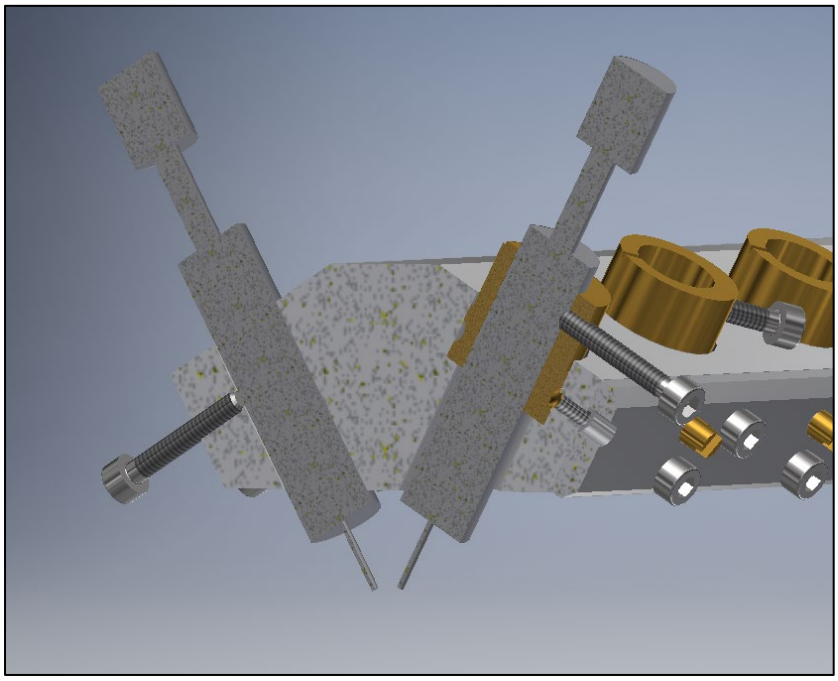

Figure 3-6: 3D section view of the printhead with section taken through the first valves set showing Microvalves in the V block

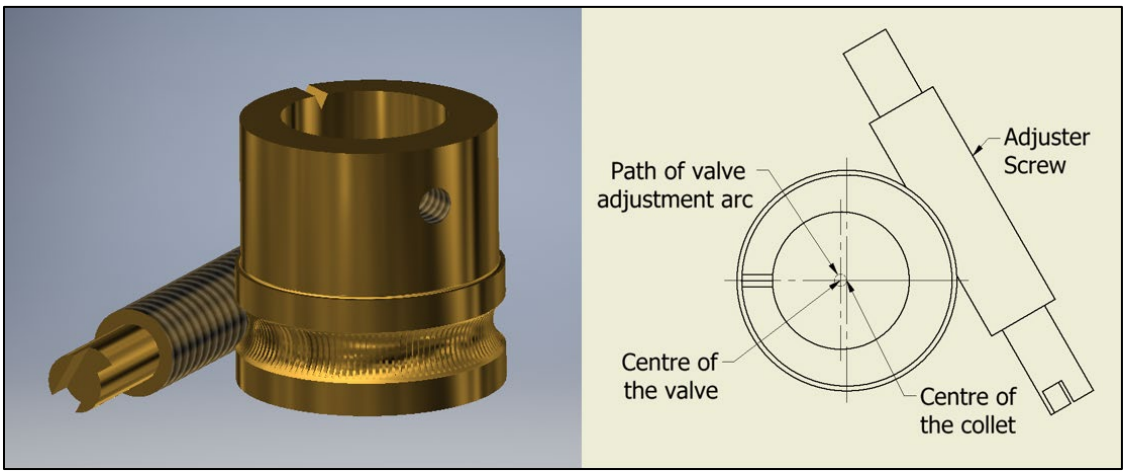

Figure 3-7: CAD image (left) and 2D drawing (right) of the adjustable collet showing the off centre or eccentric through hole that the valve is set in for adjustment

It is important that one of the valve holding collets be adjustable and one remain stationary as this allows for fine adjustment of the valves ensuring that they are impringing effectively whilst also minimising error during the adjustment process. As the valve is set in the collet off centre this allows for adjustment in both the X and Y directions with just one action rather than two, in ture this minimises error.

The V block currently mounts on to a separate plate which in turn is mounted on to the bioprinter, as shown inFigure 3-8. There is one large fastening screw to hold the block in place and two dowel pins to ensure he block is always located in the same position. This allows for fast and accurate assembly and disassembly of the V block.

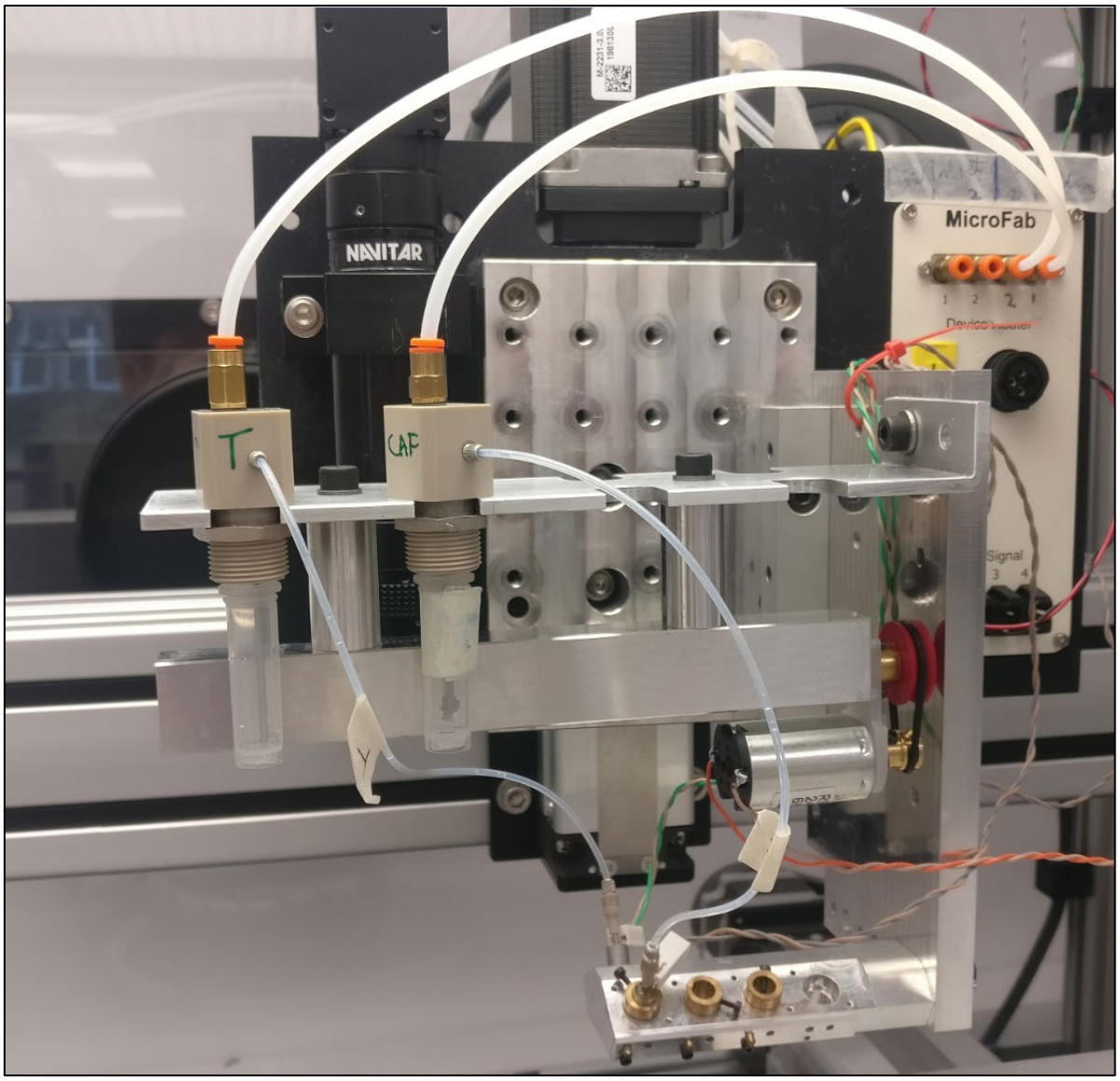

Figure 3-8: The version 2 ReJI system set up used for the experiments presented in this thesis.

3.4.2 **Manifolds and reservoirs**

The system is supplied by adding the bio-ink to a small 1.5 ml reservoir. This then screws into a reservoir manifold (Horizon instruments, C-05a-SM). The reservoir manifold has a pneumatic push fit connector through which the pneumatic back pressure can be supplied. It also has a 0.62 MINSTAC® threaded hole allowing for the use 0.62 MINSTAC® tubing to connect to the INKX0514950A VHS Solenoid valves. The manifolds and reservoirs can be seen in Figure 5.

3.4.3 **Agitation**

It is important when printing cellular inks that the ink is agitated in order to keep the cells evenly dispersed and to avoid the cells sedimenting in the reservoir. Currently this is achieved by adding a 2 mm gold plated stirring magnet to the reservoir, this is then agitated by magnets fixed to an external rotating shaft driven by a 12 V DC motor, the speed of which can be varied using a 10K potentiometer. The addition of a motor agitator was made during the course of this project.

3.4.4 **Valves and controllers**

The valves used in the ReJI system are INKX0514950A VHS Solenoid valves supplied by Lee Valves. The valves are controlled through the use of an adjustable spike and hold driver (IECX0501350A - The Lee Company, USA). This driver applies a two stage signal, first an initial spike voltage which acts to initially energize the solenoid, this is only applied for a short time, usually only slightly longer than the response time of the solenoid. In the VHS solenoid valves this is 62 µs. The solenoid is then held in the energized position by the lower hold voltage. The recommended spike and hold voltages are spike: 24 V, hold: 3.2 V, these must be supplied continually to the driver. This was provided by an external power supply unit (ISO-Tech, UK).

In addition a simple 5V unipolar trapezoidal control waveform is supplied via the JetDrive® software to control the duration of the spike and hold wave, the control wave duration, used for printing during this project is 800 µs, however this may be adjusted for larger or smaller droplet volumes. The resting signal was 0 V and the frequency was 400Hz.

The spike and hold driver will control the duration of the spike time and can be tuned and adjusted manually by turning the brass potentiometer screw on the driver, the default spike time is 62 µs, which is recommended. Sending a 5 V, 800 µs, signal wave to the driver will result in the driver supplying a 62 µs spike time and a 738 µs hold time to the valve. Figure 3-9below shows the control and spike and hold waveform.

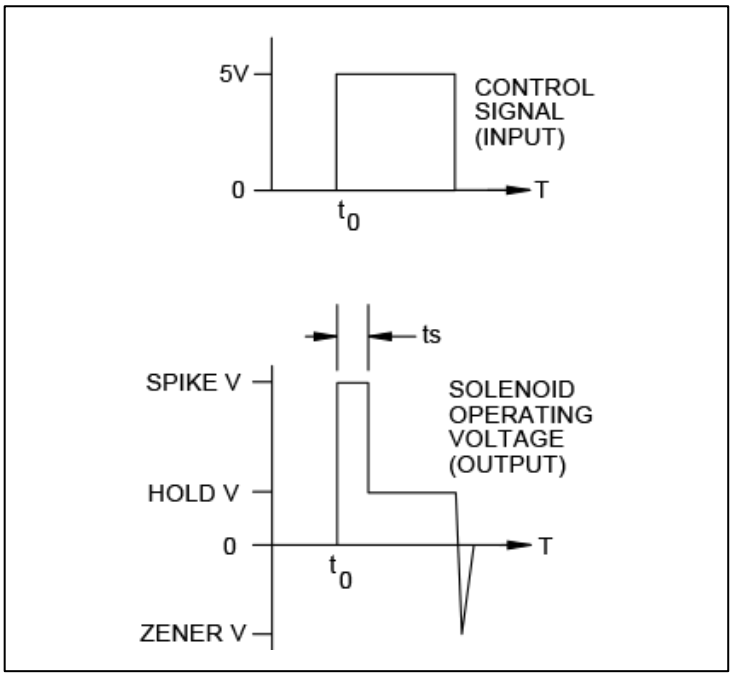

Figure 3-9: Control signal waveform. Bottom – Spike and hold waveform. Taken from [227]

3.4.5 **Pneumatic Pressure**

In order to ensure droplet volume was consistent throughout, a range of pneumatic back pressures were tested for the gel precursor and the crosslinking solution at different cell densities. The lowest back pressure that could effectively jet a droplet was chosen. This was assessed by jetting multiple droplets onto a substrate with backpressures varying between 290-550 mmHg and assessing the droplets and the nozzle for droplet size, ink build up or retention at the nozzle or splashing on the substrate.

For printing low density gels the pneumatic back pressure for the crosslinking solution containing the cells was set to 450 mmHg and for the higher cell density crosslinking solution the back pressure was set to 500 mmHg. The back pressure applied to the CAF precursor remained constant at 550 mmHg.

3.5 Design Iterations

In order to develop the ReJI system design from that of a tested prototype to a commercially viable printhead the system has gone through two main design iterations. These are described in greater detail below.

3.5.1 **Printhead version 2 design**

3.5.1.1 Design requirements

The main design requirements for the development of Version 2 were as follows:

- Simple to assemble and disassemble before and after print sessions.
- A working method of accurately adjusting valves to ensure that the head can be easily calibrated for droplet impingement.
- Include a reservoir agitation method.
- Improve cable management and system assembly.
- Ensure all components can be easily removed for cleaning and sterilisation when needed.

3.5.1.2 Print Head Mounting

The proposed solution was to create a frame comprising of two new mounting plates, the physical assembly can be seen in Figure 3-8and the CAD design image below inFigure 3-10. Each of these mounting plates would include both clearance and threaded holes of standard sizes and spacings. This not only allowed for easy mounting to, and removal from the current Jetlab® machine, but also compatibility with other printing setups making installation and removal very easy. Furthermore standardising all of the holes in order to accommodate a commonly used fitting size, such as an M6 bolt, allows for easier interchanging of parts, fewer problems in locating spares and a reduced level of required inventory, as well as making it quicker and easier to design, manufacture and fit new components when they are needed as key features such as fitting holes sizes and spacing are already known.

As well as this, 4 mm dowel holes were added to the valve mounting plate. These were specified to be a close sliding fit and as the dowel pins to be used were toleranced to g6 and the holes were specified to H7. The dowel pins were then specified to be an interference fit in the valve block so they could not be removed. This would allow for quick and accurate location, installation, and removal of the valve block from the mounting plate without compromising on accuracy. The valve block also had one threaded hole for an M6 screw so it could be held in place when assembled.

When compared to the previous arrangement of ‘G’ clamping the valve block in place this solution would offer a great deal more reliability. The final feature of the new mounting plates is that they were designed to offer a great deal more space for mounting new parts, electronic components and wiring than is currently available on the machine. This makes it a great deal simpler to design and install upgrades to the ReJI system in the future and to ensure proper cable management is maintained to ensure electronic circuits are always safe and reduce the

need for manually troubleshooting electronic failures that often arise due to incorrect installation.

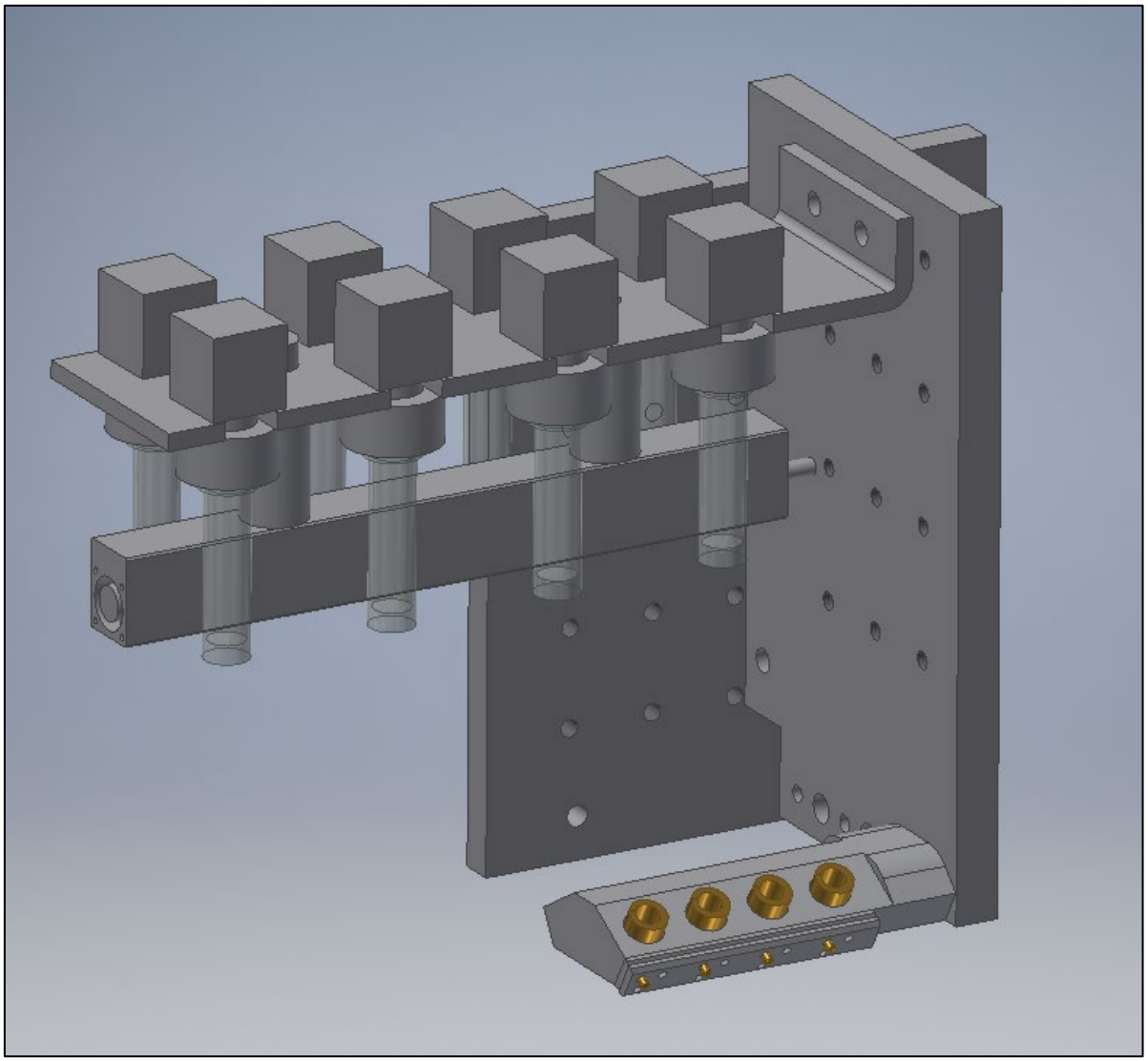

Figure 3-10: ReJI deposition head assembly, design iteration 1 CAD image

3.5.2 **Eccentric collet**

On the existing prototype ReJI head an eccentric collet had been trialled as a solution to accurately adjust the valve position. Due to the design being similar to that of a worm wheel gear arrangement, the collet being the wheel and the screw acting as the work gear, this solution is very effective in that the 'worm wheel' arrangement provides gearing, meaning not only is a very fine manual adjustment possible, but it is also very difficult to back drive making it difficult to disturb the position of the valves if they are touched or upset accidentally. As the hole the valve is set in is off centre from the centre of the collet, as the collet is rotated, rather than the valve rotate on its axis it moves around a circle with a radius of 0.1 mm, allowing for

adjustment in both the x and y directions whilst minimising the input from the opterator to only one action, thus reducting human error. Additionally, by only having an adjustable collet on one of the two impinging valves, this also minimises potential for setup error.

With the initial proof of concept worm wheel collet, the valve had to be fixed in place using an adhesive, making it difficult and time consuming to remove or adjust. This lead to researchers circumventing the collet arrangement and instead setting the valves in place using temporary fixes that allowed valves to be changed quickly if damaged, making it difficult to ensure proper alignment and impingement was taking place.

Figure 3-11 below shows the now implemented collet design (left) and the original collet design (right), note that the thread cannot be seen on the CAD models but this is represented by the channel around the circumference of the part. The new design not only incorporates a raised collar with the addition of a threaded hole for a grub screw to lock the valve in place, but also a new threaded hole has been added to the valve block in which another grub screw can be used to set the position of the entire collet and valve assembly. This is complex to manufacture and has required the production of a bespoke manufacturing jig for cutting the thread around the edge of the collet. The jig works by positioning the collet in place on a lathe bed through a hole through its centre, whist a thread tap held in the lathe chuck is introduced perpendicularly to the collet. Figure 3-12 shows the jig mounted in position cutting a thread.

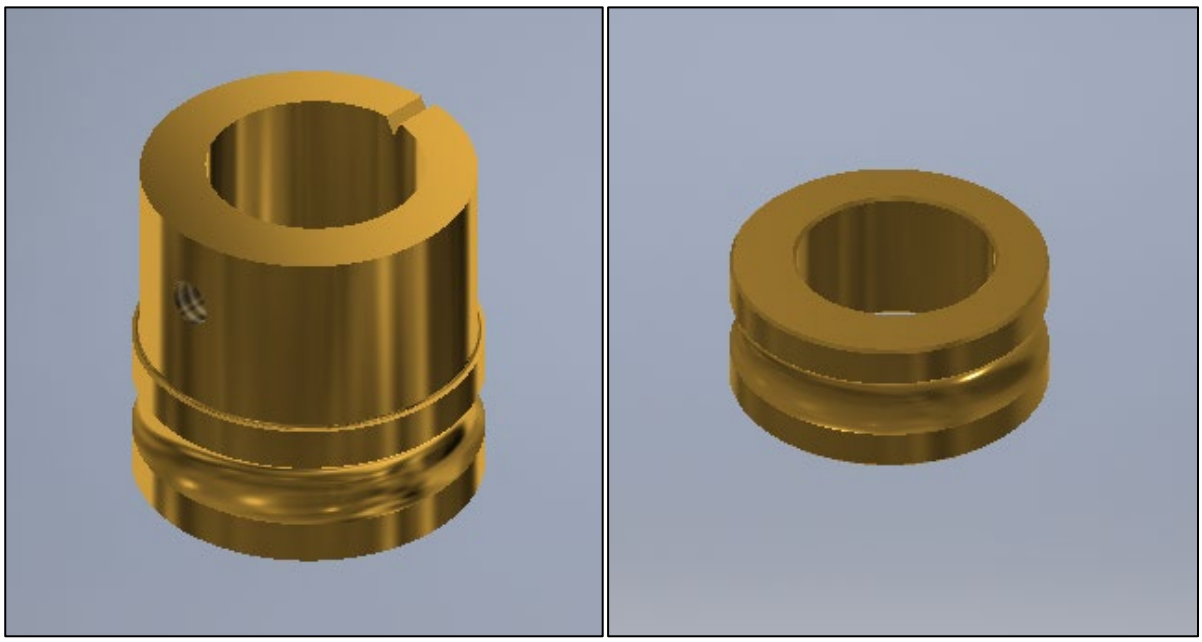

Figure 3-11: CAD images of the (Left) New eccentric collet design. (Right) Old collet design

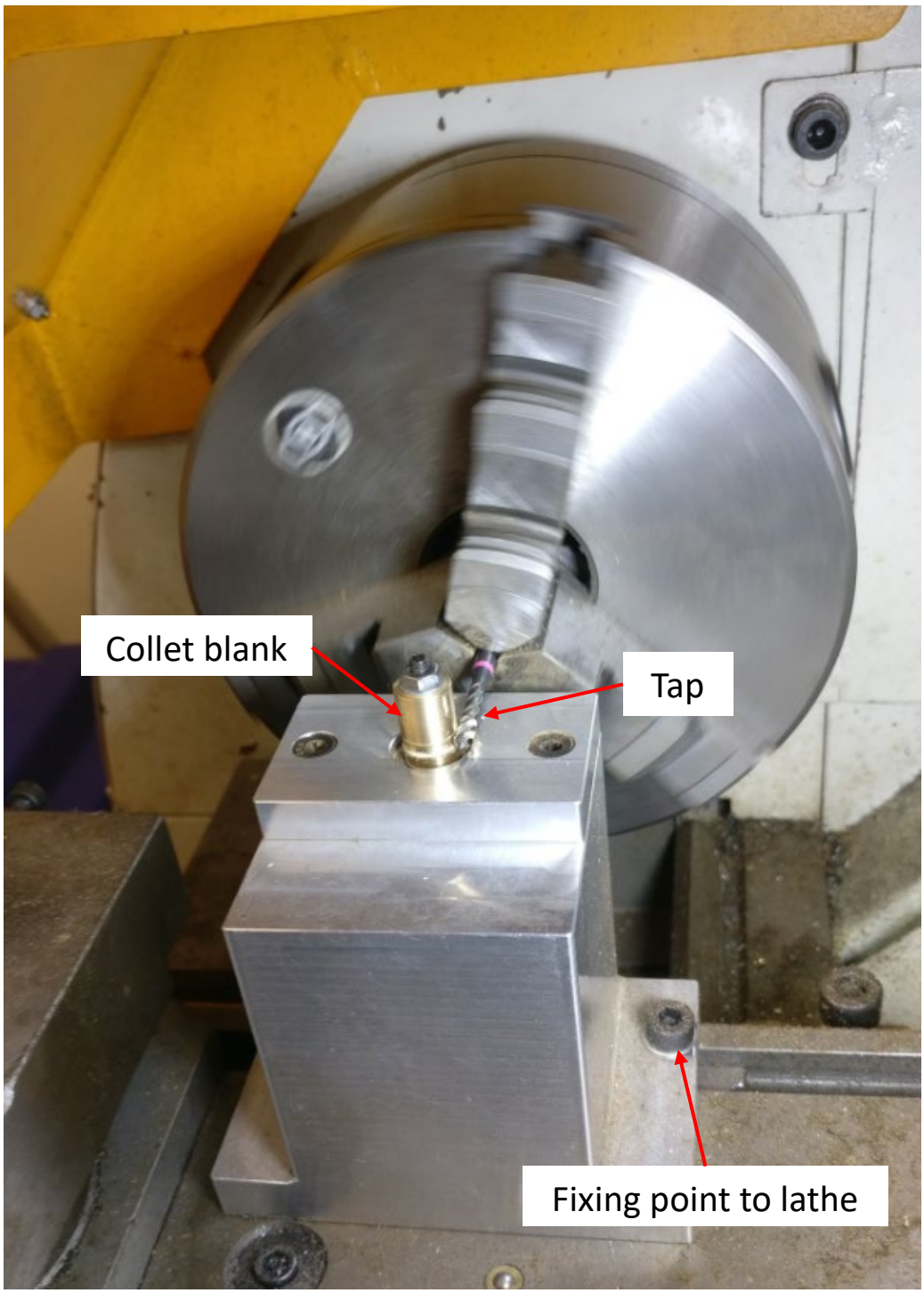

Figure 3-12: Collet thread cutting jig in the process of cutting a thread on a collet

The rotation of the thread tap causes the collet to rotate as the thread it cut into its edge. As this component requires a bespoke manufacturing process this means that it can currently only be manufactured in the Newcastle University Stephenson Building workshop.

3.5.3 **Agitation**

In order to address the agglomeration and sedimentation of the cells when printing without manually agitating the ink, an agitation system was added. This was a simple system

comprising of a shaft with four balanced magnets set into it, rotated by a small 12V dc motor. The shaft is suspended in a housing that is situated between two rows of ink reservoirs. If agitation is needed in any given reservoir then a small magnet can then be placed in that reservoir, which when the shaft rotates will agitate the bioink causing the cells to be resuspended. Figure 3-14 is an illustration demonstrating the effect of the magnetic agitation system.

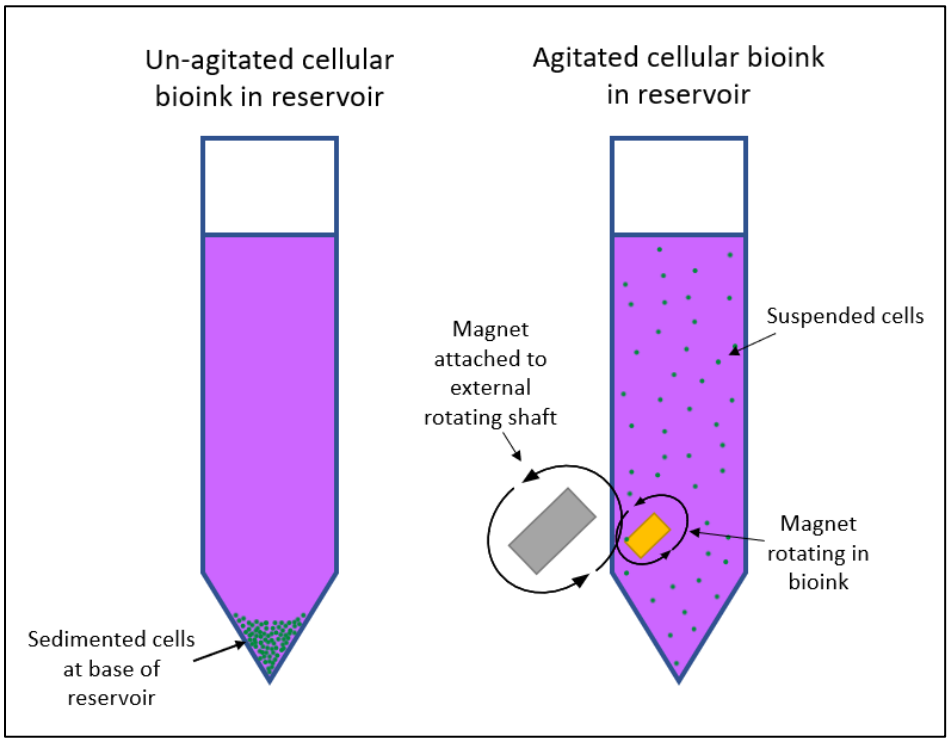

Figure 3-13: Illustration demonstrating the effect of the magnetic agitation system

As can be seen in Figure 3-8 and Figure 3-10 the bracket that holds the reservoirs has space for up to eight individual reservoirs, one for each space on the valve block, this should allow for the ReJI system to fully utilise it's eight valve print head, which was not possible on the previous configuration that could only hold 2 reservoirs at once.

3.6 Printhead version 3

The purpose of printhead version 3 was to produce a demonstrator printhead that could be fitted to a commercial 3D bioprinter. For this reason, simplicity of use for the user and also achieving a minimal size envelope to reduce inertia on machines with moving printheads rather than moving machine beds were prioritised.

3.6.1 **Reservoirs, Manifolds and Connector tubes**

3.6.1.1 Design requirements

The main design requirements for the development of Version 2 were as follows:

- Reduce the 'size envelope' of the printhead in order to minimise inertia on systems where the printhead is the moving component
- Reduce the size of the MINSTAC reservoir tubes in order to reduce clogging
- Remove the complex manifolds and replace with a simpler reservoir design that is easier to use/fill
- Introduce modular design and different size 'v-blocks'

3.6.1.2 Design changes

New designs were produced for the ink reservoirs and pneumatic manifolds. With the new designs, rather than having to unscrew the reservoir which can be quite intricate, reservoirs are now all push fit for quicker removal and replacement. A pressure seal is maintained between the manifolds and the reservoirs by means of an o-ring on the manifold, and the manifold being held in place by a coil spring. This new design also allows for reservoirs to be mounted closer together, creating an almost modular design with the smallest print head set up, the 'V2 head' comprising of only 1 pair of reservoirs and 1 pair of valves, to the largest set up, the 'V8 head' comprising of 4 pairs of valves and 4 reservoirs.

The reservoirs mount directly above the valves minimising the required length of the 0.62 MINSTAC threaded tube required to connect the reservoirs to the microvalves. This minimises the risk of tubes clogging from agglomerated cells or fibrous proteins present in the bioinks which was an issue with the previous design iterations. The 'v block' design and the method of agitation remain the same as in previous iterations. Figure 3-15 shows the CAD model for the second iteration print head 'V2' and 'V4' print head configurations. Figure 3-16 depicts a 'V4' print head and reservoir mounter to a Regemat 3D bioprinter. Overall, the new design is simpler, easier to maintain, clean and use.

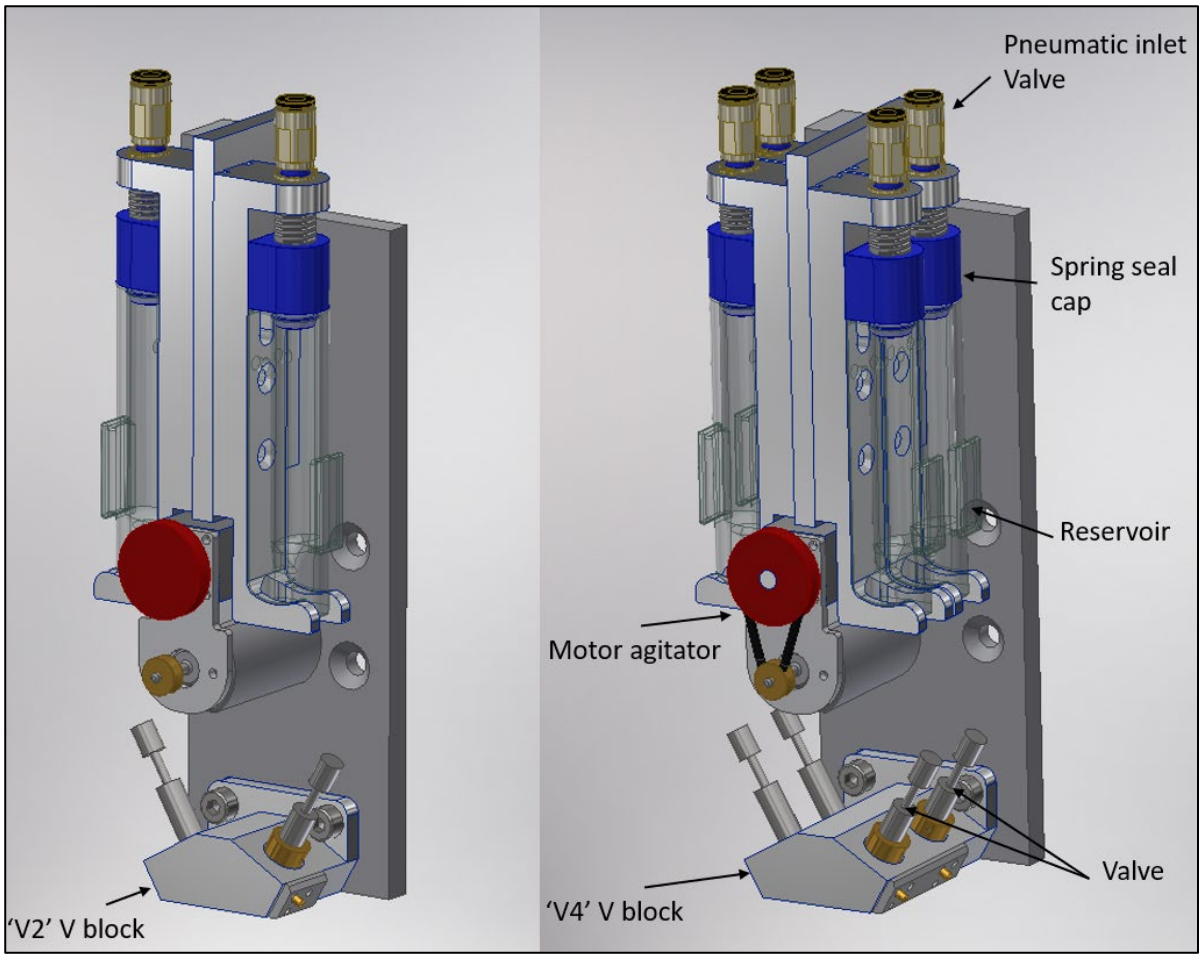

Figure 3-14: CAD model of ReJI printhead with V2 and V4 print head configurations

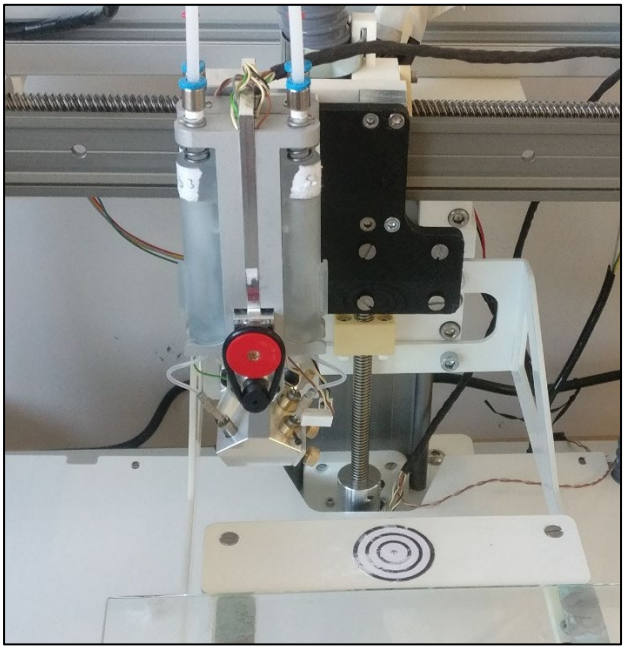

Figure 3-15: V4 ReJI print head in situ on a Regemat 3D bioprinter

Chapter 4. Material preparation and characterisation methods

This chapter describes methods which have been used across the range of experiments presented in this thesis. Methods that relate only to a particular experiment are reported in the relevant chapter.

4.1 Cell Culture

The TC28a2 chondrocyte cell line was cultured in Dulbecco's Modified Eagle Medium/Nutrient Mixture F-12 (Gibco™ DMEM/F-12, high glucose, Fisher scientific) adding 10% FBS (Fetal Bovine Serum, Gibco, Fisher scientific) and 5000 Uml−1 penicillin/streptomycin (Sigma Aldrich).

The Saos-2 osteosarcoma cell line was cultured in McCoy's 5A (Modified) Medium (Fisher scientific) adding 20% FBS (Fetal Bovine Serum, Gibco, Fisher scientific) and 5000 Uml−1 penicillin/streptomycin (Sigma Aldrich). 20% FBS was used as it was found that this helped the cells to proliferate faster.

For TC28a2/Saos-2 co cultures in this study the medium mixing method was used, mainly for ease and simplicity, but also because this ensure that if any measurable improvement is found in the cell growth in co-culture that this is not due to the medium being supplemented with additional soluble growth factors. The two media types used in this work are for the TC28a2 and Saos-2 cells are F12/DMEM and MCCoys 5a medium respectively. These are both general cell growth media and is has been shown that these can be used interchangeably between each of these cell types with no adverse effects [228,229]. As the cell mix ratio in printed co-cultures was 1:1 this was the same ratio used for the media combination.

Cells were cultured in a Thermoforma incubator at 37°C, 21% O_2 and 5% CO_2 in 175cm^2 (T175) corning tissue culture flasks. When cells reached 75-85% confluence they were passaged and split into separate T175 flasks with a seed density of 750,000 – 1x10^6 cells per flask. In doing this firstly media containing dead cells was aspirated off and then the adherent cells were washed with 10 ml Dulbecco's Phosphate Buffered Saline (DPBS; Sigma Aldrich). The cells were then incubated at 37°C with 2 ml Trypsin/EDTA (0.25%, gibco) for 3 minutes in order to detach the cells. 8 ml of medium was added per flask to neutralise the medium and remove the suspended cells. At this point two 10 µl aliquots were taken and cells were counted using a haemocytometer. The 10 ml cell solution was then centrifuged in a 15 ml falcon at 1200 RPM for 5 minutes. Following centrifugation the supernatant was removed and the cells were

suspended in supplemented medium and seeded into flasks. Cells were passaged approximately every 3-4 days.

The above process was also used in order to detach cells from culture flasks prior to printing. However prior to printing, after the supernatant was removed the cells were re-suspended in the gel crosslinking solution and agitated with a magnetic stirrer during the print to ensure the cell density throughout the print remained constant by preventing cells from sedimenting and forming clumps in the bioink reservoir.

The passage number for the TC28a2 cells at the time of printing was 26, for the Saos-2 cells the passage number was 8 at the time of printing.

4.1.1 **Cryopreservation**

Following trypsanisation at 75-85% confluency and centrifuging to remove the supernatant cells were resuspended in freezing medium comprised of 10% v/v dimethyl sulphoxide (Sigma Aldrich) in FBS. The final concentration of cells in freezing medium for preservation was $1x10^6$ cells/ml.

Cells suspended in freezing medium were then aliquoted into 1 ml cryopreservation tubes (Corning, USA) and placed in a Mr. Frosty™ Freezing Container (Fisher Scientific). The Freezing container was placed in a -80 freezer for 2-3 days to ensure a gradual rate of freezing before the cryopreservation tubes were transferred in to liquid nitrogen for long term storage at -196^{o}C.

When thawing, cryopreservation tubes were removed from the liquid nitrogen and placed in a 37^{o}C water bath until partially thawed. The sample was the transferred to a minimum of 10 mL of cold cell culture medium and centrifuged at 1200RPM for 5 minutes. After removing the supernatant the pellet was then resuspended in cell culture media at the desired concentration for seeding in to a cell culture flask.

4.1.2 **Cell counting**

Cell were counted using an Invitrogen EVOS M5000 and a Neubauer Improved Haemocytometer Counting Chamber (Hawksley, UK). After cells are detached from the culture flask and are suspended in media, but before they are centrifuged, a 20 µL aliquot was taken and 10 µL added to each side of the haemocytometer. The number of cells were then counted in each of the outside diagonal grid boxes and this was averaged. This was then repeated on the camber on the other side of the haemocytometer and compared with the first average.

4.2 Bio-ink preparation for 3D gel cultures

All of the printed gel cultures in this report were CAF (collagen, alginate and fibrinogen) gels. These were produced using the ReJI method, mixing a crosslinking solution with a gel precursor at a 1:1 ratio. CAF was chosen as it was already established that it could be printed effectively using the ReJI system and because it made a successful culture environment [4]

4.2.1 Gel Precursor Preparation

The gel precursor used is comprised of collagen (6 mg/mL Pepsin Soluble Collagen in 0.01M HCl, Collagen solutions), alginate (Alginic acid sodium salt from brown algae, *Sigma - 180947*) and fibrinogen (Fibrinogen from bovine plasma, *Sigma - F8630*) solutions mixed with a 1:2:8 ratio respectively. The components (Table 4-1) and process used were as follows:

Stock solution	**Concentration**	**Quantity (stock solution)**	**Storage**	**Shelf life**	**Working Solution**	**Notes**
Fibrinogen	10% w/v	1 g Fibrinogen per 10 ml PBS	Fridge	5 Days	37 mg/ml Add 1.7 ml PBS to 1 ml stock solution	30 mins to make stock. Add fibrinogen to PBS then leave on agitator at approx. 35°C
Alginate	2.5% w/v	2.5 g Sodium alginate per 100 ml of PBS	Fridge	2-3 months	-	Use PBS without calcium and magnesium. Mix on Agitator plate at approx. 35°C for approx. 1 hour
Collagen	0.6% w/v	Ready to use from bottle	Fridge	-	-	6 mg/mL Pepsin Soluble Collagen

Table 4-1: CAF gel components, storage and notes

4.2.1.1 *Alginate – Mix time approx. 2 hrs*

1. Place a heated agitator plate under hood set to 35°C.
2. Add PBS to the beaker that the stock solution will be prepared with, along with a suitably sized magnetic stirrer.
3. Gradually add sodium alginate over 30 mins to 1.5 hrs dependent on the amount of alginate added and stock solution batch size.
4. Leave the beaker on the heated agitator plate until sodium alginate is completely dissolved.

4.2.1.2 *Fibrinogen - Mix time approx. 30 mins*

1. Add PBS to a falcon under hood
2. Add fibrin to PBS, this can be added all at once.
3. Leave on agitator plate at approx. 35 degC for 20-30 mins.
4. Add 1.7 ml of PBS per 1 ml of stock solution to make working solution
5. Aspirate up and down with micro-pipette
6. Filter working solution through a yellow Corning Falcon™ cell strainer - mesh size 100µm

4.2.1.3 *CAF Gel precursor*

1. Add alginate to filtered fibrinogen working solution
2. Aspirate up and down with micro-pipette
3. Add collagen to alginate and fibrinogen
4. Aspirate up and down with micro-pipette
5. Filter CAF gel precursor through cell strainer

4.2.2 **Crosslinking solution**

The crosslinking solution used was Thrombin (T4648-10KU, Sigma). 20 ml of high glucose media is added to a 10,000 unit bottle and this is then separated in to 20, 1 ml Eppendorfs and stored at -20°C. When thawing each 1 ml of thrombin before printing 16 µl of 6% $CaCl_2$ is added.

When used in cellular bioprinting the cells are first centrifuged and the supernatant removed. The cells are then re-suspended in the thrombin solution and at this point are ready for

printing. Cells have been kept suspended in the thrombin solution for up to an hour for longer prints with no noticeable effect on the health of the cells.

4.3 Printer set-up and scripting

4.3.1 Print Settings

The alginate and CAF precursors were printed at a pressure of 0.6 bar, the $CaCl_2$ and Thrombin solutions were both printed at a pressure of 0.5 bar. The waveform was the same as described in 3.4.4. The stage velocity was set to 35 mm/s for all prints.

A number of test gels were printed to assess the efficacy of each bioink prior to each experiment.

4.3.2 Droplet volume

When using the ReJI, printing materials with an equal droplet volume from each valve is recommended. Average droplet volume is assessed by printing droplets on to a substrate and measure the total mass of the droplets dispensed by each valve independently, then by dividing this mass by the number of droplets dispensed and multiplying by the density of the printed bioink it is possible to get an average droplet mass. The equation for average droplet volume is as follows:

$$Average\ droplet\ volume\ (ml) = \frac{Mass\ of\ droplets\ printed\ (g)}{Density\ of\ ink\left(\frac{g}{ml}\right) \times Number\ of\ droplets}$$

Equation 4-1: Average droplet volume using mass of droplets printed, density of printed ink and number of droplets printed

All printing was performed using the in house designed ReJI bioprinter head mounted to a JetLab® 4 XL (MicroFab, USA) printing work station combined with the JetDrive® printer drive electronics unit. The valves used were INKX0514950A VHS Solenoid valves (Lee Valves, USA).

Droplet volume could also be approximated from images taken with the stroboscopic camera however this was less reliable. It is important that droplet volume is calculated as accurately as possible as this is one of the main influencing factors for setting the valve back pressure i.e. if one valve is dispensing significantly smaller droplets than it's counterpart then backpressure can be raised to ensure an even mix is achieved. Droplet volume may be influenced by factors such as viscosity.

4.3.3 **Maintenance and cleaning**

Prior to and following printing, valves, reservoirs, manifolds and any other components used in the bioprinter head that come in to contact with bioink were flushed to ensure they were cleaned, sterilised and without blockages. The pre-print flushing process was as follows:

1. De-ionised water
2. Ethanol
3. De-ionised water

The post printing flushing process was as follows:

1. De-ionised water
2. DPBS
3. Trypsin – This is left to sit in the system for 5-10 mins
4. De-ionised water
5. Ethanol
6. De-ionised water

Rigidly following this flushing process vastly decreased the number of blockages in the microvalves between printing sessions. When valve blockages occurred that could not be cleared by simply flushing, valves were left to soak for at least 24 hours at room temperature in either trypsin (if they had been used for thrombin and cells) or 1 U/ml dispase solution in DMEM/F12 (Stemcell Technologies, UK) (if they had been used for CAF precursor). This removed the majority of blockages encountered. This process was followed for all print sessions including when printing cellular gels.

4.3.4 **Software and print patterns**

Print patterns may be defined in a number of ways but a html script must be written for each print pattern to be read by the Jetlab® software. One method commonly used is to define the print pattern with a bitmap image which is then referenced in the html script. When read by the script each white pixel within the drawn bitmap image will be read as a droplet signal, settings such as the distance between each droplet can also then be defined in the script.

The method used for the production of the gel cultures tested in this report was a html script that deposits one gel droplet per well in a 96 well plate one each print pass before returning on the second pass to produce a second droplet and continuing to do so until the gels are fully printed. This ensures a consistent cell density throughout the print process across all of the

gels. The script was set to print 'on the fly' with a bed speed of 35 mm/s. This means that droplets are deposited whilst the printer bed is moving, rather than the printer stopping at each point a droplet is deposited.

4.4 Gel printing and culture

Gels were printed into CELLSTAR® flat bottom 96-multiwell plates. Printing gels in this method resulted in a cylindrical shape construct, 7 mm in diameter and 3mm in height. Figure 4-1 shows an example of one of these printed gels.

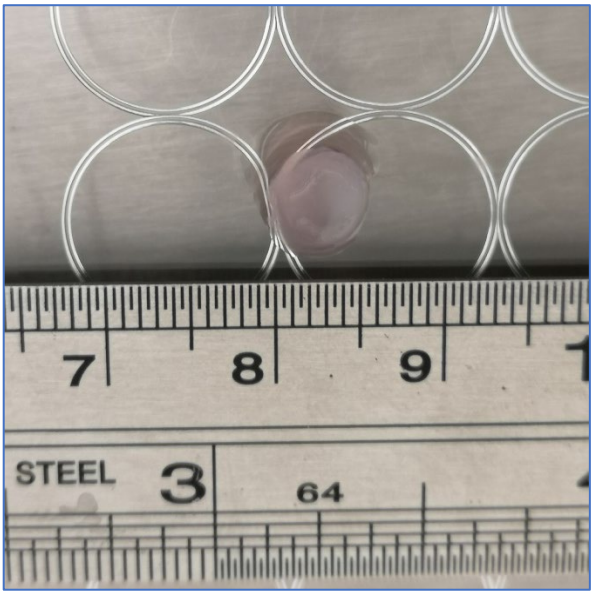

Figure 4-1: CAF hydrogel 3D printed using the ReJI method printed directly into a 96 well plate

For cell-encapsulated gels, cells were added to the crosslinking solution at the required cell density. For the printing of stratified co-cultures, first layer of gel containing a single cell type was printed at half the height of the gels printed for single cell culture, i.e. 1.5 mm; then the second layer containing the different cell type was printed on top to make a total gel thickness of 3 mm, Figure 4-2 demonstrates this. Figure 4-3 is an image of a co-culture cross section where cells have been stained with a cell tracker dye prior to printing, TC28a2 cells have been stained red and Saos-2 cells have been stained green. In this sample the layers are slightly uneven in height as the gel was damaged during the imaging process but the image shows the separated layers of cells.

Once printed, gels were manually transferred to 24-multiwell plates for culturing and 2 ml of the relevant cell culture media to each cell type was added to each well. For the co-culture

gels a 1:1 blend of the relevant media for the cell types used was added instead. Gels were cultured in a Thermoforma incubator at 37°C, 20% O_2 and 5% CO_2 in 24 well plates. Every 48 hours the supernatant was removed and replaced with fresh culture media.

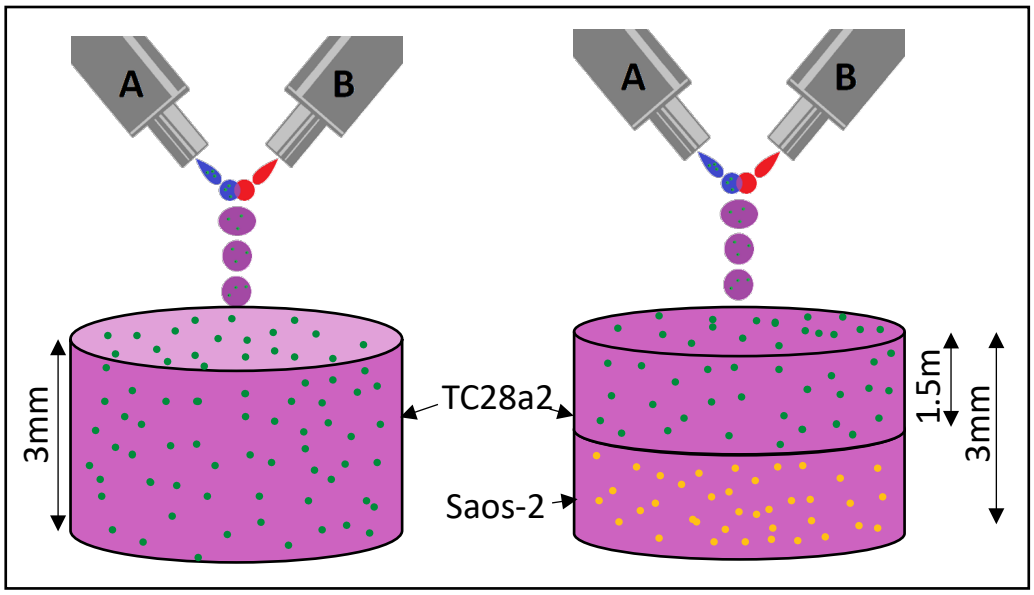

Figure 4-2: Diagram showing the structure of the printed mono-culture gel (left) and co-culture gel (right) and the dimensions of layer heights

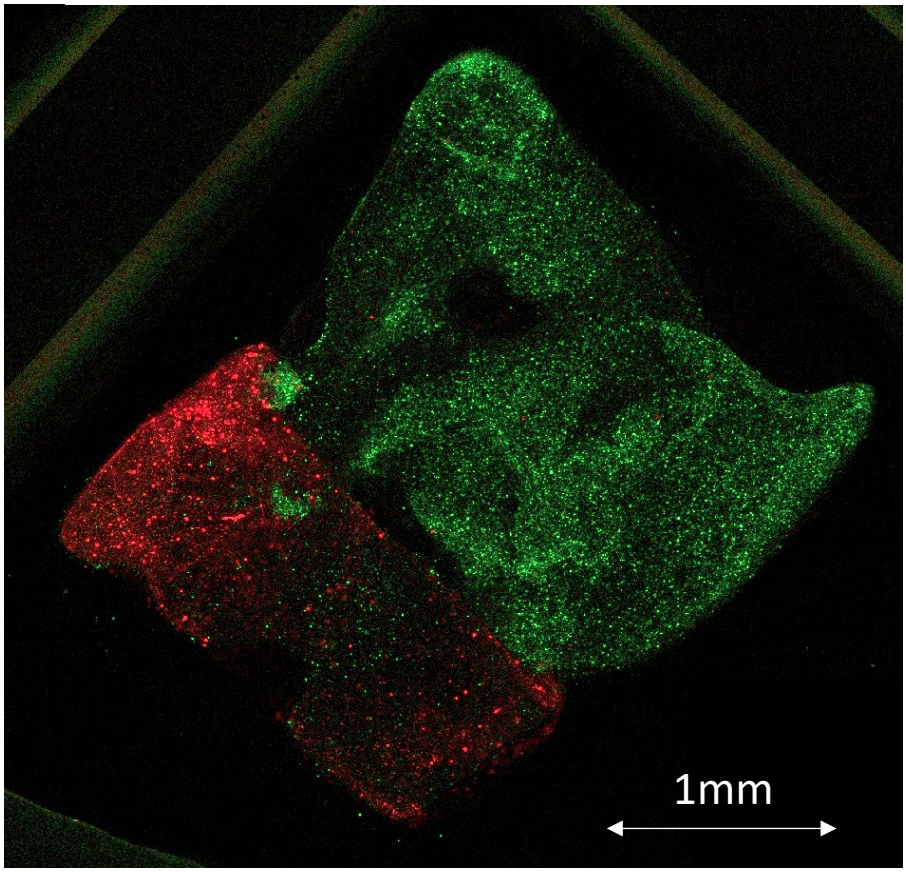

Figure 4-3: Sectioned gel co-culture with chondrocytes stained with a red cell tracker dye and osteoblasts stained with a green cell tracker dye

4.5 Characterisation of printed gels

4.5.1 Cell Viability

4.5.1.1 Live/Dead 3D fluorescence Imaging

For each gel the culture media was removed, and gels were washed with DPBS twice. Gels were stained using LIVE/DEAD ® Viability/Cytotoxicity Kit for mammalian cells (Thermofisher). From the kit calcein and ethidium homodimer-1 were added to DPBS at ratios of 1:500 and 1:2000 respectively. Each gel was fully coated in in 200 µl of the solution and incubated at 37°C for 15 minutes.

Gels were then imaged on a Zeiss LSM800 in confocal mode on the 20x 0.8 Plan Apochromat lens using settings specific for Calcein and Ethidium Homodimer (488nm excitation for both and 410-532nm emission (Calcein) and 611-700 (EthD) respectively). They were imaged using the GaAsP-Pmt1 and GaAsP-Pmt2 detectors of the Zeiss LSM800 in confocal mode, with a pinhole of 53um diameter (1.68AU) giving an optical section of 0.940um. The x/y sampling was set at 512x512 at a scan zoom of 0.5x (giving a scaling of 1.248um per pixel) and 251 z slices were taken over 235um to create the Z stack. Images were post-processed using the Imaris post processing software which could be used to locate the stained cell nuclei in order to accurately perform a cell count. Cell percentage viability presented was calculated by dividing the number of live cells by the total number of live and dead cells counted in the image. Imaging was performed on day 0 immediately after print, day 1 and day 3. These time points were chosen in order to give a representation of the effect that the printing process has on the cells. If there was a significant drop in cell viability after day 3 this is unlikely to be related to the printing process.

Three gels were imaged at each time point, gels were sliced in two and two images were taken of each gel in different areas in order to ensure that anomalous areas of particularly low, or high, cell densities were accounted for and that the images gave an accurate representation of the cell density throughout the gel. This also ensured that the live/dead assay had fully permeated the centre of the gel and was able to show if there were any areas that the culture media couldn't reach causing a necrotic core.

The Imaris image analysis software was used to perform the cell count. The process for doing this involves first manually analysing a number of randomly selected slices in the confocal Z stack in order to measure the diameter of the cell nuclei. Three live and three dead cells were

measured per gel and an average taken. It is important this is carried out for both live and dead cells as often these can vary in size. Once an average nucleus diameter is found the analysis software can then search for all cells with a nucleus of this diameter with either a red or green staining in the gel. This can then be converted to a 'spots' image which replaces the entire geometry of the cell with a sphere and these spheres can be counted. When cell density is so high that individual cell nuclei cannot be identified then the software can be used to create a surface map of the cells and the percentage live/dead can be compared by volume of green cells to red. However this volume method is much less accurate due to the size disparity between live and dead cells so this method was avoided.

4.5.1.2 Hydrogel digestion and Live/Dead

Additionally gels were digested and cells removed so a Live/Dead cell count could be performed more accurately using a cell counter. In order to digest gels, first the supernatant was removed from the gels in the well plates and the gels were washed three times with PBS. Gels were then removed from 24 well culture plates and placed in 48 well plates. 0.5 ml of room temperature 1 U/ml dispase solution in DMEM/F12 (Stemcell Technologies, UK) was added to each well and the well was placed on a Stuart SSM1 orbital plate shaker at 100rpm for 5 mins. Gels were then incubated at 37^{o}C for one hour. After one hour gels were removed from the incubator and pipetted up and down using a 1 ml pipette tip. Gels were then incubated for a further hour at 37^{o}C. Following this, gels were pipetted up and down again and finally centrifuged and the dispase solution removed from the pellet. For the live dead assay the pellet was then re-suspended in the DPBS Live/Dead solution described above.

Cells were imaged using a Tali cell counter with red and green filters compatible with the live/dead assay stainings. 3 samples of each cell density and culture type were imaged at each time point. Imaging was performed on day 1, day 3 and day 7 following printing.

4.5.2 **ECM production**

4.5.2.1 Sample fixation for cartilage/bone marker stainings

At each relevant timepoint, the gels were removed and placed in a 48-multiwell plate and washed twice with DPBS (Dulbeccos Phosphate Buffered Saline, *Sigma - D8537*); then approx.. 500 µl of 4% PFA (Paraformaldehyde Solution, 4% in PBS, Thermo Scientific™ - AAJ19943K2) or enough to fully cover the sample, was added to and left each well containing a sample and left overnight at 4°C. The PFA was then aspirated from the well plates and samples were again washed with DPBS twice before being covered with DPBS.

4.5.2.2 *Sample preparation for Immunohistochemical Staining*

After following the above process, the DPBS was removed and all of the gels were blocked with 0.1% Triton X-100 for 20 minutes and then blocked with 3% goat serum at room temperature for 1 hour and 15 minutes. Following this:

For staining for ECM markers:

- The gels were incubated overnight with primary antibodies at 4°C against collagen II 1:200 (Collagen II Rabbit anti-Bovine, Human, Mouse, Ovine, Rat, Polyclonal, Invitrogen™, Fisher Scientific - PA126206), and aggrecan 1:200 (Aggrecan Mouse anti-Bovine, Canine, Equine, Feline, Guinea Pig, Human, Ovine, Porcine, Rabbit, Rat, Clone: BC-3, Invitrogen™, Fisher Scientific - 11555772).
- The gels were then incubated at room temperature with Goat anti-Mouse IgG (H+L) Highly Cross-Adsorbed Secondary Antibody, Alexa Fluor Plus 647 (Thermofisher - A32728) and Goat anti-Rabbit IgG (H+L) Highly Cross-Adsorbed Secondary Antibody, Alexa Fluor Plus 488(Thermofisher - A32731) at a concentration of 1:200 diluted in DPBS for 45 minutes.
- Finally ,1 µl of 0.1% Hoechst 33342 solution (Thermofisher – 62249) was added to each sample and incubated at room temperature for 15 minutes.
- Between each stage the gels were washed three times with DPBS.

For staining for bone markers:

- The samples were then incubated overnight with primary antibodies at 4°C against Osteocalcin Antibody 1:100 (PA5-96529 – Thermofisher), and 1:100 Osteopontin Monoclonal Antibody ((2F10), eBioscience™).
- The samples were then incubated at 37°C with Goat anti-Mouse IgG (H+L) Highly Cross-Adsorbed Secondary Antibody, Alexa Fluor Plus 647 and Goat anti-Rabbit IgG (H+L) Highly Cross-Adsorbed Secondary Antibody, Alexa Fluor Plus 488 at a concentration of 1:200 diluted in DPBS for 45 minutes.
- Finally, 1 µl of 0.1% Hoechst 33342 solution was added to each sample and incubated at room temperature for 15 minutes.
- Between each stage the samples were washed three times with DPBS.

After removing the DPBS, samples were taken to the Leica CM1590 cryostat for cryosectioning. A small amount of OCT (optimal cutting temperature) compound was placed

on the sample dies, which were pre-chilled to -20°C. Once the OCT had begun to set slightly at the edges, the gel samples were placed in the middle and covered entirely in OCT. The dies were then returned to the -20°C machine bed to fully freeze. Once fully frozen the die with the sample was placed on the cryotome head, which was also set at -20°C and 20 µm slices were made which were collected on pre-coated slides.

All samples were imaged using the EVOS M5000 fluorescence microscope with an Olympus 10X Aprochromat objective, using settings specific for Hoechst 33342, Alexa Fluor Plus 488 and Alexa Fluor Plus 647 using the following excitation and emission setings:

- Hoechst 33342 - 357-444 nm exitation and 447-460 nm emission
- Alexa Fluor Plus 488 - 470-522 nm exitation and 525-550 nm emission
- Alexa Fluor Plus 647 – 628-640 nm exitation and 685-740 nm emission

4.5.3 **Alizarin Red Mineralisation Staining Protocol**

Two grams of Alizarin Red S (Sigma - A5533) were added to 100 ml of distilled water, then vortexed and buffered using 0.1% NH_4OH until the pH was between 4.1-4.3 read using the pH meter (Mettler-Toledo FiveEasy Benchtop F20 pH/mV Meter). The alizarin red staining solution was then filtered using a 0.22 µm syringe filter.

Media was removed from the gels and these were washed twice with DPBS and approx. 500 µl of 10% neutral buffered formalin was added to each well to cover the gels. These were then left for 45mins before removing the formalin and washing the gels twice with PBS. Gels were then covered with the alizarin red staining solution and incubated at room temperature for 45min in the dark.

The Alizarin red staining solution was then aspirated, and the gels were washed with DPBS three times. Gels were then covered with DPBS and left on a Stuart SSM1 orbital plate shaker overnight at 80 rpm. Gels were then imaged using a Leica DFC310 FX microscope.

4.5.4 **ELISA analysis**

Additionally to the qualitative stainings, cultures were measured quantitatively by analysing the media supernatant using kit ELISAs. The two ELISAs chosen were human collagen I (HCol1) and Aggrecan (PG).

4.5.4.1 *Human Collagen 1 ELISA*

The HCol1 ELISA (Human Pro-Collagen I alpha 1 DuoSet ELISA - DY6220-05) was carried out using the following process. Fist the following solutions were prepared:

- Wash solution – 5 PBS tablets (Thermofisher – 18912014) and 0.5 ml of tween were added to 1000 ml of deionised H_2O
- Stop Solution – 26.7 ml of H_2SO_4 (Fisher Scientific - 10294300) were added to 47.3 ml of ultrapure H_2O
- Reagent Diluent (RD) – 1% BSA (Sigma - A9418-5G) in DPBS

On day 1, 25 µl of the capture antibody was added to 2475 µl of capture antibody for a 96-multiwell plate. 25 µl of capture antibody is added to each well. The plate was then sealed and incubated overnight on a plate rocker at room temperature.

On day 2 the ELISA plate was washed three times using the wash solution on a plate washer using a 150 µl wash volume. 150 µl of RD was added then added to all wells to block the plate. Standards were then prepared in the following dilutions (Table 4-2).

	pg/ml	Quantity for one plate
Tube 1	2000	2 µl + 198 µl
Tube 2	1000	100 µl from 1+100RD
Tube 3	500	100 µl from 2+100RD
Tube 4	250	100 µl from 3+100RD
Tube 5	125	100 µl from 4+100RD
Tube 6	62.5	100 µl from 5+100RD
Tube 7	31.25	100 µl from 6+100RD
Blank	0	100 µl RD

Table 4-2: HCol1 ELISA standards dilutions

In a round bottom 96-multiwell multiwell dilution plate dilute samples using RD to the desired dilutions. The plate was then washed and 25 µl of the samples from the dilution plate are added to the ELISA plate. The plate was then sealed and incubated for 2 hours on a Stuart SSM1 orbital shaker at 700 rpm at room temperature. The plate was then washed again and the detection antibody is then diluted 1:100 in RD and 25 µl is added to each well, the plate was then re-sealed and incubated on the plate rocker at room temperature for another 2 hours.

Streptavidin-HRP (thermofisher - N100) was then diluted in RD in a 1:40 ratio. Following additional plate wash 25 µl of the of the diluted strep solution was added to each well of the ELISA plate which is sealed and incubated for 20 mins at room temperature away from light.

The substrate solution was prepared mixing A and B (from kit) in a 1:1 mix. Following a final plate wash 25 µl of A+B solution was added to each well. This is then incubated away from light until a blue colour begins to develop. 25 µl of stop solution was then added to each well, turning the solution yellow this is then read on a microplate reader at excitation/emission maxima of 450/570 nm.

Results were then analysed by correcting for background, and adjusting for the gradient of the standard curve as well as the dilution factor of the ELISA, which in this case was 2000 for media taken from high density samples and 500 for media taken from low density samples. Different dilution factors were tested independently ahead of carrying out the actual ELISA.

A two way ANOVA was carried out on each separate set of results for each culture type and Tukey's multiple comparisons test was used for directly comparing variance between timepoints between each culture type with an alpha value of 0.05. For the purpose of the ELISAs the supernatant was used from both high and low cell density gels for each culture type. Additionally, a media sample was taken from an acellular control gel at each timepoint as well as media from a blank control well with no cells seeded in it.

For the purpose of this ELISA samples were taken from 3 different gels at each timepoint and ran in technical duplicate.

4.5.4.2 Aggrecan Proteoglycan ELISA

The standard protocol of the Aggrecan Proteoglycan (PG) kit ELISA (Thermofisher - KAP1461) was followed. This was as follows:

50 µl of the standard, control and diluted sample was added to each well followed by 100 µl of incubation buffer. This was then incubated for 2 hours at room temperature on a horizontal plate shaker at 700 rpm.

The liquid is then aspirated from each well and the plate is washed 3 times using the supplied BioSource wash solution.

200 µl of anti-PG conjugate is then added to each well and the plate is incubated for a further hour at room temperature on a horizontal plate shaker set at 700 rpm. The liquid is then

aspirated from the well and the plate is washed three times. Immediately following the was 100 µl of Chromogenic solution is added to each well and this is incubated for a further 15 minutes at room temperature on a horizontal plate shaker set to 700 rpm. After adding the chromogenic solution the plate is kept covered from light.

200 µl of stop solution is added to each well and absorbances are read at 450 nm and 490 nm (reference filter 630 nm)

4.5.5 **Young's modulus**

The Young's modulus was calculated for TC28a2, Saos-2 and TC28a2/Saos-2 co-cultures for both high and low cell density gel cultures. An acellular gel was also analysed at each time point as a control measure.

The process for calculating the Young's modulus involved fist measuring the gel dimensions in order to ascertain height and cross sectional area. Gels were then placed in a Shimadzu Autograph AGS-X with a 1kN load cell and the compression foot was lowered until it had just began touching the gel, this was ascertained by the force feedback measured on the machine. This was then zeroed and the gel was pre-loaded to 0.05N. The displacement in mm was also recorded during pre-loading. The gels were then loaded to 0.1N, the displacement was recorded throughout. Displacement and loads, as well as gel measurements could then be used to calculate Young's modulus. Three samples were measured at each time point.

4.5.6 **Mass retention**

Gels were weighed at immediately after print, and at days 3, 7 and 14 to assess the mass retention over this period. This was done by removing the gels from the culture media and placing them on a pre-weighed petri dish, the mass of the dish could then be subtracted from the overall mass of the dish and the gels. Three gels were weighed at each time point and an average was taken of these. Excess moisture was removed from each gell by placing it on a paper towel before weighing.

4.6 Statistical analysis

In all cases where a summary chart is presented a two way ANOVA with Tukey's multiple comparisons test has been carried out on the data. Number of asterisks indicate the level of significance with alpha equal to 0.05, i.e. $P \leq 0.05$ is represented by *, $P \leq 0.01$ is **, $P \leq 0.001$ is *** and $P > 0.05$ is not significant and not represented on the graph.

Chapter 5. ReJI Acellular Print Performance Benchmarking

The aim of the research presented in this chapter was to assess the ability of the ReJI process to accurately deposit gel droplets at a range of stand-off heights from the substrate and also to assess the effect of the two main calibration methods used when printing at different heights.

For the prints reported in this chapter an acellular alginate gel was used, with the solutions prepared as described in the methods chapter, section 4.2.

5.1 Materials and Methods

5.1.1 Bio-ink preparation for printer calibration

For the purpose of the calibration prints, an alginate gel precursor was used. This was chosen as it is simple and quick to make, constituent components are inexpensive, it was already established that this material could be easily printed by the ReJI system and the alginate gel crosslinks quickly and effectively. The gel precursor was prepared using 100 ml of DPBS (Dulbeccos Phosphate Buffered Saline, Sigma - D8537) placed on a heated magnetic stirrer and warmed to approximately 35 degrees. 1.25g of Alginic acid sodium salt (Sigma – 180947) was then gradually added whilst stirring using a stirrer magnet until fully dissolved to make a 1.25% w/v alginate working solution.

The corresponding cross linking solution was Calcium chloride based. To prepare, 1.5 g of granular Calcium Chloride (Sigma C1016-100G) was added to 1 ml of DPBS. This was then vortexed until fully dissolved. This concentration was chosen as it was the highest $CaCl_2$ concentration that could be effectively printed without clogging the microvalves.

5.1.2 Printer calibration

The first operational feature that must be calibrated is the valve alignment. Valves must be aligned correctly so that the droplets will collide in the air correctly. This can be done by eye (calibration method 1) or by using a stroboscopic camera operating at a frequency that is the same or higher than that of the valves to image the droplets as they are dispensed (calibration method 2).

Calibration method 1 involves printing a straight line of 20 droplets on to a substrate. Valves are adjusted whilst printing until the two droplets are seen to impinge and only one droplet is deposited onto the substrate at a time, rather than two separate un-impinged droplets.

For calibration method 2 the printer stroboscopic camera was used alongside the Aphelion image processing software (ADCIS, France) incorporated within the Jetdrive printer control program.

As droplets were deposited from the microvalve nozzles, a strobe pulse was generated synchronously with the valve actuation. The strobe delay could then be adjusted to view the ejected droplets at a number of points in their trajectory ensuring that they were able to impinge correctly (Figure 5-1). If they did not impinge then they could be adjusted using the adjustable collet until impinging was observed. Each of the major grid lines in Figure 5-1 represents 1 mm, meaning the stroboscopic images can be used to simply estimate droplet volume mathematically by measuring the approximate length and diameter of the droplets. This could then be compared with the method of average droplet volume measurement described in 4.3.2 to ensure consistency.

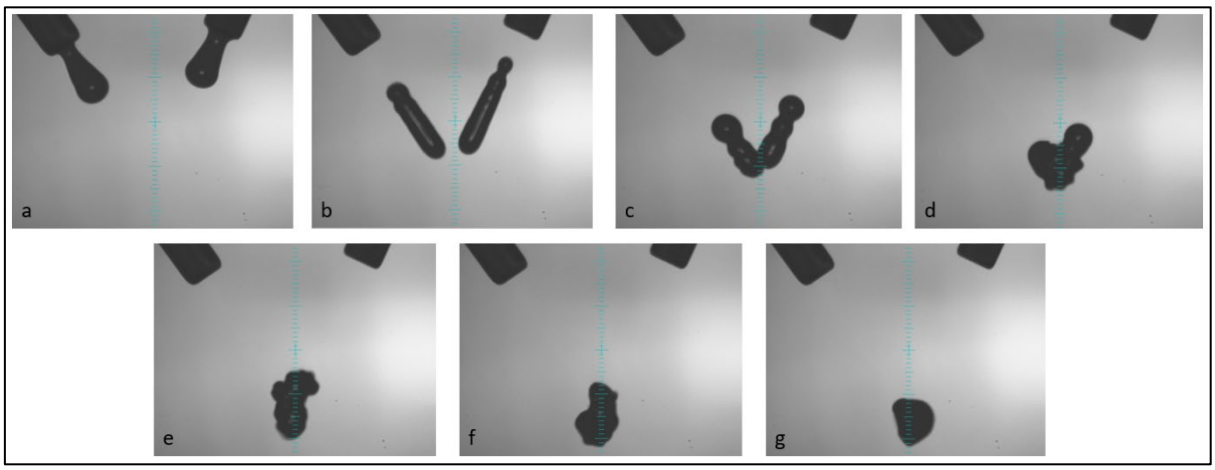

Figure 5-1: Images showing droplets ejected from the microvalves in the ReJI head at different stages in the impingement process for the purpose of printer calibration. Major gridlines in images represent 1 mm.

5.1.3 **Print Parameters**

The alginate precursor used for calibration was printed at a pressure of 0.6 bar, the $CaCl_2$ solution was printed at a pressure of 0.5 bar, this was experimentally calibrated by using the average droplet volume calculation as described in 4.3.2. The waveform was the same as described in 3.4.4. The stage velocity was set to 35 mm/s. During setup the distance between the two nozzle tips is set to nominally 1.5 mm however this can vary slightly dusing calibration due to the rotation of the adjustable valve.

Reagent	Total Print Speed (s)	Drops/s	Resolution approx. (µl)	Back pressure (bar)
Calcium Chloride	12.34	35	0.5	0.5
Alginate precursor	12.34	35	0.5	0.6

Table 5-1: Summary of print parameters for Calcium chloride and Alginate calibration prints

5.2 Study Design

5.2.1 Droplet array and 3D gel

Following calibration a 4 x 4 single layer droplet array was printed with the gap between each droplet set to 3 mm. This lead to a grid size of approximately 10 mm x10 mm when printed. The height of the print head from the substrate was gradually increased and the print quality assessed at each height. Additionally, a small number of 4 x 4 gels 16 layers in height with a gap between droplets of 1 mm were printed resulting in a gel approximately 5 mm x 5 mm x 3 mm, to demonstrate the effect printing multiples layers has on crosslinking efficiency.

5.2.2 Assessment techniques

Assessment of print efficacy was qualitative and mainly based on a visual assessment of the patterns printed. In a successful print pattern, the grid would remain square throughout with no deviation, have no additional droplet splatter or splashing, there would be no droplet overlap where droplets have not successfully impinged, and all droplets would be mostly spherical and uniform in size. These factors are important as they demonstrate how accurately the ReJI can deposit small volumes of ink, additionally, splashing, droplet volume and droplet overlap are all indicators of successful droplet impingement. Ineffective prints would deviate from this.

5.3 Results

Figure 5-2 below shows a number of 4x4 grids printed at standoff distances (the distance between the tip of the print nozzles to the substrate) ranging from 3 mm to 11 mm from the print substrate. The printed grids in the images were calibrated using the first method described in section 6.2.1 whereby a line of 20 droplets was printed at a 3 mm standoff height and the valves adjusted until they were seen to have impinged on the substrate.

As can be seen in the image the initial printed grid at a 3mm standoff (Figure 5-2 (a)) appears to be a successful print. Importantly there are 4 distinct rows of droplets with no additional splashes or sprays of gel precursor or crosslinking agent and the grid is uniform and square in shape. Additionally all droplets are spherical in shape.

Looking at Figure 5-2 (b-e) it can be seen that as the stand off increases from 3 mm to 5 mm and greater, the instances of droplets falling outside of the 4x4 grid boundary, droplets splashing, or droplets not impinging increase, in Figure 5-2 (e) it would appear that only a small number of droplets in the centre of the spread of printed droplets have successfully impinged. Additionally, From heights of 5 mm and greater, droplets begin to look more elongated and less spherical, this may be because using this calibration method results in droplets impinging on the substrate rather than in the air, and as the distance increases the distance between where the two opposing droplets land on the substrate resulting in an elongated droplet and as the height increases, eventually droplets not impinging at all (see Figure 5-3 a.i). Another phenomenon that can be observed in Figure 5-2 (e) is droplet overlap, this is where the two nozzles miss each other completely, do not impinge and the end result is a printed grid of gel precursor and a printed grid of crosslinking agent very close together but unimpinged.

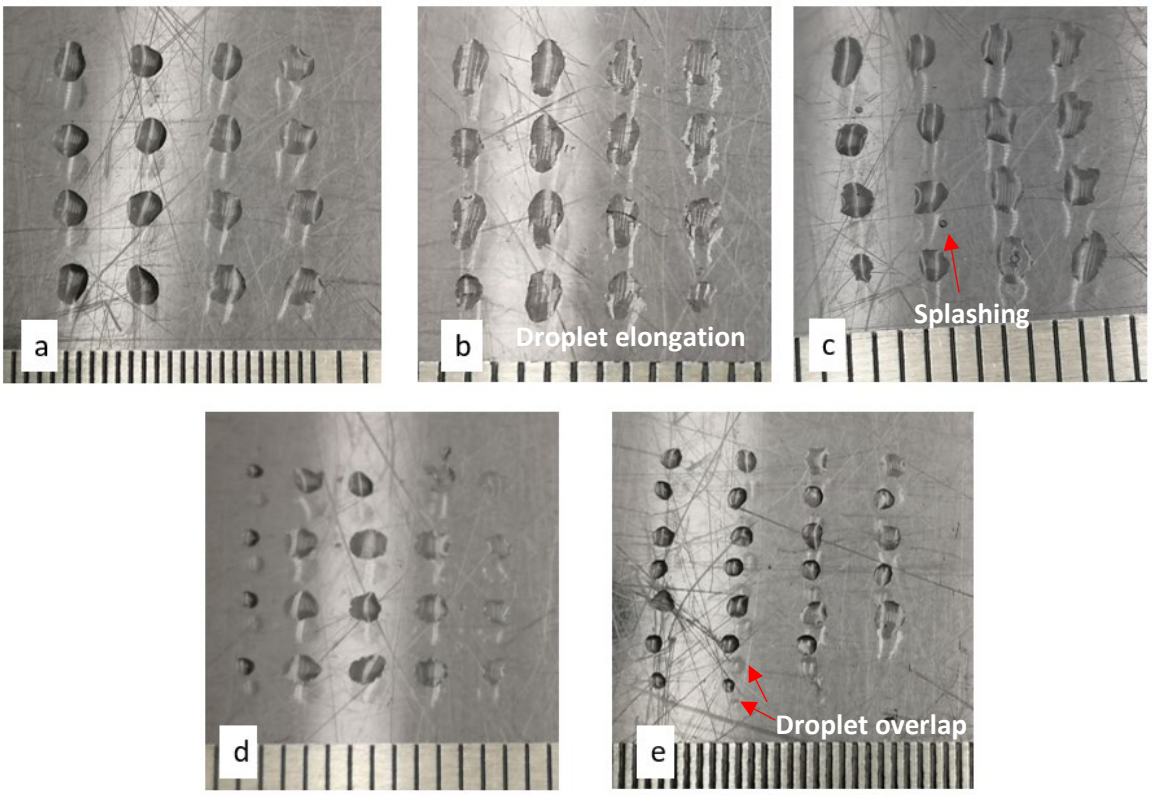

Figure 5-2: 4x4 grids of alginate gel droplets calibrated using calibration method 1 at a 3 mm standoff distance printed at standoff distances of (a) 3 mm (b) 5 mm (c) 7 mm (d) 9 mm and (e) 11 mm

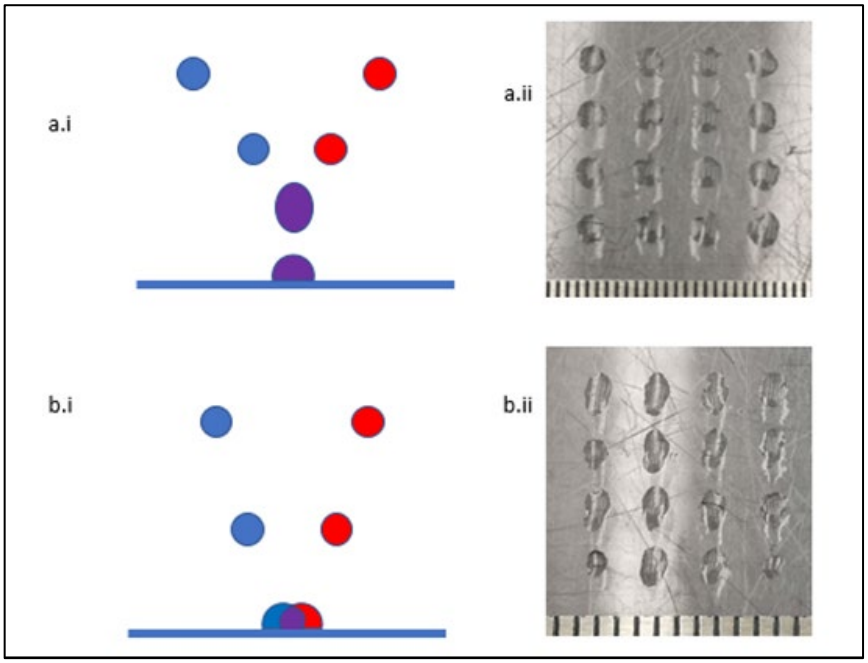

Figure 5-3: a.i: Droplet impingement in air and how this effects crosslinking by increasing surface area contact between the gel precursor and substrate, a.ii: Accurately printed spherical droplets resulting from this method, b.i: Ineffective droplet impingement resulting in inefficient crosslinking and wastage of reagents, b.ii: Elongated, not fully crosslinked droplets resulting from this

Figure 5-4shows 4x4 grids printed at standoffs of 3 mm, 5 mm, 7 mm, 9 mm and 11mm from the print substrate having calibrated the ReJI head prior to printing using the stroboscopic camera. Using calibration method 2 all of the droplets seem to have impinged and printed successfully. The only real significant change in increasing the standoff difference when the print head has been calibrated in this method appears to be the droplets are slightly less spherical, rather than this being due to ineffective impingement, this is likely due to them striking the print substrate at a higher velocity having fallen a greater distance.

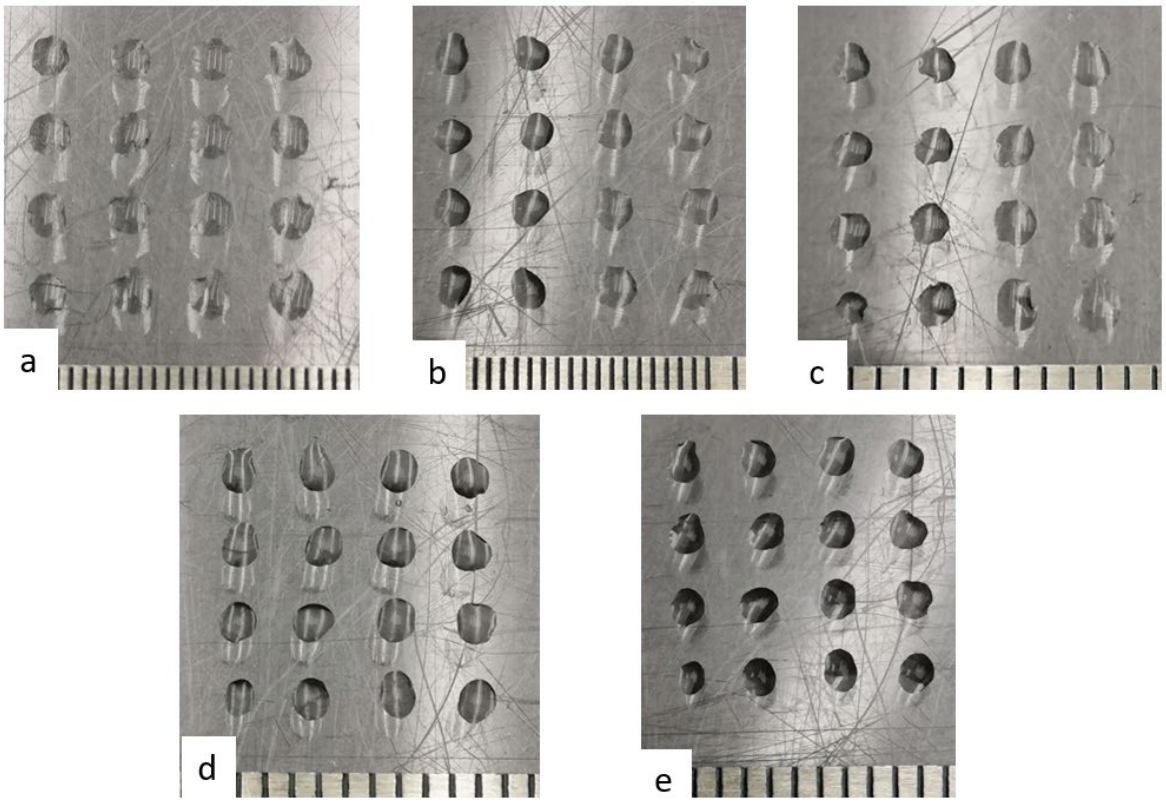

Figure 5-4: 4x4 grids of alginate gel droplets calibrated using Calibration method 2 printed at standoff distances of (a) 3mm (b) 5mm (c) 7mm (d) 9mm and (e) 11mm

An additional observation in printing using the ReJI method is that as the layers of droplets continue to build the efficacy of the print increases as gel droplets are able to combine with layers above and below and as a result there is less wasted un-crosslinked material. Figure 5-5 shows a printed 12 layer hydrogel with the individual gel droplets visible, demonstrating the quality of the printed gels.

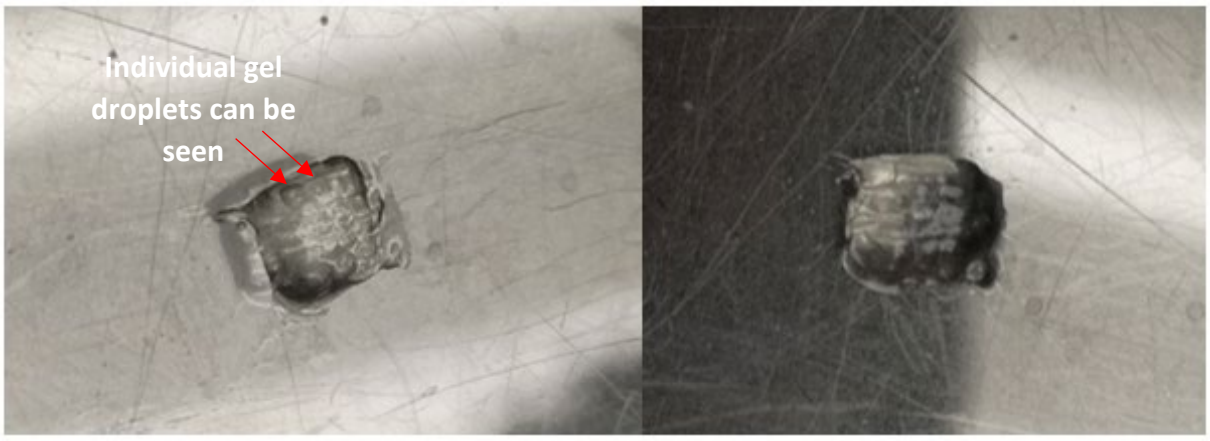

Figure 5-5: A printed 12 layer hydrogel 5 mm x 5 mm x 3 mm in size with the individual printed gel droplets visible

5.4 Discussion

The results of the printer calibration experiments show that the ReJI system is capable of repeatably depositing an accurate grid of uniform droplets.

When comparing calibration methods, it is apparent that although the method of printing a droplet line and adjusting the valves during the print is faster than calibrating using the stroboscopic camera, as the print height increases this calibration method reveals itself to be significantly less effective. Splashing is more common and droplets become less spherical and more elongated suggesting that the droplets are impinging on the substrate rather than in the air. This is important as when the droplets impinge in the air and the droplets come into contact they spread, increasing their surface area and allowing them to mix more thoroughly. When the droplets impinge on the substrate full mixing does not occur leaving some uncross linked ink and only a small amount of crosslinked gel in the centre, making the process significantly less effective and efficient, Figure 5-2 demonstrates this and Figure 5-1 (d-e) show correct impingement with images taken with stroboscopic camera. Using the stroboscopic camera, the printer only started to demonstrate very minor deviations in sphericity at a height of 11 mm and some very minor splashing at 15 mm. The ability to print accurately at different print heights, specifically the height of 1 1mm is key in demonstrating the ReJI system can act as an effective high throughput bioprinter capable of making large batches of gel cultures for applications such as drug testing research. Printing accurately at a standoff height of 11 mm would allow for the ReJI system to print directly in to 96 and 384 well plates which are used for these applications. Furthermore, the ReJI system can be further adapted for even higher throughput through the addition of more valve pairs meaning the process is scalable. Finally, the ability to accurately print small droplets of very high cell density gel is very significant. In other processes capable of printing similar cell densities, for example microextrusion, there is a lack of this level of accuracy. One application where very small droplets of high cellular density gels may be needed is in tumour invasion models where a droplet of cell laden gel needs to be applied accurately to a specified area on a small section of tissue so the cell invasion from the gel can be observed. In this application if gels are too large or applied to the wrong area of the tissue then the tissue can sometimes be effectively blocked of oxygen or nutrients found in the culture medium resulting in the tissue dying. Again, this demonstrates another potential application for the ReJI system.

Chapter 6. Benchmarking of Post-ReJI-print Cell Behaviour within an Osteochondral Co-culture

6.1 Introduction

The aim of this chapter is to assess the efficacy of the ReJI system as a 3D bioprinter for printing cell filled hydrogel scaffolds by assessing how accurately the printing process can print specified cell densities and the effect of printing different cell densities on cell viability, both in mono-culture and stratified co-cultures.

6.2 Study Design

Cell filled CAF hydrogel cultures were printed at densities of $4x10^6$ cells/ml and $40x10^6$ cells/ml containing Saos-2 osteosarcoma cells and TC28a2 chondrocyte cells. The printed co-cultures were comprised of separate layers of CAF gel containing each cell type (see Figure 4-2 and Figure 4-3) equating to the same overall volume of the single cell culture gels. These cell types were chosen as they are the main component cell types of the osteochondral interface found in cartilage tissue. This is also why the co-culture models were printed as a stratified co-culture rather than with all of the cells mixed in to on gel, in order to act as a more representative model of an osteochondral interface.

The gels were cultured over a 72-hour period and assessed through live/dead analysis both by staining the cells in situ and imaging using confocal microscopy, and by digesting the cells using dispase and analysing using fluorescence based cell counting methods.

6.3 Results

6.3.1 *A*ssessing Cell Viability and printed Cell Density

6.3.1.1 Live/Dead analysis using 3D confocal microscopy

Figure 6-1 below shows the average percentage viability of the Saos-2 and TC28a2, and co-cultures at both $4x10^6$ cells/ml and $40x10^6$ cells/ml print densities analysed using confocal microscopy. For simplicity, only pairwise comparisons between samples of similar density or cell type at each timepoint (i.e. high density vs high density or High density TC28a2 vs low density TC28a2), and comparisons between similar culture types at different timepoints (i.e. Day 3 high density TC28a2 vs Day 14 High density TC28a2) are displayed on the chart.

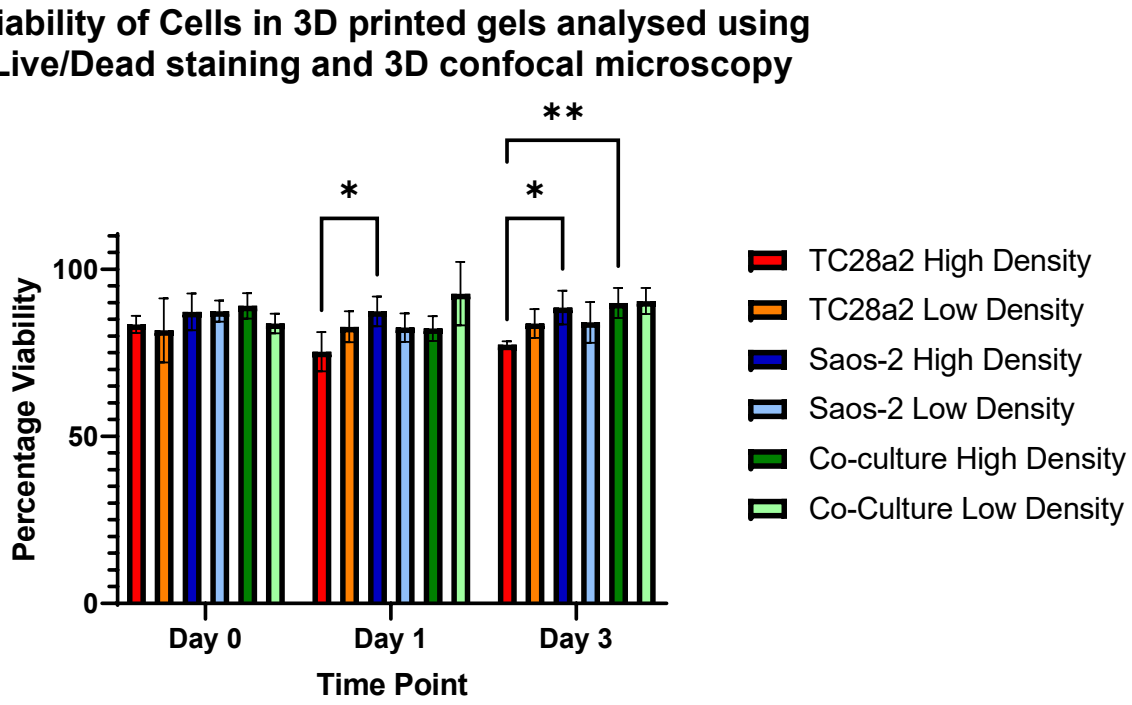

*Figure 6-1: The Percentage viability of cell filled 3D printed hydrogels, containing TC28a2, Saos-2 and co-cultures of TC28a2/ Saos-2 cell types respectively, indicated by the percentage of counted live cells to total number of cells counted using the live/dead assay and imaged with 3D confocal microscopy. Asterisks indicate the level of significance with alpha equal to 0.05, i.e. P ≤0.05 is represented by *, P ≤0.01 is **, P ≤0.001 is *** and P >0.05 is not significant and not represented on the graph.*

It can be seen that in all cell types at all densities and at all time points the percentage viability does not fall below 75% and in most cases this is above 80%. It is worth noting that the cell viability in the high density TC28a2 cultures is significantly lower than the other high density culture types at day 3, and significantly lower than the Saos-2 viability at day 1. However the average viability is still very high and does not change significantly in the high density TC28a2 culture over the 72 hour period.

Figure 6-2 and Figure 6-3 below show images at different stages in the process of counting the cell nuclei of TC28a2 cells in a low and high cellular density gels respectively demonstrating how the cell counting function works. At stage 'a' (labelled in Figure 6-2 and Figure 6-3) the confocal image can be seen, stage 'b' shows the 'spots' image, this is where the nuclei are identified and each cell is replaced with a single point. At stage b the number of live and dead cells can usually be counted however in some instances this is more difficult, for example

when comparing the cells in very high cellular density gels, or when comparing cells at more advanced time points when there appears to be a change in the cell morphology. This can be seen in the day 3 images in Figure 6-2 and in the images in Figure 6-3. In these instances it is possible to produce a 'surface' image as shown at stage 'c' in Figure 6-2 and Figure 6-3 to deduce viability volumetrically.

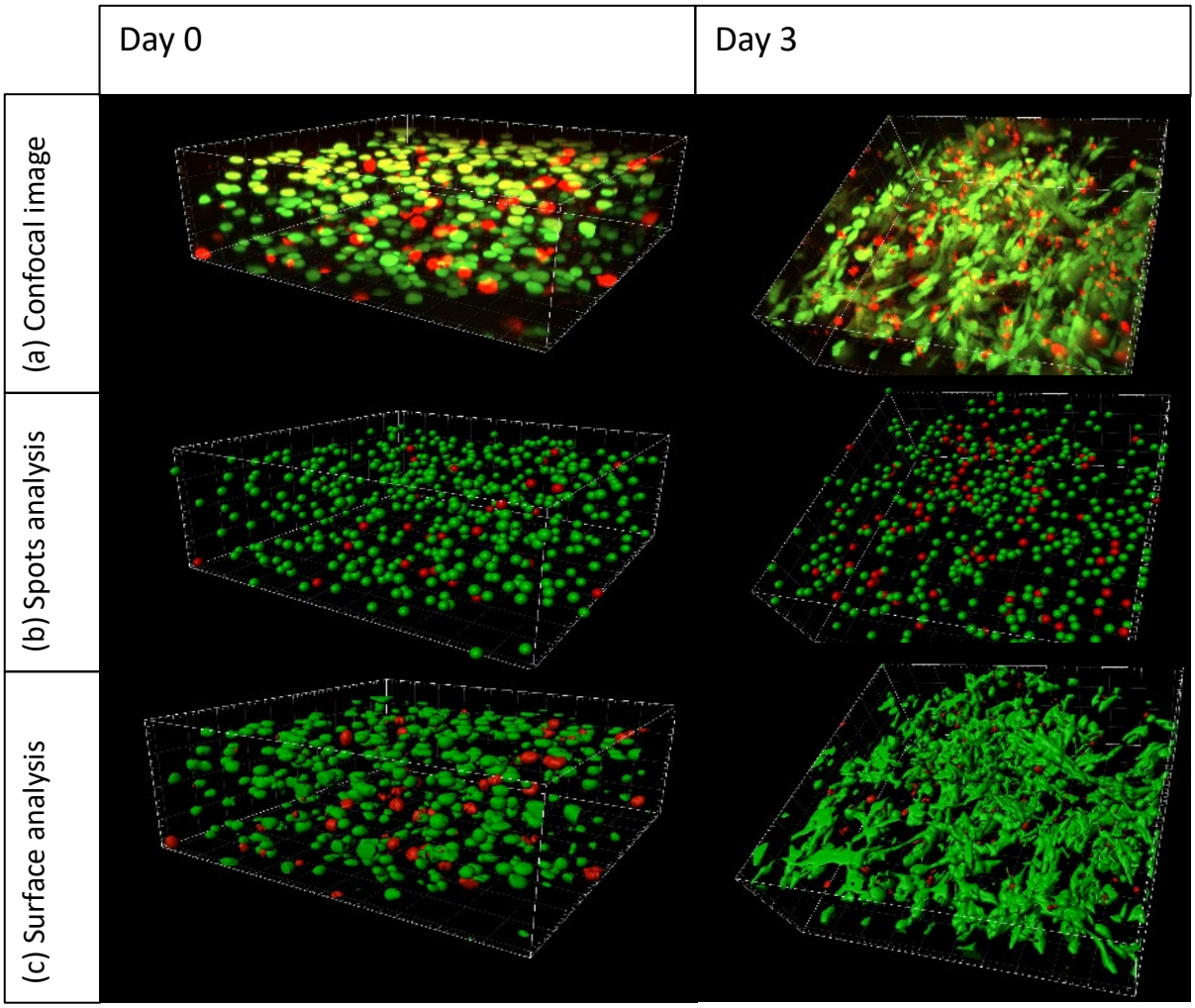

Figure 6-2: The different stages of confocal image analysis in a 4x10^6 cells per ml density gel containg TC28a2 cells. The box outlined is 500x500x200µm in size. (a) Confocal image of hydrogel containing cells stained with Live/dead viability kit (b) Cells in the confocal image converted to 'spots' by the Imaris imaging software (c) Cells and their full morphology represented by a surface rendering by Imaris

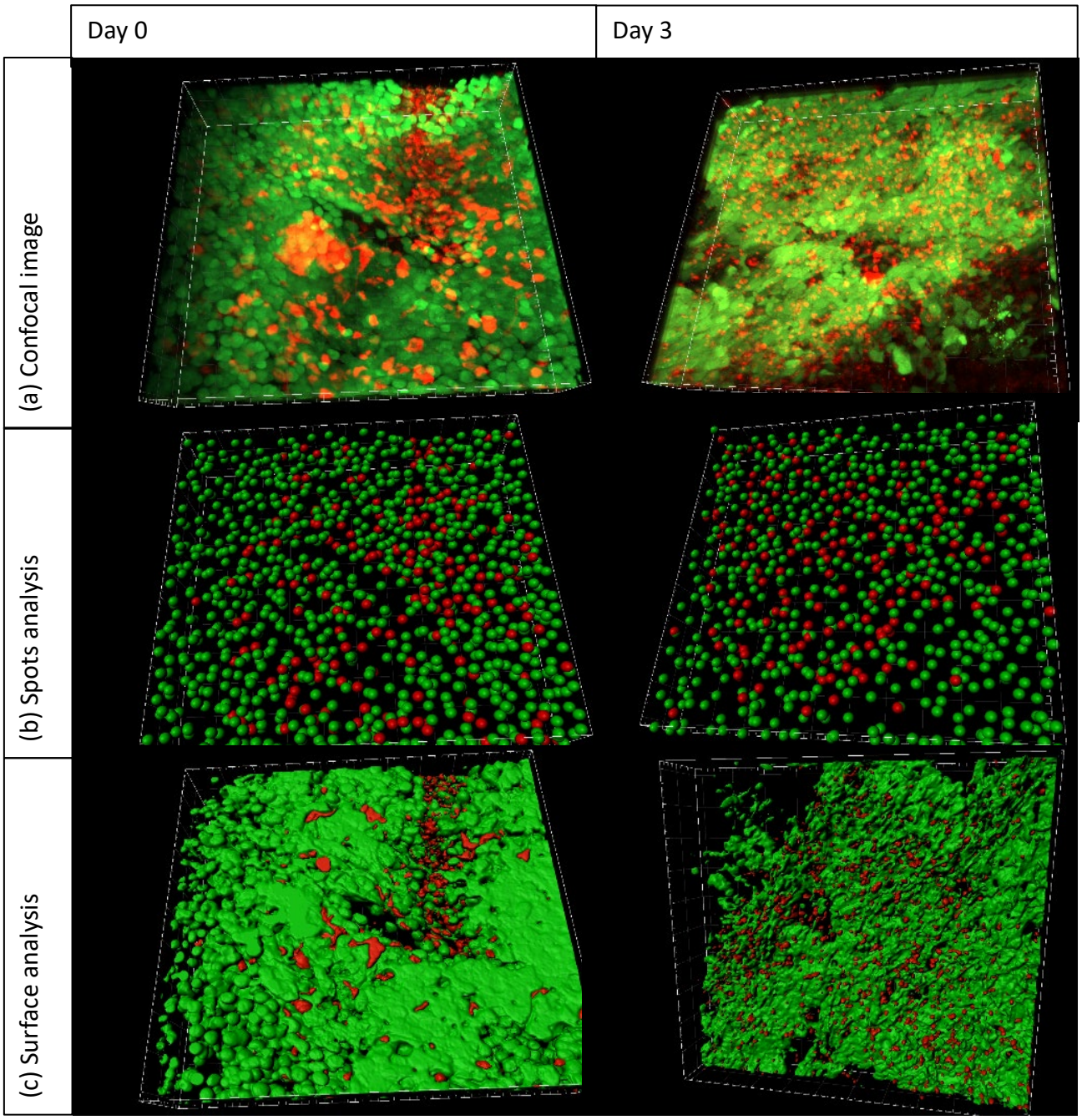

Figure 6-3: The different stages of confocal image analysis in a 40x10^6 cells per ml density gel containg TC28a2 cells. The box outlined is 500x500x200µm in size. (a) Confocal image of hydrogel containing cells stained with Live/dead viability kit (b) Cells in the confocal image converted to 'spots' by the Imaris imaging software (c) Cells and their full morphology represented by a surface rendering by Imaris

6.3.1.2 *Live/Dead analysis using Hydrogel Digestion and 2D Fluorescence imaging*

Figure 6-4 shows the counted cell concentration (cells per ml) of cells in digested hydrogels immediately after printing, counted using a Tali cell counter and fluorescence stainings. The cell types used in this method were Tc28a2, Saos-2 and Tc28a2/Saos-2 co-cultures. The results clearly show that the ReJI process has been effective in accurately printing the desired number of cells in each type of hydrogel culture based on the number of cells counted before adding to the bioink.

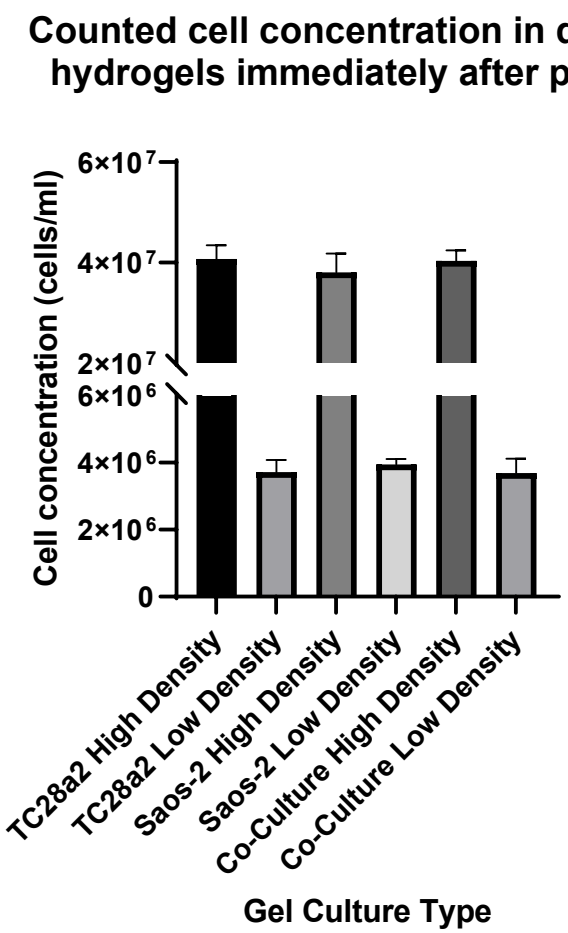

Figure 6-4: Counted cell concentration (cells per ml) of cells in digested hydrogels immediately after printing, counted using a Tali cell counter and fluorescence stainings

The average cell concentration for each culture type as well as the percentage error is presented in Table 6-1 below.

Culture Type	Average cell concentration	Percentage Error
TC28a2 High Density	41000000	1.8
TC28a2 Low Density	3700000	7.1
Saos-2 High Density	38000000	4.8
Saos-2 Low Density	4000000	1.3
Co-Culture High Density	40000000	0.91
Co-Culture High Density	3700000	7.8

Table 6-1: Average cell concentrations counter post-print and percentage error based on number of cells counted prior to print shown to 2 significant figures

Figure 6-5 below shows the percentage viability of the dissolved hydrogels using the Tali fluorescence counting method.

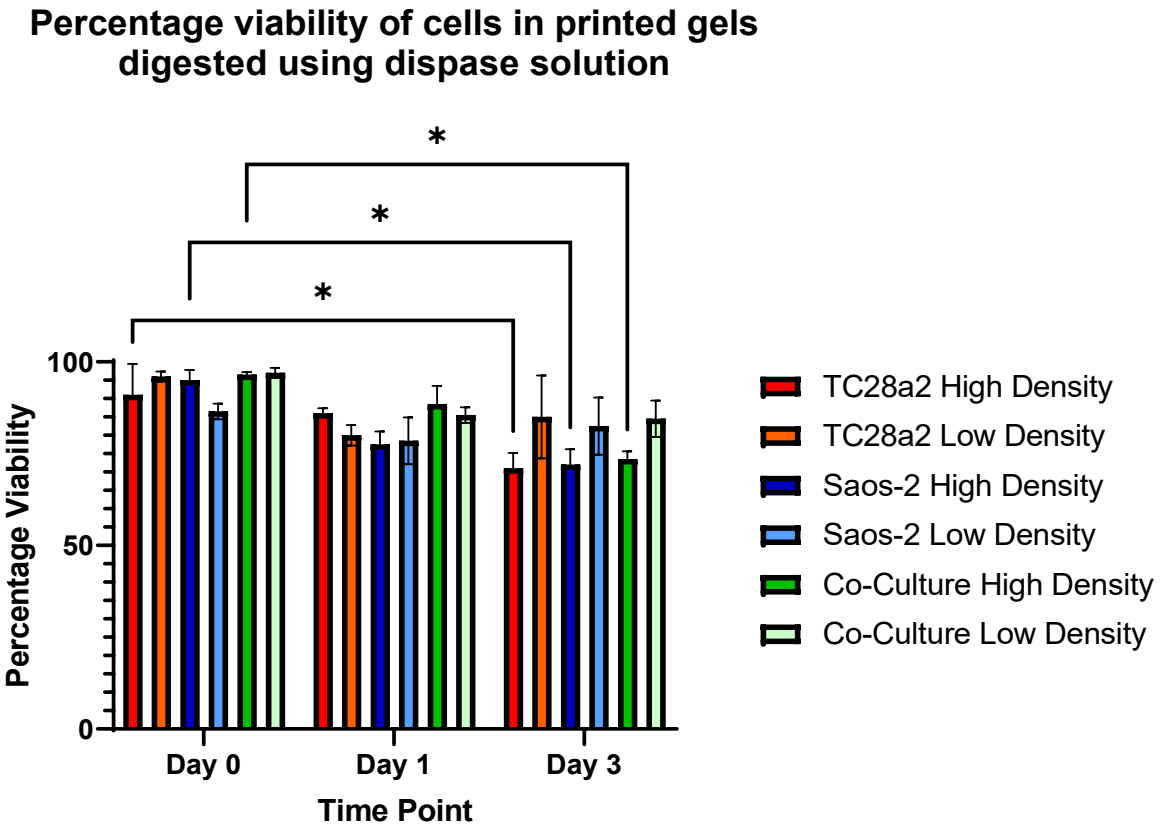

*Figure 6-5 The Percentage viability of cell filled 3D printed hydrogels, containing TC28a2, Saos-2 and TC28a2/Saos-2 co-cultures respectively, indicated by the percentage of counted live cells to total number of cells counted using the Tali cell counter and fluorescence stainings. Asterisks indicate the level of significance with alpha equal to 0.05, i.e. P ≤0.05 is represented by *, P ≤0.01 is **, P ≤0.001 is *** and P >0.05 is not significant and not represented on the graph.*

As can be seen in Figure 6-5 there is no Significant difference between the viability of any of the cell types, at any of the printed densities, at any of the time points. The only significant differences observed are between the high density gels at day 0 vs day 3 signifying that there is a significant decrease in viability in the high density gels after 3 days. However, this decrease occurs in all of the high density gels of all culture types indicating it is due to some feature of the high cell density gels. Furthermore in comparing the high cell density to low cell density gels of the same cell type at day 3 there is no significant difference.

Figure 6-6 shows the comparison between using the 3D (confocal microscopy) and 2D (digestion) analysis methods for assessing cell percentage viability in high density (a) and low density (b) gels.

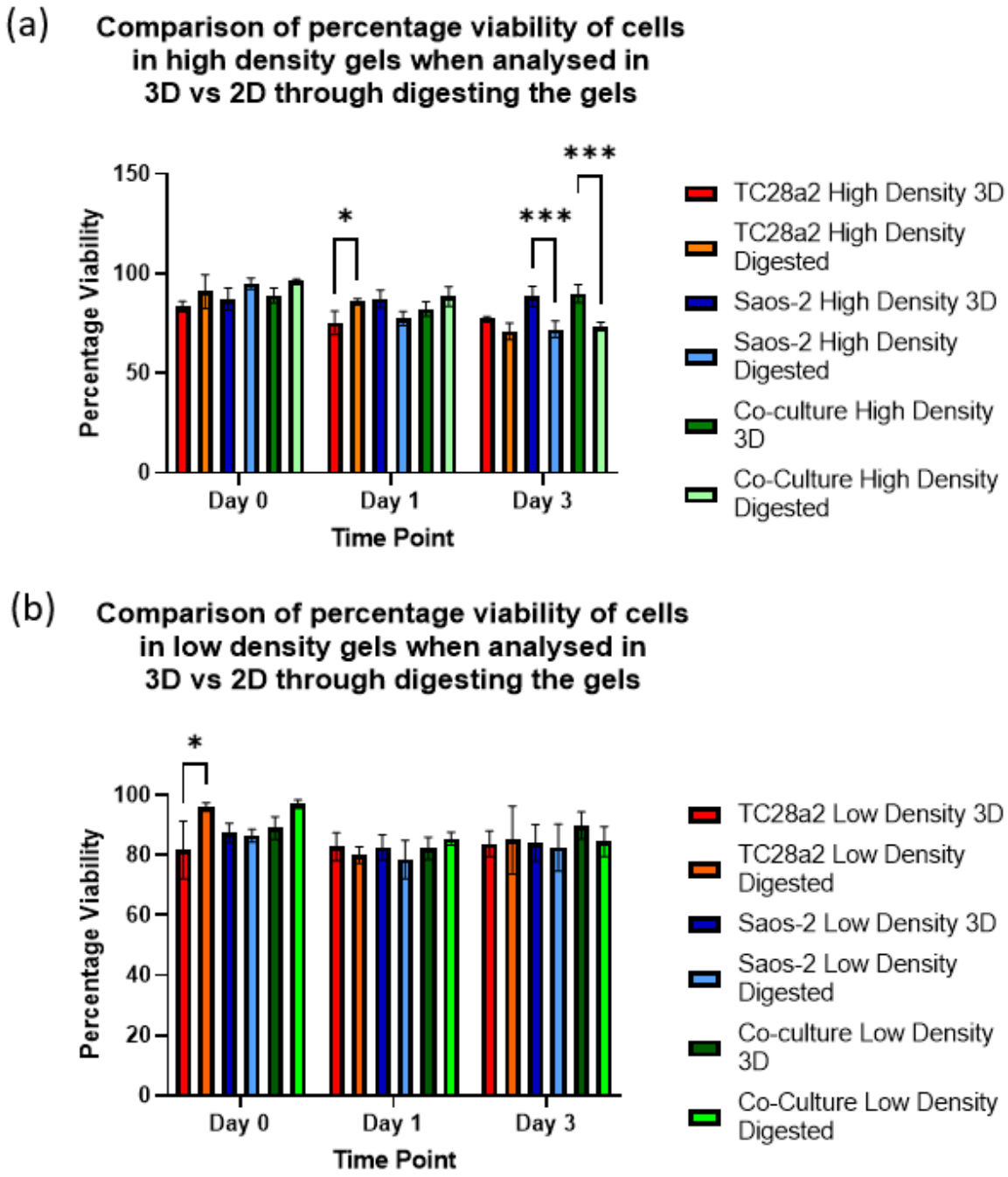

*Figure 6-6: Comparison between using the 3D (confocal microscopy) and 2D (digestion) analysis methods for assessing cell percentage viability in (a) high density and (b) low density gels. Asterisks indicate the level of significance with alpha equal to 0.05, i.e. P ≤0.05 is represented by *, P ≤0.01 is **, P ≤0.001 is *** and P >0.05 is not significant and not represented on the graph.*

6.4 Discussion

6.4.1 Live/Dead analysis using 3D confocal microscopy

It is worth noting that the two way ANOVA carried out on these results showed no statistically significant difference between the high and low density cultures at each timepoint, and so, statistically there is no significant drop in viability at the higher cell density.

The print viability results are overall very positive and show that gels do not appear to be harmed or affected adversely by the printing process. In all low density gels the percentage viability was higher than 80% at all time points. In the high density gels the viability was slightly lower but still higher than 75% in all cases. This may be due to the tenfold increase in cell density leading to an increase in viscosity and in turn the shear stress exerted on the cells during printing, or this may be due to increased competition in higher cell density prints. In addition to this, although the cell density has increased by tenfold, in most cases the percentage viability remains in excess of 80%. One reason for this is that an increase in cell density may lead to an increase in hydrogel stiffness which, if unrepresentative of the native tissue of the cell type analysed, may have a negative effect on viability. Lam et al. found that an increase in cell density resulted in a reduced viability in neuronal cultures for this reason [230], although as the viability in this case remains high, this is not thought to be an influencing factor.

In addition to this most samples seem to exhibit the same trend, that is that following an initially high percentage viability immediately after print, there is either no increase, or a slight dip in viability at day one. This then, in most cases this increases to the initial viability found at day 0, or in some cases in excess of this at day 3.

There are two main drawbacks with this method. The first of which is that it is only possible to analyse small areas of the gels at once, this means that samples had to be manually dissected and analysed at multiple points throughout the gel and the percentage viability is an average of the areas analysed. In order for this method to produce the most representative results possible for the entire gel samples had to be imaged both at the edges, and at various points throughout the centre of the gel. This does not appear to have effected the accuracy of the results and has in-fact helped to establish that there are no internal areas of necrosis, even in the high cell density prints, similar to those found within organoids.

The second drawback is that in the higher cell density gels at later timepoints when the cells begin to spread out through the gels it can become difficult to count individual cells due to the sear volume of the cells within the gels. As mentioned previously percentage viability can be assessed by instead analysing the volume of red to green occupied within the imaged volume however as the cells are spread out and occupying larger volumes, and as this is not a comparison of counted nuclei, this may not necessarily give very accurate results. For the purpose of the experiments carried out in this thesis the method of comparing volumes was not used and the 'spots' method was used exclusively however the accuracy of this could be improved. This is one of the reasons the live/dead analysis was also carried out on 2D dissolved gels.

6.4.2 **Live/Dead analysis using Hydrogel Digestion and 2D Fluorescence imaging**

The first advantage of using a method of gel digestion to count all of the cells within a printed gel is that it can establish, accurately, if the cell concentration within the gels is what was expected during the print process. Figure 6-4 shows that in all of the printed gels that were digested and analysed immediately after printing the cell concentration (cell/ml) were exactly what was expected. Clearly in the high cell density gels the standard deviation from the mean counted concentrations account for a much greater number of cells than in the low. However that was to be expected given that as the cell density increases this significantly, the error involved in in processes such as cell counting (both before and after printing) also increases. That said, the mean counted concentrations are still what was expected. In comparing the percentage error calculated using the cell concentration counted immediately after printing and the cell concentration counted prior to printing, the percentage error in the high cell density gels is actually lower than in the low cell density gels.

This is a significant result as it demonstrates the ReJI system is capable of printing 3D gel filled structures with a significantly high ($40x10^6$ cells/ml) cell concentration. Due to the complexities of printing cells at this concentration there are not a great deal of comparable studies however advances in extrusion bioprinters have allowed for the production of cartilaginous tissue by using 20×10^6 cells ml^{-1} nanocellulose bio-inks [231] or by adopting 40×10^6 cells ml^{-1} multi-material bio-inks [1]. What's more the ReJI can do this in an accurate drop by drop method and directly into multiwell plates, demonstrating the capability of the process for high throughput applications. There are very few if any processes that can reliably, and with a high rate of throughput 3D print cell laden gels and none (at the time of writing)

that can do this with gels of such high cellular concentration. This suggests that high throughput applications such as drug/toxicology testing could be a viable application for the ReJI process.

The second advantage of using the gel digestion method to analyse the cells within the gels is that the cells can be stained with fluorescent dyes and the percentage viability of all of the cells within the gel, not just those within a small area, can be counted. The results shown in Figure 6-5 are very positive. On day 0 the lowest average percentage viability is in the low density Saos-2 gels and this is 86.5%, which is still a very high viability for gels within hydrogels [232]. Additionally the day 0 results demonstrate that there is clearly no negative effect from the increased viscosity when printing solutions containing high cell concentrations as there is no statistically significant difference between any of the high and low density prints in any of the cell types immediately after print.

The cell viability remains high in all cases up until day 3 with the only significant drops in viability being in the high cell density gels from day 0 to day 3. The lowest average viability at day 3 is in the high density TC28a2 cultures however this is still above 70% which can be considered a high viability for cells within hydrogels [232]. Given that the results at day 0 do not demonstrate that the print process has an effect on the viability based on cell density, it is likely that the drop in viability at day 3 is due to the level of competition between the cells in the high density gels. Additionally, the fact that the low density gels do not also demonstrate a significant drop in viability reinforces this argument.

Figure 6-6 compares the results from using each of the two methods for the analysis of percentage viability. First looking at Figure 6-6 (b) there is only one statistically significant difference in results, this is in the TC28a2 cells at day one. There is no immediately obvious reason for why this may be, although the standard deviation in the results analysed using the 3D method is quite large the viability is still very high. There is no significant variation between any of the other results at any of the other time points in the low-density gels. When looking at the comparison of high-density gels in Figure 6-6 (a) the differences are more apparent. At day 0 whilst there are no significant differences between the methods, the average viability counted using the digestion method is higher than the average counted using confocal microscopy in all cases. This is the same at day 1 however this reverses at day 3 with the percentage viability counted in the Saos-2 and co-cultures using confocal microscopy being significantly higher than that counted using digestion. The reason for this is likely that

immediately after printing, cells are still spherical in morphology, with space between each cell. This makes cell counting using confocal microscopy easier, however by day 3, cells begin to change morphology and spread, there is less space between cells and they become very difficult to count using confocal microscopy and digital analysis techniques (see Figure 6-4). Likewise in low cell density gels cell morphology changes by day 3 (see Figure 6-3) however there is still sufficient distance between cells to allow for accurate counting, unlike in the high-density gels. However, when digesting the gels in order to count cells, this is never an issue. Additionally, using the confocal method is significantly more time consuming with the imaging of each gel sample taking 30-60 mins when compared to the 5 min analysis time using the digestion method, although it can take up to 2 hours for the gels to dissolve prior to counting, this is still faster if imaging gels in any significant number. Finally, the digestion method is significantly cheaper than the confocal microscopy method.

Ultimately this is a very positive result for the ReJI process as a whole as it shows the system can be used to print very high cellular density gels and maintain a high print viability. Furthermore it shows that all of the necessary cell types required for this project to produce an effective osteochondral co culture can be printed using the ReJI process with a high viability.

Chapter 7. The Effect of Cell Density on Maturation of 3D ReJI Printed Osteochondral Co-cultures

7.1 Introduction

The aim of this chapter is to investigate the efficacy of 3D printed CAF hydrogels as an *in vitro* 3D cell culture environment for osteochondral models. Building on the work from chapter 6, where it was established that high cellular density hydrogels could be printed effectively, this chapter seeks to analyse the effect of cell density (cells/ml) on the performance of these osteochondral models.

7.2 Study Design

3D hydrogels containing cells both in single cell culture and in co-culture were printed using the ReJI method. Stratified 'layered' co-cultures were printed in order to attempt to replicate a layered osteochondral interface as in the cell viability study.

Over a 14 day time period samples were assessed to determine levels of relevant indicators of ECM production within the gels, that include markers for assessing (1) bone formation, such as osteocalcin and osteopontin, and (2) cartilage formation, such as collagen II and aggrecan.

Further to this, the levels of collagen I and aggrecan found in the gel culture supernatant were measured quantitatively by ELISA to provide a quantitative measure of mineralisation and ECM production respectively.

Initially gels containing TC28a2 human chondrocyte cells and Saos-2 osteosarcoma cells were analysed. Osteoblasts and chondrocytes were chosen as they are common cell types found in the osteochondral interface. This is also why the co-cultures were printed in stratified layers, as this is more representative as an interface model, rather than having both cell types mixed in to one single gel. These particular cell lines were chosen because they are numerous, the fast growth rate is beneficial for *in vitro* models and as such these are commonly used for this purpose [233,234].

7.3 Results

7.3.1 Immunohistochemical Staining

The image results of the 2D immunohistochemical stainings for aggrecan and collagen II, carried out on 20 µm thick hydrogel sections of the $40x10^6$ cells/ml TC28A2/SAOS-2 hydrogel co-cultures, are presented below in Figure 7-1 and Figure 7-2. Figure 7-1 shows the

chondrocyte area of the co-culture and Figure 7-2 shows the osteoblastic area of the same gel at all timepoints. Images of hydrogels with other cell densities, cell types and staining combinations are shown in Appendix I.

Images in all cases show the presence of the relevant cartilage/ bone marker they have been stained for. Looking at the individual image channels (blue, green, red),it is clear that the staining process has been effective. It is apparent that the majority of cartilage and bone markers can be found surrounding cell nuclei, which is to be expected.

There does appear to be some increase in the concentration of cartilage and bone markers between day 3 and day 14 in all cases.

TC28a2 and Saos-2 Cell filled CAF Hydrogel co-cultures with printed cell density $40x10^6$/ml			
Timepoint	Day 3	Day 7	Day 14
Merged	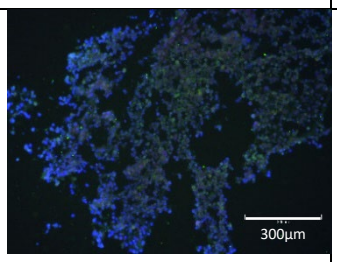	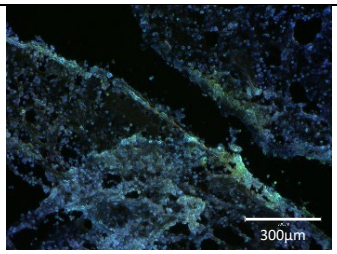	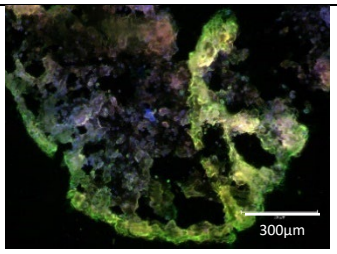
Hoechst	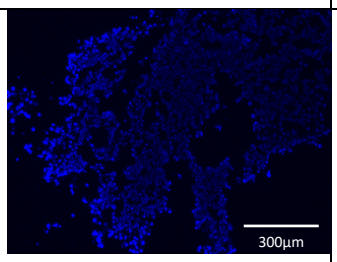	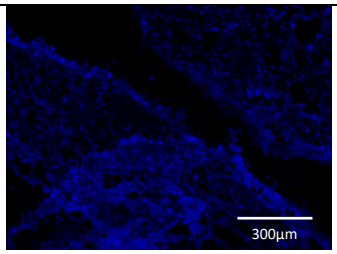	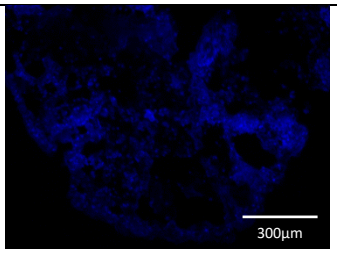
Collagen II	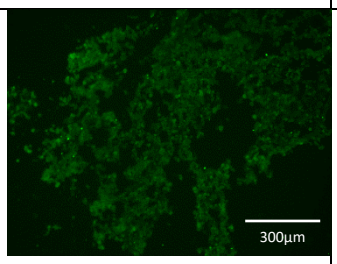	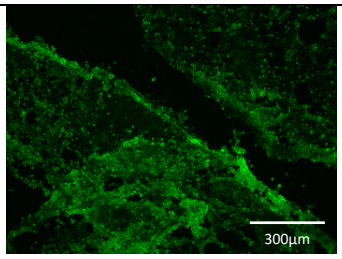	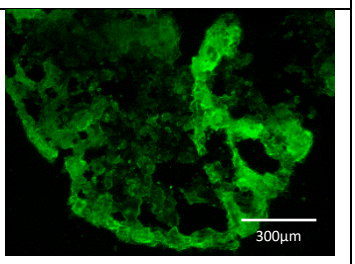
Aggrecan	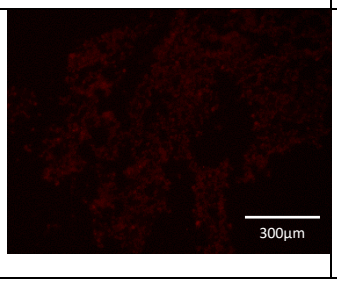	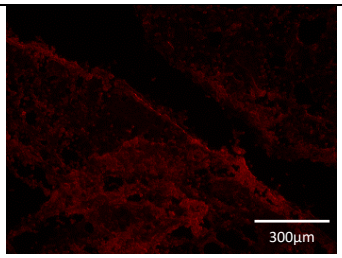	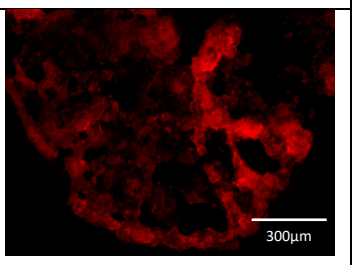

Figure 7-1: Immunohistochemical staining images of 20 µm thick hydrogel sections containing TC28a2 chondrocyte cells and Saos-2 osteosarcoma cells printed at a density of $40x10^6$ cells per ml of gel. Sections were stained to show the presence of cell nuclei (blue), Collagen II (green) and Aggrecan (red). Above images show the chondrocyte region of the gel co-culture.

TC28a2 and Saos-2 Cell filled CAF Hydrogel co-cultures with printed cell density $40x10^6$/ml			
Timepoint	Day 3	Day 7	Day 14
Merged	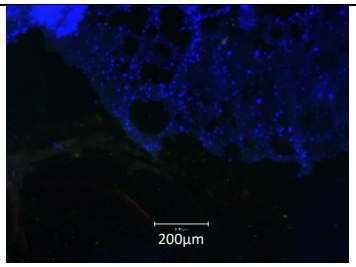	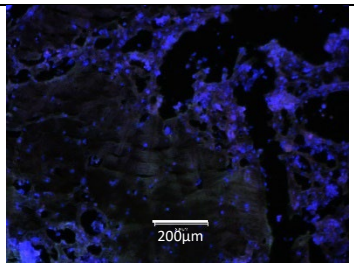	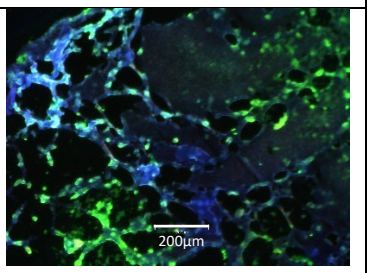
Hoechst	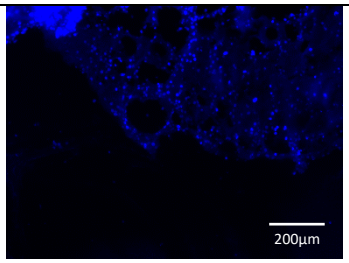	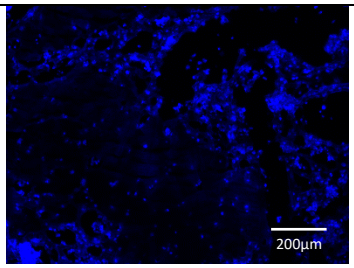	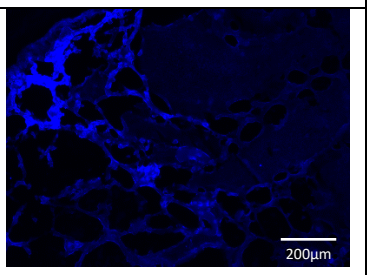
Osteocalcin	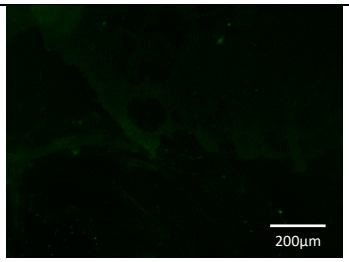	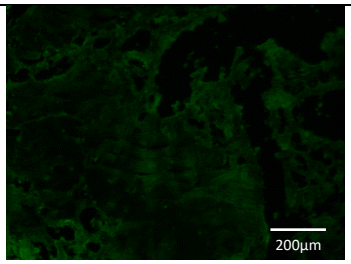	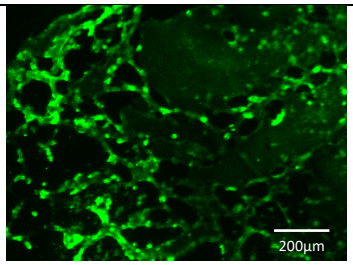
Osteopontin	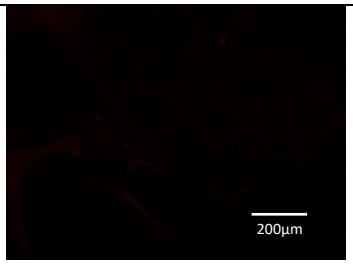	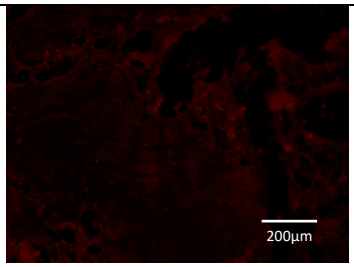	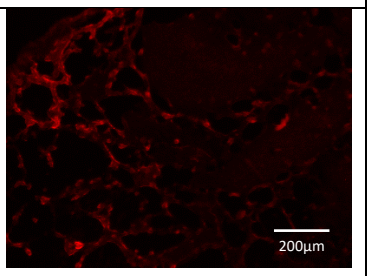

Figure 7-2: Immunohistochemical staining images of 20 µm thick hydrogel sections containing TC28a2 chondrocyte cells and Saos-2 osteosarcoma cells printed at a density of $40x10^6$ cells per ml of gel. Sections were stained to show the presence of cell nuclei (blue), Collagen II (green) and Aggrecan (red). Above images show the chondrocyte region of the gel co-culture.

7.3.2 **Mineralisation**

Figure 7-3 shows the alizarin red stained gels after 7 and 14 days of incubation. At day 7 only a few traces of staining can be seen. However, at day 14 in both samples there is some mineralisation beginning to take place. These can be seen from the red/purple staining that appears to be forming around ridges and features in the gels indicated by the arrows in the image.

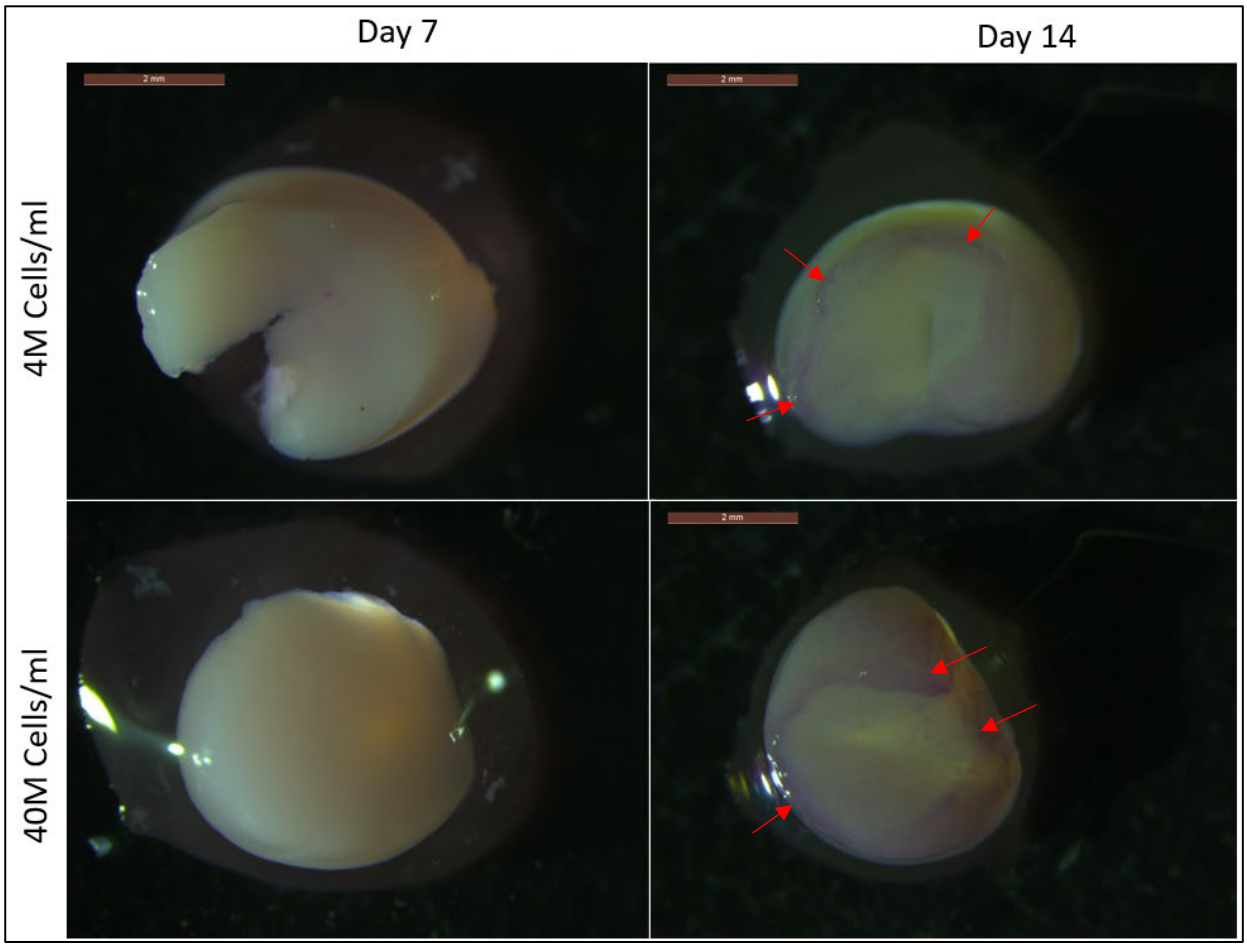

Figure 7-3: Saos-2 printed gels of 40x10^6 Cells/ml and 4x10^6 Cells/ml print density stained with alizarin red to show mineralisation at Day 7 and Day 14 after print. Arrows indicate areas of concentrated staining

Figure 7-4 and Figure 7-5 show a dyed low and high density Saos-2 gel respectively at day 14 at higher magnifications. It is apparent to see that there is mineralisation occurring at day 14, that is more evident in the high cell density samples than in the lower density samples.

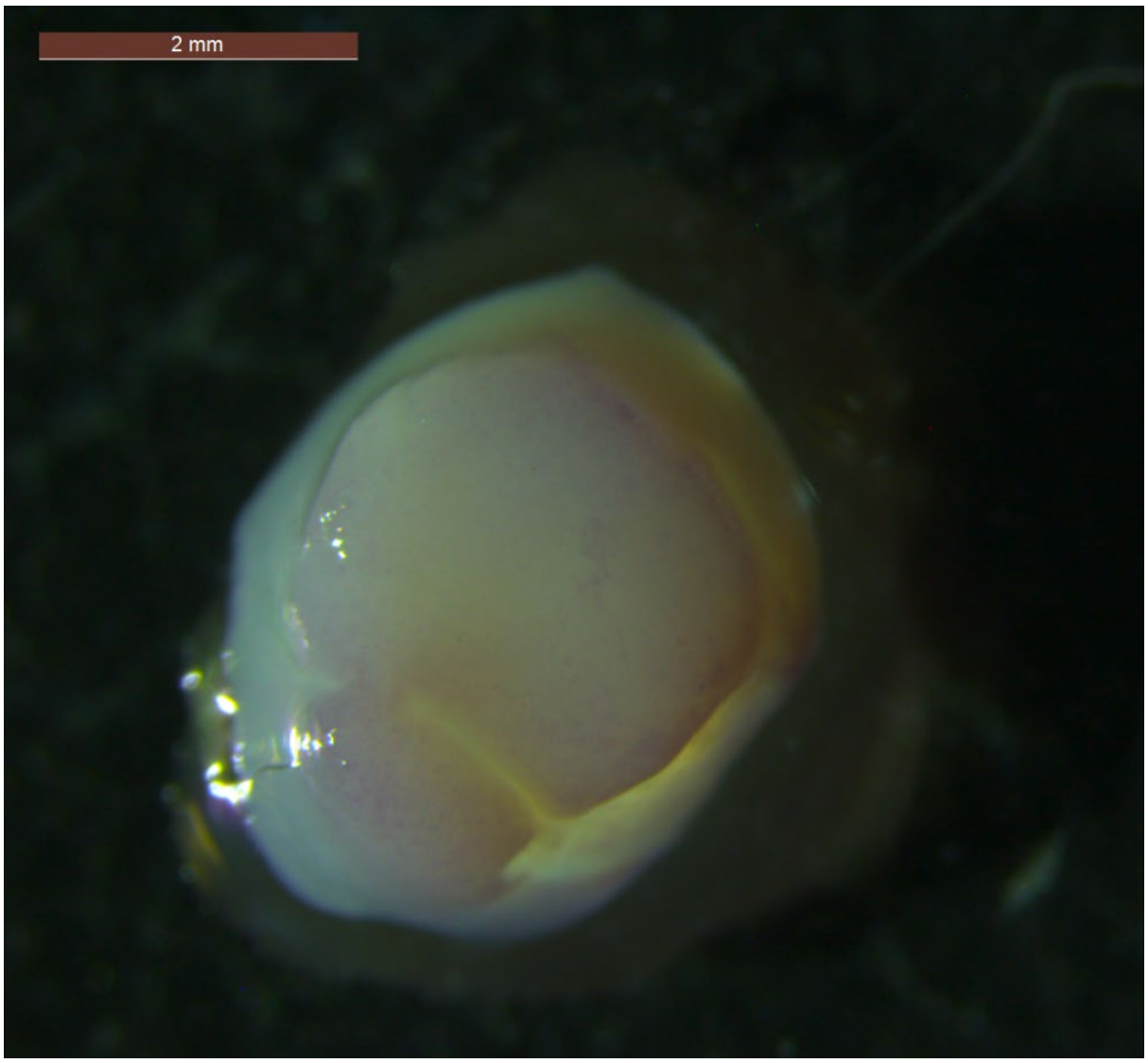

Figure 7-4: Saos-2 printed gel of 4x10^6 Cells/ml print density stained with alizarin red to show mineralisation at Day 14 after print.

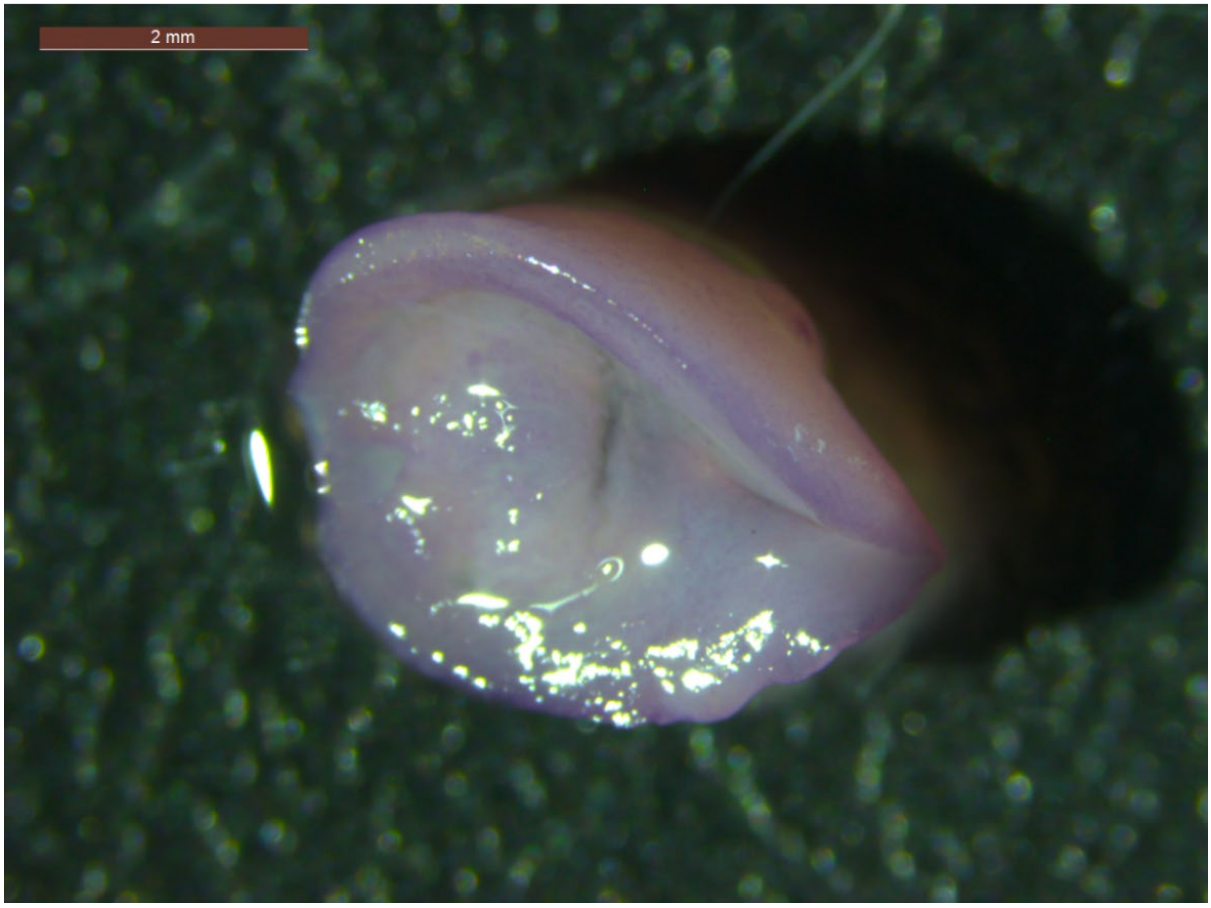

Figure 7-5: Saos-2 printed gel of 40x10^6 Cells/ml print density stained with alizarin red to show mineralisation at Day 14 after print.

7.3.3 **Human Collagen I ELISA**

Figure 7-6 shows the HCol1 (human collagen I) concentration for all culture types at day 3, 7 and 14. For simplicity, only pairwise comparisons between samples of similar density or cell type at each timepoint (i.e. high density vs high density or High density TC28a2 vs low density TC28a2), and comparisons between similar culture types at different timepoints (i.e. Day 3 high density TC28a2 vs Day 14 High density TC28a2) are displayed on the chart. A baseline correction has been performed using media taken from an acellular gel as the control.

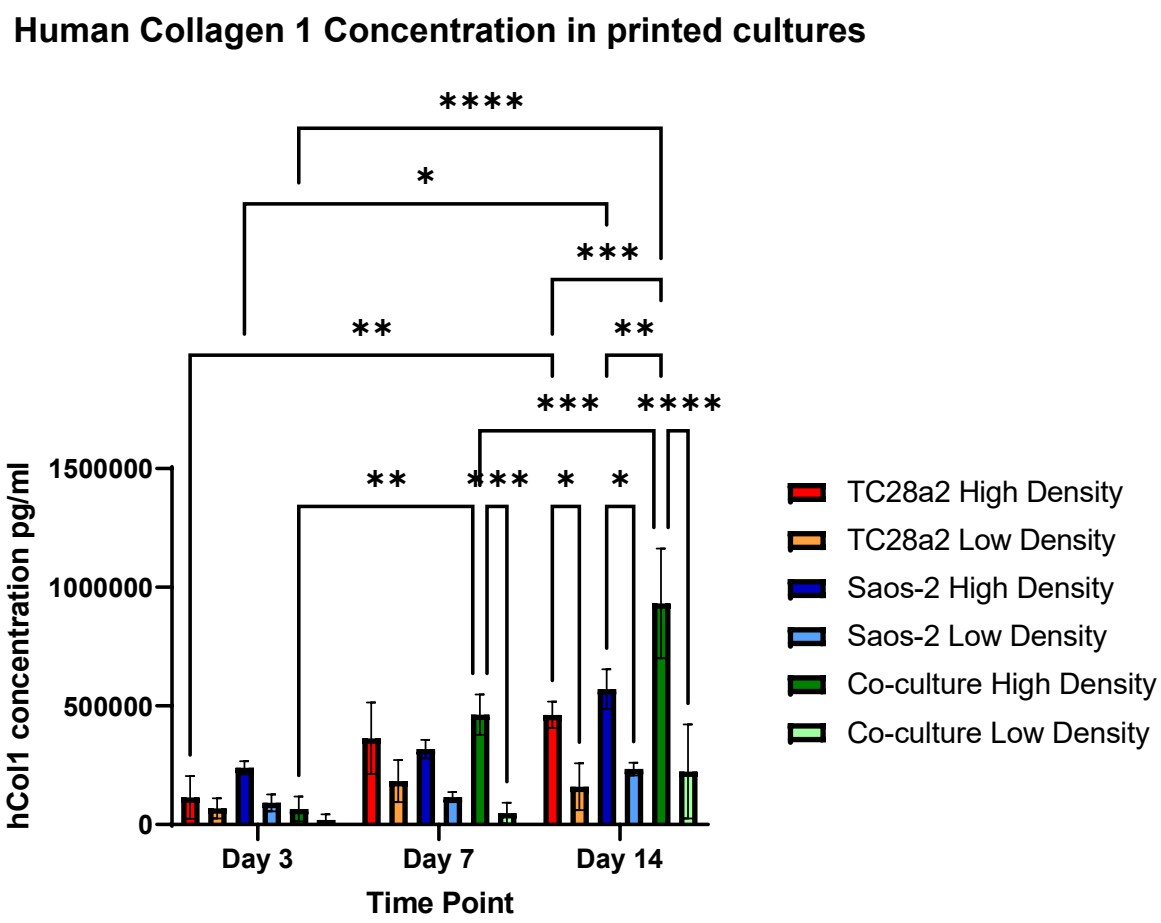

*Figure 7-6: HCol1 concentration measured in pg/ml in the supernatant removed from hydrogel cultures containing Tc28a2 chondrocyte cells, Saos-2 osteosarcoma cells and co-cultures of both, with printed cell densities of 40x10^6 cells/ml (high density), 4x10^6 cells/ml (low density) at day 3, day 7 and day 14 after printing. Asterisks indicate the level of significance with alpha equal to 0.05, i.e. P ≤0.05 is represented by *, P ≤0.01 is **, P ≤0.001 is *** and P >0.05 is not significant and not represented on the graph.*

All culture types exhibit an increase in HCol1 as time in culture progresses as was hypothesised.

In the case of the low density TC28a2 cultures, based on the statistical analysis at day 7 and day 14 there is no statistically significant change in the collagen concentration, i.e. ECM formation has 'levelled out' rather than continuing to increase as it does in the high density samples.

In all cases the high density cultures contained a higher HCol1 concentration that the corresponding low density cultures. Additionally, at day 7 all of the high density cultures

display a statistically similar HCol1 concentration, however at day 14 the concentration found in the high density co-cultures is significantly higher than that found in any other culture type. At day 14 all of the low-density cultures exhibit a similar HCol1 concentration. The high density co-cultures are the only culture type that exhibit a significant increase between each timepoint.

7.3.4 **Aggrecan ELISA**

Figure 7-7 shows the Aggrecan concentration for all culture types at day 3, day 7 and day 14. For simplicity, only pairwise comparisons between samples of similar density or cell type at each timepoint (i.e. high density vs high density or High density TC28a2 vs low density TC28a2), and comparisons between similar culture types at different timepoints (i.e. Day 3 high density TC28a2 vs Day 14 High density TC28a2) are displayed on the chart. A baseline correction has been performed using media taken from an acellular gel as the control.

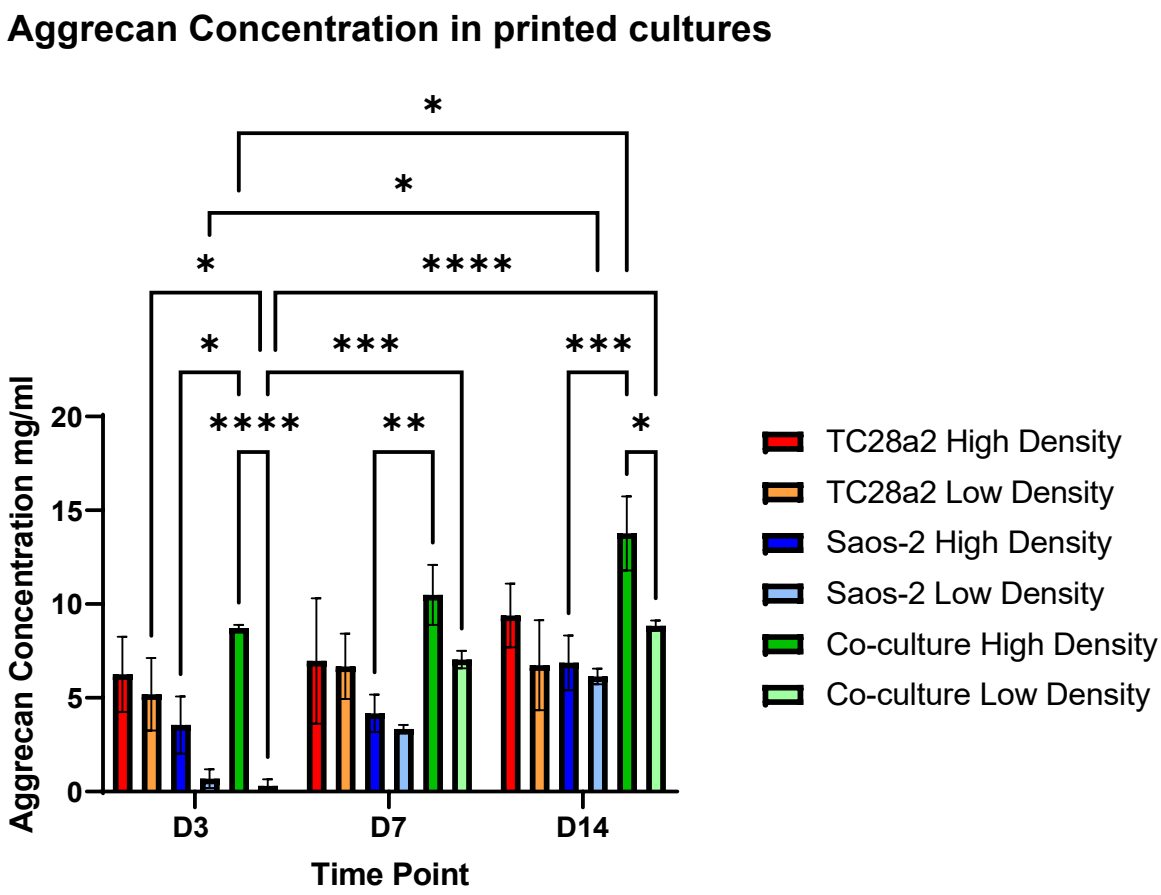

*Figure 7-7: Aggrecan (PG) concentration measured in mg/ml in the supernatant removed from hydrogels containing TC28a2 chondrocyte cells and Saos-2 osteosarcoma cells, and co-cultures of both with printed cell densities of 40x10^6 cells/ml (high density), 4x10^6 cells/ml (low density). Asterisks indicate the level of significance with alpha equal to 0.05, i.e. P ≤0.05 is represented by *, P ≤0.01 is **, P ≤0.001 is *** and P >0.05 is not significant and not represented on the graph.*

In all cases some amount of aggrecan is detected. This is higher in the high density samples and lower in the low density samples. The co culture samples exhibit a higher concentration than the monoculture samples and this trend is visible in both high and low cell density cultures. The TC28a2 cultures exhibit a higher average concentration than the SAOS-2 samples, likely because aggrecan is more of an indicator of cartilage production than mineralisation.

7.3.5 **Gel mass retention**

Figure 7-8 shows the average mass of the gel cultures weighed at days 0, 3, 7 and 14. For clarity significance is illustrated only for high density/low density comparisons with a single

cell type at each timepoint. However a two way anova has also been carried out as well as multiple comparisons between all samples using Tukey's multiple comparisons test. As it is not indicated on the graph it is also worth mentioning that the drop in average mass for each culture type when comparing day 0 and day 14 is significant in each case with all of the differences having a P value of less than 0.0001.

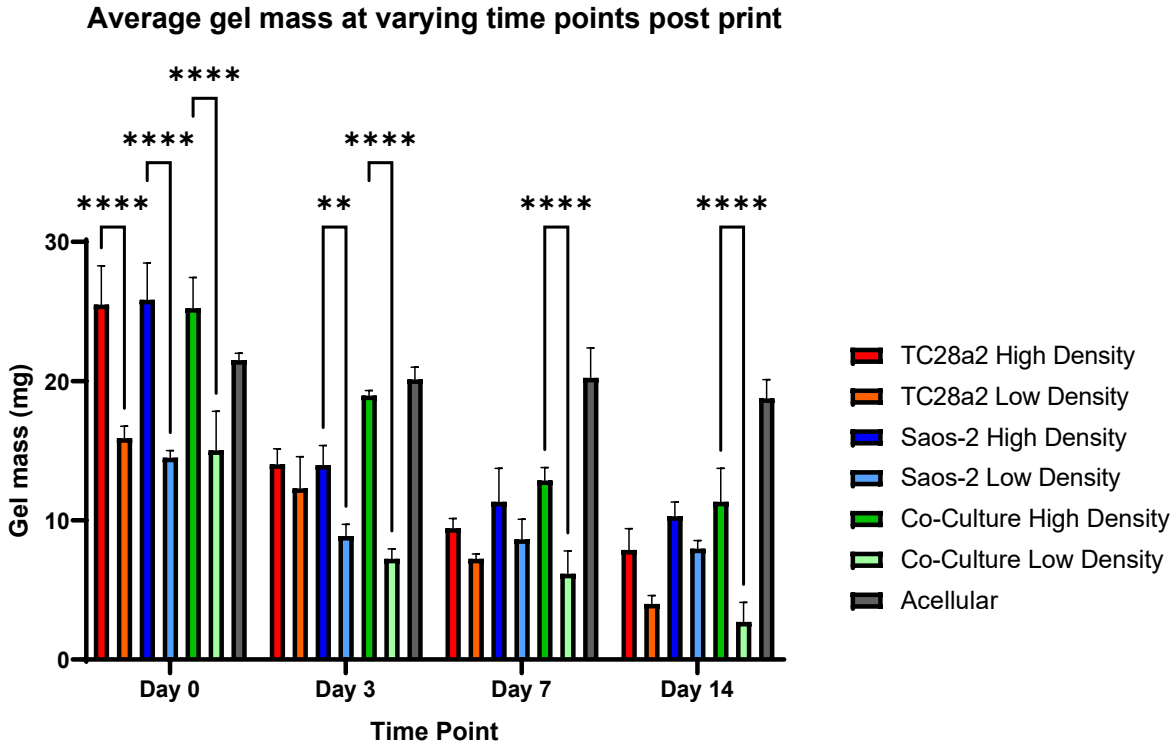

*Figure 7-8: Average gel mass immediately after print and at days 3. 7 and 14 post print. For clarity significance is illustrated only for high density/low density comparisons with a single cell type at each timepoint. Asterisks indicate the level of significance with alpha equal to 0.05, i.e. P ≤0.05 is represented by *, P ≤0.01 is **, P ≤0.001 is *** and P >0.05 is not significant and not represented on the graph.*

The results clearly indicate that the cellular gels lose mass and break down significantly over a two-week period. The high cellular density gels are heavier immediately after print and throughout the two-week time period the high cell density gels remain heavier than their low density counterparts. Conversely the acellular gels remain a similar mass across the two week period with no significant decrease in mass or gel size. On day 0 all of the gels are of a similar size, however Figure 7-9 shows a comparison of TC28a2 and Saos-2 high and low density gels against two acellular gels at day 7 and the decrease in volume of the gels is apparent, with the low density gels (centre) reducing in volume significantly more than the high density gels.

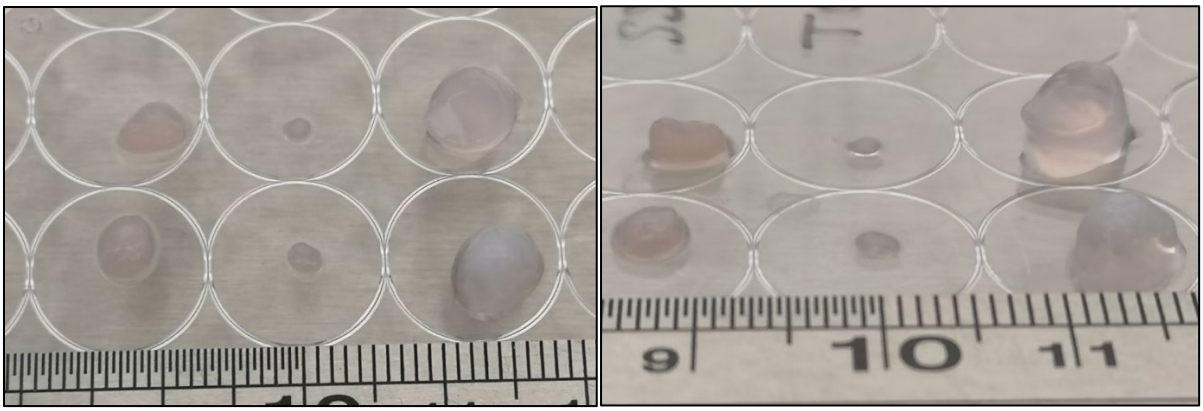

Figure 7-9: Left hand image shows - TC28a2 high cell density gel (top left), TC28a2 low density gel (top centre), Saos-2 high density gel (bottom left), Saos-2 low density gel (bottom centre) and two acellular gels (top right and bottom right) 7 days after print. Right hand image shows the same gels from a different elevation to demonstrate gel height

Figure 7-10 shows the Young's modulus of the cell laden hydrogel cultures at day 1, day 3 and day 7 time points. For clarity significance is illustrated only for high density/low density comparisons with a single cell type at each timepoint. However a two way ANOVA has also been carried out as well as multiple comparisons between all samples using Tukey's multiple comparisons test. Not indicated on the graph is that all culture types display a significant increase in their Youngs modulus between days 1-7 and between days 3-7 with a P value of less than 0.0001 in all cases. There is no significant difference between high and low cell density in any of the cell types at any of the time points with the exception of the co-cultures at day 7 wherein the high-density co-culture has a significantly higher Young's modulus than the low. However the average Young's modulus is lower in the low density gels than in the high density for all cell types. The acellular gel exhibits no significant change and at day 7 it is significantly lower than all other culture types with a P value less than 0.0001 in all comparison cases. The significant increase in Youngs modulus from day 3 to day 7, particularly in the high cell density gels demonstrates that the presence of the cells, and additionally the cell density has a significant effect on the Young's modulus of the gels.

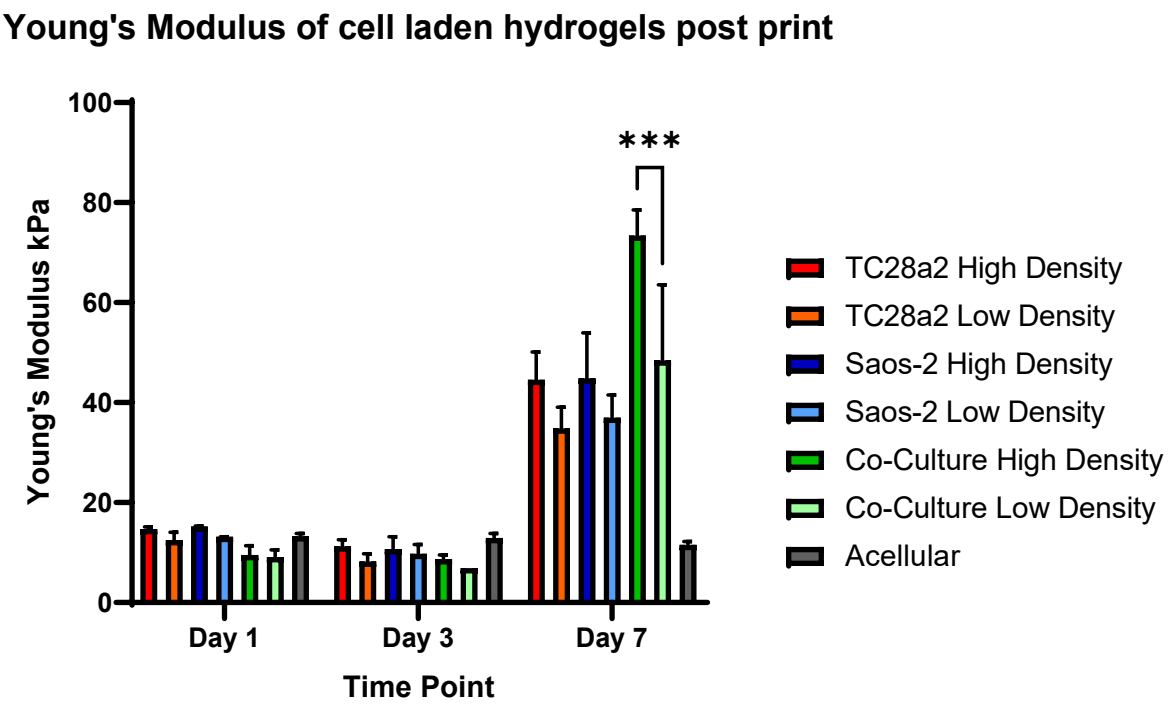

*Figure 7-10: Young's Modulus of cell laden hydrogels at days 1. 3 and 7 post print. For clarity significance is illustrated only for high density/low density comparisons with a single cell type at each timepoint. Asterisks indicate the level of significance with alpha equal to 0.05, i.e. P ≤0.05 is represented by *, P ≤0.01 is **, P ≤0.001 is *** and P >0.05 is not significant and not represented on the graph.*

7.4 Discussion

A number of different time points were considered in order to evaluate the ECM formation in the bioprinted constructs. Particularly, days 3 and 7 were chosen to assess if there would be any early ECM formation in the gels, due to the effect of increased cell density or the influence of cells in co-culture. Day 14 was the timepoint at which it was expected that ECM may likely be detected as ECM production usually takes place over a timescale of the order of several weeks [235,236].

7.4.1 Immunohistochemical staining

TC28a2 chondrocyte laden gel samples were stained for collagen II and aggrecan. These were chosen as collagen II and aggrecan are ECM components that are both found in abundance in cartilage and act as cartilage markers [237,238]. It can be assumed that if the gels are functioning as an effective 3D culture environment for the chondrocyte cells then an ECM will begin to form, and cartilage markers will be produced and detectable. Similarly, osteocalcin and osteopontin are bone markers and detecting them in the osteoblast cultures would suggest that the osteoblasts are functioning correctly.

Most of the sectioned samples show some evidence of either cartilage or bone markers at day 3. This may be because the staining was able to penetrate through the thinner sections easier than through the 3D gel, although it is more likely a function of the imaging process. It is easier to image in greater detail a thin section than an opaque 3D gel, so this combination of more effective imaging and staining is likely to give a more accurate estimation of the distribution of cartilage and bone markers within the gel.

In all samples cartilage and bone markers are more prominent in areas where there is a higher concentration of cells, this would be expected as this is where ECM formation is likely to begin [239]. Additionally, it would appear that there are less cartilage and bone markers present in the day 3 samples than in the later day 7 and Day 14 samples. The day 14 samples appear to have the highest concentration of cartilage and bone markers and it appears that there is a higher concentration in the higher cell density prints than in the low. Also it would appear that in almost all cases the co-culture samples have a higher concentration of cartilage and bone markers than in the corresponding single cell type culture with the only possible exception being the high density TC28a2 laden cells appear to have a greater amount of collagen II and aggrecan expressed at day 3 than in the high density co-culture at day 3. However, this difference is likely to be minimal. It is significant that at day 7 both high and low density co-cultures have produced collagen II and aggrecan, the higher density gels showing a much larger amount of both. This is a significant finding as this type of aggrecan production in a chondrocyte laden hydrogel is often not observed until much later timepoints. For instance Skaalure et al. in their study of aggrecan production in chondrocytes in PEG hydrogels seeded a similar Density of cells (50M cells/ml) manually on to gels. The levels of aggrecan found in their studies at week 6 seems to correspond in the high density TC28a2 samples at day 7 [240].

It is clear from the images that the high density gels have produced more ECM than the low density gels which very clearly shows that printing gels with a higher cell density is more likely to lead to the faster production of mature cartilage tissue. At day 14 it is difficult to interpret if there is a difference between the high density co-cultures and the high density single cell gels, although it can be seen from the day 7 images that the co-cultures begin to produce both collagen II and aggrecan faster. However, it is clear from these results that the seeded cell density is important in ECM production with the higher density gels being more effective. Furthermore, studies of ECM production in hydrogels usually do not detect significant levels at such early timepoints, with studies usually taking place over at least several weeks

[235,236,241]. This early ECM production shows that the gels are a suitable culture medium for the rapid production of mature tissue.

Another observation is that in most cases, at earlier timepoints cells appear to just be arranged in clumps or clusters with no real organisation. However, at later timepoints there is a clear structure between areas containing cells. Cells appear to be linked in strands, or web like formations containing large areas of visible porosity. This may be because as cells begin to arrange themselves within the gel and form ECM they do so in such a way that nutrients from culture media can diffuse through the gel and reach all of the cells. This may account for the reason that there were no large areas of necrosis, or 'necrotic cores' similar to those found in organoids found in the sectioned gels. The fact that cells are able to move freely enough within the gel to reorganise themselves to grow as efficiently as possible truly demonstrates the efficacy of the CAF hydrogels as a 3D cell culture scaffold. Figure 7-11 demonstrates this well, Figure 7-11 (a) shows a low density co-culture after 3 days in culture, there is some porosity in the gel and cells are beginning to organise but are largely unstructured and spread evenly throughout, at day 14 (Figure 7-11 (b)) the cells are clearly organised along collagen fibres that have formed within the gel and surrounding almost all cell nuclei is the visible presence of aggrecan. Anseth et al. have observed similar gel migration patterns in PEG gels with cells starting off spherical in shape immediately after seeding and extending their morphology as they move through the gels and proliferate [109] however cell movement in 3D is still an area of considerable interest as it differs significantly from 2D cell behaviour.

Finally the control images shown in Figure 7-2 clearly show that formulation of cartilage ECM markers appears to be most prominent in areas containing chondrocytes and not in the osteoblastic region, and although there is some indication of collagen and aggrecan formation by day 14 this may be due to the gradual migration and mixing of cells through the gel causing cartilage ECM to begin to be formed in all regions.

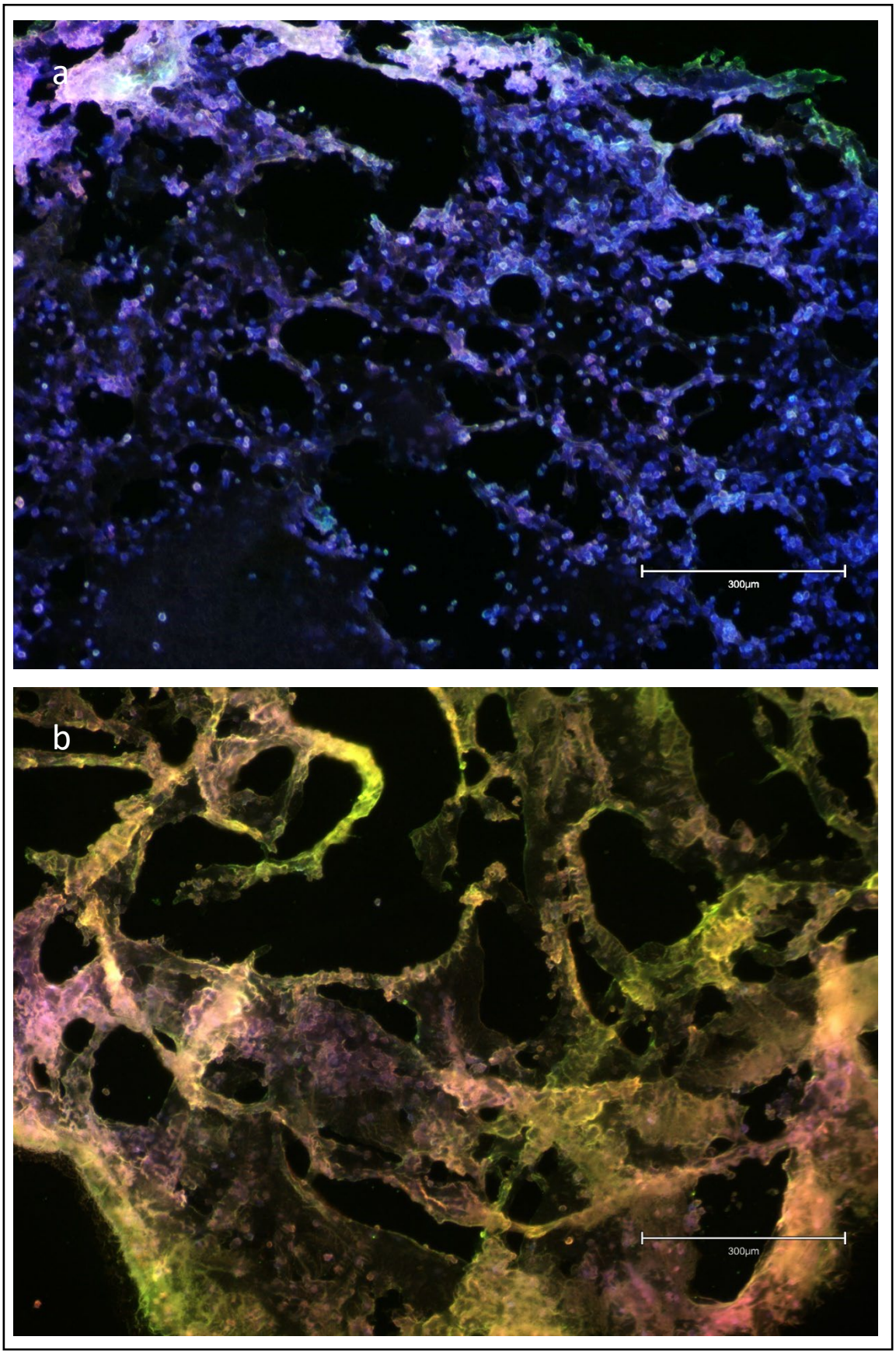

Figure 7-11: TC28a2 and Saos-2 co-culture printed with a cell density of 4x10^6 cells/ml at day 3 (a) and day 14 (b), stained with Hoechst 33342 (blue), and for Collagen II (green) and Aggrecan (red) (individual filter images can be seen in Figure 11-6)

Interestingly, although increased cell density seems to have an effect on the amount of ECM markers produced, it does not necessarily appear to have an impact on cell organisation. In fact it would appear that in the lower density gels the cells begin to organise along the fibres earlier whilst in the higher cell density gels, the gels still appear to form a fibrous structure, but the cells remain in highly populated clusters. Figure 7-12 shows gels stained with Hoechst and for collagen II and aggrecan at day 7. The gel co-cultures appear to show a greater presence of collagen II and aggrecan than the single cell culture gels in both high and low density, however the low cell density gels clearly show greater organisation along fibres. This is likely due to the cells in the low cell density gels having greater mobility within the gels, as they are not fully surrounded by other cells they are able to degrade their local matrix and spread further, unlike the cells in the high density gels [109].

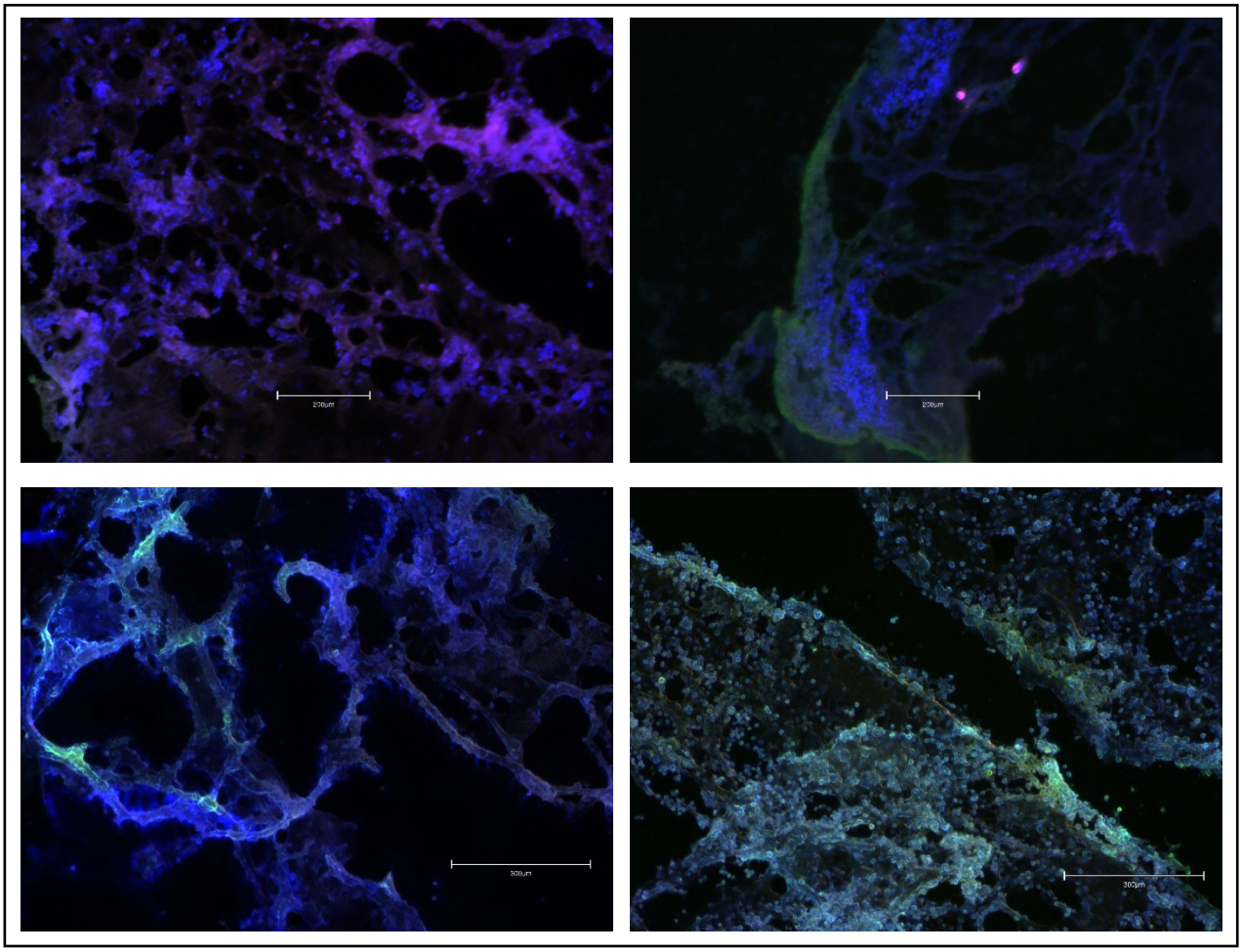

Figure 7-12 Low density TC28a2 culture (top left), High density TC28a2 culture (top right), Low density TC28a2 and Saos-2 co-culture (bottom left) and High density TC28a2 and Saos-2 co-culture (bottom right) at day 7 stained with Hoechst 33342 (blue), and for Collagen II (green) and Aggrecan (red)

Based on the results presented it would appear that the printed cell density relative effect on the rate that ECM formation occurs, i.e. as the cell density increases so doe sthe ECM production. This is likely because there are more cells in close contact acting together. This can be seen both when comparing the results for each time point but also in that the indicators of ECM formation are found in timepoints as early as day 3 and day 7. As stated previously it was not expected that bone and cartilage markers would be detected at these early timepoints as these are usually not usually detected in significant levels until later timepoints. However, the presence of these markers demonstrates all cell types growing effectively and producing ECM in the gels. Additionally, the cell growth does not appear to be impaired in the stratified co-cultures examined. In fact, in the co-cultures the production of ECM appears to be accelerated when compared to the single cell cultures of similar cell density. There are few studies that directly compare the influence of cell concentration on the rate of ECM

production, and this field is further narrowed when considering these are 3D printed cultures with cells suspended in natural hydrogels. Assessing the effect of cell density on ECM production, specifically high cell densities (greater than $1x10^7$) with an effective repeatable bioprinting method certainly demonstrates the novelty and effectiveness of the ReJI bioprinting system.

It is worth noting that no additional growth factors were added to the cell culture medium in any of these experiments. In further studies it would be interesting to assess the effect on the addition of growth factors for example TGF-β3, as this is widely believed to aid in early and rapid mineralisation and cartilage formation respectively [242–244]. Instead, the effect of printed cell density as well as the effect of growing cells in co-culture was prioritised. This could be explored in future work.

7.4.2 **Mineralisation**

Calcium deposits and mineralisation are one of the main indicators of *in vitro* bone growth [245]. In this study the gels were monitored over a 14 day period to remain consistent with the time points used in the ECM production experiments. Similar studies concerned with the rate of mineralisation of osteoblasts study samples over a longer time frame, often between 3 and 8 weeks as it can take longer of signs of mineralisation to appear [246,247].

From the samples shown in Figure 7-3 in the first 7 days there is no significant visible mineralisation. However, at day 14, in both the high and low density prints there are visible deposits of stained calcium where mineralisation is occurring. Calcium deposits such as this do not usually present in similar growth scaffolds and culture environments until significantly later timepoints [246,247] and so detecting calcium deposits at such an early time point shows that the CAF gels provide a suitable culture environment for the osteosarcoma cells and allow for bone formation. Based on Figure 7-4 and Figure 7-5, it could be argued that in the higher cell density prints, there is a slightly higher concentration of calcium than in the lower density prints. Whilst it appears that there are more areas of stained mineralisation, this is difficult to interpret. However, the fact that there is any mineralisation apparent in either of these gels, especially the lower cell density gel, at such early time points suggests that the CAF gels are a very suitable growth scaffold for the Saos-2 cells. The calcium deposits also appear to form in higher concentration around ridges, edges and features such as defects or pits in the gels, suggesting that cells may prefer to grow on or around these features. This may suggest that

with the introduction of additional mechanical features to the gel, i.e. culturing the gel onto a hard porous scaffolds, or meshes, mineralisation will occur earlier.

7.4.3 **ELISA analysis**

7.4.3.1 HCol1 ELISA

The ELISA results clearly indicate that as culture time increases so does the HCol1 concentration inferring that as culture time increases so does the quantity of ECM formed by the cells, which corroborates the results found in the immunohistochemistry images.

The results also strongly support the fact that as the cell density increases, so does the rate of ECM production, indicating that the fastest way to produce mature 3D printed tissue is to print with the highest cell density possible.

Additionally, based on the HCol1 concentration, the formation of ECM in co-cultures is vastly greater than that found in the single cell cultures. Moreover at day 14 the high density co-culture is significantly higher than all other high and low cell density cultures, highlighting that the co-cultures produce ECM as a much faster rate than most of the single cell cultures. This supports the evidence found in the immunohistochemical images suggesting that when the TC28a2 and Saos-2 cells are grown in stratified co-culture, they produce more ECM and do so at a greater rate. This not only demonstrates that the 3D printed CAF gels provide a suitable 3D growth environment for the chondrocytes and osteoblasts individually but that they also facilitate interaction between the two cell types which allows them to grow and form ECM quicker, more effectively and in greater quantity.

It is worth noting that although the difference in cell seeding density between high and low cell density cultures is tenfold, the difference in HCol1 detected between high- and low-density cultures is not. There may be a number of reasons for this however the most likely reason is that the HCol1 is detected in the culture media and has been excreted from the gel, it is not a measure of the amount of HCol1 found within the gel. The amount of HCol1 excreted from the gel is unlikely to be just governed by cell density and gel volume but also the gel surface area, which remains the same for both high and low cell density cultures. It could also be argued that the cell activity and as a result amount of ECM produced is also governed by confluence level of the cells, i.e. the more overconfluent the gels are the less ECM the cells will produce [248] however as the levels of HCol1 continue to increase at day 14 in the high

density gels in all samples, this appears to be unlikely. It is more likely that the amount of collagen released into the media is a function of gel surface area.

Finally, addressing the decrease in HCol1 concentration from day 1 to day 7 in the high density Saos-2 cultures relative to the TC28a2 cultures. One possible explanation, as mentioned above is that immediately after print cells begin to proliferate and in doing so produce greater amounts of ECM, after 7 days this proliferation begins to slow down as gels become over confluent and gradually as dead cells begin to remove themselves from the gels cells are then able to continue to proliferate and produce ECM. However, as discussed above, this seems unlikely, and what is more anomalous is the significantly high level of HCol1 detected at day one in the Saos-2. This may just be due to the particular behaviour of the osteosarcoma cells. Another, more likely explanation for this may be simply that bone markers such as collagen I are produced at a slower rate than cartilage markers, the alizarin red mineralisation staining seems to support this as significant mineralisation was not detected until day 7, this is supported in literature where significant amounts of bone markers are not observed in similar culture studies for up to several weeks. This would also explain why the Saos-2 collagen 1 production overtakes that of the TC28a2 cells by day 14. It would be expected that a greater concentration of HCol1 would be detected in the osteoblast cultures than in the chondrocyte cultures as the HCol1 functions as more of a bone marker than that of cartilage and this goes some way to support that.

7.4.3.2 Aggrecan (PG) ELISA

Based on the data presented in Figure 7-7 it is clear that the factor that has the largest impact on aggrecan production is the growth of cells in co-culture. Whilst at all timepoints the average aggrecan concentration in the high density cultures is always higher than the corresponding low density cultures, this difference is not significant in any cases with the exception of the co-culture samples. The aggrecan detected in the high density co-culture samples is significantly higher than the corresponding low density samples at both days 1 and 14, additionally it is significantly higher than the aggrecan found in the Saos-2 high density samples at all timepoints but never significantly higher than that found in the TC28a2 samples.

It was hypothesised that the TC28a2 samples would have a higher concentration of aggrecan than the Saos-2 samples, as aggrecan is more of an indicator of cartilage production than mineralisation, meaning it is more likely to be found in the chondrocyte supernatant than in the osteoblast. However, it is interesting that the co-cultures exhibit higher aggrecan

concentration that the chondrocyte cultures. This clearly indicates that cells growing in 3D co-culture begin to form greater amounts of ECM at a greater rate. This reinforces the findings in the immunohistochemical images.

When comparing high- and low-density samples it is clear that there is a greater concentration of aggrecan in the high cell density samples. Whilst the difference does not reflect the 10 fold difference in cell density, as stated previously this is likely to be influenced by the surface area of the gel. The ELISA does at least show that the high-density gels deposit more aggrecan (PG) into the supernatant, which shows they are producing a greater amount of ECM.

Additionally the concentration of aggrecan collected in all samples is high, significantly higher than that found in similar studies of cell laden hydrogels [249,250] and in some instances even comparable to levels of aggrecan detected in serum extracted from the human Supraspinatus Tendon which is approximately 4.2 µg/ml [251]. Again this clearly demonstrates the effectiveness of the CAF hydrogels for supporting high cell density 3D cell culture and the importance of seeded cell density in these cultures.

7.4.4 **Mass retention**

It is clear from the mass retention results that the breakdown of the CAF gels is related to the presence of cells. The acellular gels exhibit no significant loss of mass over the entire two week period whereas all of the cellular gels all lose a significant amount of mass. Additionally it is worth noting that the low density gels decrease at a higher rate than the high cell density gels. This suggests that the gel degradation may not be based on cell metabolic activity alone, as the high cell density gels are much more active than the low. It may be that the cells in the high density gels depositing a greater amount of ECM at earlier timepoints result in the production of an internal structure that aids in retaining gel mass.

Kloxin *et al.* have observed in PEG based hydrogels, that in order for cells to spread, move and proliferate, the cells secrete an enzyme to degrade their surrounding matrix. This allows them to gradually extend their morphology. From initially being very small and rounded, they are able to spread and eventually divide [110,252]. Additionally it has been found that in hydrogels with higher stiffness (or Modulus as these are directly proportional), the rate of cellular proliferation decreases [120]. This may be because the gel scaffold is more difficult to degrade, or, in the case of the high cell density hydrogels this may be because as the confluence level is increased there is less room within the scaffold for the cells to move in to as the confluence

level is so high, resulting in less gel degradation. Figure 6-2 and Figure 6-3 illustrate this last point well. In the low density gels cells are small and rounded within the gels but at day 3 they are larger and the morphology is more spread out. In the high cell density gel (Figure 6-3) the cells are rounded immediately after print but at day 3 it is very difficult to detect a change in morphology due to the density of cells present within the gel. This may also be why at day 3 the percentage viability is lower in the high density gels than in the lower density gels, as there is less space for the cells to proliferate in to. 2D studies have found that as confluence level increases the metabolic activity decreases [248], however to our knowledge this has not previously been demonstrated in 3D gel culture. It is likely that a combination of the lower rate of ECM production, the lower gel stiffness and the cells having more space to move in to, results in a greater rate of production of enzymes from the cells in order to break the gels down, explaining why at day 7 the low density gels are significantly smaller in volume than the high density. Figure 7-13 taken from Kloxin *et al.* [109] demonstrates the process by which cells degrade the local gel matrix. However the process of monitoring the changes in local gel mechanics due to cell degradation remains a challenge.

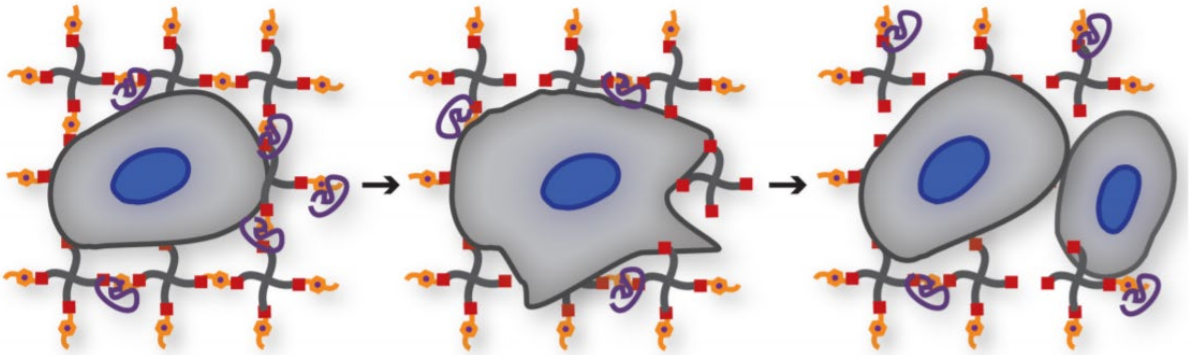

Figure 7-13: Cells initially exhibit a rounded morphology (left). Cells secrete enzymes (purple coils) that break down the local gel matrix and enable cells to begin to change morphology and spread (centre) allowing for cell division (right). Taken from [109]

7.4.5 **Young's Modulus**

The results demonstrated for the gel modulus are very interesting. Firstly it is worth noting that the modulus in the acellular control gels does not change across the 7 day time period. This infers that any change in the gel modulus is due to the influence of the cells within the gels.

Whilst there is no statistically significant change between the average gel modulus at day 1 and day 3 there is a small drop in the average modulus for all culture types at day 3. This may be due to the fact that the cells have begun to degrade the local gel matrix to allow for morphology change and proliferation, however by day 3 they have not yet begun to significantly proliferate or deposit ECM to an extent that it would affect the gel modulus. Additionally this lower starting gel modulus may allow for the cells to begin proliferation at a faster rate [232]. However, it is clear that by day 7 there is a significant increase in the gel modulus. This may be due to a number of factors including cell proliferation, the change in cell morphology, or through the deposition of ECM. Based on the images presented in 5.3.1 and the fact that the high cell density gels exhibit the greatest increase in modulus at day 7, it is likely that the key factor for this increase in modulus is the rate of ECM production, this is further supported by the co-cultures exhibiting the highest Young's modulus whilst also exhibiting the greatest amount of ECM markers of any of the culture types at day 7.

Although the lower gel stiffness and lower density of cells may allow for a greater rate of proliferation in the low density gels and as a result a higher percentage viability, this does not translate to a greater amount of ECM produced, this appears to be more dependent on the total amount of cells, explaining why the increase in Young's modulus is greater in the high density gels than in the low density, even though in most of the cases this difference is not statistically significant. This further supports the argument that the cell density has a significant impact on the rate of ECM production in the CAF hydrogels.

It is worth noting that the Young's modulus of anticular cartilage can vary anywhere between 0.2-0.9 MPa. The Young's modulus of the tested hydrogels is much lower than this, as would be expected as this is not mature cartilage, however the rapid increase over the 14 day period demonstrates that the printed gels may be a suitable method for the growth of mature cartilage if cultured over a longer period.

7.5 Conclusion

The aim of this chapter was to demonstrate the effect of cell concentration on the production of ECM in 3D gel cultures and in doing so to also demonstrate the effectiveness of the CAF gels as a 3D culture environment. Through immunofluorescence and immunohistochemical staining it was established that ECM formation begins by time points as early as 3 days which is significantly earlier than would be expected based on similar literature [235,236] and by one week cells begin to organise themselves around fibres in gels and form structures. Through

immunohistochemical imaging it has been established that the high cell density gels produce significantly more indicators of ECM production (collagen II, aggrecan, osteopontin and osteocalcin) than their low cell density counterparts, and this is supported by quantitative ELISA analysis and the compression testing.

There was a significant increase in ECM markers observed at day 14 and again this was supported b the alizarin red mineralisation staining and the gel young's modulus testing. Cells begin to organise and form structures earlier in low cell density cultures, which is supported by literature [109] and also explains why the low density gels degrade faster than high density gels, as the cells have more room to move and so they degrade more of the local matrix.

All of the above is evidence that in 3D culture, an increased cell density leads to faster rate of ECM production, a greater amount of ECM produced and ultimately, when using 3D cultures as tissue models, will contribute to the production of mature tissue at a faster rate. When considering the use of the REJI system as a high throughput bioprinter for the production of tissue models this is very beneficial, as it means it is a repeatable, reliable method for producing cultures, that can also reduce the overall cell culture time needed through the ability to print high cell densities. There are few studies that compare the effect of cell concentration on printed 3D cultures and as such this demonstrates the novelty and effectiveness of the system.

Chapter 8. Feasibility Study of REJI Printing on Precision Cut Liver Slices for a Tumour Invasion Model

8.1 Introduction

The Aim of this chapter was to investigate the use of ReJI printing of cancer cells within a CAF gel onto a liver tissue substrate as proof of concept for the use of ReJI as the cell deposition method within a cancer invasion assay

8.2 Study Design

Sections of rat liver were provided by Professor Fiona Oakley (Newcastle University Fibrosis Research Group) as well as Hep-53.4 murine liver hepatoma cells and 3T3 murine embryonic fibroblasts. Using the ReJI system, CAF gels containing cells were printed directly on to the liver slices.

Cells were stained with a tracker and liver slices were later imaged to assess cell dispersion throughout the tissue, imaging was carried out by Amy Collins (Newcastle University Fibrosis Research Group).

Figure 8-1 shows a simple schematic of the process used for printing on to liver tissue slices.

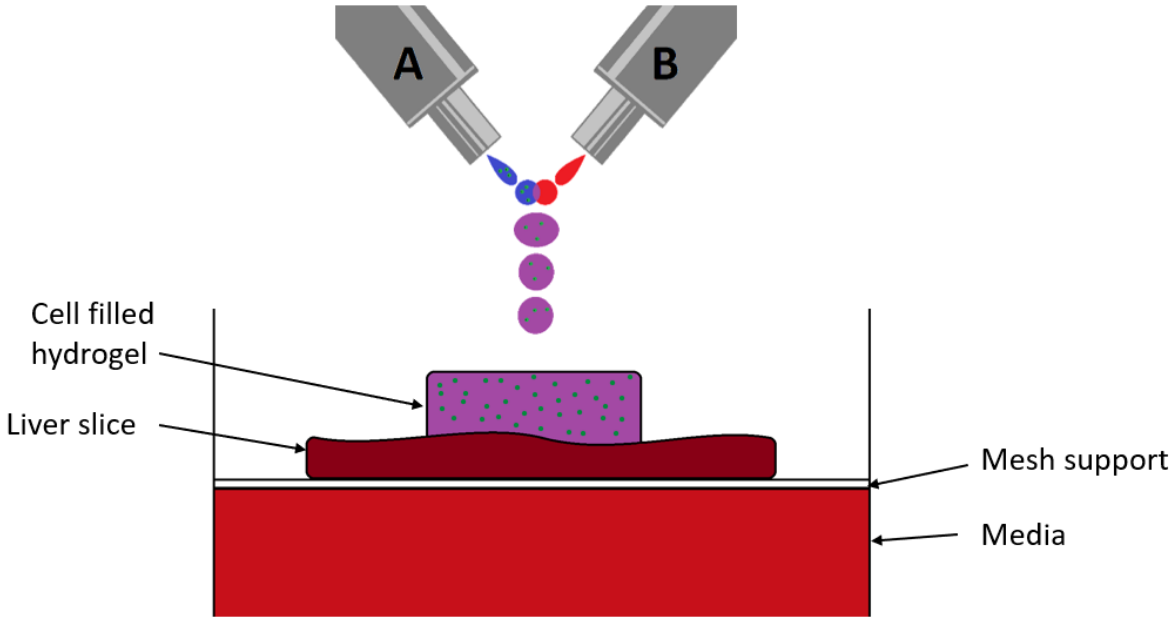

Figure 8-1: Schematic showing the ReJI head printing a cell filled hydrogel on to an uneven tissue substrate of unknown stiffness

8.3 Methods

8.3.1 Tissue Preparation and culture

The process for preparing and culturing the liver tissue is detailed as follows as per Paish et al. [96]. Liver tissue was cored using a 8 mm Stiefel biopsy punch (Medisave, Weymouth, UK). Cores were transferred to a metal mould, submerged in 3% low geling temperature agarose (A9414; Sigma-Aldrich, Poole, UK), and placed on ice for 2-5 minutes. Agarose embedded liver cores were superglued to the vibratome mounting stage, submersed in the media chamber containing 4°C Hank's balanced salt solution+ , and cut using a Leica VT1200S vibrating blade microtome (Leica Biosystems, Milton Keynes, UK) at a speed 0.3 mm/sec, amplitude 2 mm, and thickness (step size) of 250 µm. Slices were transferred onto 8-µm-pore Transwell inserts and cultured in a modified tissue culture plate (BioR plate) and rocked on the bioreactor platform (patent PCT/GB2016/053310) at a flow rate of 18.136 µL/sec. All slices were cultured in DMEM (D5796-500ML; SigmaAldrich), supplemented with 1% penicillin/streptomycin and l-glutamine, 1× insulin transferrin-selenium X, and 2% fetal bovine serum (Thermo Fisher Scientific, Cramlington, UK), and 100 nM of dexamethasome (Cerilliant, Texas, USA) at 37°C, supplemented with 5% CO2. Media was changed daily.

A 15:1 ratio of Hep-53.4 murine liver hepatoma cells transfected with tdTomato and 3T3 murine embryonic fibroblasts transfected with eGFP, supplemented with 40 ng/ml hepatocyte growth factor and 20 ng/ml epidermal growth factor were suspended in thrombin and printed into CAF gels directly on to tissue sections with a cell density of $40x10^6$ cells/ml.

Following printing, for immunofluorescence imaging, samples were placed in a 12 well plate with enough culture media added to cover them completely, samples were then imaged using an EVOS M5000 fluorescence microscope. For Multiphoton imaging samples were stained for 15 mins with Hoechts 33342 (1:1000 in PBS), washed with PBS then mounted (live or fixed) on a microscope slide in a gene frame. Samples were then imaged with a Zeiss LSM800 NLO Multiphoton microscope.

8.3.2 Printing

Tissue slices were arranged on to cell strainers which were in turn placed into dishes containing cell culture medium (Figure 8-2). This was to prevent the tissue from drying out by keeping the cell strainer mesh wet, also the time that the slices were out of the transwells for printing was minimised, again to ensure the tissue was not out of culture for too long.

The print seed density used was $40x10^6$ cells per ml. Two gel thicknesses were printed for testing, these were 4 and 8 printed layers thick. 24 tissue samples were provided which allowed for 8 gel sizes to be printed in triplicate cultured in two separate multiwell plates. The gels printed were simple square shapes and the gel dimensions defined by the number of droplets in x and y were as follows:

Plate 1

1. Single droplet - 4 layers
2. 2x2 - 4 layers
3. 3x3 – 4 layers
4. 4x4 – 4 layers

Plate 2

1. Single droplet – 8 layers
2. 2x2 – 8 layers
3. 3x3 – 8 layers
4. 4x4 – 8 layers

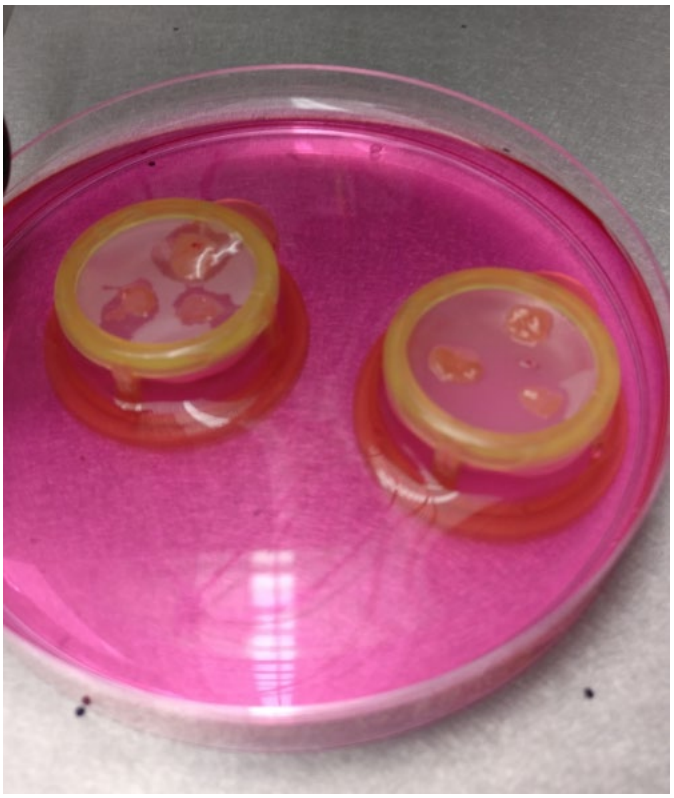

Figure 8-2: Liver tissue slices arranged on cell strainers in a dish containing culture media

8.4 Results

Figure 8-3 shows tissue samples in the multi well plates with printed gels on top. Printing cells of all specified sizes directly on to the tissue substrate was a success and it was possible to manipulate the sections, with the printed gels on to back into the transwell inserts for culture. Media was then replenished and the tissue was returned to the incubator.

Figure 8-3: Tissue samples with printed gels on to. Left shows a 4 layer single droplet gel and right shows a 4 layer 2x2 gel

Figure 8-4 is a multi-photon image showing the red He-53.4 cancer cells invading the blue stained liver tissue from the gel. The left image shows the second generation harmonics, which highlight collagen, meaning the large green area indicates the hydrogel, the right image removes the harmonics. The arrows indicate the penetration depth of some of the cells, which is up to 80 µm of a total 250 µm.

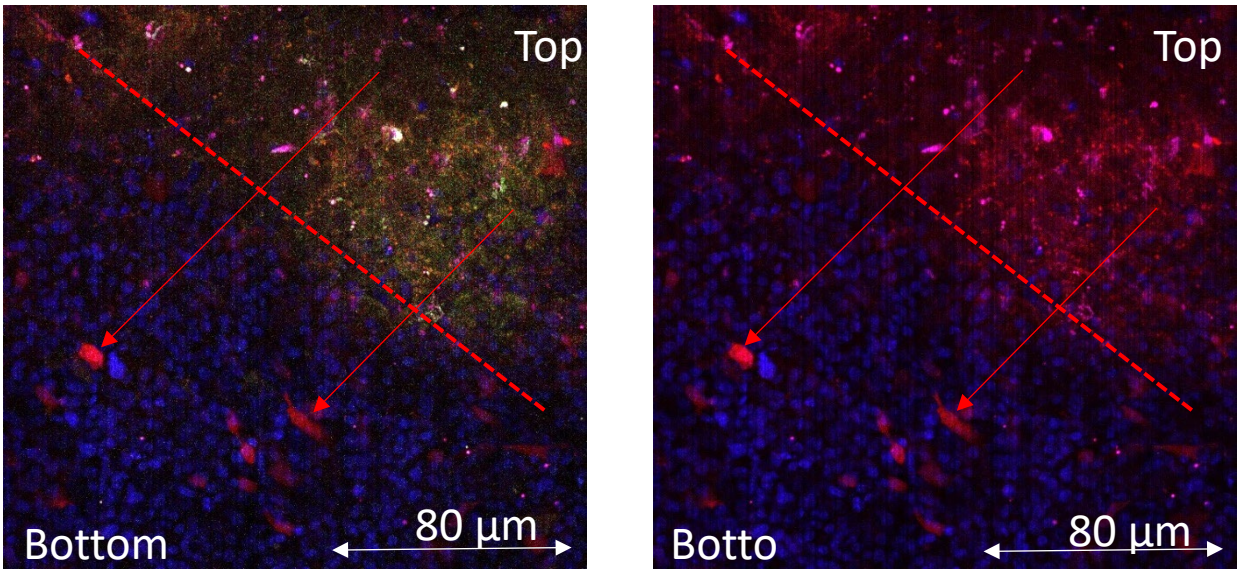

Figure 8-4: Multi-photon image showing He-53.4 transfected with tdTomato(red) invading the liver tissue (blue stained with Hoechst 33342). The red dotted line is the boundary between the tissue and the gel (left) Image showing second generation harmonics (right) second generation harmonics removed

printing. Here it can be seen that after their initial homogenous spread across the tissue substrate from the printing process, by day 3 in culture the cells begin to migrate to one area together, and proliferate.

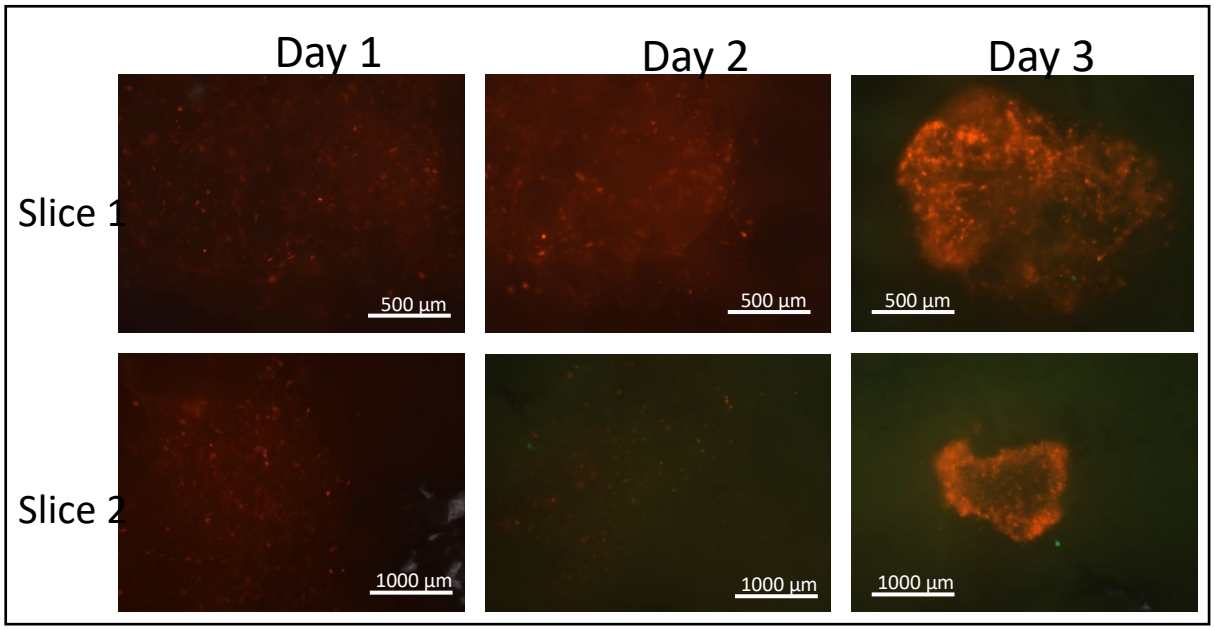

Figure 8-5: Fluorescence imaging of two tissue slices showing He-53.4 transfected with tdTomato(red) 24, 48 and 72 hours after printing cell filled gels directly onto the slices.

Figure 8-6 shows a multi-photon image of the He-53.4 and 3T3 cells interspersed all the way through the liver tissue.

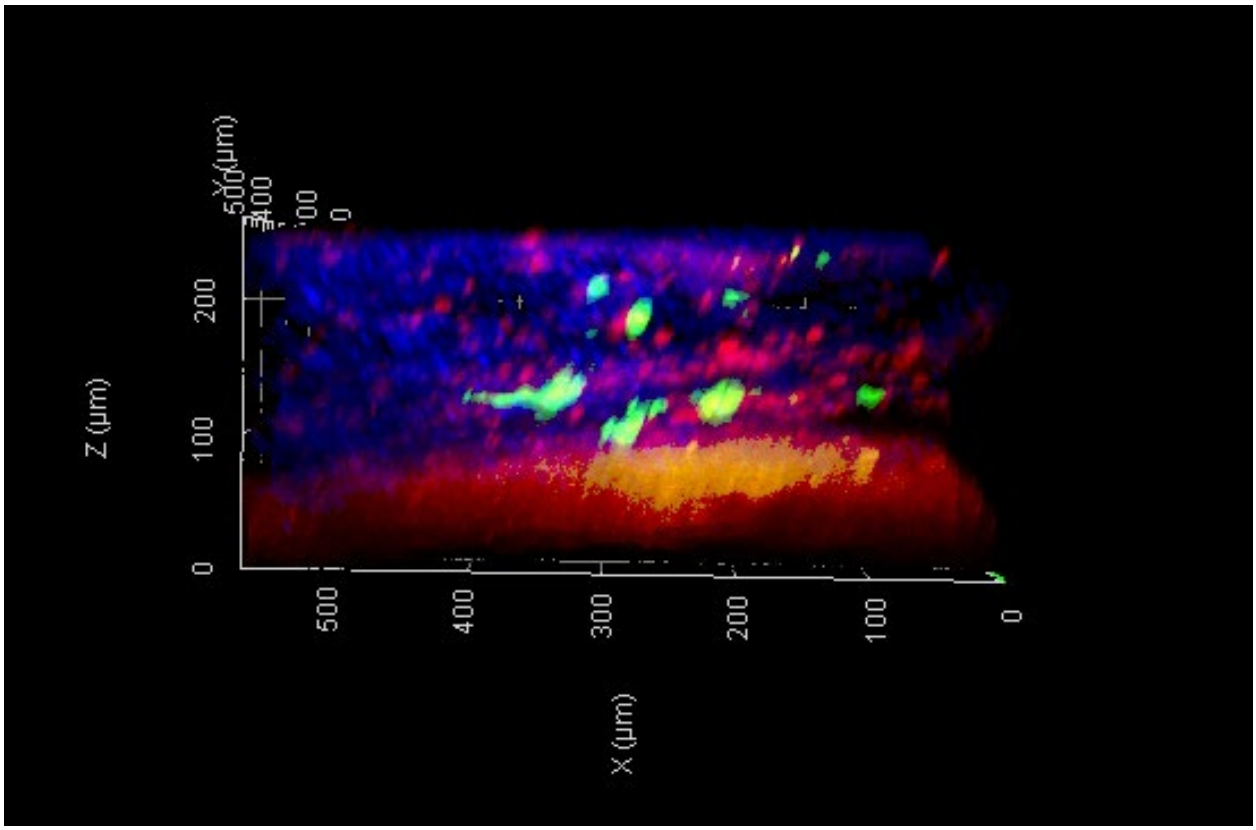

Figure 8-6: Multi-photon image of the He53.4 cells (red) and 3T3 fibroblast cells (green) interspersed all the way through the liver tissue section (blue)

8.5 Discussion

The results of the printing process demonstrate that the ReJI system is capable, with a high degree of accuracy, of printing directly on to a soft tissue substrate. In doing so, and with drop on demand accuracy, this demonstrates a significant additional application for the ReJI system. This is the first instance that the ReJI has been used to print directly on to tissue. Being able to print directly on to a soft tissue substrate can be beneficial for a number of reasons, for example, printing onto less stiff substrates can actually improve print accuracy by reducing splashing or droplet spread, whilst also decreasing the stress on cells [40,253,254]. The culture of cancer cells using 3D scaffold has been studied for decades and it is well established that the accurate replication of the native micro-tissue has a huge impact on the cell growth in vitro [255]. Whilst hydrogels have commonly been used for this process for a number of reasons including the ease of manufacture, the ability to control mechanical factors such as stiffness and for the ability to embed cells uniformly within the gel [16,204,256], for an application such as modelling liver cancer cell invasion, using actual liver tissue as the matrix is one of the most representative in vitro methods. To this end studies have been carried out in order to decellularize human liver tissue so that it can be repopulated with cells for study. Mazza et al. demonstrated that this could be successfully carried out on an entire human liver which could then be repopulated with derived human liver cells. The repopulated liver sections showed good viability, motility, proliferation and even successful remodelling of the ECM [257]. However the process of seeding cells onto the scaffold in order to ensure all cells attached appears difficult, with cells being manually seeded, drop by drop on to the scaffold with a hypodermic needle. To avoid manual processes such as this, especially when considering methodologies such as this for high throughput applications 3D bioprinting techniques can be applied [258,259] to automate the process of cell seeding. Additionally, depositing the cells on the tissue suspended in a printed low stiffness gel has the advantage of ensuring cells are deposited in exactly the point where they are desired, with the gel preventing them from just washing off the tissue, and if a low stiffness gel that naturally degrades (such as CAF) is used, the cells are able to migrate from the gel, and if the method is successful directly into the matrix. Paish et al. have demonstrated the effectiveness of their novel technique for the sectioning and culture of human and rodent liver for use as scaffolds and through combining this with the ability of the ReJI system to accurately print drop on demand hydrogels on to tissue substrates, a high throughput method of seeding cells directly on to tissue has been demonstrated.

Furthermore Figure 8-3 to Figure 8-6 show that not only does the process of printing cell filled gels on to tissues work but also that cells to indeed begin to migrate into the tissue. Aside from acting as an effective tissue model for drug screening applications this could provide future studies with a highly accurate platform for studying cell motility and proliferation a very accurate 3D in vitro model. For example Figure 8-5 demonstrates that immediately after printing, cells are homogenously spread across the tissue substrates, as was desired from using the ReJI system in the seeding process. However at day 3, cells have clearly begun to migrate towards each other and have also began proliferation. Clearly this demonstrates that the CAF gel as a scaffold provides enough rigidity to deposit the cells where they are needed but is not so strict that it restricts cell motility, additionally this is true of the liver slices as the cells were observed to have penetrated through the full depth of the liver slice by day 3 (Figure 8-6). This high motility also shows that the liver slices in combination with the gel seeding process is ideally suited to the research of cancer invasion in tissue.

Finally the concept of 'in situ' or 'in vivo' bioprinting has been discussed for some time [55], and there have been a number of successful studies in recent years that have developed techniques for undertaking this [64,65,260,261]. The ability to directly apply the required cell type to the damaged area in vivo often allows for a much faster rate of cell growth, proliferation and in some cases repair of the damaged tissue. Ultimately if the ReJI is to be used to produce implants for cartilage or tissue repair, this demonstration of the system's ability to print detailed gels in a specified size and area directly on to soft tissue are certainly the first steps in demonstrating that the ReJI is capable of this.

Chapter 9. Discussion and Conclusions

9.1 Summary of work

9.1.1 Printhead Design

A large proportion of the work in this project was based around developing the ReJI system to a point where it could be reliably used to produce accurate hydrogel cell scaffolds.

This involved the design manufacture and installation of completely new printhead systems and a system of calibration for printing.

The version 3 printhead incorporates:

- An on-board agitator
- Quick-change reservoirs
- Different 'v-block' heads that allow for up to 4 different bioinks to be loaded for printing simultaneously.
- The ability to remove and sterilise each component individually

Due to the software limitations of the Jetlab 4 machine in Newcastle University, the ReJI printhead can currently only print one ink type at a time, however the simultaneous deposition of multiple inks has been achieved when installing the print head on a Regemat 3D machine.

9.1.2 Characterisation of 3D CAF hydrogels

The most demanding aspect of this body of work was the development of suitable characterisation methods for 3D hydrogels. Although there are many examples of processes that have been carried in literature, it became apparent that if hydrogel formations differed even slightly this can have a significant impact on the effectiveness of an assay or analysis method.

One of the main difficulties is that conventional assays, are designed for cells grown in 2D culture, where the assay has a large amount of surface area contact with the cells. In 3D, diffusion of the assay through the gel becomes a significant issue. The assay may not be able to diffuse fully thoughout the gel in the recommended assay time and if the assay time is altered, for example be extending the time to allow for better diffusion throughout the gel, cells at the edges of the gel may now be over exposed, making them appear to be more 'active' than those in the centre. It cannot be guaranteed that the activity of all the cells within the

gel are represented, this makes comparison between 3D with 2D culture very difficult, and it is also difficult to compare gels of different densities as higher cell density gels are likely to inhibit diffusion.

Similar issues are encountered with immunofluorescence staining, and even histological methods are complicated, as the processes that are commonly used to dehydrate tissues before embedding them alters the structure of the hydrogel significantly and can make them too brittle to section effectively in some instances.

This lead to the development of the gel digestion methods, and whilst it was demonstrated that the cell viability was not significantly effected by the digestion process, assays such as metabolic activity would likely give a less reliable comparison as even just the action of removing the cells from the gel may have an effect on their metabolic activity and any assay carried out on extracted cells would assess their metabolic activity after extraction, which is likely to differ from when they suspended in the gel.

One potential solution for this may be to extract small sections of gel using an instrument such as a biopsy punch and using a designated 3D assay such as the Cell Titer-Glo® 3D Cell Viability Assay.

In this body of work novel methods have been developed and presented for:

- Assessing cell viability in 3D
- Safely digesting gels without damaging encapsulated cells
- Staining for quantitively assessing ECM and bone markers
- Qualitatively assessing ECM and bone markers by ELISA

All of these methods required individual development, tailoring, and deviation from standard protocols to work suitably with the CAF hydrogels.

9.1.3 **Printer calibration and post-print cell behaviour within a cell filled gel**

Through developing a successful calibration method, the system's ability to accurately print hydrogels on a drop-on-demand basis is demonstrated. Multi-layer gels appear to be more successful than monolayer, or single droplet gels printed as the multiple layers allow for additional mixing of any of the remaining bioink that did not crosslink during the printing process. However, with accurate calibration and adjustment of print settings, there was very

little un-crosslinked ink, with the alginate and CAF based gels used due to the effectiveness of the in-air droplet mixing.

Cell viability of the cells in the printed hydrogels were assessed at various timepoints post-print and the viability was found to be high (above 75%, in all cases). This included cells printed in high cell density gels ($40x10^6$ cells/ml), as well as those printed in stratified co-cultures. Additionally, the number of cells counted within the gels immediately post-printing was found to accurately represent the number seeded prior to printing.

The accurate and viable printing of hydrogels using microvalve technology, containing cells at a high cellular density (of the order of 10^7) has not been demonstrated in any other studies.

9.1.4 **The production of an osteochondral co-culture**

A 3D printed stratified osteochondral interface model was produced by printing a layer of chondrocyte cells encapsulated in CAF gel on top of a layer of printed osteoblast cells also encapsulated in CAF gel.

Gels were printed in cell densities of $40x10^6$ cells/ml and $4x10^6$ cells/ml. The rate of ECM production was evaluated through the analysis of various ECM markers through immunofluorescence and immunohistochemical staining, as well as quantitatively by ELISA analysis. Additionally, gel mass retention and Young's modulus were assessed.

ECM production in chondrocyte cells and mineralisation in osteoblasts occurred at a faster rate in higher cell density gels and in co-culture with the high cell density co-cultures having the highest levels of ECM and bone markers in all cases.

Additionally, compression testing showed a dramatic increase in the Young's modulus of cellular gels from days 3-7, which is when cells begin to proliferate and deposit ECM, Young's modulus was also found to be higher in high cell density gels and co-cultures.

The production of stratified 3D printed co-cultures, and a direct comparison of the performance of high and low density cultures through the comparison of growth markers, such as indicators of ECM production or bone markers has not been demonstrated in similar studies.

9.1.5 **3D printed hydrogels for use in cancer invasion models**

The ReJI process was used for printing hydrogels containing cancer cells directly on to a tissue substrate (liver sections) in order to study cell motility for use as a cancer invasion model. Gels

of varying sizes were analysed and cells were found to migrate from the CAF gel and through the liver tissue. Furthermore, after 72 hours, cells were found to proliferate and migrate towards each other. There are no other current examples in literature of bioprinting onto viable tissue substrates.

9.2 General Discussion

9.2.1 Machine Development

At the beginning of this project there was a working ReJI system although it is fair to say that this was more of a proof-of-concept system than a fully functioning bioprinter system. Some of the design features were not functioning as had been intended during the design, resulting in researchers circumventing important aspects of assembly, this made things like calibration and valve alignment more difficult and overall had an impact on the reliability of the system.

The main efforts of the design work during this project have focused on making the system easy to assemble, disassemble and operate for all researchers using the ReJI head. Assembly and disassembly were of particular importance as the Jetlab machine that the system is mounted on is also used by the research group for different printheads, so ensuring that the ReJI head could be easily changed between sessions and calibrated easily when set up was of utmost importance. Furthermore this will still be of importance in the future if the system is sold as an attachment for existing bioprinter base models.

Ease of operation and maintenance are some off the most important features in the area of bioprinter design. The majority of users that work on bioprinter systems are often from a biological background. Very few have a background in machine design or are confident with carrying out machine maintenance unless it is straightforward enough to carry out without making any mistakes or damaging the system. Therefore, designing systems such that they have the least number of components possible and the lowest margin of error in assembly and calibration are priorities.

Finally, arguably the most important feature of any bioprinting system, other than its ability to print bioinks, is the ability of the user to clean the system. If the system cannot be cleaned effectively and efficiently then after a single use bacteria and other sources of infection will begin to build within the system and it will become unusable. All of the ReJI components, including reservoirs, tubes and microvalves can be removed and thoroughly flushed with

cleaners, additionally all of the components except the microvalves (as the internal mechanisms are sensitive) can be cleaned through sonication.

With design iteration 2, the first ReJI system developed for commercial purposes was produced. This included minimising the physical size of the head in order to reduce the inertia when moving on a 3-axis machine, the introduction of spring-loaded reservoirs for quick changing of inks and the ability to customise the system for 'V blocks' of different sizes.

Ultimately the design developments in this project have been successful in creating both a print head that is simple and effective to use in a research setting but also a commercially viable bioprinter head design that will be simple to make and assemble in small batch amounts. As mentioned previously the next step will be fully integrating parametric design techniques with the CAD models so that when a custom order is placed, the relevant design parameters need only be input into a spreadsheet and the CAD model will update automatically to reflect the changes. From there a STEP file or a drawing can be produced for part manufacture.

9.2.2 Drop-on-demand printing of high cell density hydrogels

The viability and behaviour of cells post-print are some of the most important characteristics of drop-on-demand bioprinting. The ability to accurately print a desired cell density effectively, and to do so with an acceptably high cell viability, are tantamount to a successful bioprinting process. Drop-on-demand printing using microvalves offers a higher accuracy and an acceptable cell density (conventionally approx. 10^6) with a considerably high viability, greater than 80% on average [262], when compared to processes such as microextrusion, and although it is not traditionally capable of printing the cell density associated laser assisted bioprinting, the affordability and accessibility of the technology has meant that is very common in the field of bioprinting. One of the main drawbacks of the process is that it is commonly limited by the viscosity of the ink [263–265].

Through the use of the ReJI system, a method of accurately depositing individual droplets of hydrogel that would otherwise be too viscous to print through a single microvalve has been demonstrated. Additionally gels containing $40x10^6$ cells/ml have been produced, a density that is tenfold greater than any other similar systems in comparable literature, higher even than any similar impingement based methods [67–69]. The viability of the cells within these hydrogels is comparable to that found in literature in the lower cell density gels [262], and

remains high in the high cell density gels. The process demonstrated in this body of work sets a standard for the ability to accurately deposit cell filled hydrogels in either single droplets or as larger tissue models with both low and high (up to 40 M cells/ml) cell densities.

9.2.3 The effect of printed cell density on the production of ECM (and mature tissue in general)

The ability to effectively produce high cell density hydrogel tissue scaffold using a high throughput method such as bioprinting has significant implications for applications such as the production of tissue models for drug screening. There are numerous models for drug screening applications currently including 2D culture, aggregate and insert based 3D models, and for studies that progress to the more advanced stages animal models are the current 'gold standard' [195]. However many of the current in vitro models fail to accurately represent the native microtissue or provide the correct environment for cell-cell or cell-ECM interaction. Furthermore, due to expense, low throughput as well as animal welfare concerns and the fact that studies carried out on animals may still fail in human trials due to specific immunogenic properties of the drugs going undetected in animal trials [194,266], additional, more representative, in vitro methods are sought after for early stage drug screening applications.

For applications such as drug screening where a high number of test samples are required, the model production method must also be of a significantly high throughput. Importantly, the production method is not just the point at which cells are seeded on to the growth substrate but this also includes all of the cell culture time up until the tissue model is sufficiently mature and representative enough of native tissue to allow for representative drug testing. Studies have shown that one way of producing mature tissue at an increased rate is by increasing the cell density in the tissue model [267], however few studies have comprehensively investigated this effect and there are none (known to the author) that are able to test this premise using a 3D bioprinting method.

This body of work not only effectively demonstrates a high throughput method of printing cells encapsulated in 3D hydrogels in both high and low cell densities, but it also demonstrates that cultures containing higher cell densities produce markers of ECM and mineralisation at a greater rate. Through direct comparison, this affirms that higher cell density hydrogels will form a more representative model of mature tissue faster than low cell density. Further to this, cells printed in co-culture produced even greater amounts of bone and ECM markers,

demonstrating that not only can a stratified co-culture model be produced, but that growing cells in co-culture has a positive effect on the maturation of the tissue model.

One of the aims of this body of work was to produce a stratified 3D printed osteochondral interface model. Whilst a stratified osteochondral interface model has been produced and has been found to be a more effective tissue culture environment than the single cell cultures, in terms of the production of ECM and bone markers, it is not possible to compare the printed osteochondral co-culture model to the tissue found within an osteochondral interface within the remit of this work. However the benefits of cell density and culture type have clearly been demonstrated

9.2.4 **Printing onto a tissue substrate and the production of a cancer invasion model**

The need for in vitro tissue models more representative of the human body is not limited to the treatment of OA but is an important requirement in all fields where drug screening is required, not least of all on cancer research. When considering the effectiveness of drug treatments on cancer cells 2D models provide an inaccurate representation and common in vitro 3D models such as aggregate based models are unable to represent the cell motility accurately due to the lack of cell-ECM interactions. To this end hydrogels and also human tissue, such as liver tissue, have been used as cell scaffold, and cell growth, proliferation and motility within these scaffolds can be monitored. However using these methods throughput can often be limited by the need to individually seed droplets of media containing cells on to the scaffold until all cells can be observed to be absorbed.

In this thesis the ReJI method is used to 3D print small quantities of high cellular density hydrogel directly on to liver sections. This demonstrates a method of immediately increasing throughput. Furthermore, cells were observed to have successfully migrated from the hydrogel site and through the liver tissue, where they were found to migrate toward each other and proliferate. In addition to this demonstrating an additional, significant, high throughput requirement for the ReJI system, it also demonstrates the ability of the system to print on delicate, uneven substrates of uneven stiffness which in turn opens the door to a diverse range of applications.

9.3 Conclusions

The research presented in this body of work has demonstrated the versatility of the ReJI system, and its applications in the production of in vitro hydrogel tissue culture models.

9.3.1 **Machine Developement**

The ReJI system design was developed from a prototype system to a functioning commercially available 3D bioprinting system.

9.3.2 **ReJI System Performance**

The ability to accurately print hydrogels on a drop-on-demand basis was demonstrated through the printed calibration process. This provides a cost-effective alternative to laser assisted bioprinting.

The ability to print high cellular density hydrogels ($40x10^6$ cells/ml) was demonstrated and the viability of those cells was assessed post-print. This demonstrated the ability of the system to produce high cell density hydrogels with drop-on-demand accuracy with no negative effect on cell viability, something which has not been reported using microvalve technology, even in similar impingement-based methods.

9.3.3 **Osteochondral Model**

It can be concluded that printed cell density has a significant effect on the maturation rate of 3D printed tissue. This was assessed though the analysis of ECM and bone markers as well as through mechanical testing. Additionally, the system was used to produce a chondrocyte-osteoblast stratified osteochondral co-culture. High cell density cultures demonstrated higher levels of ECM and bone markers, with co-culture performing better than single cell culture models. This was supported by mechanical testing.

9.3.4 **Cancer invasion model**

The ReJI system was used in the development in a cancer invasion model, by printing high cell density hydrogels on to liver tissue sections. This demonstrated the ability of the system to print on to uneven, soft tissue and the effectiveness of the high density 3D printed hydrogels as a part of tumour invasion models.

9.4 Future work

A number of areas for future work have been identified in this work. Firstly there is still the potential for significant design modification. The groundwork has been laid for parametric design processes to be employed to speed up the production of custom orders however this could be explored further. Additionally the effect that parameters such as the valve angle have on impingement should be explored as this could have a significant effect on the ease with which the ReJI effectively prints into 96 well plates, simplifying high throughput printing. A number of variations on the reservoir have been designed, including some with and without handles, and some with side fill access, however a reservoir that could be rapidly loaded and unloaded, that does not need to use the MINSTAC tubing, which is prone to clogging, whilst still allowing for easy valve adjustment would be an effective modification.

In the majority of the ReJI 'V blocks' the angle between the valves was maintained constant at 120 degrees. However, the desire to use the ReJI system for high throughput bioprinting also lead to the desire to explore different valve angles to aid in droplet impingement and print accuracy. One such modification is that by making the angle between the valves shallower (in this case 110 degrees) the droplets will impinge later in the air, further away from the nozzle. This may in turn reduce the possibility of splashback or droplet inaccuracies occurring. In turn, this would then help increase accuracy when printing in to 96 and 384 multiwell plates. Figure 9-1 shows the CAD model of a ReJI 'V4' head designed with a 110 degree angle rather than a 120 degree angle.

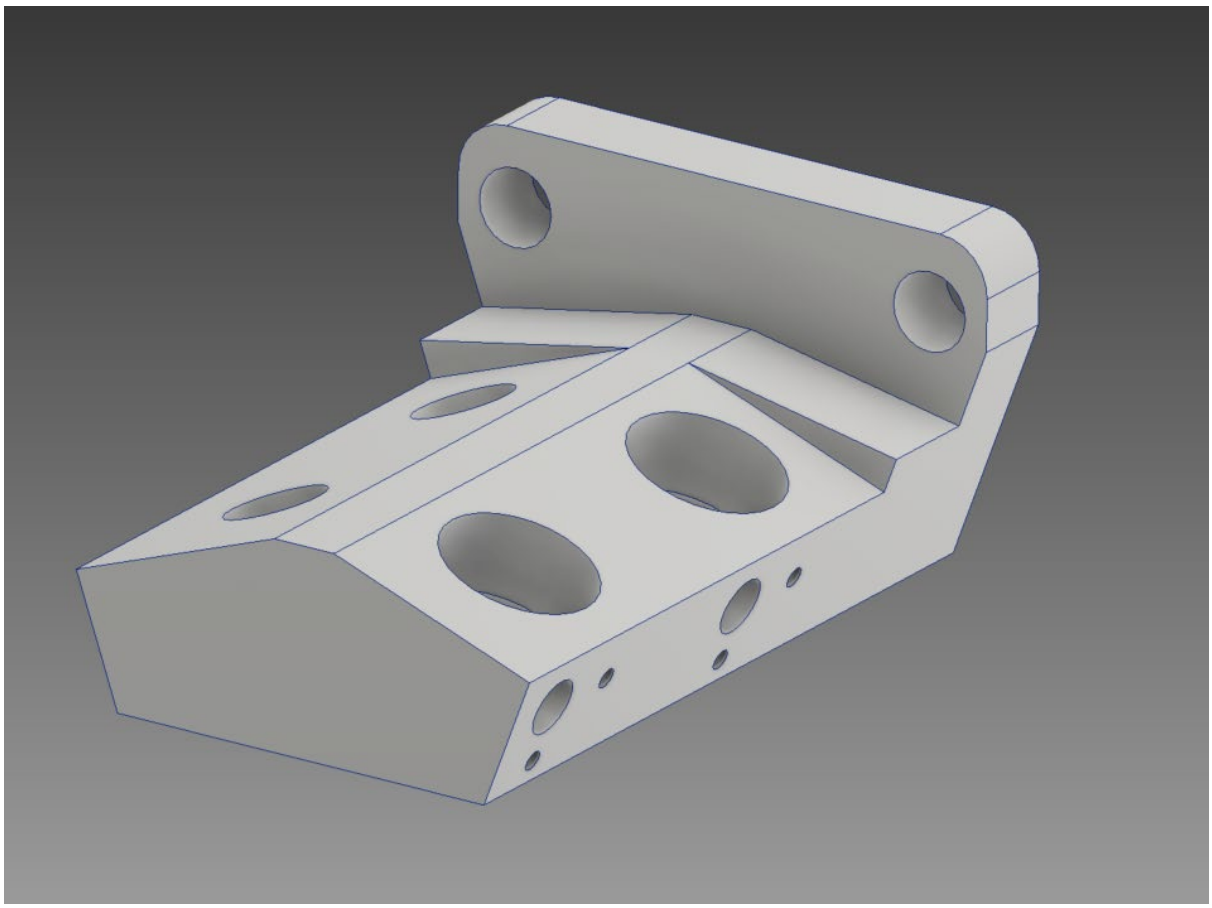

Figure 9-1: ReJI V4 head with a 110 degree valve angle

Given that there is now a greater demand for modification of the 'V Blocks' and blocks with slightly different features such as the number of valves required, and the differing valve angles, the groundwork has been started to create a parametrically controlled 'V Block' model to aid in manufacture. This involved choosing key parameter that may be changes, such as the number of required valve pairs, and the block angle and linking these with real design parameters such as length in the case of the number of valve pairs i.e. a V8 block is 4 times the length of a V2 block. A spreadsheet with these key parameters can be linked with the Inventor CAD model and when a different block variant is required the user needs only to input the key parameters i.e. number of valves pairs or block angle, and the CAD model will then update automatically. From there a STEP file can be produced and sent for manufacture. This will make the manufacture of small custom orders of ReJI heads much simpler in the future.

The most difficult ReJI process for the user is still the calibration and so a method of autocalibration could be assessed. Initial studies were carried out to use the existing worm wheel arrangement but rather than using a manual adjustment method this would be

adjusted via a linked servo motor. However the process for assessing effective impingement was initially going to be based on a test print and the number of droplets this produced on the substrate (based on Calibration method 1, section 5.3.1) and this was found to be ineffective. Additionally methods of assessing the images taken using the stroboscopic camera in real time and using these to inform the automatic calibration of the valves were explored but found to be too computationally demanding. There may be some other method that could be explored to allow for autocalibration.

The development of an in-house machine or the use of a Regemat machine to conduct a study with the simultaneous printing of multiple bioink types would also be interesting and demonstrate throughput scalability of the technology.

The effect of additional cell types such as MSCs in the stratified osteochondral co-culture would be an interesting future study as these are known to produce chondrocyte growth factors. Given how much more effective the co-culture models were, exploring the addition of another cell type would be interesting. Additionally, the effect of the addition of growth factors on ECM production could be explored. To assess the effectiveness of the 3D printed culture models the next stage in development would be direct comparison to other common culture models including insert and aggregate based as well as animal testing.

One area of research that could benefit from significant future work is the in vitro culture of hydrogel models. Currently common methods for hydrogel culture are adapted from 2D culture with gels often just suspended in media. The culture requirements for different tissue types vary significantly, for example it has been demonstrated that some cells produce greater levels of ECM markers when subject to mechanical stimuli [141]. In order to increase the accuracy of any in vitro tissue model, ensuring the culture environment is as similar as possible to in vivo conditions is paramount. To this end bioreactor design for emerging novel tissue models is positioned to be one of the most important areas for development in the future. Even factors such as the substrate that the gels are printed on to, or cultured on could have an effect on cell growth and behaviour. For example, if cells are printed on to a stiff scaffold that they are likely to attach to, they may be more likely to produce markers of ECM and bone than if they are left suspended in media. Replicating in vivo conditions as closely as possible is key.

The development of gel characterisation methods was a continual challenge throughout this project with little reference material to draw from and even the slightest differences in gel composition of cell density having an effect on the effectiveness of the analysis techniques used. The development of reliable protocols for characterising basic cell functions such as metabolic activity, or for gel imaging, gel digestion, quantification of deposited markers of ECM or other important indicators of culture performance, would have a significant impact on the quality of any research outputs in this field. This work goes some way to stabilising some effective protocols however the ability to analyse printed hydrogels is just as important as the ability to produce them and this area should not be neglected.

Finally, an additional application, the production of cancer invasion models, was demonstrated. The ability to deliver a concentrated gel scaffold containing cells accurately on to a uneven soft tissue substrate indicates a great deal of potential applications for future work. For example, coating surgical implants with cell laden gels to improve cartilage regeneration for OA, the development of more complex or higher throughput cancer invasion models, or even the adaptation of the ReJI method for in situ bioprinting are all possible areas of future work.

Chapter 10. References

[1] Kang HW, Lee SJ, Ko IK, Kengla C, Yoo JJ, Atala A. A 3D bioprinting system to produce human-scale tissue constructs with structural integrity. Nature Biotechnology 2016. https://doi.org/10.1038/nbt.3413.

[2] Baharvand H, Hashemi SM, Ashtiani SK, Farrokhi A. Differentiation of human embryonic stem cells into hepatocytes in 2D and 3D culture systems in vitro. International Journal of Developmental Biology 2006. https://doi.org/10.1387/ijdb.052072hb.

[3] Murphy S v., Atala A. 3D bioprinting of tissues and organs. Nature Biotechnology 2014. https://doi.org/10.1038/nbt.2958.

[4] da Conceicao Ribeiro R, Pal D, Ferreira AM, Gentile P, Benning M, Dalgarno K. Reactive jet impingement bioprinting of high cell density gels for bone microtissue fabrication. Biofabrication 2019. https://doi.org/10.1088/1758-5090/aaf625.

[5] Benning M, Dalgarno K. Printing apparatus and method. WO2019008373A1, 2017.

[6] Berenbaum F. Osteoarthritis as an inflammatory disease (osteoarthritis is not osteoarthrosis!). Osteoarthritis and Cartilage 2013. https://doi.org/10.1016/j.joca.2012.11.012.

[7] Glyn-Jones S, Palmer AJR, Agricola R, Price AJ, Vincent TL, Weinans H, et al. Osteoarthritis. The Lancet 2015;386:376–87. https://doi.org/10.1016/S0140-6736(14)60802-3.

[8] Birgersdotter A, Sandberg R, Ernberg I. Gene expression perturbation in vitro - A growing case for three-dimensional (3D) culture systems. Seminars in Cancer Biology 2005. https://doi.org/10.1016/j.semcancer.2005.06.009.

[9] Miki Y, Ono K, Hata S, Suzuki T, Kumamoto H, Sasano H. The advantages of co-culture over mono cell culture in simulating in vivo environment. Journal of Steroid Biochemistry and Molecular Biology 2012. https://doi.org/10.1016/j.jsbmb.2011.12.004.

[10] Giverso C, Preziosi L. Influence of the mechanical properties of the necrotic core on the growth and remodelling of tumour spheroids. International Journal of Non-Linear Mechanics 2019. https://doi.org/10.1016/j.ijnonlinmec.2018.10.005.

[11] Stebbings R, Findlay L, Edwards C, Eastwood D, Bird C, North D, et al. "Cytokine Storm" in the Phase I Trial of Monoclonal Antibody TGN1412: Better Understanding the Causes to Improve PreClinical Testing of Immunotherapeutics. The Journal of Immunology 2007. https://doi.org/10.4049/jimmunol.179.5.3325.

[12] Schlander M, Hernandez-Villafuerte K, Cheng CY, Mestre-Ferrandiz J, Baumann M. How Much Does It Cost to Research and Develop a New Drug? A Systematic Review and Assessment. Pharmacoeconomics 2021;39. https://doi.org/10.1007/s40273-021-01065-y.

[13] Paul SM, Mytelka DS, Dunwiddie CT, Persinger CC, Munos BH, Lindborg SR, et al. How to improve RD productivity: The pharmaceutical industry's grand challenge. Nature Reviews Drug Discovery 2010;9:203–14. https://doi.org/10.1038/nrd3078.

[14] Visk D. Will Advances in Preclinical In Vitro Models Lower the Costs of Drug Development? . Applied In Vitro Toxicology 2015. https://doi.org/10.1089/aivt.2015.1503.

[15] Petersen OW, Ronnov-Jessen L, Howlett AR, Bissell MJ. Interaction with basement membrane serves to rapidly distinguish growth and differentiation pattern of normal and malignant

human breast epithelial cells. Proc Natl Acad Sci U S A 1992. https://doi.org/10.1073/pnas.89.19.9064.

[16] Caliari SR, Burdick JA. A practical guide to hydrogels for cell culture. Nature Methods 2016. https://doi.org/10.1038/nmeth.3839.

[17] Groll J, Boland T, Burdick J, Blunk T, Cho D--W, Dalton PD, et al. Biofabrication: Reappraising the definition in an evolving field. 2016.

[18] Zhang K, Fu Q, Yoo J, Chen X, Chandra P, Mo X, et al. 3D bioprinting of urethra with PCL/PLCL blend and dual autologous cells in fibrin hydrogel: An in vitro evaluation of biomimetic mechanical property and cell growth environment. Acta Biomaterialia 2017. https://doi.org/10.1016/j.actbio.2016.12.008.

[19] Russell S, Wojtkowiak J, Neilson A, Gillies RJ. Metabolic Profiling of healthy and cancerous tissues in 2D and 3D. Scientific Reports 2017. https://doi.org/10.1038/s41598-017-15325-5.

[20] Horn TJ, Harrysson OLA. Overview of current additive manufacturing technologies and selected applications. Science Progress 2012. https://doi.org/10.3184/003685012X13420984463047.

[21] Raibert M. BigDog, the rough-terrain quadruped robot. IFAC Proceedings Volumes (IFAC-PapersOnline), 2008. https://doi.org/10.3182/20080706-5-KR-1001.4278.

[22] Zheng F, Fu F, Cheng Y, Wang C, Zhao Y, Gu Z. Organ-on-a-Chip Systems: Microengineering to Biomimic Living Systems. Small 2016. https://doi.org/10.1002/smll.201503208.

[23] Wegst UGK, Bai H, Saiz E, Tomsia AP, Ritchie RO. Bioinspired structural materials. Nature Materials 2015. https://doi.org/10.1038/nmat4089.

[24] Patra S, Young V. A Review of 3D Printing Techniques and the Future in Biofabrication of Bioprinted Tissue. Cell Biochemistry and Biophysics 2016. https://doi.org/10.1007/s12013-016-0730-0.

[25] Do AV, Khorsand B, Geary SM, Salem AK. 3D Printing of Scaffolds for Tissue Regeneration Applications. Advanced Healthcare Materials 2015. https://doi.org/10.1002/adhm.201500168.

[26] Jakab K, Norotte C, Marga F, Murphy K, Vunjak-Novakovic G, Forgacs G. Tissue engineering by self-assembly and bio-printing of living cells. Biofabrication 2010. https://doi.org/10.1088/1758-5082/2/2/022001.

[27] Kelm JM, Lorber V, Snedeker JG, Schmidt D, Broggini-Tenzer A, Weisstanner M, et al. A novel concept for scaffold-free vessel tissue engineering: Self-assembly of microtissue building blocks. Journal of Biotechnology 2010. https://doi.org/10.1016/j.jbiotec.2010.03.002.

[28] Sonntag F, Schilling N, Mader K, Gruchow M, Klotzbach U, Lindner G, et al. Design and prototyping of a chip-based multi-micro-organoid culture system for substance testing, predictive to human (substance) exposure. Journal of Biotechnology 2010. https://doi.org/10.1016/j.jbiotec.2010.02.001.

[29] Williams DF. On the mechanisms of biocompatibility. Biomaterials 2008. https://doi.org/10.1016/j.biomaterials.2008.04.023.

[30] Nair K, Gandhi M, Khalil S, Yan KC, Marcolongo M, Barbee K, et al. Characterization of cell viability during bioprinting processes. Biotechnology Journal 2009. https://doi.org/10.1002/biot.200900004.

[31] Hölzl K, Lin S, Tytgat L, van Vlierberghe S, Gu L, Ovsianikov A. Bioink properties before, during and after 3D bioprinting. Biofabrication 2016;8. https://doi.org/10.1088/1758-5090/8/3/032002.

[32] West JL, Hubbell JA. Polymeric biomaterials with degradation sites for proteases involved in cell migration. Macromolecules 1999. https://doi.org/10.1021/ma981296k.

[33] Wu L, Leijten JCH, Georgi N, Post JN, van Blitterswijk CA, Karperien M. Trophic effects of mesenchymal stem cells increase chondrocyte proliferation and matrix formation. Tissue Engineering - Part A 2011. https://doi.org/10.1089/ten.tea.2010.0517.

[34] Binder KW, Allen AJ, Yoo JJ, Atala A. Drop-on-demand inkjet bioprinting: A primer. Gene Therapy and Regulation 2011. https://doi.org/10.1142/S1568558611000258.

[35] Xu T, Jin J, Gregory C, Hickman JJ, Boland T. Inkjet printing of viable mammalian cells. Biomaterials 2005. https://doi.org/10.1016/j.biomaterials.2004.04.011.

[36] Zhang X, Zhang Y. Tissue Engineering Applications of Three-Dimensional Bioprinting. Cell Biochemistry and Biophysics 2015. https://doi.org/10.1007/s12013-015-0531-x.

[37] Iwami K, Noda T, Ishida K, Morishima K, Nakamura M, Umeda N. Bio rapid prototyping by extruding/aspirating/refilling thermoreversible hydrogel. Biofabrication 2010. https://doi.org/10.1088/1758-5082/2/1/014108.

[38] Guillotin B, Souquet A, Catros S, Duocastella M, Pippenger B, Bellance S, et al. Laser assisted bioprinting of engineered tissue with high cell density and microscale organization. Biomaterials 2010. https://doi.org/10.1016/j.biomaterials.2010.05.055.

[39] Xu T, Kincaid H, Atala A, Yoo JJ. High-throughput production of single-cell microparticles using an inkjet printing technology. Journal of Manufacturing Science and Engineering, Transactions of the ASME 2008. https://doi.org/10.1115/1.2903064.

[40] Tirella A, Vozzi F, de Maria C, Vozzi G, Sandri T, Sassano D, et al. Substrate stiffness influences high resolution printing of living cells with an ink-jet system. Journal of Bioscience and Bioengineering 2011. https://doi.org/10.1016/j.jbiosc.2011.03.019.

[41] Xu T, Gregory CA, Molnar P, Cui X, Jalota S, Bhaduri SB, et al. Viability and electrophysiology of neural cell structures generated by the inkjet printing method. Biomaterials 2006. https://doi.org/10.1016/j.biomaterials.2006.01.048.

[42] Cui X, Dean D, Ruggeri ZM, Boland T. Cell damage evaluation of thermal inkjet printed chinese hamster ovary cells. Biotechnology and Bioengineering 2010. https://doi.org/10.1002/bit.22762.

[43] Yang EH, Lee C, Mueller J, George T. Leak-tight piezoelectric microvalve for high-pressure gas micropropulsion. Journal of Microelectromechanical Systems 2004;13:799–807. https://doi.org/10.1109/JMEMS.2004.835767.

[44] Demirci U, Montesano G. Single cell epitaxy by acoustic picolitre droplets. Lab on a Chip 2007. https://doi.org/10.1039/b704965j.

[45] Christensen K, Xu C, Chai W, Zhang Z, Fu J, Huang Y. Freeform inkjet printing of cellular structures with bifurcations. Biotechnology and Bioengineering 2015;112. https://doi.org/10.1002/bit.25501.

[46] Wijshoff H. The dynamics of the piezo inkjet printhead operation. Physics Reports 2010;491. https://doi.org/10.1016/j.physrep.2010.03.003.

[47] Kim JD, Choi JS, Kim BS, Chan Choi Y, Cho YW. Piezoelectric inkjet printing of polymers: Stem cell patterning on polymer substrates. Polymer (Guildf) 2010. https://doi.org/10.1016/j.polymer.2010.03.038.

[48] Barron JA, Ringeisen BR, Kim H, Spargo BJ, Chrisey DB. Application of laser printing to mammalian cells. Thin Solid Films, 2004. https://doi.org/10.1016/j.tsf.2003.11.161.

[49] Colina M, Serra P, Fernández-Pradas JM, Sevilla L, Morenza JL. DNA deposition through laser induced forward transfer. Biosensors and Bioelectronics, 2005. https://doi.org/10.1016/j.bios.2004.08.047.

[50] Gruene M, Deiwick A, Koch L, Schlie S, Unger C, Hofmann N, et al. Laser printing of stem cells for biofabrication of scaffold-free autologous grafts. Tissue Engineering - Part C: Methods 2010. https://doi.org/10.1089/ten.tec.2010.0359.

[51] Li J, Chen M, Fan X, Zhou H. Recent advances in bioprinting techniques: Approaches, applications and future prospects. Journal of Translational Medicine 2016. https://doi.org/10.1186/s12967-016-1028-0.

[52] Moldovan NI, Hibino N, Nakayama K. Principles of the kenzan method for robotic cell spheroid-based three-dimensional bioprinting. Tissue Engineering - Part B: Reviews 2017. https://doi.org/10.1089/ten.teb.2016.0322.

[53] What is the Kenzan Method for 3D Bioprinting from Cyfuse's Regenova System? - 3D Printing Media Network n.d. https://www.3dprintingmedia.network/kenzan-method-3d-bioprinting-cyfuses-regenova-system/ (accessed June 3, 2021).

[54] Itoh M, Nakayama K, Noguchi R, Kamohara K, Furukawa K, Uchihashi K, et al. Scaffold-free tubular tissues created by a bio-3D printer undergo remodeling and endothelialization when implanted in rat aortae. PLoS ONE 2015. https://doi.org/10.1371/journal.pone.0136681.

[55] Campbell PG, Weiss LE. Tissue engineering with the aid of inkjet printers. Expert Opinion on Biological Therapy 2007. https://doi.org/10.1517/14712598.7.8.1123.

[56] Wang M, He J, Liu Y, Li M, Li D, Jin Z. The trend towards in vivo bioprinting. International Journal of Bioprinting 2015. https://doi.org/10.18063/IJB.2015.01.001.

[57] Murdock MH, Badylak SF. Biomaterials-based in situ tissue engineering. Current Opinion in Biomedical Engineering 2017. https://doi.org/10.1016/j.cobme.2017.01.001.

[58] Ozbolat IT. Bioprinting scale-up tissue and organ constructs for transplantation. Trends in Biotechnology 2015. https://doi.org/10.1016/j.tibtech.2015.04.005.

[59] Li X, Lian Q, Li D, Xin H, Jia S. Development of a robotic arm based hydrogel additive manufacturing system for in-situ printing. Applied Sciences (Switzerland) 2017. https://doi.org/10.3390/app7010073.

[60] Ravnic DJ, Leberfinger AN, Koduru S v., Hospodiuk M, Moncal KK, Datta P, et al. Transplantation of Bioprinted Tissues and Organs: Technical and Clinical Challenges and

Future Perspectives. Annals of Surgery 2017. https://doi.org/10.1097/SLA.0000000000002141.

[61] Keriquel V, Guillemot F, Arnault I, Guillotin B, Miraux S, Amédée J, et al. In vivo bioprinting for computer- and robotic-assisted medical intervention: Preliminary study in mice. Biofabrication 2010. https://doi.org/10.1088/1758-5082/2/1/014101.

[62] Skardal A, Mack D, Kapetanovic E, Atala A, Jackson JD, Yoo J, et al. Bioprinted Amniotic Fluid-Derived Stem Cells Accelerate Healing of Large Skin Wounds. STEM CELLS Translational Medicine 2012. https://doi.org/10.5966/sctm.2012-0088.

[63] Cohen DL, Lipton JI, Bonassar LJ, Lipson H. Additive manufacturing for in situ repair of osteochondral defects. Biofabrication 2010. https://doi.org/10.1088/1758-5082/2/3/035004.

[64] O'Connell CD, di Bella C, Thompson F, Augustine C, Beirne S, Cornock R, et al. Development of the Biopen: A handheld device for surgical printing of adipose stem cells at a chondral wound site. Biofabrication 2016. https://doi.org/10.1088/1758-5090/8/1/015019.

[65] Hakimi N, Cheng R, Leng L, Sotoudehfar M, Ba PQ, Bakhtyar N, et al. Handheld skin printer:: In situ formation of planar biomaterials and tissues. Lab on a Chip 2018. https://doi.org/10.1039/c7lc01236e.

[66] Visser CW, Kamperman T, Karbaat LP, Lohse D, Karperien M. In-air microfluidics enables rapid fabrication of emulsions, suspensions, and 3D modular (bio)materials. Science Advances 2018. https://doi.org/10.1126/sciadv.aao1175.

[67] Gesim. Bioinstruments and Microfluidics n.d.

[68] Albanna M, Binder KW, Murphy S v., Kim J, Qasem SA, Zhao W, et al. In Situ Bioprinting of Autologous Skin Cells Accelerates Wound Healing of Extensive Excisional Full-Thickness Wounds. Scientific Reports 2019. https://doi.org/10.1038/s41598-018-38366-w.

[69] Sakurada S, Sole-Gras M, Christensen K, Wallace DB, Huang Y. Liquid-absorbing system-assisted intersecting jets printing of soft structures from reactive biomaterials. Additive Manufacturing 2020. https://doi.org/10.1016/j.addma.2019.100934.

[70] Montalbano G, Toumpaniari S, Popov A, Duan P, Chen J, Dalgarno K, et al. Synthesis of bioinspired collagen/alginate/fibrin based hydrogels for soft tissue engineering. Materials Science and Engineering C 2018;91. https://doi.org/10.1016/j.msec.2018.04.101.

[71] Hong H, Stegemann JP. 2D and 3D collagen and fibrin biopolymers promote specific ECM and integrin gene expression by vascular smooth muscle cells. Journal of Biomaterials Science, Polymer Edition 2008. https://doi.org/10.1163/156856208786052380.

[72] Sun T, Jackson S, Haycock JW, MacNeil S. Culture of skin cells in 3D rather than 2D improves their ability to survive exposure to cytotoxic agents. Journal of Biotechnology 2006. https://doi.org/10.1016/j.jbiotec.2005.12.021.

[73] Edmondson R, Broglie JJ, Adcock AF, Yang L. Three-dimensional cell culture systems and their applications in drug discovery and cell-based biosensors. Assay and Drug Development Technologies 2014. https://doi.org/10.1089/adt.2014.573.

[74] Tibbitt MW, Anseth KS. Hydrogels as extracellular matrix mimics for 3D cell culture. Biotechnology and Bioengineering 2009. https://doi.org/10.1002/bit.22361.

[75] Katt ME, Placone AL, Wong AD, Xu ZS, Searson PC. In vitro tumor models: Advantages, disadvantages, variables, and selecting the right platform. Frontiers in Bioengineering and Biotechnology 2016. https://doi.org/10.3389/fbioe.2016.00012.

[76] Nath S, Devi GR. Three-dimensional culture systems in cancer research: Focus on tumor spheroid model. Pharmacology and Therapeutics 2016. https://doi.org/10.1016/j.pharmthera.2016.03.013.

[77] Bhadriraju K, Chen CS. Engineering cellular microenvironments to improve cell-based drug testing. Drug Discovery Today 2002. https://doi.org/10.1016/S1359-6446(02)02273-0.

[78] Woodfield TBF, Malda J, de Wijn J, Péters F, Riesle J, van Blitterswijk CA. Design of porous scaffolds for cartilage tissue engineering using a three-dimensional fiber-deposition technique. Biomaterials 2004. https://doi.org/10.1016/j.biomaterials.2003.10.056.

[79] Melissaridou S, Wiechec E, Magan M, Jain MV, Chung MK, Farnebo L, et al. The effect of 2D and 3D cell cultures on treatment response, EMT profile and stem cell features in head and neck cancer. Cancer Cell International 2019. https://doi.org/10.1186/s12935-019-0733-1.

[80] Tung YC, Hsiao AY, Allen SG, Torisawa YS, Ho M, Takayama S. High-throughput 3D spheroid culture and drug testing using a 384 hanging drop array. Analyst 2011. https://doi.org/10.1039/c0an00609b.

[81] Kojima N, Takeuchi S, Sakai Y. Rapid aggregation of heterogeneous cells and multiple-sized microspheres in methylcellulose medium. Biomaterials 2012. https://doi.org/10.1016/j.biomaterials.2012.02.065.

[82] Aijian AP, Garrell RL. Digital Microfluidics for Automated Hanging Drop Cell Spheroid Culture. Journal of Laboratory Automation 2015. https://doi.org/10.1177/2211068214562002.

[83] Fennema E, Rivron N, Rouwkema J, van Blitterswijk C, de Boer J. Spheroid culture as a tool for creating 3D complex tissues. Trends in Biotechnology 2013. https://doi.org/10.1016/j.tibtech.2012.12.003.

[84] Aguilar IN, Smith LJ, Olivos DJ, Chu TMG, Kacena MA, Wagner DR. Scaffold-free bioprinting of mesenchymal stem cells with the regenova printer: Optimization of printing parameters. Bioprinting 2019. https://doi.org/10.1016/j.bprint.2019.e00048.

[85] Daly AC, Davidson MD, Burdick JA. 3D bioprinting of high cell-density heterogeneous tissue models through spheroid fusion within self-healing hydrogels. Nature Communications 2021. https://doi.org/10.1038/s41467-021-21029-2.

[86] Meretoja V v., Dahlin RL, Kasper FK, Mikos AG. Enhanced chondrogenesis in co-cultures with articular chondrocytes and mesenchymal stem cells. Biomaterials 2012. https://doi.org/10.1016/j.biomaterials.2012.05.042.

[87] Hendriks J, Riesle J, van Blitterswijk CA. Co-culture in cartilage tissue engineering. Journal of Tissue Engineering and Regenerative Medicine 2007. https://doi.org/10.1002/term.19.

[88] Sekiya I, Vuoristo JT, Larson BL, Prockop DJ. In vitro cartilage formation by human adult stem cells from bone marrow stroma defines the sequence of cellular and molecular events during chondrogenesis. Proc Natl Acad Sci U S A 2002. https://doi.org/10.1073/pnas.052716199.

[89] Grimaud E, Heymann D, Rédini F. Recent advances in TGF-β effects on chondrocyte metabolism potential therapeutic roles of TGF-β in cartilage disorders. Cytokine and Growth Factor Reviews 2002;13:241–57. https://doi.org/10.1016/S1359-6101(02)00004-7.

[90] Sailor LZ, Hewick RM, Morris EA. Recombinant human bone morphogenetic protein-2 maintains the articular chondrocyte phenotype in long-term culture. Journal of Orthopaedic Research 1996. https://doi.org/10.1002/jor.1100140614.

[91] Elder BD, Athanasiou KA. Systematic assessment of growth factor treatment on biochemical and biomechanical properties of engineered articular cartilage constructs. Osteoarthritis and Cartilage 2009. https://doi.org/10.1016/j.joca.2008.05.006.

[92] Liu X, Sun H, Yan D, Zhang L, Lv X, Liu T, et al. In vivo ectopic chondrogenesis of BMSCs directed by mature chondrocytes. Biomaterials 2010. https://doi.org/10.1016/j.biomaterials.2010.08.052.

[93] Acharya C, Adesida A, Zajac P, Mumme M, Riesle J, Martin I, et al. Enhanced chondrocyte proliferation and mesenchymal stromal cells chondrogenesis in coculture pellets mediate improved cartilage formation. Journal of Cellular Physiology 2012. https://doi.org/10.1002/jcp.22706.

[94] Aung A, Gupta G, Majid G, Varghese S. Osteoarthritic chondrocyte-secreted morphogens induce chondrogenic differentiation of human mesenchymal stem cells. Arthritis and Rheumatism 2011. https://doi.org/10.1002/art.30086.

[95] Wu L, Prins HJ, Helder MN, van Blitterswijk CA, Karperien M. Trophic effects of mesenchymal stem cells in chondrocyte Co-Cultures are independent of culture conditions and cell sources. Tissue Engineering - Part A 2012. https://doi.org/10.1089/ten.tea.2011.0715.

[96] Paish HL, Reed LH, Brown H, Bryan MC, Govaere O, Leslie J, et al. A Bioreactor Technology for Modeling Fibrosis in Human and Rodent Precision-Cut Liver Slices. Hepatology 2019. https://doi.org/10.1002/hep.30651.

[97] Restouin A, Aresta S, Prébet T, Borg JP, Badache A, Collette Y. A simplified, 96-well-adapted, ATP luminescence-based motility assay. Biotechniques 2009. https://doi.org/10.2144/000113250.

[98] Vis MAM, Ito K, Hofmann S. Impact of Culture Medium on Cellular Interactions in in vitro Co-culture Systems. Frontiers in Bioengineering and Biotechnology 2020. https://doi.org/10.3389/fbioe.2020.00911.

[99] Goers L, Freemont P, Polizzi KM. Co-culture systems and technologies: Taking synthetic biology to the next level. Journal of the Royal Society Interface 2014. https://doi.org/10.1098/rsif.2014.0065.

[100] Zhu S, Ehnert S, Rouß M, Häussling V, Aspera-Werz RH, Chen T, et al. From the clinical problem to the basic research—Co-culture models of osteoblasts and osteoclasts. International Journal of Molecular Sciences 2018. https://doi.org/10.3390/ijms19082284.

[101] Eckermann CW, Lehle K, Schmid SA, Wheatley DN, Kunz-Schughart LA. Characterization and modulation of fibroblast/endothelial cell co-cultures for the in vitro preformation of three-dimensional tubular networks . Cell Biology International 2011. https://doi.org/10.1042/cbi20100718.

[102] Traphagen SB, Titushkin I, Sun S, Wary KK, Cho M. Endothelial invasive response in a co-culture model with physically-induced osteodifferentiation. Journal of Tissue Engineering and Regenerative Medicine 2013. https://doi.org/10.1002/term.554.

[103] Nakaoka R, Hsiong SX, Mooney DJ. Regulation of chondrocyte differentiation level via co-culture with osteoblasts. Tissue Engineering 2006. https://doi.org/10.1089/ten.2006.12.2425.

[104] Battiston KG, Cheung JWC, Jain D, Santerre JP. Biomaterials in co-culture systems: Towards optimizing tissue integration and cell signaling within scaffolds. Biomaterials 2014. https://doi.org/10.1016/j.biomaterials.2014.02.023.

[105] Jiang J, Nicoll SB, Lu HH. Co-culture of osteoblasts and chondrocytes modulates cellular differentiation in vitro. Biochemical and Biophysical Research Communications 2005. https://doi.org/10.1016/j.bbrc.2005.10.025.

[106] Jiang J, Tang A, Ateshian GA, Edward Guo X, Hung CT, Lu HH. Bioactive stratified polymer ceramic-hydrogel scaffold for integrative osteochondral repair. Annals of Biomedical Engineering 2010. https://doi.org/10.1007/s10439-010-0038-y.

[107] Korpayev S, Kaygusuz G, Şen M, Orhan K, Oto Ç, Karakeçili A. Chitosan/collagen based biomimetic osteochondral tissue constructs: A growth factor-free approach. International Journal of Biological Macromolecules 2020. https://doi.org/10.1016/j.ijbiomac.2020.04.109.

[108] Xue R, Chung B, Tamaddon M, Carr J, Liu C, Cartmell SH. Osteochondral tissue coculture: An in vitro and in silico approach. Biotechnology and Bioengineering 2019. https://doi.org/10.1002/bit.27127.

[109] Kloxin AM, Kloxin CJ, Bowman CN, Anseth KS. Mechanical properties of cellularly responsive hydrogels and their experimental determination. Advanced Materials 2010. https://doi.org/10.1002/adma.200904179.

[110] Fairbanks BD, Schwartz MP, Halevi AE, Nuttelman CR, Bowman CN, Anseth KS. A versatile synthetic extracellular matrix mimic via thiol-norbornene photopolymerization. Advanced Materials 2009. https://doi.org/10.1002/adma.200901808.

[111] Lutolf MP, Raeber GP, Zisch AH, Tirelli N, Hubbell JA. Cell-responsive synthetic hydrogels. Advanced Materials 2003. https://doi.org/10.1002/adma.200304621.

[112] Raeber GP, Lutolf MP, Hubbell JA. Mechanisms of 3-D migration and matrix remodeling of fibroblasts within artificial ECMs. Acta Biomaterialia 2007. https://doi.org/10.1016/j.actbio.2007.03.013.

[113] Frey MT, Wang YL. A photo-modulatable material for probing cellular responses to substrate rigidity. Soft Matter 2009. https://doi.org/10.1039/b818104g.

[114] Giepmans BNG, Adams SR, Ellisman MH, Tsien RY. The fluorescent toolbox for assessing protein location and function. Science (1979) 2006. https://doi.org/10.1126/science.1124618.

[115] VanEngelenburg SB, Palmer AE. Fluorescent biosensors of protein function. Current Opinion in Chemical Biology 2008. https://doi.org/10.1016/j.cbpa.2008.01.020.

[116] Wirtz D. Particle-tracking microrheology of living cells: Principles and applications. Annual Review of Biophysics 2009. https://doi.org/10.1146/annurev.biophys.050708.133724.

[117] Baker EL, Bonnecaze RT, Zaman MH. Extracellular matrix stiffness and architecture govern intracellular rheology in cancer. Biophysical Journal 2009. https://doi.org/10.1016/j.bpj.2009.05.054.

[118] Maskarinec SA, Franck C, Tirrell DA, Ravichandran G. Quantifying cellular traction forces in three dimensions. Proc Natl Acad Sci U S A 2009. https://doi.org/10.1073/pnas.0904565106.

[119] Reinhart-King CA, Dembo M, Hammer DA. Cell-cell mechanical communication through compliant substrates. Biophysical Journal 2008. https://doi.org/10.1529/biophysj.107.127662.

[120] Banerjee A, Arha M, Choudhary S, Ashton RS, Bhatia SR, Schaffer D v., et al. The influence of hydrogel modulus on the proliferation and differentiation of encapsulated neural stem cells. Biomaterials 2009. https://doi.org/10.1016/j.biomaterials.2009.05.050.

[121] Grant PK, Szep G, Patange O, Halatek J, Coppard V, Csikász-Nagy A, et al. Interpretation of morphogen gradients by a synthetic bistable circuit. Nature Communications 2020. https://doi.org/10.1038/s41467-020-19098-w.

[122] Chen CS, Mrksich M, Huang S, Whitesides GM, Ingber DE. Geometric control of cell life and death. Science (1979) 1997. https://doi.org/10.1126/science.276.5317.1425.

[123] Chen A, Davis BH. UV irradiation activates JNK and increases αI(I) collagen gene expression in rat hepatic stellate cells. Journal of Biological Chemistry 1999. https://doi.org/10.1074/jbc.274.1.158.

[124] Shoulders MD, Raines RT. Collagen structure and stability. Annual Review of Biochemistry 2009. https://doi.org/10.1146/annurev.biochem.77.032207.120833.

[125] Doyle AD, Carvajal N, Jin A, Matsumoto K, Yamada KM. Local 3D matrix microenvironment regulates cell migration through spatiotemporal dynamics of contractility-dependent adhesions. Nature Communications 2015. https://doi.org/10.1038/ncomms9720.

[126] Kim H do, Guo TW, Wu AP, Wells A, Gertler FB, Lauffenburger DA. Epidermal growth factor-induced enhancement of glioblastoma cell migration in 3D arises from an intrinsic increase in speed but an extrinsic matrix-and proteolysis-dependent increase in persistence. Molecular Biology of the Cell 2008. https://doi.org/10.1091/mbc.E08-05-0501.

[127] Corning. Corning® Matrigel® Matrix. Https://WwwCorningCom/Catalog/Cls/Documents/Faqs/CLS-DL-CC-026Pdf 2022.

[128] Lawrie AS, McDonald SJ, Purdy G, Mackie IJ, Machin SJ. Prothrombin time derived fibrinogen determination on Sysmex CA-6000(TM). Journal of Clinical Pathology 1998. https://doi.org/10.1136/jcp.51.6.462.

[129] Bian W, Juhas M, Pfeiler TW, Bursac N. Local tissue geometry determines contractile force generation of engineered muscle networks. Tissue Engineering - Part A 2012. https://doi.org/10.1089/ten.tea.2011.0313.

[130] Paxton JZ, Wudebwe UNG, Wang A, Woods D, Grover LM. Monitoring sinew contraction during formation of tissue-engineered fibrin-based ligament constructs. Tissue Engineering - Part A 2012. https://doi.org/10.1089/ten.tea.2011.0535.

[131] Lin CC, Anseth KS. PEG hydrogels for the controlled release of biomolecules in regenerative medicine. Pharmaceutical Research 2009. https://doi.org/10.1007/s11095-008-9801-2.

[132] Lu Y, Aimetti AA, Langer R, Gu Z. Bioresponsive materials. Nature Reviews Materials 2016;2. https://doi.org/10.1038/natrevmats.2016.75.

[133] Khan F, Tanaka M. Designing smart biomaterials for tissue engineering. International Journal of Molecular Sciences 2018;19. https://doi.org/10.3390/ijms19010017.

[134] Nguyen QT, Hwang Y, Chen AC, Varghese S, Sah RL. Cartilage-like mechanical properties of poly (ethylene glycol)-diacrylate hydrogels. Biomaterials 2012;33. https://doi.org/10.1016/j.biomaterials.2012.06.005.

[135] Kloxin AM, Kasko AM, Salinas CN, Anseth KS. Photodegradable hydrogels for dynamic tuning of physical and chemical properties. Science (1979) 2009. https://doi.org/10.1126/science.1169494.

[136] Lutolf MP, Lauer-Fields JL, Schmoekel HG, Metters AT, Weber FE, Fields GB, et al. Synthetic matrix metalloproteinase-sensitive hydrogels for the conduction of tissue regeneration: Engineering cell-invasion characteristics. Proc Natl Acad Sci U S A 2003. https://doi.org/10.1073/pnas.0737381100.

[137] Phelps EA, Enemchukwu NO, Fiore VF, Sy JC, Murthy N, Sulchek TA, et al. Maleimide cross-linked bioactive PEG hydrogel exhibits improved reaction kinetics and cross-linking for cell encapsulation and in situ delivery. Advanced Materials 2012. https://doi.org/10.1002/adma.201103574.

[138] Burdick JA, Anseth KS. Photoencapsulation of osteoblasts in injectable RGD-modified PEG hydrogels for bone tissue engineering. Biomaterials 2002. https://doi.org/10.1016/S0142-9612(02)00176-X.

[139] Akmal M, Anand A, Anand B, Wiseman M, Goodship AE, Bentley G. The culture of articular chondrocytes in hydrogel constructs within a bioreactor enhances cell proliferation and matrix synthesis. Journal of Bone and Joint Surgery - Series B 2006. https://doi.org/10.1302/0301-620X.88B4.16498.

[140] Mabvuure N, Hindocha S, S. Khan W. The Role of Bioreactors in Cartilage Tissue Engineering. Current Stem Cell Research & Therapy 2012. https://doi.org/10.2174/157488812800793018.

[141] Cochis A, Grad S, Stoddart MJ, Farè S, Altomare L, Azzimonti B, et al. Bioreactor mechanically guided 3D mesenchymal stem cell chondrogenesis using a biocompatible novel thermo-reversible methylcellulose-based hydrogel. Scientific Reports 2017. https://doi.org/10.1038/srep45018.

[142] Huh D, Matthews BD, Mammoto A, Montoya-Zavala M, Yuan Hsin H, Ingber DE. Reconstituting organ-level lung functions on a chip. Science (1979) 2010. https://doi.org/10.1126/science.1188302.

[143] Pörtner R, Nagel-Heyer S, Goepfert C, Adamietz P, Meenen NM. Bioreactor design for tissue engineering. Journal of Bioscience and Bioengineering 2005. https://doi.org/10.1263/jbb.100.235.

[144] Branco MC, Pochan DJ, Wagner NJ, Schneider JP. Macromolecular diffusion and release from self-assembled β-hairpin peptide hydrogels. Biomaterials 2009. https://doi.org/10.1016/j.biomaterials.2008.11.019.

[145] Stellwagen NC. Apparent pore size of polyacrylamide gels: Comparison of gels cast and run in Tris-acetate-EDTA and Tris-borate-EDTA buffers. Electrophoresis 1998. https://doi.org/10.1002/elps.1150191004.

[146] Carrion B, Janson IA, Kong YP, Putnam AJ. A safe and efficient method to retrieve mesenchymal stem cells from three-dimensional fibrin gels. Tissue Engineering - Part C: Methods 2014. https://doi.org/10.1089/ten.tec.2013.0051.

[147] Loebsack AB, Halberstadt CR, Holder WD, Culberson CR, Beiler RJ, Greene KG, et al. The development of an embedding technique for polylactide sponges. Journal of Biomedical Materials Research 1999. https://doi.org/10.1002/(SICI)1097-4636(1999)48:4<504::AID-JBM16>3.0.CO;2-Y.

[148] World Health Organization. No Title. World Health Organization 2021:Chronic rheumatic conditions. https://www.who.int/chp/topics/rheumatic/en/ (accessed May 31, 2021).

[149] Hiligsmann M, Cooper C, Arden N, Boers M, Branco JC, Luisa Brandi M, et al. Health economics in the field of osteoarthritis: An Expert's consensus paper from the European Society for Clinical and Economic Aspects of Osteoporosis and Osteoarthritis (ESCEO). Seminars in Arthritis and Rheumatism 2013. https://doi.org/10.1016/j.semarthrit.2013.07.003.

[150] Loeser RF, Collins JA, Diekman BO. Ageing and the pathogenesis of osteoarthritis. Nature Reviews Rheumatology 2016. https://doi.org/10.1038/nrrheum.2016.65.

[151] Aurich M, Squires GR, Reiner A, Mollenhauer JA, Kuettner KE, Poole AR, et al. Differential matrix degradation and turnover in early cartilage lesions of human knee and ankle joints. Arthritis and Rheumatism 2005. https://doi.org/10.1002/art.20740.

[152] Burrage PS, Mix KS, Brinckerhoff CE. Matrix metalloproteinases: Role in arthritis. Frontiers in Bioscience 2006. https://doi.org/10.2741/1817.

[153] Karsenty G. An Aggrecanase and Osteoarthritis. New England Journal of Medicine 2005. https://doi.org/10.1056/nejmcibr051399.

[154] Bondeson J, Wainwright SD, Lauder S, Amos N, Hughes CE. The role of synovial macrophages and macrophage-produced cytokines in driving aggrecanases, matrix metalloproteinases, and other destructive and inflammatory responses in osteoarthritis. Arthritis Research and Therapy 2006. https://doi.org/10.1186/ar2099.

[155] Intema F, Hazewinkel HAW, Gouwens D, Bijlsma JWJ, Weinans H, Lafeber FPJG, et al. In early OA, thinning of the subchondral plate is directly related to cartilage damage: Results from a canine ACLT-meniscectomy model. Osteoarthritis and Cartilage 2010. https://doi.org/10.1016/j.joca.2010.01.004.

[156] Intema F, Sniekers YH, Weinans H, Vianen ME, Yocum SA, Zuurmond AMM, et al. Similarities and discrepancies in subchondral bone structure in two differently induced canine models of osteoarthritis. Journal of Bone and Mineral Research 2010. https://doi.org/10.1002/jbmr.39.

[157] Bhosale AM, Richardson JB. Articular cartilage: Structure, injuries and review of management. British Medical Bulletin 2008. https://doi.org/10.1093/bmb/ldn025.

[158] Buckwalter JA, Mankin HJ, Grodzinsky AJ. Articular cartilage and osteoarthritis. Instr Course Lect 2005. https://doi.org/10.1136/ard.51.9.1028-a.

[159] Hu X, Xu J, Li W, Li L, Parungao R, Wang Y, et al. Therapeutic "Tool" in Reconstruction and Regeneration of Tissue Engineering for Osteochondral Repair. Applied Biochemistry and Biotechnology 2020. https://doi.org/10.1007/s12010-019-03214-8.

[160] Weinans H, Siebelt M, Agricola R, Botter SM, Piscaer TM, Waarsing JH. Pathophysiology of peri-articular bone changes in osteoarthritis. Bone 2012. https://doi.org/10.1016/j.bone.2012.02.002.

[161] Cox LGE, van Donkelaar CC, van Rietbergen B, Emans PJ, Ito K. Decreased bone tissue mineralization can partly explain subchondral sclerosis observed in osteoarthritis. Bone 2012. https://doi.org/10.1016/j.bone.2012.01.024.

[162] Buckland-Wright C. Subchondral bone changes in hand and knee osteoarthritis detected by radiography. Osteoarthritis and Cartilage 2004. https://doi.org/10.1016/j.joca.2003.09.007.

[163] Dieppe P, Cushnaghan J, Young P, Kirwan J. Prediction of the progression of joint space narrowing in osteoarthritis of the knee by bone scintigraphy. Annals of the Rheumatic Diseases 1993. https://doi.org/10.1136/ard.52.8.557.

[164] Sanchez C, Pesesse L, Gabay O, Delcour JP, Msika P, Baudouin C, et al. Regulation of subchondral bone osteoblast metabolism by cyclic compression. Arthritis Rheum 2012. https://doi.org/10.1002/art.33445.

[165] Bastow ER, Byers S, Golub SB, Clarkin CE, Pitsillides AA, Fosang AJ. Hyaluronan synthesis and degradation in cartilage and bone. Cellular and Molecular Life Sciences 2008. https://doi.org/10.1007/s00018-007-7360-z.

[166] Marcelino J, Carpten JD, Suwairi WM, Gutierrez OM, Schwartz S, Robbins C, et al. CACP, encoding a secreted proteoglycan, is mutated in camptodactyly- arthropathy-coxa vara-pericarditis syndrome. Nature Genetics 1999. https://doi.org/10.1038/15496.

[167] Ludwig TE, McAllister JR, Lun V, Wiley JP, Schmidt TA. Diminished cartilage-lubricating ability of human osteoarthritic synovial fluid deficient in proteoglycan 4: Restoration through proteoglycan 4 supplementation. Arthritis and Rheumatism 2012. https://doi.org/10.1002/art.34674.

[168] Dieppe PA, Lohmander LS. Pathogenesis and management of pain in osteoarthritis. Lancet, 2005. https://doi.org/10.1016/S0140-6736(05)71086-2.

[169] Clohisy JC, Calvert G, Tull F, McDonald D, Maloney WJ. Reasons for revision hip surgery: A retrospective review. Clinical Orthopaedics and Related Research, 2004. https://doi.org/10.1097/01.blo.0000150126.73024.42.

[170] Ghalme SG, Mankar A, Bhalerao Y. Biomaterials in Hip Joint Replacement. International Journal of Materials Science and Engineering 2016. https://doi.org/10.17706/ijmse.2016.4.2.113-125.

[171] Crowe JF, Sculco TP, Kahn B. Revision Total Hip Arthroplasty: Hospital Cost and Reimbursement Analysis. Clinical Orthopaedics and Related Research 2003. https://doi.org/10.1097/01.blo.0000072469.32680.b6.

[172] Erggelet C, Vavken P. Microfracture for the treatment of cartilage defects in the knee joint – A golden standard? Journal of Clinical Orthopaedics and Trauma 2016. https://doi.org/10.1016/j.jcot.2016.06.015.

[173] Harris JD, Siston RA, Pan X, Flanigan DC. Autologous chondrocyte implantation: A systematic review. Journal of Bone and Joint Surgery - Series A 2010. https://doi.org/10.2106/JBJS.J.00049.

[174] Niemeyer P, Albrecht D, Andereya S, Angele P, Ateschrang A, Aurich M, et al. Autologous chondrocyte implantation (ACI) for cartilage defects of the knee: A guideline by the working group “Clinical Tissue Regeneration” of the German Society of Orthopaedics and Trauma (DGOU). Knee 2016. https://doi.org/10.1016/j.knee.2016.02.001.

[175] Fedorovich NE, Schuurman W, Wijnberg HM, Prins HJ, van Weeren PR, Malda J, et al. Biofabrication of osteochondral tissue equivalents by printing topologically defined, cell-laden hydrogel scaffolds. Tissue Engineering - Part C: Methods 2012. https://doi.org/10.1089/ten.tec.2011.0060.

[176] Jeong CG, Atala A. 3D printing and Biofabrication for load bearing tissue engineering. Advances in Experimental Medicine and Biology, 2015. https://doi.org/10.1007/978-3-319-22345-2_1.

[177] di Bella C, Duchi S, O'Connell CD, Blanchard R, Augustine C, Yue Z, et al. In situ handheld three-dimensional bioprinting for cartilage regeneration. Journal of Tissue Engineering and Regenerative Medicine 2018. https://doi.org/10.1002/term.2476.

[178] Evans CH, Ghivizzani SC, Robbins PD. Gene Delivery to Joints by Intra-Articular Injection. Human Gene Therapy 2018;29. https://doi.org/10.1089/hum.2017.181.

[179] Frisbie DD, McIlwraith CW. Gene therapy: future therapies in osteoarthritis. Vet Clin North Am Equine Pract 2001;17. https://doi.org/10.1016/S0749-0739(17)30059-7.

[180] Evans CH, Ghivizzani SC, Robbins PD. Arthritis gene therapy and its tortuous path into the clinic. Translational Research 2013. https://doi.org/10.1016/j.trsl.2013.01.002.

[181] Thysen S, Luyten FP, Lories RJU. Targets, models and challenges in osteoarthritis research. DMM Disease Models and Mechanisms 2015. https://doi.org/10.1242/dmm.016881.

[182] Rey-Rico A, Madry H, Cucchiarini M. Hydrogel-Based Controlled Delivery Systems for Articular Cartilage Repair. BioMed Research International 2016. https://doi.org/10.1155/2016/1215263.

[183] Tat SK, Pelletier JP, Mineau F, Caron J, Martel-Pelletier J. Strontium ranelate inhibits key factors affecting bone remodeling in human osteoarthritic subchondral bone osteoblasts. Bone 2011. https://doi.org/10.1016/j.bone.2011.06.005.

[184] Hurley ET, Yasui Y, Gianakos AL, Seow D, Shimozono Y, Kerkhoffs GMMJ, et al. Limited evidence for adipose-derived stem cell therapy on the treatment of osteoarthritis. Knee Surgery, Sports Traumatology, Arthroscopy 2018. https://doi.org/10.1007/s00167-018-4955-x.

[185] Pas HI, Winters M, Haisma HJ, Koenis MJ, Tol JL, Moen MH. Stem cell injections in knee osteoarthritis: a systematic review of the literature. Br J Sports Med 2017. https://doi.org/10.1136/bjsports-2016-096793.

[186] Armoiry X, Cummins E, Connock M, Metcalfe A, Royle P, Johnston R, et al. Autologous Chondrocyte Implantation with Chondrosphere for Treating Articular Cartilage Defects in the Knee: An Evidence Review Group Perspective of a NICE Single Technology Appraisal. Pharmacoeconomics 2019. https://doi.org/10.1007/s40273-018-0737-z.

[187] Gandjour A. Willingness to pay for new medicines: A step towards narrowing the gap between NICE and IQWiG. BMC Health Services Research 2020. https://doi.org/10.1186/s12913-020-5050-9.

[188] Paul SM, Mytelka DS, Dunwiddie CT, Persinger CC, Munos BH, Lindborg SR, et al. How to improve RD productivity: The pharmaceutical industry's grand challenge. Nature Reviews Drug Discovery 2010. https://doi.org/10.1038/nrd3078.

[189] Imaduwage KP, Lakbub J, Go EP, Desaire H. Rapid LC-MS Based High-Throughput Screening Method, Affording No False Positives or False Negatives, Identifies a New Inhibitor for Carbonic Anhydrase. Scientific Reports 2017. https://doi.org/10.1038/s41598-017-08602-w.

[190] Thakur M, Rahman W, Hobbs C, Dickenson AH, Bennett DLH. Characterisation of a peripheral neuropathic component of the rat monoiodoacetate model of osteoarthritis. PLoS ONE 2012. https://doi.org/10.1371/journal.pone.0033730.

[191] Kuyinu EL, Narayanan G, Nair LS, Laurencin CT. Animal models of osteoarthritis: Classification, update, and measurement of outcomes. Journal of Orthopaedic Surgery and Research 2016. https://doi.org/10.1186/s13018-016-0346-5.

[192] McCoy AM. Animal Models of Osteoarthritis: Comparisons and Key Considerations. Veterinary Pathology 2015. https://doi.org/10.1177/0300985815588611.

[193] Kyostio-Moore S, Nambiar B, Hutto E, Ewing PJ, Piraino S, Berthelette P, et al. STR/ort mice, a model for spontaneous osteoarthritis, exhibit elevated levels of both local and systemic inflammatory markers. Comparative Medicine 2011.

[194] Malfait AM, Little CB, McDougall JJ. A commentary on modelling osteoarthritis pain in small animals. Osteoarthritis and Cartilage 2013. https://doi.org/10.1016/j.joca.2013.06.003.

[195] Teeple E, Jay GD, Elsaid KA, Fleming BC. Animal models of osteoarthritis: Challenges of model selection and analysis. AAPS Journal 2013. https://doi.org/10.1208/s12248-013-9454-x.

[196] Chapman KL, Holzgrefe H, Black LE, Brown M, Chellman G, Copeman C, et al. Pharmaceutical toxicology: Designing studies to reduce animal use, while maximizing human translation. Regulatory Toxicology and Pharmacology 2013. https://doi.org/10.1016/j.yrtph.2013.03.001.

[197] Liu J, Li L, Suo H, Yan M, Yin J, Fu J. 3D printing of biomimetic multi-layered GelMA/nHA scaffold for osteochondral defect repair. Materials and Design 2019. https://doi.org/10.1016/j.matdes.2019.107708.

[198] He A, Liu L, Luo X, Liu Y, Liu Y, Liu F, et al. Repair of osteochondral defects with in vitro engineered cartilage based on autologous bone marrow stromal cells in a swine model. Scientific Reports 2017. https://doi.org/10.1038/srep40489.

[199] Kilian D, Ahlfeld T, Akkineni AR, Bernhardt A, Gelinsky M, Lode A. 3D Bioprinting of osteochondral tissue substitutes – in vitro-chondrogenesis in multi-layered mineralized constructs. Scientific Reports 2020. https://doi.org/10.1038/s41598-020-65050-9.

[200] Markstedt K, Mantas A, Tournier I, Martínez Ávila H, Hägg D, Gatenholm P. 3D bioprinting human chondrocytes with nanocellulose-alginate bioink for cartilage tissue engineering applications. Biomacromolecules 2015. https://doi.org/10.1021/acs.biomac.5b00188.

[201] Schuurman W, Levett PA, Pot MW, van Weeren PR, Dhert WJA, Hutmacher DW, et al. Gelatin-methacrylamide hydrogels as potential biomaterials for fabrication of tissue-engineered cartilage constructs. Macromolecular Bioscience 2013. https://doi.org/10.1002/mabi.201200471.

[202] Castilho M, Mouser V, Chen M, Malda J, Ito K. Bi-layered micro-fibre reinforced hydrogels for articular cartilage regeneration. Acta Biomaterialia 2019. https://doi.org/10.1016/j.actbio.2019.06.030.

[203] Schmitmeier S, Langsch A, Jasmund I, Bader A. Development and characterization of a small-scale bioreactor based on a bioartificial hepatic culture model for predictive pharmacological

in vitro screenings. Biotechnology and Bioengineering 2006. https://doi.org/10.1002/bit.21089.

[204] Härmä V, Virtanen J, Mäkelä R, Happonen A, Mpindi JP, Knuuttila M, et al. A comprehensive panel of three-dimensional models for studies of prostate cancer growth, invasion and drug responses. PLoS ONE 2010. https://doi.org/10.1371/journal.pone.0010431.

[205] Weigelt B, Lo AT, Park CC, Gray JW, Bissell MJ. HER2 signaling pathway activation and response of breast cancer cells to HER2-targeting agents is dependent strongly on the 3D microenvironment. Breast Cancer Research and Treatment 2010. https://doi.org/10.1007/s10549-009-0502-2.

[206] Liao MJ, Cheng CZ, Zhou B, Zimonjic DB, Mani SA, Kaba M, et al. Enrichment of a population of mammary gland cells that form mammospheres and have in vivo repopulating activity. Cancer Research 2007. https://doi.org/10.1158/0008-5472.CAN-06-4493.

[207] Gupta PB, Chaffer CL, Weinberg RA. Cancer stem cells: Mirage or reality? Nature Medicine 2009. https://doi.org/10.1038/nm0909-1010.

[208] Chambers AF, Groom AC, MacDonald IC. Dissemination and growth of cancer cells in metastatic sites. Nature Reviews Cancer 2002. https://doi.org/10.1038/nrc865.

[209] Clark AG, Vignjevic DM. Modes of cancer cell invasion and the role of the microenvironment. Current Opinion in Cell Biology 2015. https://doi.org/10.1016/j.ceb.2015.06.004.

[210] Friedl P, Wolf K. Tumour-cell invasion and migration: Diversity and escape mechanisms. Nature Reviews Cancer 2003. https://doi.org/10.1038/nrc1075.

[211] Bissell MJ, Hines WC. Why don't we get more cancer? A proposed role of the microenvironment in restraining cancer progression. Nature Medicine 2011. https://doi.org/10.1038/nm.2328.

[212] Hirschhaeuser F, Menne H, Dittfeld C, West J, Mueller-Klieser W, Kunz-Schughart LA. Multicellular tumor spheroids: An underestimated tool is catching up again. Journal of Biotechnology 2010. https://doi.org/10.1016/j.jbiotec.2010.01.012.

[213] Sant S, Johnston PA. The production of 3D tumor spheroids for cancer drug discovery. Drug Discovery Today: Technologies 2017. https://doi.org/10.1016/j.ddtec.2017.03.002.

[214] Zanoni M, Piccinini F, Arienti C, Zamagni A, Santi S, Polico R, et al. 3D tumor spheroid models for in vitro therapeutic screening: A systematic approach to enhance the biological relevance of data obtained. Scientific Reports 2016. https://doi.org/10.1038/srep19103.

[215] Kim SA, Lee EK, Kuh HJ. Co-culture of 3D tumor spheroids with fibroblasts as a model for epithelial-mesenchymal transition in vitro. Experimental Cell Research 2015. https://doi.org/10.1016/j.yexcr.2015.05.016.

[216] Liu T, Lin B, Qin J. Carcinoma-associated fibroblasts promoted tumor spheroid invasion on a microfluidic 3D co-culture device. Lab on a Chip 2010. https://doi.org/10.1039/c000022a.

[217] Mano JF. Designing biomaterials for tissue engineering based on the deconstruction of the native cellular environment. Materials Letters 2015. https://doi.org/10.1016/j.matlet.2014.11.061.

[218] Nunes AS, Barros AS, Costa EC, Moreira AF, Correia IJ. 3D tumor spheroids as in vitro models to mimic in vivo human solid tumors resistance to therapeutic drugs. Biotechnology and Bioengineering 2019;116. https://doi.org/10.1002/bit.26845.

[219] Brekhman V, Neufeld G. A novel asymmetric 3D in-vitro assay for the study of tumor cell invasion. BMC Cancer 2009;9. https://doi.org/10.1186/1471-2407-9-415.

[220] Zimmermann M, Box C, Eccles SA. Two-dimensional vs. Three-dimensional in vitro tumor migration and invasion assays. Methods in Molecular Biology 2013;986. https://doi.org/10.1007/978-1-62703-311-4_15.

[221] Gunti S, Hoke ATK, Vu KP, London NR. Organoid and spheroid tumor models: Techniques and applications. Cancers (Basel) 2021;13. https://doi.org/10.3390/cancers13040874.

[222] Bilandzic M, Stenvers KL. Assessment of ovarian cancer spheroid attachment and invasion of mesothelial cells in real time. Journal of Visualized Experiments 2014. https://doi.org/10.3791/51655.

[223] Vinci M, Gowan S, Boxall F, Patterson L, Zimmermann M, Court W, et al. Advances in establishment and analysis of three-dimensional tumor spheroid-based functional assays for target validation and drug evaluation. BMC Biology 2012;10. https://doi.org/10.1186/1741-7007-10-29.

[224] de Wever O, Hendrix A, de Boeck A, Eertmans F, Westbroek W, Braems G, et al. Single cell and spheroid collagen type i invasion assay. Methods in Molecular Biology 2014;1070. https://doi.org/10.1007/978-1-4614-8244-4_2.

[225] Li Z, Li X, Gao X, Zhang Y, Shi W, Ma H. Nitroreductase detection and hypoxic tumor cell imaging by a designed sensitive and selective fluorescent probe, 7-[(5-Nitrofuran-2-yl)methoxy]-3 H -phenoxazin-3-one. Analytical Chemistry 2013;85. https://doi.org/10.1021/ac400750r.

[226] Mosadegh B, Lockett MR, Minn KT, Simon KA, Gilbert K, Hillier S, et al. A paper-based invasion assay: Assessing chemotaxis of cancer cells in gradients of oxygen. Biomaterials 2015;52. https://doi.org/10.1016/j.biomaterials.2015.02.012.

[227] The Lee Company. LEE SOLENOID VALVE DRIVE CIRCUIT SCHEMATICS 2021:1. https://www.theleeco.com/engineering/electrical-engineering/lee-solenoid-valve-drive-circuit-schematics/ (accessed January 17, 2021).

[228] Víctor Álvarez J, Filgueira CH, González A de la F, Mejeras CC, Iglesias AB, Tomatsu S, et al. Enzyme-loaded gel core nanostructured lipid carriers to improve treatment of lysosomal storage diseases: Formulation and in vitro cellular studies of elosulfase alfa-loaded systems. Pharmaceutics 2019. https://doi.org/10.3390/pharmaceutics11100522.

[229] Chen X, Zhang C, Wang X. Long noncoding RNA DLEU1 aggravates osteosarcoma carcinogenesis via regulating the miR-671-5p/DDX5 axis. Artificial Cells, Nanomedicine and Biotechnology 2019. https://doi.org/10.1080/21691401.2019.1648285.

[230] Lam D, Enright HA, Peters SKG, Moya ML, Soscia DA, Cadena J, et al. Optimizing cell encapsulation condition in ECM-Collagen I hydrogels to support 3D neuronal cultures. Journal of Neuroscience Methods 2020. https://doi.org/10.1016/j.jneumeth.2019.108460.

[231] Martínez Ávila H, Schwarz S, Rotter N, Gatenholm P. 3D bioprinting of human chondrocyte-laden nanocellulose hydrogels for patient-specific auricular cartilage regeneration. Bioprinting 2016. https://doi.org/10.1016/j.bprint.2016.08.003.

[232] Bachmann B, Spitz S, Schädl B, Teuschl AH, Redl H, Nürnberger S, et al. Stiffness Matters: Fine-Tuned Hydrogel Elasticity Alters Chondrogenic Redifferentiation. Frontiers in Bioengineering and Biotechnology 2020. https://doi.org/10.3389/fbioe.2020.00373.

[233] Claassen H, Schicht M, Brandt J, Reuse K, Schädlich R, Goldring MB, et al. C-28/I2 and T/C-28a2 chondrocytes as well as human primary articular chondrocytes express sex hormone and insulin receptors-Useful cells in study of cartilage metabolism. Annals of Anatomy 2011. https://doi.org/10.1016/j.aanat.2010.09.005.

[234] Prideaux M, Wijenayaka AR, Kumarasinghe DD, Ormsby RT, Evdokiou A, Findlay DM, et al. SaOS2 osteosarcoma cells as an in vitro model for studying the transition of human osteoblasts to osteocytes. Calcified Tissue International 2014. https://doi.org/10.1007/s00223-014-9879-y.

[235] Barreto-Henriksson H, Llorente M, Larsson A, Brisby H, Gold J, Schuster E, et al. Determination of mechanical and rheological properties of a cell-loaded peptide gel during ECM production. International Journal of Pharmaceutics 2019. https://doi.org/10.1016/j.ijpharm.2019.04.028.

[236] Levett PA, Melchels FPW, Schrobback K, Hutmacher DW, Malda J, Klein TJ. A biomimetic extracellular matrix for cartilage tissue engineering centered on photocurable gelatin, hyaluronic acid and chondroitin sulfate. Acta Biomaterialia 2014. https://doi.org/10.1016/j.actbio.2013.10.005.

[237] Eyre D. Collagen of articular cartilage. Arthritis Research 2002. https://doi.org/10.1186/ar380.

[238] Roughley PJ, Mort JS. The role of aggrecan in normal and osteoarthritic cartilage. Journal of Experimental Orthopaedics 2014. https://doi.org/10.1186/s40634-014-0008-7.

[239] Frantz C, Stewart KM, Weaver VM. The extracellular matrix at a glance. Journal of Cell Science 2010. https://doi.org/10.1242/jcs.023820.

[240] Skaalure SC, Chu S, Bryant SJ. An Enzyme-Sensitive PEG Hydrogel Based on Aggrecan Catabolism for Cartilage Tissue Engineering. Advanced Healthcare Materials 2015. https://doi.org/10.1002/adhm.201400277.

[241] Henriksson HB, Svanvik T, Jonsson M, Hagman M, Horn M, Lindahl A, et al. Transplantation of human mesenchymal stems cells into intervertebral discs in a xenogeneic porcine model. Spine (Phila Pa 1976) 2009. https://doi.org/10.1097/BRS.0b013e31818f8c20.

[242] Takuma A, Kaneda T, Sato T, Ninomiya S, Kumegawa M, Hakeda Y. Dexamethasone Enhances Osteoclast Formation Synergistically with Transforming Growth Factor-β by Stimulating the Priming of Osteoclast Progenitors for Differentiation into Osteoclasts. Journal of Biological Chemistry 2003. https://doi.org/10.1074/jbc.M300213200.

[243] Fromigué O, Marie PJ, Lomri A. Differential effects of transforming growth factor β2, dexamethasone and 1,25-Dihydroxyvitamin D on human bone marrow stromal cells. Cytokine 1997. https://doi.org/10.1006/cyto.1997.0209.

[244] Danišovič Ľ, Varga I, Polák Š. Growth factors and chondrogenic differentiation of mesenchymal stem cells. Tissue and Cell 2012. https://doi.org/10.1016/j.tice.2011.11.005.

[245] Castillo Diaz LA, Saiani A, Gough JE, Miller AF. Human osteoblasts within soft peptide hydrogels promote mineralisation in vitro. Journal of Tissue Engineering 2014. https://doi.org/10.1177/2041731414539344.

[246] Uchihashi K, Aoki S, Matsunobu A, Toda S. Osteoblast migration into type I collagen gel and differentiation to osteocyte-like cells within a self-produced mineralized matrix: A novel system for analyzing differentiation from osteoblast to osteocyte. Bone 2013. https://doi.org/10.1016/j.bone.2012.09.001.

[247] Kim S, Kim SS, Lee SH, Eun Ahn S, Gwak SJ, Song JH, et al. In vivo bone formation from human embryonic stem cell-derived osteogenic cells in poly(d,l-lactic-co-glycolic acid)/hydroxyapatite composite scaffolds. Biomaterials 2008;29:1043–53. https://doi.org/10.1016/j.biomaterials.2007.11.005.

[248] Uzarski JS, DiVito MD, Wertheim JA, Miller WM. Essential design considerations for the resazurin reduction assay to noninvasively quantify cell expansion within perfused extracellular matrix scaffolds. Biomaterials 2017. https://doi.org/10.1016/j.biomaterials.2017.02.015.

[249] Esfandiariy E, Hashemibeni B, Hatef M, Ansar M, Mardani M, Zarkesh-Esfahani S, et al. A comparative study of aggrecan synthesis between natural articular chondrocytes and differentiated chondrocytes from adipose derived stem cells in 3D culture. Advanced Biomedical Research 2012. https://doi.org/10.4103/2277-9175.98145.

[250] Kim SA, Sur YJ, Cho M la, Go EJ, Kim YH, Shetty AA, et al. Atelocollagen promotes chondrogenic differentiation of human adipose-derived mesenchymal stem cells. Scientific Reports 2020;10:1–18. https://doi.org/10.1038/s41598-020-67836-3.

[251] Matuszewski PE, Chen YL, Szczesny SE, Lake SP, Elliott DM, Soslowsky LJ, et al. Regional variation in human supraspinatus tendon proteoglycans: Decorin, biglycan, and aggrecan. Connective Tissue Research 2012. https://doi.org/10.3109/03008207.2012.654866.

[252] Deforest CA, Polizzotti BD, Anseth KS. Sequential click reactions for synthesizing and patterning three-dimensional cell microenvironments. Nature Materials 2009. https://doi.org/10.1038/nmat2473.

[253] Son Y, Kim C, Yang DH, Ahn DJ. Spreading of an inkjet droplet on a solid surface with a controlled contact angle at low weber and Reynolds numbers. Langmuir 2008. https://doi.org/10.1021/la702504v.

[254] Stringer J, Derby B. Limits to feature size and resolution in ink jet printing. J Eur Ceram Soc 2009. https://doi.org/10.1016/j.jeurceramsoc.2008.07.016.

[255] Aggeler J, Ward J, Mackenzie Blackie L, Barcellos-Hoff MH, Streuli CH, Bissell MJ. Cytodifferentiation of mouse mammary epithelial cells cultured on a reconstituted basement membrane reveals striking similarities to development in vivo. Journal of Cell Science 1991. https://doi.org/10.1242/jcs.99.2.407.

[256] Matai I, Kaur G, Seyedsalehi A, McClinton A, Laurencin CT. Progress in 3D bioprinting technology for tissue/organ regenerative engineering. Biomaterials 2020. https://doi.org/10.1016/j.biomaterials.2019.119536.

[257] Mazza G, Rombouts K, Rennie Hall A, Urbani L, Vinh Luong T, Al-Akkad W, et al. Decellularized human liver as a natural 3D-scaffold for liver bioengineering and transplantation. Scientific Reports 2015. https://doi.org/10.1038/srep13079.

[258] Singh S, Choudhury D, Yu F, Mironov V, Naing MW. In situ bioprinting – Bioprinting from benchside to bedside? Acta Biomaterialia 2020. https://doi.org/10.1016/j.actbio.2019.08.045.

[259] Gudapati H, Dey M, Ozbolat I. A comprehensive review on droplet-based bioprinting: Past, present and future. Biomaterials 2016. https://doi.org/10.1016/j.biomaterials.2016.06.012.

[260] Duchi S, Onofrillo C, O'Connell CD, Blanchard R, Augustine C, Quigley AF, et al. Handheld Co-Axial Bioprinting: Application to in situ surgical cartilage repair. Scientific Reports 2017. https://doi.org/10.1038/s41598-017-05699-x.

[261] Keriquel V, Oliveira H, Rémy M, Ziane S, Delmond S, Rousseau B, et al. In situ printing of mesenchymal stromal cells, by laser-assisted bioprinting, for in vivo bone regeneration applications. Scientific Reports 2017. https://doi.org/10.1038/s41598-017-01914-x.

[262] Horvath L, Umehara Y, Jud C, Blank F, Petri-Fink A, Rothen-Rutishauser B. Engineering an in vitro air-blood barrier by 3D bioprinting. Scientific Reports 2015. https://doi.org/10.1038/srep07974.

[263] Lee W, Debasitis JC, Lee VK, Lee JH, Fischer K, Edminster K, et al. Multi-layered culture of human skin fibroblasts and keratinocytes through three-dimensional freeform fabrication. Biomaterials 2009. https://doi.org/10.1016/j.biomaterials.2008.12.009.

[264] Lee V, Singh G, Trasatti JP, Bjornsson C, Xu X, Tran TN, et al. Design and fabrication of human skin by three-dimensional bioprinting. Tissue Engineering - Part C: Methods 2014. https://doi.org/10.1089/ten.tec.2013.0335.

[265] Ng WL, Lee JM, Yeong WY, Win Naing M. Microvalve-based bioprinting-process, bio-inks and applications. Biomaterials Science 2017. https://doi.org/10.1039/c6bm00861e.

[266] Hay M, Thomas DW, Craighead JL, Economides C, Rosenthal J. Clinical development success rates for investigational drugs. Nature Biotechnology 2014. https://doi.org/10.1038/nbt.2786.

[267] Mudera V, Smith AST, Brady MA, Lewis MP. The effect of cell density on the maturation and contractile ability of muscle derived cells in a 3D tissue-engineered skeletal muscle model and determination of the cellular and mechanical stimuli required for the synthesis of a postural phenotype. Journal of Cellular Physiology 2010. https://doi.org/10.1002/jcp.22271.

Chapter 11. Appendix I

The image results of the 2D immunohistochemical stainings for all relevant bone and cartilage markers (osteocalcin, osteopontin, collagen II and aggrecan) carried out on both the $40x10^6$ cells/ml and $4x10^6$ cells/ml cell density hydrogel monocultures and co-cultures are presented below in Figure 11-1 to Figure 11-7.

TC28a2 Cell filled CAF Hydrogels with printed cell density $40x10^6$/ml			
Timepoint	Day 3	Day 7	Day 14
Merged	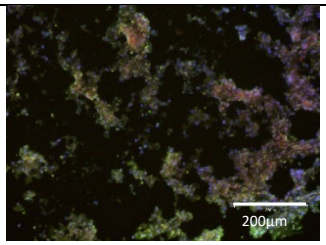	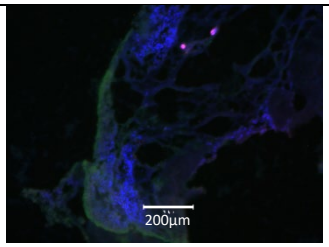	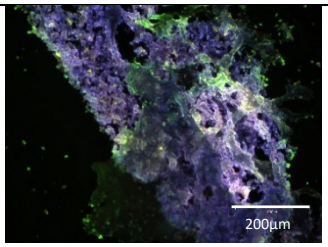
Hoechst	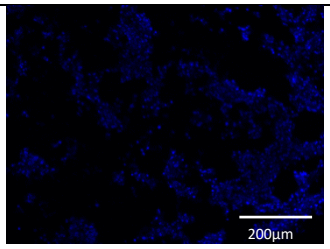	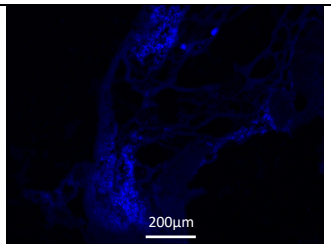	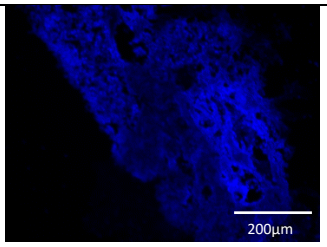
Collagen II	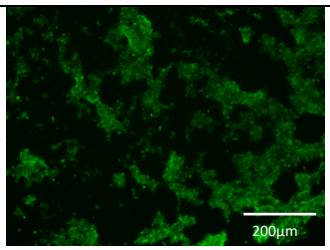	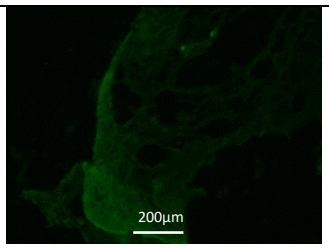	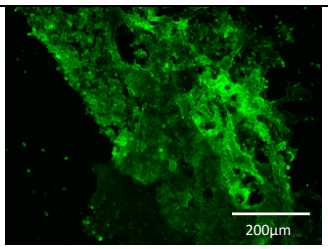
Aggrecan	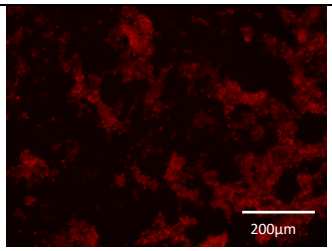	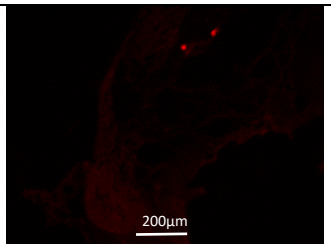	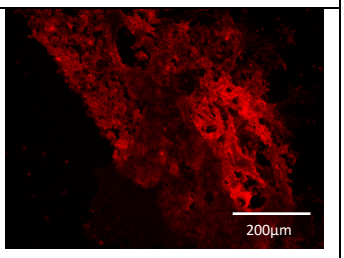

Figure 11-1 : Immunohistochemical staining images of 20µm thick hydrogel sections containing TC28a2 chondrocyte cells printed at a density of $40x10^6$ cells per ml of gel. Sections were stained to show the presence of cell nuclei (blue), Collagen II (green) and Aggrecan (red).

Saos-2 Cell filled CAF Hydrogels with printed cell density $40x10^6$/ml			
Timepoint	Day 3	Day 7	Day 14
Merged	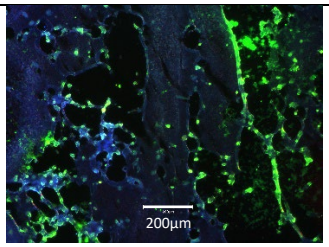	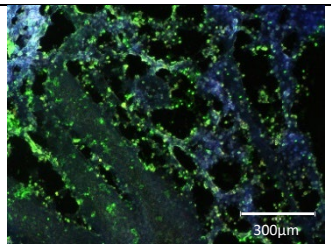	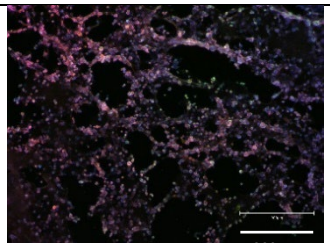
Hoechst	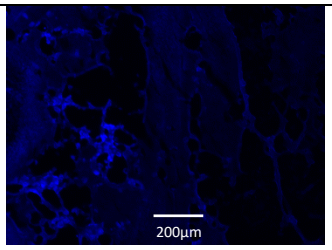	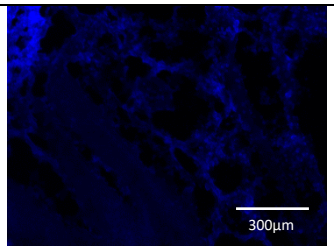	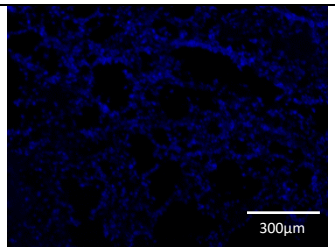
Osteocalcin	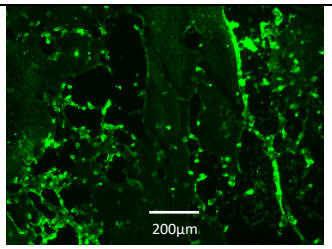	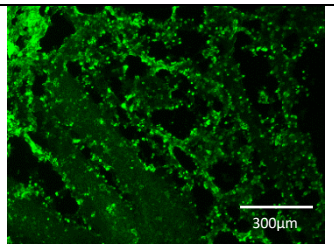	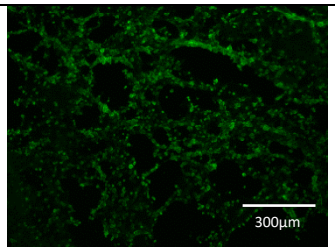
Osteopontin	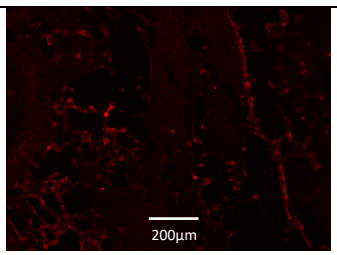	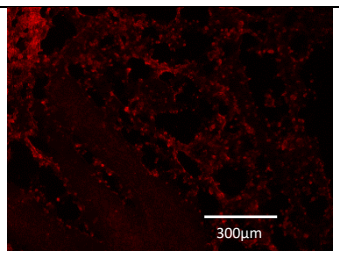	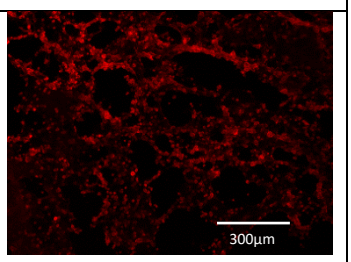

Figure 11-2: Immunohistochemical staining images of 20µm thick hydrogel sections containing Saos-2 osteosarcoma cells printed at a density of $40x10^6$ cells per ml of gel. Sections were stained to show the presence of cell nuclei (blue), Osteocalcin (green) and Osteopontin (red).

TC28a2 and Saos-2 Cell filled CAF Hydrogel co-cultures with printed cell density $40x10^6$/ml			
Timepoint	Day 3	Day 7	Day 14
Merged	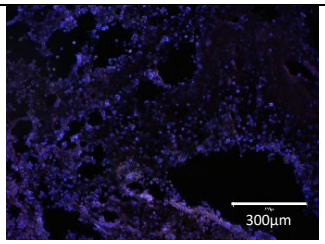	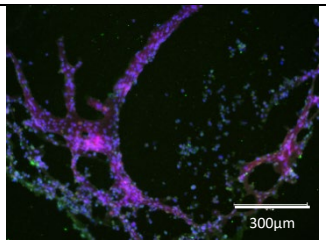	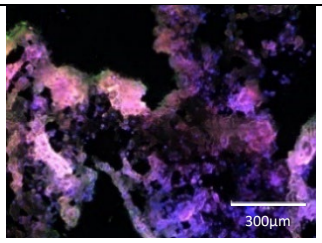
Hoechst	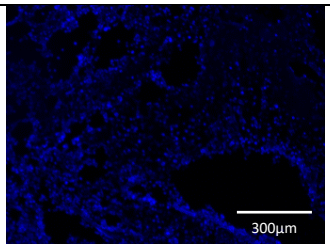	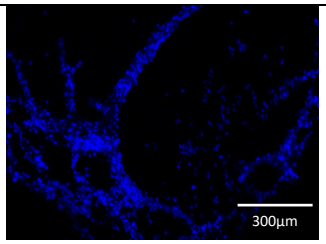	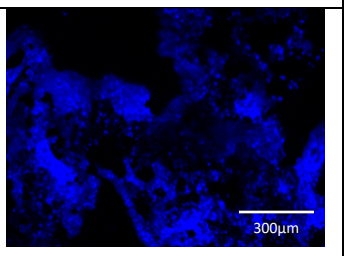
Osteocalcin	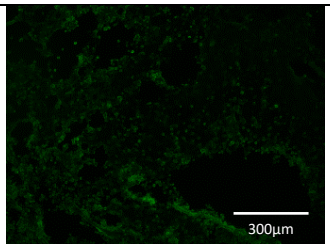	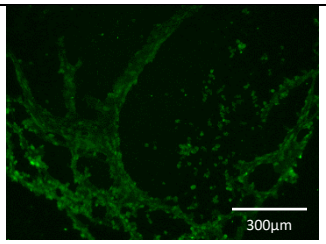	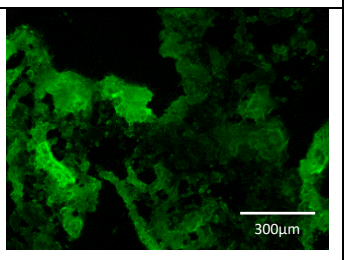
Osteopontin	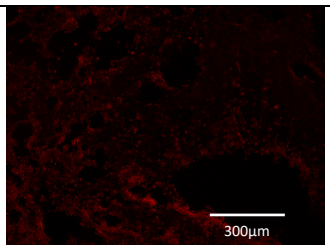	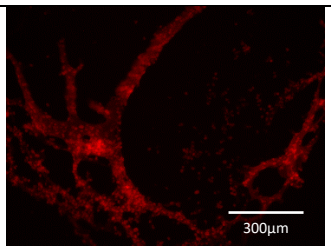	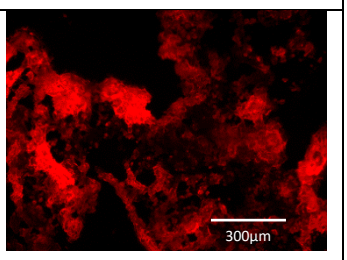

Figure 11-3: Immunohistochemical staining images of 20µm thick hydrogel sections containing TC28a2 chondrocyte cells Saos-2 osteosarcoma cells printed at a density of $40x10^6$ cells per ml of gel. Sections were stained to show the presence of cell nuclei (blue), Osteocalcin (green) and Osteopontin (red).

TC28a2 Cell filled CAF Hydrogels with printed cell density $4x10^6$/ml			
Timepoint	Day 3	Day 7	Day 14
Merged	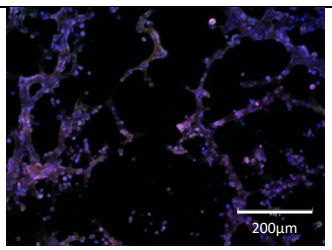	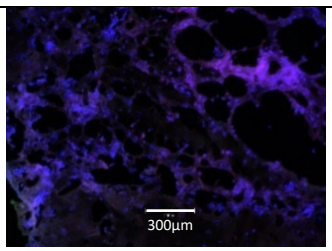	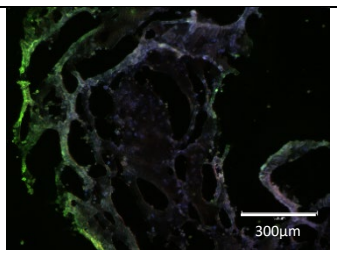
Hoechst	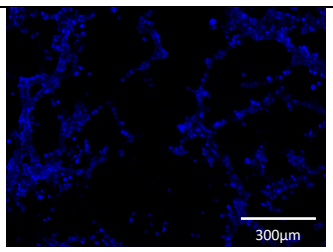	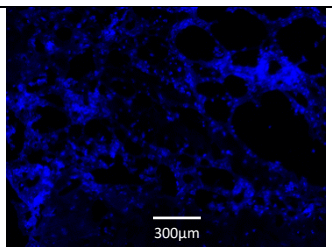	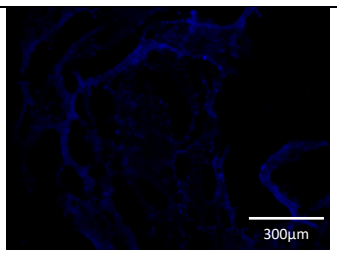
Collagen II	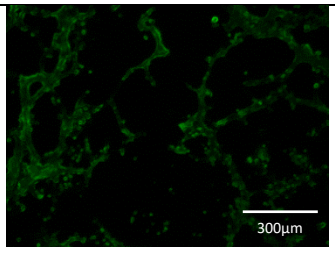	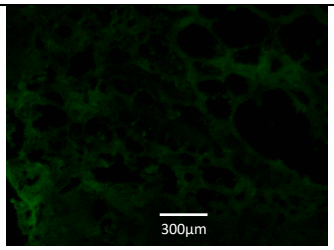	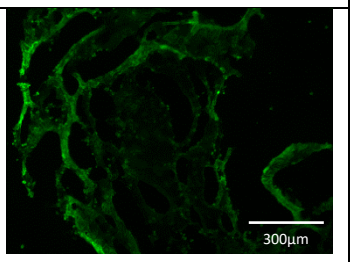
Aggrecan	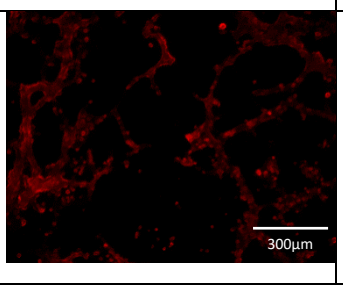	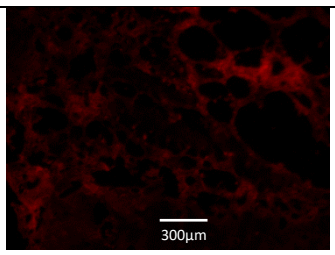	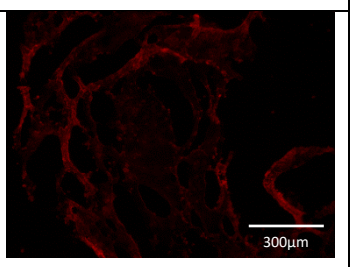

Figure 11-4: Immunohistochemical staining images of 20µm thick hydrogel sections containing TC28a2 chondrocyte cells printed at a density of $4x10^6$ cells per ml of gel. Sections were stained to show the presence of cell nuclei (blue), Collagen II (green) and Aggrecan (red).

Saos-2 Cell filled CAF Hydrogels with printed cell density $4x10^6$/ml			
Timepoint	Day 3	Day 7	Day 14
Merged	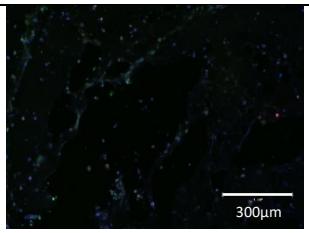	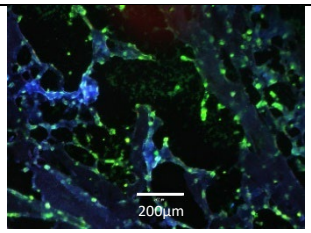	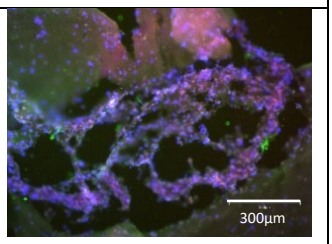
Hoechst	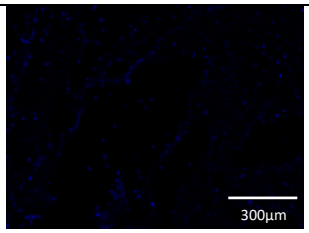	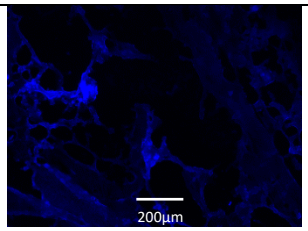	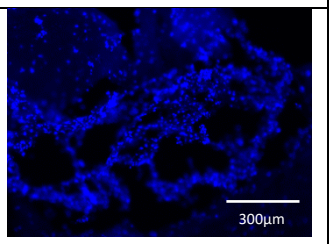
Osteocalcin	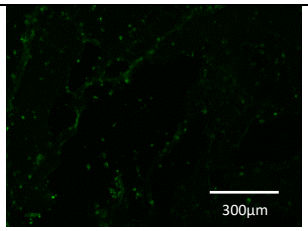	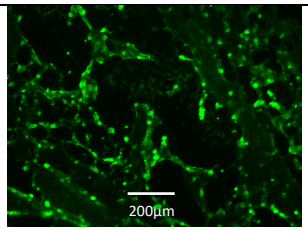	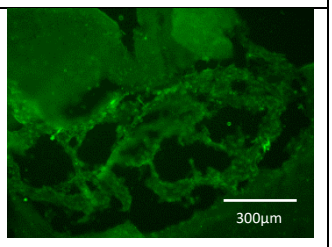
Osteopontin	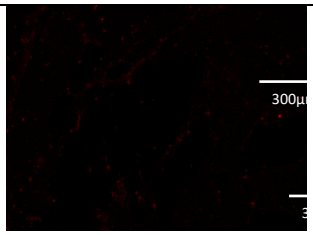	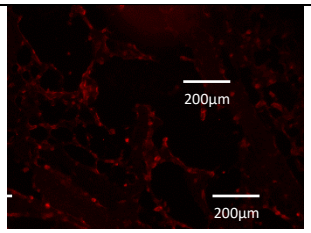	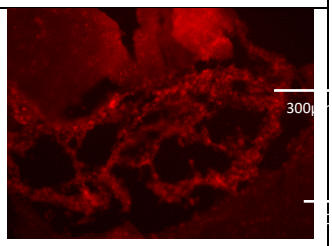

Figure 11-5: Immunohistochemical staining images of 20µm thick hydrogel sections containing Saos-2 osteosarcoma cells printed at a density of $4x10^6$ cells per ml of gel. Sections were stained to show the presence of cell nuclei (blue), Osteocalcin (green) and Osteopontin (red).

TC28a2 and Saos-2 Cell filled CAF Hydrogel co-cultures with printed cell density $4x10^6$/ml			
Timepoint	Day 3	Day 7	Day 14
Merged	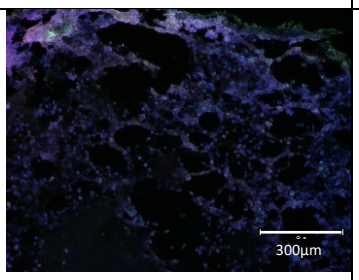	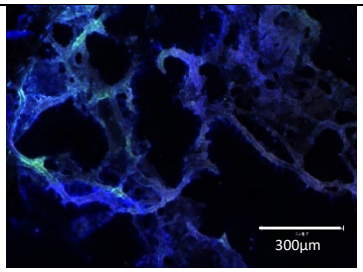	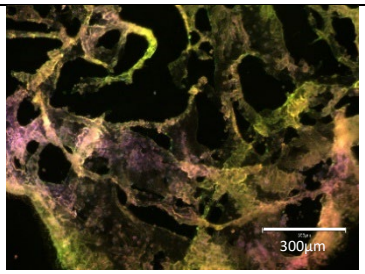
Hoechst	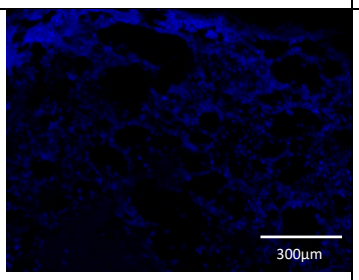	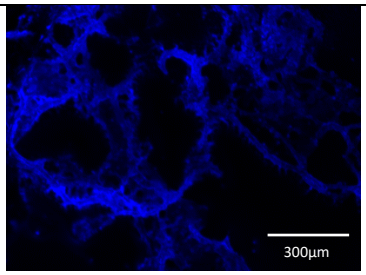	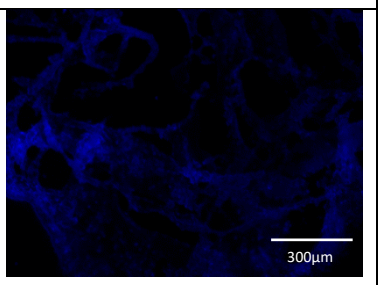
Collagen II	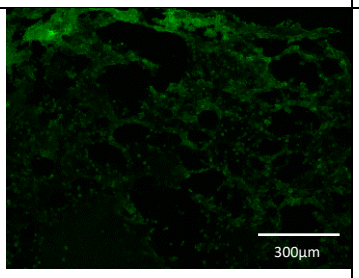	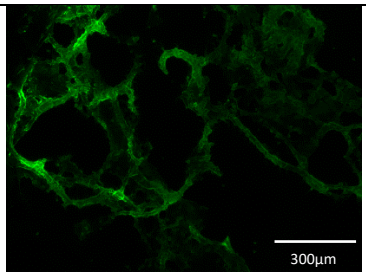	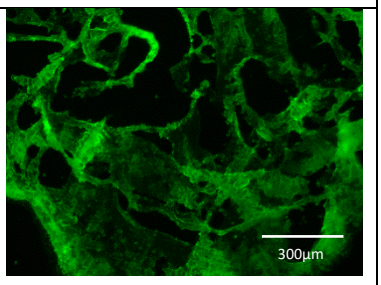
Aggrecan	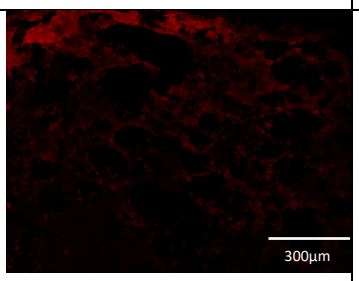	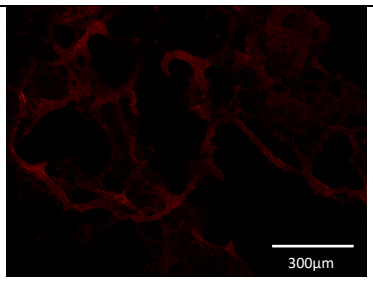	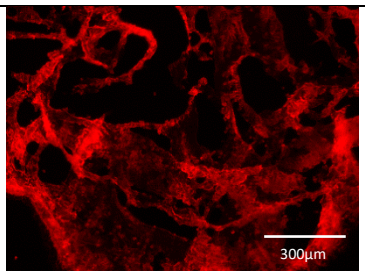

Figure 11-6: Immunohistochemical staining images of 20µm thick hydrogel sections containing TC28a2 chondrocyte cells and Saos-2 osteosarcoma cells printed at a density of $4x10^6$ cells per ml of gel. Sections were stained to show the presence of cell nuclei (blue), Collagen II (green) and Aggrecan (red).

TC28a2 and Saos-2 Cell filled CAF Hydrogel co-cultures with printed cell density $4x10^6$/ml			
Timepoint	Day 3	Day 7	Day 14
Merged	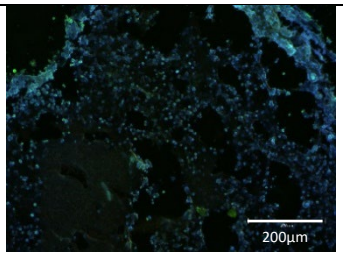	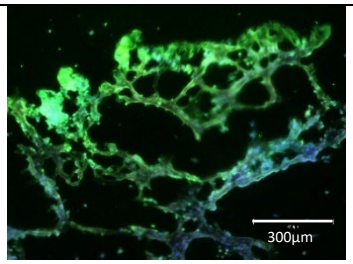	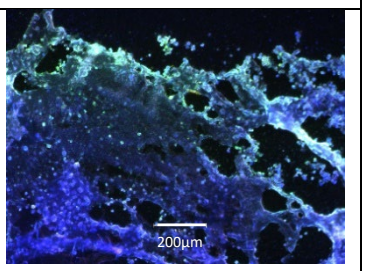
Hoechst	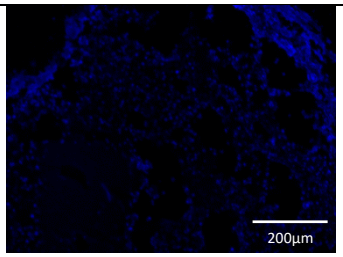	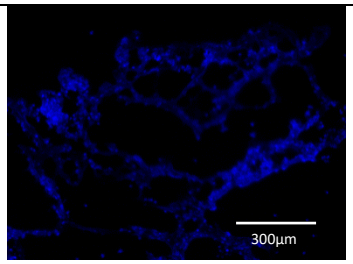	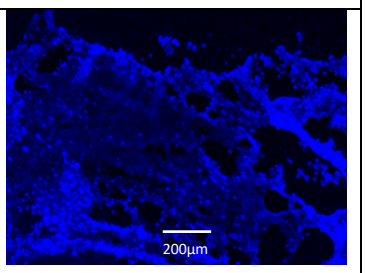
Osteocalcin	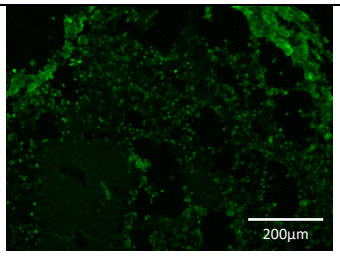	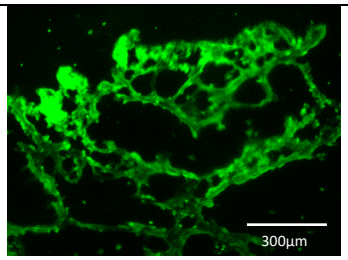	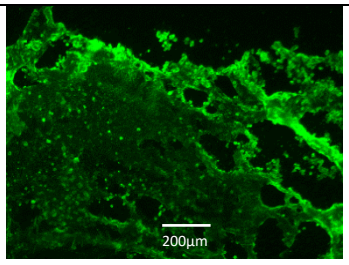
Osteopontin	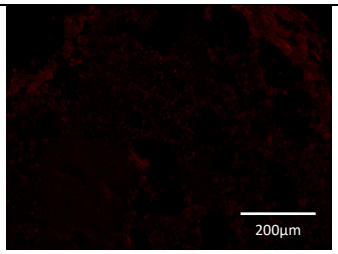	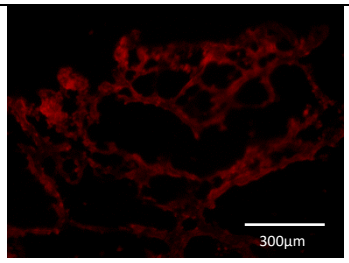	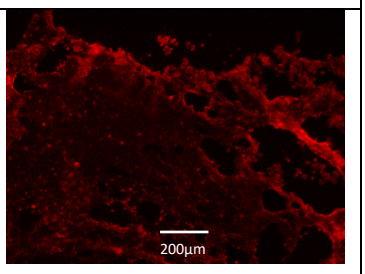

Figure 11-7: Immunohistochemical staining images of 20µm thick hydrogel sections containing TC28a2 chondrocyte cells Saos-2 osteosarcoma cells printed at a density of $4x10^6$ cells per ml of gel. Sections were stained to show the presence of cell nuclei (blue), Osteocalcin (green) and Osteopontin (red).